UNIVERSITY OF MANCHESTER

Organic Finishes on Coil Coated Steels

A thesis submitted to The University of Manchester for the degree of Doctor of Philosophy in the Faculty of Science & Engineering

2018

Lee A. Farren

School of Materials

Contents

Word Count: 50,250

Table of Figures

Abstract

The replacement of hexavalent chromium corrosion inhibitors from paints is an important venture due to the effects of those compounds on the environment and detrimental health effects. The procedure of replacement is made more urgent by imminent changes on the legality of using these compounds within the European Union. Whilst replacements have been devised, in many cases these replacements are less versatile, less effective and their mechanisms less understood.

In aid of this, a methodology was produced that allows some understanding of the potential of an inhibitor on complex metallic systems, without the time restraints involved with more traditional methods, such as atmospheric testing. This methodology, simultaneous electrochemical impedance, utilises multiple zero resistance ammeters attached to a single overriding potentiostat to gain electrochemical information on multiple metals whilst maintaining the mixed potential of the coupled system, and was verified using previously defined inhibitor systems.

Three commercial polyphosphate inhibitors were analysed using this technique and were shown to have distinct behaviours on a simple steel/zinc couple. Strontium aluminium polyphosphate exhibited a delayed inhibition response which was absent when the distance between working electrodes was decreased, which was theorized to be due to the mechanism of action requiring the presence of anodically produced zinc ions. This was tested and confirmed through an x-ray photoelectron spectroscopy study which externally introduced zinc ions and showed an increase in the phosphorus content seen on the steel surface. The concentration of externally added zinc required for this effect was tested and determined to be approximately between 1 and 2 mM.

Subsequently, alternative cationic species were added to determine whether the efficacy of the phosphorus surface deposition could be potentially improved through other in-paint additives. Calcium was shown to be effective, with magnesium showing some effect on strontium aluminium polyphosphate. Aluminium cations appeared to have little effect.

Additionally, the use of the simultaneous electrochemical impedance methodology was shown to have some use in analysing even more complex materials with a zinc/steel/aluminium model. The use of pure aluminium may cause some issues in analysis due to the protective oxide layer. Magnesium aluminium polyphosphate results suggest that it may initially interfere with this oxide layer production.

Declaration

The author declares that no portion of the work presented here has been submitted in support of an application for another degree or qualification of this or any other University

Copyright Statement

The ownership of certain Copyright, patents, designs, trademarks and other intellectual property (the “Intellectual Property”) and any reproductions of copyright works in the thesis, for example graphs and tables (“Reproductions”, which may be described in this thesis, may not be owned by the author and may be owned by third parties. Such Intellectual Property and Reproductions cannot and must not be made available for use without the prior written permission of the owner(s) of the relevant Intellectual Property and/or Reproductions.

Acknowledgements

Whilst a thesis can be considered to be the celebration and accumulation of the research accomplishments of an individual, it is certain that it would not be possible without the support of those who surround us. As such, I would like to use this section to personally thank those people who have aided over the last several years.

To Professor Stuart Lyon and Dave Francis, as supervisors of the academic and industrial parts of the project respectively, who have been vital in keeping the project from becoming unmanageable and unwieldy. Both important beacons of guidance throughout the entire process, and without whom this piece of work would not be what it is today.

To Dr. Suzanne Morsch, with whom I have shared an office as desk neighbour, for being an ever-present sounding board and one of the greatest outlets for unscrambling thoughts and producing sensible ideas and plans.

I would also like to acknowledge, for the support offered, the members of the AkzoNobel laboratory team: Reza Emad, Zoe Keffalinou, Nick Curry, Monika Walczak, Matthew Goodall, Yanwen Liu, Kiran Kousar and Wei Shi.

Finally, I would like to dedicate this thesis to my parents, Gary Wake and Jennifer Farren, whom without their support I would not be in the position to submit it. And, to my girlfriend Nicola Neale, whose endless patience and moral support has allowed me to complete it.

Chapter 1

Literature Review

1.1 Introduction

The works presented in this thesis were carried out to investigate the effects of corrosion inhibitor pigments on the cut edges of coil coated materials. In this literature review, the concepts, methods and materials utilised throughout the thesis will be introduced, and an overview and critical analysis of previously published research within these areas will be presented.

1.2 Corrosion Fundamentals

Introduction to Corrosion

Corrosion is defined as the 'physicochemical interaction between a metal and its environment that results in changes in the properties of the metal, and which may lead to significant impairment of the function of the metal, the environment, or the technical system, of which these form a part[1].' (ISO 8044-1999). This process occurs electrochemically, with an oxidation reaction occurring at anodic sites and balancing reduction reactions occurring at cathodic sites.

The particular electrochemical process that occurs at a metal surface is dependent on both the environment and the metal itself. Susceptibility of a metal or system to different corrosion phenomena are determined by a combination of these two factors. Later sections will deal with the corrosion behaviour of certain individual metals.

Both oxidation and reduction have multiple pathways which can be represented by chemical half-equations. A common oxidation reaction that is observed at the anode can be expressed by the general equation[2]:

$$M_{(s)} \rightarrow M^{n+}_{(aq)} + ne^{-}$$

where *M* is a metallic element, and *n* is the number of electrons removed from the element, which is dependent on the valency of the metal. The positively charged atom can then solvate

into the surrounding electrolyte as an ion, or react with other species present within the environment to form insoluble corrosion products[3].

The dissolution of the anodic site, as represented by the previous chemical half-equation, is very common. However, this does not occur in cases where the anodic site is inert. In this case, other reactions must take place to balance any cathodic activity. Commonly, this occurs through the oxidation of anionic species in solution, or, alternatively, through the release of oxygen. Examples of chemical half-equations representing these processes are:

$$2Cl^-_{(aq)} \rightarrow Cl_{2(g)} + 2e^-$$

$$2H_2O_{(l)} \rightarrow O_{2(g)} + 4H^+_{(aq)} + 4e^-$$

The electron transfer shown in the oxidation half-equation is balanced by a reduction reaction, which occurs at the cathodic site on the material. There are several reactions that can occur at the cathode. Of these, the simplest is metal deposition, also known as replating, which is effectively a reversal of the anodic dissolution process shown previously. This can be represented by the following equation[2]:

$$M^{n+}_{(aq)} + ne^- \rightarrow M_{(s)}$$

The particular reduction reaction that takes place at the cathodic site is dependent on factors such as the surface potential and local environmental effects. The oxygen reduction reaction is a common reaction seen at the cathode. The particular pathway for this reaction to occur is dependent on the environment, with two possible half-equations:[2]

$O_2 + 4H^+ + 4e^- \rightarrow 2H_2O$ (Acidic solutions)

$2H_2O + O_2 + 4e^- \rightarrow 4OH^-$ (Basic/Neutral solutions)

In the absence of a sufficient concentration of oxygen dissolved in solution, the reduction of hydrogen can occur[4]:

$$2H^+ + 2e^- \rightarrow H_2$$

In some cases, the anodic process can provide enough energy to electrolytically split water at the cathode. This most often occurs in situations where there is a reactive metal, such as magnesium, aluminium or zinc, and the concentration of dissolved oxygen is sufficiently low enough to limit oxygen reduction[5].

$$2H_2O + 2e^- \rightarrow 2OH^- + H_2$$

Corrosion can only occur when a complete cell is formed. This consists of a conductive electrolyte, an anodic site, a cathodic site and an electric bridge between anode and cathode. An electric bridge can be formed through either direct contact between the two sites, or through other means such as a wire. The electrons released at the anode spontaneously travel to the cathode to allow the cathodic reaction to occur[6]. Therefore, to maintain balance, one cannot happen without the other.

Thermodynamics of Corrosion

Free Energy

The likelihood of a particular reaction occurring is governed by Gibbs free energy, which is represented in electrochemical reactions by the equation given below[7].

$$\Delta G = -nFE$$

Where ΔG is the change in Gibbs free energy, n is the number of electrons transferred in the reaction, F is the Faraday constant and E is the potential of the reaction.

For a reaction to be favourable, the ΔG for the process will be negative. Corrosion is, in the case of most metals, a thermodynamically favourable process. This is due to the relatively high energy state of the base metal when compared to the oxide forms, and it is this energy

difference that drives corrosion[3]. This is also the reason that metals are naturally found within ore, where energy must be expended to isolate the metal. As can be seen in Figure 1.2.1, the metal exists in a higher energy state than that of the corrosion products[3]. Therefore, the free energy of the metal can be significantly reduced by being corroded, and thus there is, in most cases, a thermodynamic driving force for corrosion.

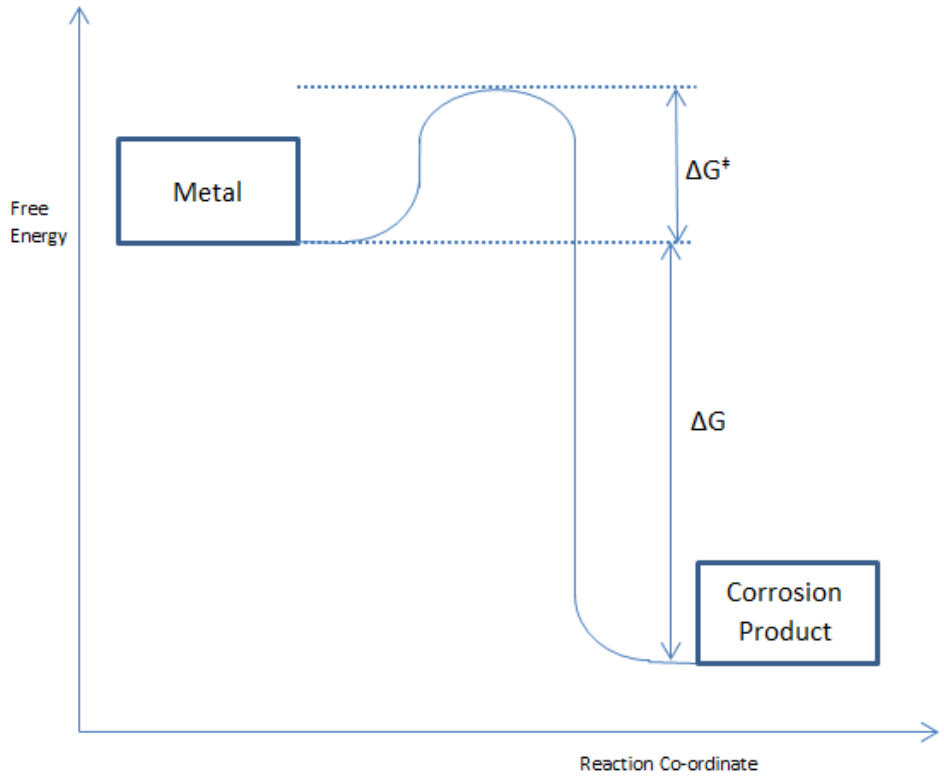

Figure 1.2.1 - An energy diagram representative of a generic metal and the products of corrosion

However, in spite of this thermodynamic driving force, metals are capable of existing as free metal. The stability of metals can be explained by $\Delta G^{\ddagger}$, the free energy of activation, which represents an energy barrier for the corrosion reaction. This ensures that corrosion is not a completely spontaneous process in reality.

Nernst Equation

An electrochemical reaction can be also be represented in its entirety by the Nernst equation[3].

$$E = E^0 - \frac{RT}{zF} lnK$$

In the Nernst equation, *E* is the potential of the cell, specific to the conditions as measured. E^0 is the standard potential of the cell, which is a measure of the potential of a reversible cell at standard state. *R* is the ideal gas constant (8.314 J K^{-1} mol^{-1}), *T* is the absolute temperature, z is the number of electrons transferred in the corrosion reaction and F is the Faraday constant (approximately 96,494 C mol^{-1}). K is the equilibrium constant for the reaction being investigated, which is dependent on the concentrations of the products and reactants.

The standard electrode potential, E^0, is the characteristic activity of a reversible electrode in standard conditions, which means the potential measured with solutes at an effective concentration of 1 mol dm^{-3} and gasses at a pressure of 1 atm. This standard measurement can be used to represent the electrochemical activity of particular elements, as elements with higher standard electrode potentials can be considered to be less active, or more noble, than those with lower or negative standard electrode potentials[7]. It is this which is the basis behind the electrochemical series. Standard electrode potentials are given with reference to the standard hydrogen electrode, which is defined as having 0 potential[7].

The measurement of the potential of individual electrodes is, however, impractical. Experimentally, only the difference in potentials between two electrodes can be measured. The need for accuracy means the use of a reference electrode. A reference electrode is used in determining the potential of a cell by providing a well-defined standard potential for comparing all other electrodes with. Several reference electrodes have been developed for use in electrochemical experiments. A common reference electrode is the saturated calomel

electrode, a mercury/mercury chloride electrode containing saturated potassium chloride that has a potential of +0.245 V when compared to the standard hydrogen electrode[8].

Pourbaix Diagrams

pH-overpotential diagrams, also known as Pourbaix diagrams, were first introduced in the 1940s by Marcel Pourbaix[9]. These diagrams show a representation of the most thermodynamically stable forms of a particular metal over a 2 dimensional range of pH values and applied potentials. A simplified Pourbaix diagram, however, only shows distinct areas of how the metal behaves in the particular environment. There are three distinct areas: immunity, where the metal remains unchanged in the system, passivation, where the metal is reacted but forms a protective surface layer, and corrosion, where general attack of the surface can occur[9]. A simplified Pourbaix diagram for iron is shown in Figure 1.2.2.

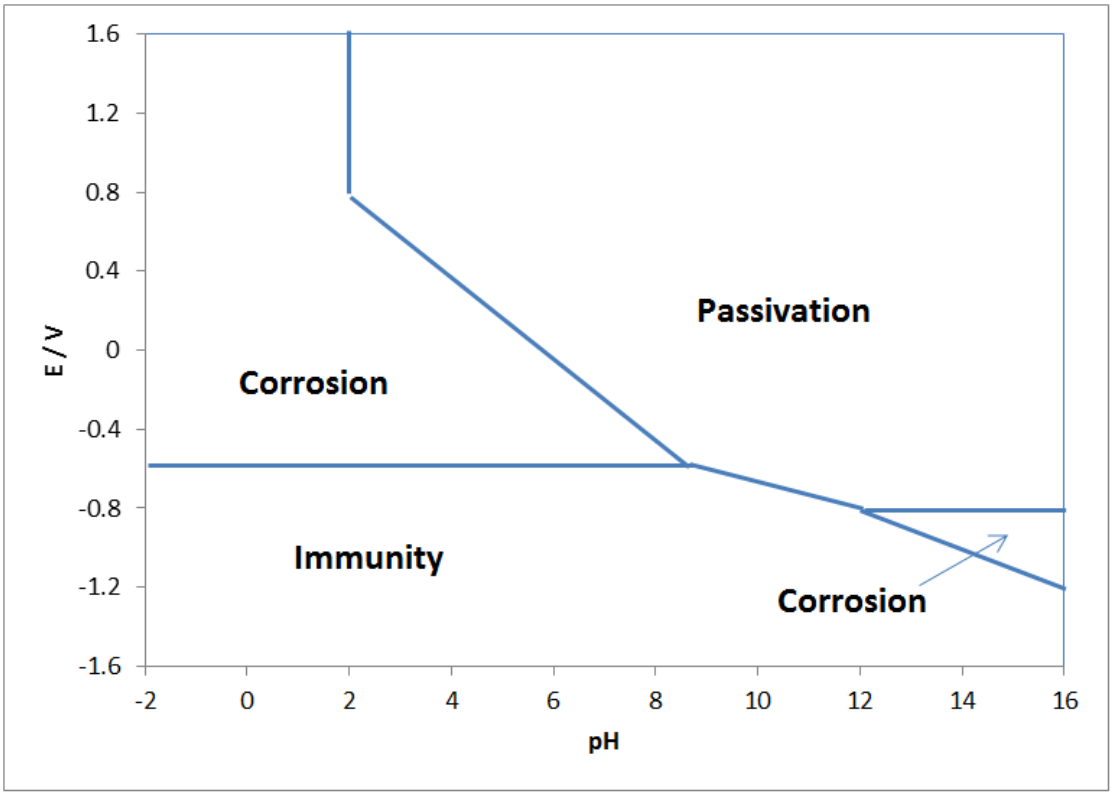

Figure 1.2.2 – A simplified Pourbaix diagram for iron

Whilst there are certainly uses for the information that can be obtained by analysis of Pourbaix diagrams, specifically the general usefulness of a material in a particular environment, it is somewhat limited. Whilst a Pourbaix diagram will give information on thermodynamic stability of a material in specific environments, it gives no details about the kinetics of those reactions. This means that the actual rate of a particular corrosion reaction, a property which is also significant, cannot be considered through the use of Pourbaix diagrams alone.

Kinetics of Corrosion

Tafel Equation

As previously mentioned, the electrochemical reactions that take place during corrosion cannot occur unless there are electrochemically equivalent reactions occurring simultaneously. As such, it can be expected that the rate of oxidation is equivalent to the rate of reduction[3]. It is therefore also the case that when a metal begins to corrode, there must always be an oxidation process and a reduction process. The potential observed for a sample undergoing these processes would be observed as a combination of the two, and would therefore lie between. Therefore, plotting the intersection of the anodic and cathodic processes provides the E_{corr}, which is the free corrosion potential, and i_{corr}, the corrosion current density[2].

In the early 1900s, Tafel discovered that the logarithm of current density of a reaction taking place in an electrochemical cell varies linearly with potentials lying away from the open circuit potential[3]. The equation describing the relationship is known as the Tafel equation, and is as shown below:

$$\eta = a + b \log i$$

Plotting a graph of η vs. log|i|, therefore, gives a graphical representation of the effect of overpotential on current density. This can be used as a way of determining the open circuit potential, E_{corr}.

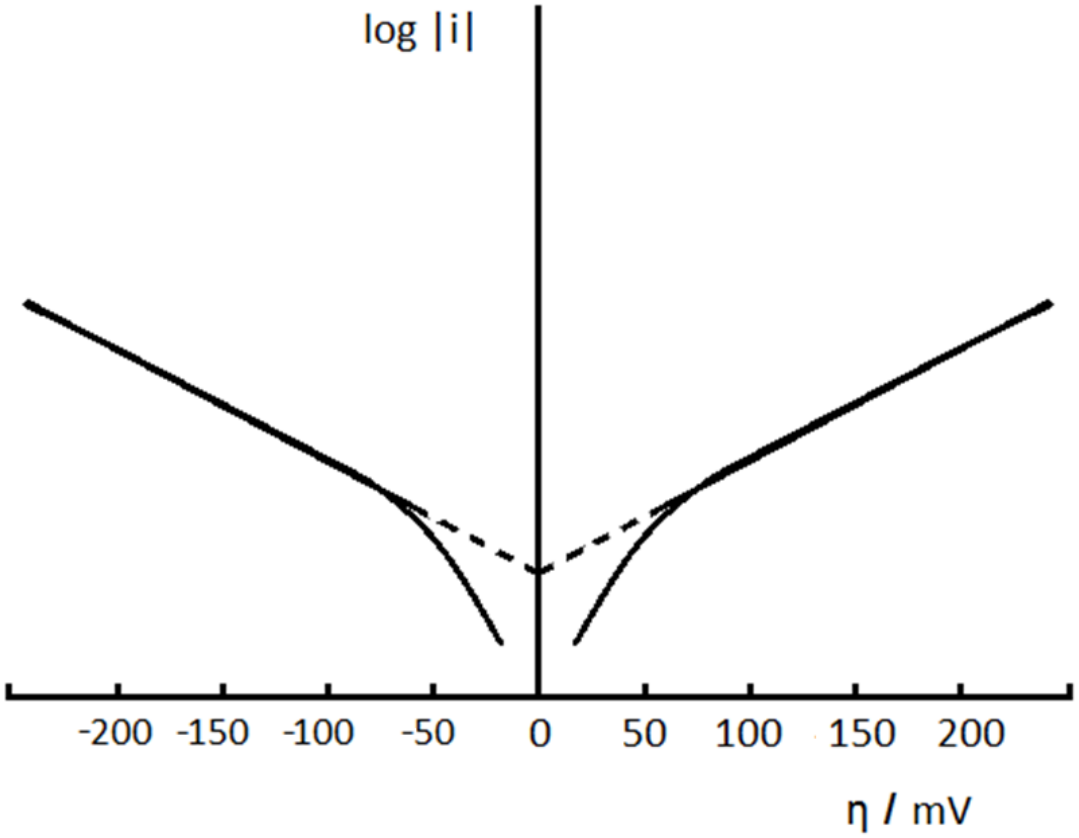

Figure 1.2.3 - A Tafel plot showing the variation in current with overpotential

As can be seen in Figure 1.2.3, there is a deviation from linearity as α approaches 0. This is due to the fact that the reaction occurring in the opposite direction becomes non-negligible at very low values of α[10]. There are also deviations from the linear path at the upper and lower limits of η. This is because the reaction at these values becomes limited by the ability for mass to be transferred at a sufficient rate[11].

Diffusion

Diffusion plays an important part in determining how corrosion occurs. As previously mentioned, metals have a thermodynamic tendency toward corrosion when immersed in electrolyte, and thus it can be considered that corrosion occurs readily upon immersion[3]. However, the onset of corrosion has the effect of lowering the thermodynamic demand for

corrosion. This is due, in part, to Le Chatelier's principle, where a system will react to oppose changes in the equilibrium position of the system[3].

The formation of the Helmholtz double layer is partially responsible for the lowering of the corrosion rate. As metal ions solvate, the surface is left with a net surplus of electrons. This surface charge maintains an attraction to the solvated cationic species, hindering diffusion away. In time, the surface has a strong electrostatic interaction with an adjacent volume of solution containing a high concentration of solvated ions[3]. As a result, the tendency for the surface to solvate is reduced, and thus, the rate of corrosion is lowered. In some cases, this may eventually lead to equilibrium between the dissolution process and replating process[12].

The phenomenon of concentration polarisation is also a result of diffusion. If it is considered that the cathodic component of a cell is the oxygen reduction reaction, then through the application of a cathodic overpotential, the thermodynamic driving force for this reaction, and consequently the rate of the reaction, can be increased. It can be asserted, however, that the highest rate that this reaction is capable of is limited by the amount of oxygen that is present at the cathode surface to be reduced. In this way, the resulting current from the cathode is limited to the rate at which oxygen can diffuse to the surface[13]. This is known as the diffusion limiting current density.

Passivity

Metals that are closer to the top of the electrochemical series as it is traditionally arranged are expected to be more prone to corrosion than those considered to be less active. However, this is not always the case. Some metals with active electromotive forces can corrode at a low rate when exposed to certain conditions[14]. This is due to a phenomenon known as passivity. Passivity occurs when the thermodynamic product of a reaction between the metal and components of the environment forms a solid material on the surface that exists as a continuous and adherent film which remains insoluble within the surroundings. A common

example of this is aluminium, which, when exposed to the air, will form a protective oxide layer that slows the rate of corrosion[14]. Similarly, passivity is observed on stainless steels, in which the chromium alloying additions form a protective chromium oxide layer on the surface[15]. In a previous section, it could be seen that the simplified Pourbaix diagram for iron shows passivity in areas of applied anodic current and alkaline environments.

Passivity may not always significantly hinder corrosion processes, however, as the effect that the formation of a surface film is dependent on the properties of that film. Taking into consideration the formation of chromium oxide on the surface of stainless steels, it can be seen that due to the electrical conductivity of the chromium oxide layer, cathodic processes may still occur at the surface. However, the dissolution of iron is hindered by the presence of chromium oxide, due to the interference with diffusion. Thus the passivation in this case can be considered to be hindering just anodic processes[16].

Forms of Corrosion

How corrosion proceeds is dependent on a number of factors. There are a number of different corrosion processes, and the susceptibility of a system to these processes is dependent on both the metal and the environment in which it is contained.

Uniform Corrosion

Uniform corrosion, also known as general attack corrosion, is a process which leads to reasonably even dissolution across the metallic surface[17]. The characteristic sign of uniform corrosion is a general reduction in the thickness of the material that is approximately evenly distributed. Two common examples of this process are seen in the degradation of unprotected iron in the atmosphere and the tarnishing of silver[17].

Due to the nature of uniform corrosion, the amount of time before it becomes an issue from a mechanical properties standpoint can often be well predicted and measured[17]. Thus, monitoring the progression of this corrosion process generally requires only basic techniques.

However, uniform corrosion can prove to be problematic, particularly when dealing with the aesthetics of materials. The nature of uniform corrosion means that most developed corrosion protection strategies can be utilised.

However, it is worth noting that uniform corrosion can never be truly uniform. As corrosion is a stochastic process, in that both cathodic and anodic processes must occur at the same time with the same magnitude but never at the same site. This fact can give rise to intrinsic variance that causes non-uniform attack on the surface.

Galvanic Corrosion

Galvanic corrosion is the preferential dissolution of one material over another. This occurs when two dissimilar metals come into electrical contact with each other whilst exposed to an electrolyte, causing a current to flow between the two. This current flows from the metal with the lower electromotive force, which becomes the anode, to that with the higher, which becomes the cathode. This happens as the potential difference between the two metals causes each to assume a different corrosion potential. This, in effect, leads to the anodic and cathodic polarisation of the constituent parts[18].

Galvanic corrosion is often perceived as occurring between two distinct pieces of metal, either through metal coatings or other attached metal blocks. However, galvanic corrosion occurs even without such well-defined dissimilar metals. For example, it is also possible for the corrosion products of a material to form a galvanic couple. This is particularly problematic in some applications where the corrosion products of one metal may leave the surface and be deposited on another metal. When this happens, there is the potential for a small galvanic cell to develop that can lead to severe corrosion around the point of deposition[19].

The risk of galvanic corrosion is increased when there is a greater difference between the electromotive forces of the two materials in the environment in which they are exposed. However, greater risk of galvanic activity does not necessarily equate to a greater rate of

galvanic corrosion, as other factors, such as tendency to passivate, must also be taken into account[20].

The rate of galvanic corrosion can be affected by various parameters, besides the properties of the selected metals. One such consideration is the ratio of the exposed areas of the anode and cathode. In situations where the cathodic area far exceeds that of the anodic area, the corrosion rate of the anodic material may see a notable increase; even in cases where the potential difference between the anodic and cathodic materials is low[21].

Differences in material geometry and electrolyte properties can also have an effect on the rate of galvanic corrosion. For example, in conditions where the electrolyte is sparingly conductive, and there is a significant pathway between the two coupled materials, a drop in the potential of the couple is observed. This is due to the increased resistance that is imparted by the electrolyte[21].

Temperature also has an effect on the rate of galvanic corrosion. Typically corrosion rate will increase with increasing temperature. However, there are cases where the cathodic and anodic sites will switch following temperature changes. For example, the couple of zinc and iron has been reported to switch in some electrolytes at higher temperatures due to the ennoblement of zinc by corrosion products[21]. Temperature gradients on single metals can also cause galvanic corrosion to occur, with areas differing in temperature becoming anodic or cathodic to the rest of the material[21].

Localised Corrosion

Pitting and crevice corrosion are two distinct forms of localised corrosion in which a particular site on the substrate surface is subjected to corrosive attack at a rate that is significantly higher than that of the rest of the surface. This is due to the development of a microenvironment at the site of corrosion which differs greatly to the bulk electrolyte. The underlying cause of this microenvironment is the distinguishing factor between crevice corrosion and pitting.

Pitting occurs in systems where there is a surface protection of the substrate, through either the use of corrosion inhibitors or the self-passivation of metals such as stainless steels or aluminium[6]. Pits initiate at a point where the surface protection breaks down, despite being in conditions in which the bulk material remains protected.

For pitting to initiate, there must be the development of a corrosive microenvironment. For example, in chloride containing environments, the microenvironment local to the pit can be acidified due to the formation of hydrochloric acid at the site. This is caused by the hydrolysis of metal chloride complexes. Chloride ions are attracted to the pit from the high concentration of counterions from anodic dissolution of the bulk metal, which in turn produces metal chloride complexes. The hydrolysis of these complexes produces free hydrochloric acid at the pit through reactions such as the following[20].

$$MCl_2 + H_2O \rightarrow M(OH)_2 + 2HCl$$

Whilst pitting can be considered to be initiated through a combination of metallurgical and solution properties, crevice corrosion occurs as a result of geometrical factors of the materials which cause an environment to be shielded or restricted. A shielded environment can cause the lowering of the rate of diffusion of dissolved species in the bulk electrolyte to the local environment[21].

As this can restrict the diffusion of dissolved oxygen to metal sites in the crevice, cathodic processes in this environment are suppressed. This leads to metal within the crevice to assume a more anodic character than the rest of the material, leading to a greater rate of anodic dissolution. The increased anodic activity within the crevice can aid the diffusion of chloride ions into the crevice through providing a greater concentration of counter ions. Through reactions similar to those mentioned for the propagation of pitting, the corrosion rate within the crevice is then increased[20].

Filiform Corrosion

Filiform corrosion is a type of corrosion that produces filament-like corrosion products. It occurs most commonly on samples that have thin coating layers, although it has been observed on bare substrates[6]. It has been shown to occur in high humidity environments, and is particularly prevalent with some salts and on certain metallic substrates. Considered to mainly be an aesthetic issue, it does not generally make significant changes to the strength of the bulk material.

It is considered to contain a small anode at the head, with an electrolyte containing tube running behind it, with the mechanism of propagation being similar to that of crevice corrosion[22]. Figure 1.2.4 shows the proposed mechanism of filiform corrosion as it proceeds under an organic film.

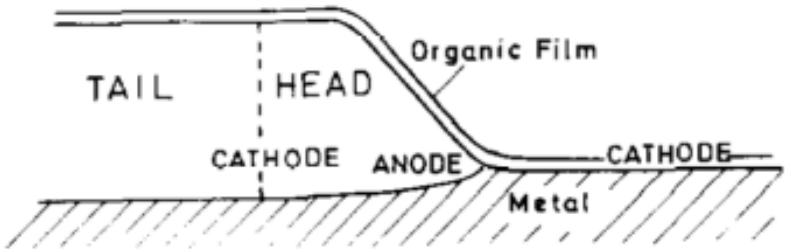

Figure 1.2.4 - Proposed structure of a filament in filiform corrosion[23]**.**

Filiform is a commonly observed form of corrosion of aluminium alloys, and the presence of filiform corrosion on aluminium alloys[24,25] and inhibiting filiform corrosion of aluminium alloys[26,27] is well documented. However, there are some reports of filiform corrosion present on steels[28,29], and of particular interest, galvanised steels[30].

It could be suggested that the added inclusions of aluminium into the zinc coatings of galvanised steels may produce coatings that are more susceptible to this form of degradation. Whilst not much research suggests filiform corrosion occurring on zinc-coated and zinc alloy-

coated steel materials, a paper by Luckeneder et al[31] reports anecdotal evidence of “filiform-like” corrosion in zinc-aluminium alloys from industrial sources.

Dealloying

Dealloying is a corrosion process where one metallic constituent of an alloy is removed preferentially. Galvanic currents generated between two of the constituent metal parts of the alloy is the major reason behind dealloying, although other factors do still have an effect[32].

Dealloying occurs in two distinct ways. The first is through uniform dealloying, which entails the selective dissolution of a particular phase that occurs at a similar rate across the surface of the material. Alternatively, dealloying can be localised, where the selective dissolution occurs with greater severity at particular parts of the material[21].

A common example of dealloying is in brass. Brass is a copper-zinc alloy containing between 15 and 40 wt% of zinc. Due to the difference in electrode potential of zinc and copper, zinc corrodes preferentially as it is an anodic when coupled to the copper[33]. This results in general dissolution of the zinc rich phases in the brass alloy, leading to a porous structure that loses all structural strength. The dealloying of brass is more commonly known as dezincification.

Dealloying has been reported to occur in the corrosion of some alloy coatings used in the coil coating industry. Sullivan et al[34] were able to observe the dealloying of eutectic phases within zinc magnesium aluminium ternary alloy structures in-situ using time lapse optical microscopy. This was independently observed by Volovitch et al[35], who speculated that the inactivity of aluminium is due to the naturally protective oxides forming on aluminium phases. By using atomic emission photoelectron spectroscopy, Salguiero Azevedo et al[36] were also able to confirm dealloying phenomena in zinc magnesium aluminium alloys, but noted that the mechanisms and phases that were preferentially dissolved was dependent on the environment.

Corrosion of Iron and Steels

The corrosion of iron is a significant problem that is well identified on a global scale. Iron oxide, or rust, present on an iron or steel surface is one of the most recognisable products of a corrosion process, and the prevention of this has been a source of research for several years. Many of the problems arising from the corrosion of iron come from the ability of iron to be readily oxidised and reduced depending on the environment.

Iron corrosion occurs generally with the metal taking the form as both the anode and the cathode, although in some cases, other materials can act as cathodes when in contact with the iron surface. The dissolution of iron at an anodic site on the metal proceeds as mentioned previously:

$$Fe_{(s)} \rightarrow Fe^{2+}_{(aq)} + 2e^{-}$$

The iron ions in solution can then react with cathodically produced hydroxide ions to form an adherent iron (II) hydroxide precipitate on the surface[37].

$$Fe^{2+}_{(aq)} + 2OH^{-}_{(aq)} \rightarrow Fe(OH)_{2\,(s)}$$

This iron (II) oxide forms a barrier layer between the free iron surface and the environment, of which oxygen must diffuse through. However, in the presence of oxygen, this iron (II) hydroxide product can be further oxidised from iron (II) to form iron (III) products, such as iron (III) oxide, hematite, or iron (III) hydroxide, which are the more characteristic compounds noted on rusty surfaces[38].

$$4Fe(OH)_2 + O_2 \rightarrow 2Fe_2O_{3\,(s)} + 4H_2O_{(l)}$$

$$4Fe(OH)_2 + 2H_2O + O_2 \rightarrow 4Fe(OH)_3$$

Whilst there are many different forms of rust that can appear on an iron surface, an oxidising environment will generally result in the production of iron (III) oxide and oxide-hydroxide

hybrids on the surface, with an iron (II) oxide lower layer. However, this is dependent on the impurities present within the environment, which can have an effect on the overall corrosion chemistry of iron. Figure 1.2.5 is an example of a potential-pH diagram for iron.

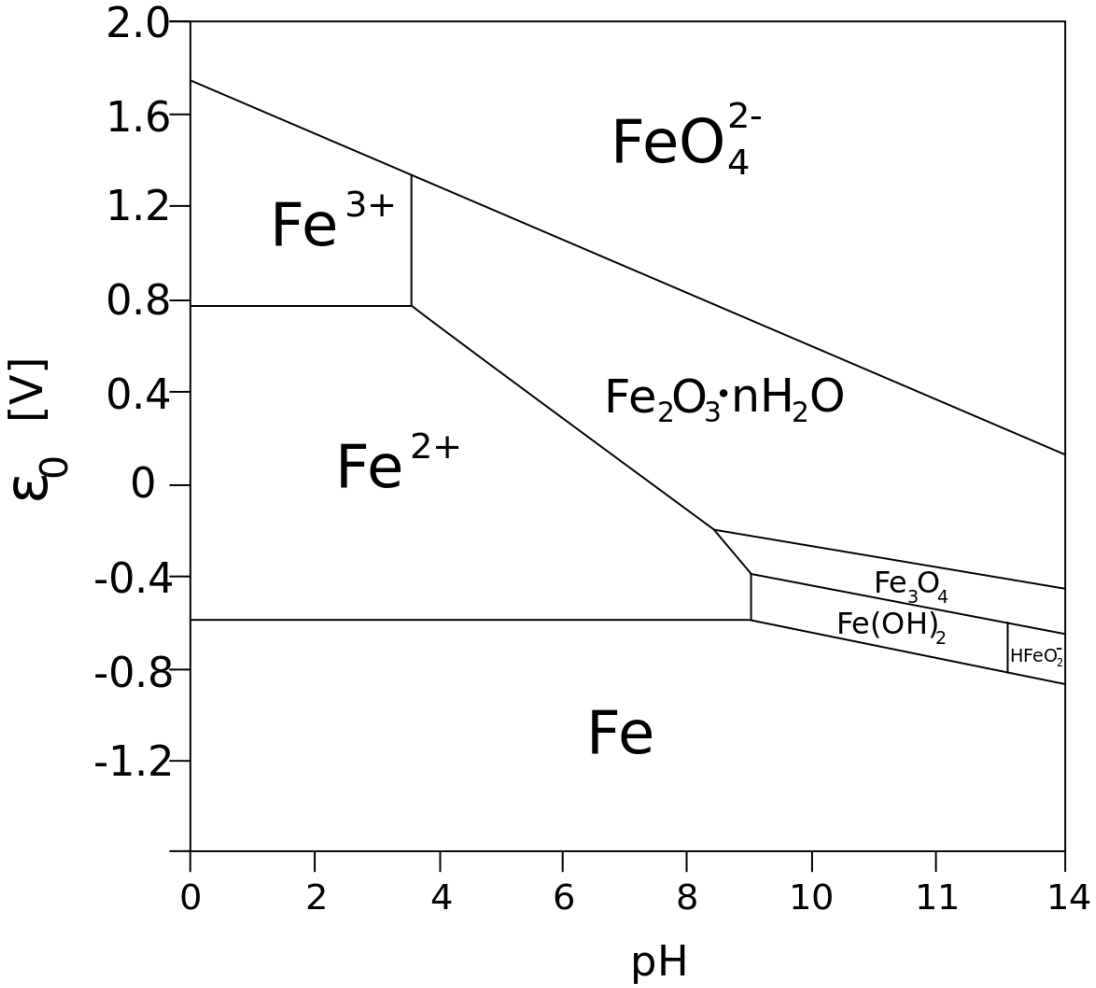

Figure 1.2.5 - A Pourbaix diagram showing the states of iron for different potentials and pH values

Corrosion of Zinc

Zinc is thermodynamically unstable in both pure water and aqueous solutions, meaning that it will dissolve over a wide range of pHs, and tends to evolve hydrogen upon dissolution. Its chemistry is dominated by the divalent form, and therefore the dissolution of zinc can be considered to be as follows[39]:

$$Zn_{(s)} \rightarrow Zn^{2+}_{(aq)} + 2e^{-}$$

Or the aided dissolution using protons in solutions[40]:

$$Zn_{(s)} + 2H^{+}_{(aq)} \rightarrow Zn^{2+}_{(aq)} + H_2$$

Zinc hydroxide, $Zn(OH)_2$, is a commonly formed product of zinc dissolution in aqueous media. It is amphoteric, which means that it is generally soluble in both acidic and alkaline environments. However, there is the possibility for the formation of an adherent zinc hydroxide layer at specific alkaline pHs, generally between 9 and 13, which can be considered protective[39].

Zinc is capable of forming many insoluble compounds with commonly observed chemicals, and can have an effect on the corrosion rate of zinc in various environments. Zinc carbonate, in particular, has been found to be instrumental in the corrosion resistance exhibited by zinc in atmospheric conditions.

$$Zn^{2+} + H_2CO_3 \rightarrow ZnCO_3(s) + 2H^{+}$$

Figure 1.2.6 shows a common example of a potential-pH diagram for zinc. This shows the large potential range where zinc is most stable in solution, and also the range of potentials (mildly alkaline conditions) where solid zinc oxide is the most stable, which is why zinc ions can precipitate at cathodic sites.

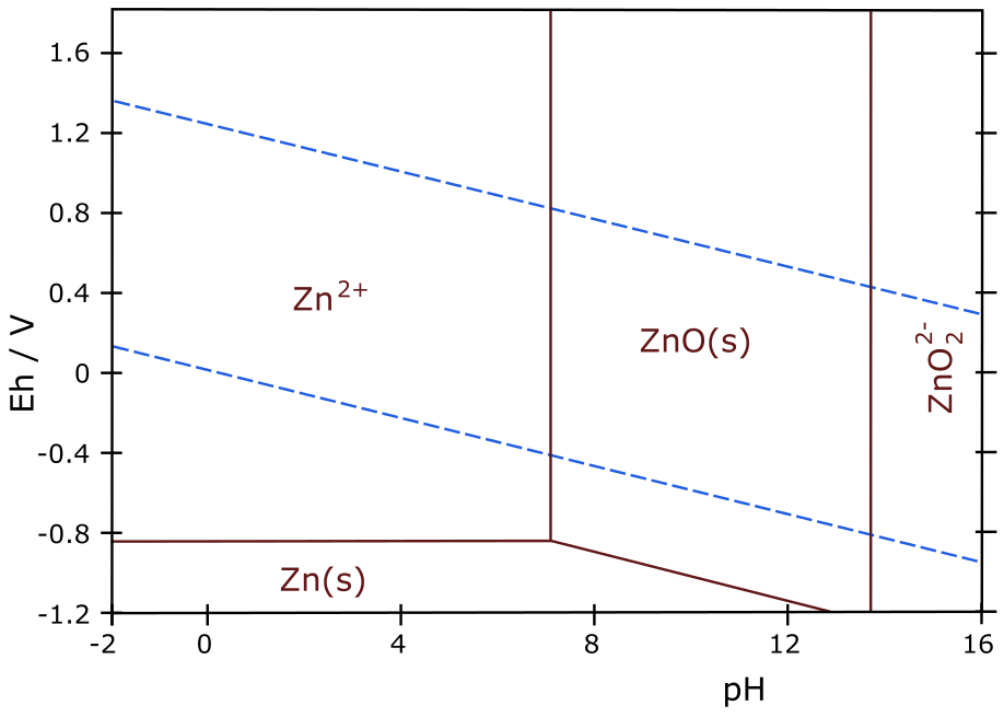

Figure 1.2.6 - A Pourbaix diagram showing the states of zinc for different potentials and pH values

1.3 Cost of Corrosion

Deterioration due to corrosion can lead to a range of problems that range in severity; from aesthetic issues to major structural damage. As such, it is an issue that must be taken into account, particularly when using metals as materials. Certainly, considerable thought has been directed towards quantifying the drain that corrosion has on the economy.

Several reports have been published on the subject of corrosion cost. H.H. Uhlig's report from 1949 on the cost of corrosion in the United States was one of the first to portray the magnitude of the economic impact of corrosion, estimating direct losses due to corrosion at around 5.5 billion dollars[41]. Direct losses refer to the cost that arises from replacement and reconditioning of corroded parts, as well as the cost of using more corrosion resistant materials where the mechanical properties of cheaper materials may be sufficient[41].

Whilst direct losses are considered to be somewhat simple to quantify, they are not responsible for all costs that can be attributed to corrosion. Indeed, there are considerable losses that are a consequence of the material degradation beyond the material itself[42]. These are referred to as indirect losses.

There are several incidents that can account for indirect losses. Whilst significant, these can be difficult to quantify. As a result, reports that take into account indirect losses use estimations for the financial implications of indirect losses. These include lost revenue through equipment downtime during maintenance on corroded parts, losing product through damaged piping or containers, contamination of products with corrosion material that can lead to the need for batch disposal and facility overdesign to deal with unpredictable or unknown corrosion activity in some cases[42].

However, whilst “cost” often has a financial implication, there are other consequences of corrosion that can be considered to be costly but are unable to be financially quantifiable. There is the potential for problems affecting the environment to arise due to corrosion. This can be through the release of dangerous chemicals through damaged components, or the need to remove natural resources to replace corrosion affected parts[43]. The loss of integrity in structure critical components can lead to situations that may result in injury or in some cases death[43].

Following the increased awareness of the issues of corrosion, case studies have been taken to determine the cost of corrosion specifically to certain industries. It has been calculated that the direct cost to the paper and pulp industry in India alone of corrosion is approximately £1.5 million per annum[44], where the application of one particular preventative measure could potentially save nearly 10% of this cost annually.

A case study of an African oil rig showed a similar annual cost due to corrosion, with product deferment, an indirect cost of corrosion, considered to be the largest contributing factor to the overall cost[45]. A study carried out in 2004 on the financial impact of corrosion on the Indian fertilizer market saw an extrapolated annual corrosion cost of just over $900,000. The projected potential savings for this industry was small, and the overall annual cost is lower than the projected costs in a previous study[46]. This suggests that the successful implementation of corrosion preventative strategies can have a noticeable impact on the financial implications of corrosion.

1.4 Introduction to Coil Coating

Coil coating is a pre-painting process that was originally developed in the 1940s by Joseph Hunter as a way of reducing bottlenecks in the production of Venetian blinds[47]. It is capable of producing nominally homogenous coatings consistently. Owing to this, products developed from coil coating lines often boast good visual properties and barrier corrosion resistances. It is performed on coiled metal sheet, which is commonly galvanised steel or aluminium.

Process

Coil coating is described as a continuous process in which an organic coating material is applied on rolled metal strip. This includes cleaning, if necessary, and chemical pre-treatment of the metal surface and either one-side or two-side, single or multiple application of paints of coating powders which are subsequently cured and/or laminated with permanent plastic films.

The process of coil coating a metal substrate contains many parts. Initially, the bare metal, which initially arrives coiled, is uncoiled into the machine. It is then mechanically spliced and joined to the end of the previous coil. It is then run through an accumulator stack ahead of being degreased and cleaned.

The metal then undergoes a chemical pretreatment, often used to provide better adhesion for the primer, or to improve corrosion resistance. Following this, the organic coating is then

applied. This is often done in multiple steps as appropriate for the application, with primer, top coat and lamination all applied and cured separately and as appropriate. It is important to note that due to the speeds that the metals go through this line (the coil is capable of reaching speeds in excess of 3 metres per second), the coatings must be able to be cured at high temperatures for short periods[48].

Following this procedure, the coated metal is then run through an exit accumulator stack before being recoiled and shipped. Figure 1.4.1 shows an example of how a coil coating line may be set up[47].

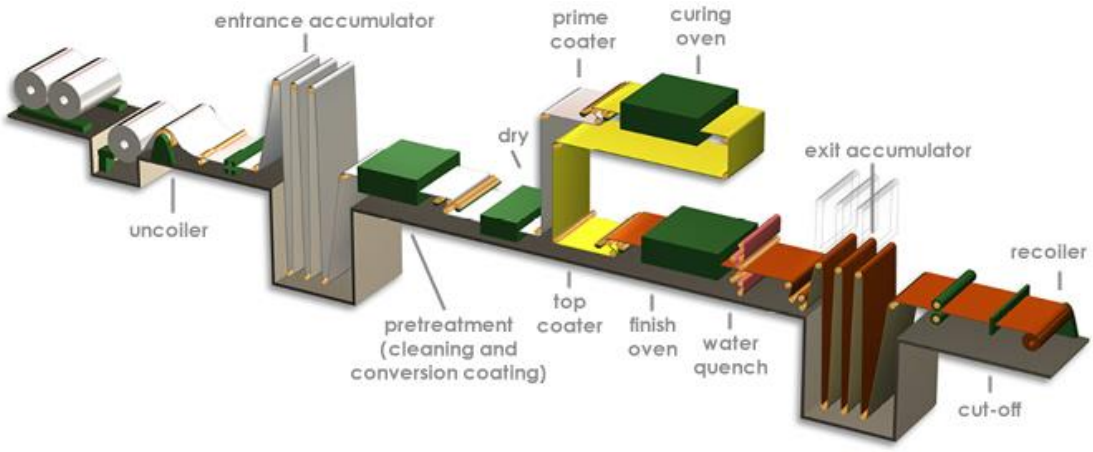

Figure 1.4.1 - A visual representation of a coil coating line[47]

Issues

Changes in and around the coil coating industry, occurring both in the recent past and imminent future, is driving research within the area. Firstly, the galvanized steel substrate that is generally used in the coil coating process has been gradually modified over the course of the last half century. Companies that produce the substrate have been moving away from traditional hot dip galvanised steels and towards more complex zinc alloys that are either cheaper or considered to provide greater corrosion protection.

Secondly, European Union legislations have been introduced that outline the timeframe for a region-wide ban on the use of hexavalent chromium compounds. Chromates are widely used as corrosion inhibitors as they are effective and are capable of working over a wide range of conditions and are commonly used in coil coating formulations.

The combination of these issues is particularly problematic when considering protection at cut edges. The cut edge is an inherent defect within coil coated materials that is produced on the machining of the material into the final product, leading to the exposure of bare substrate. Attack at this vulnerability is known as cut edge corrosion, and is one of the main failure points for coil coated materials in service[49]. Therefore, to extend the lifetime of coil coated materials, cut edges must be sufficiently protected.

The new galvanising coatings can be thinner or less effective at sacrificial protection, whilst the more complicated nature of the microstructure may change local chemistries which chromate replacements rely on for inhibitive action. Therefore, further research into the area is required.

1.5 Corrosion Protection

As previously mentioned, corrosion causes various problems in real world scenarios. The deterioration that it is responsible for can result in issues ranging from purely aesthetic problems, such as the presence of visible red rust, to potentially life-endangering structural damage. It is therefore important to understand some of the methods that can be used in limiting or protecting from corrosion.

Barrier Coatings

One way of protecting a metal is to attempt to isolate it from the environment. A common method of doing this is to coat the metal and produce a barrier between the metallic material and the environment.

Organic Coatings

Organic coatings, or paints, are a widely used commodity in corrosion protection systems. To protect effectively, an organic coating must exhibit a number of properties that combine to make a shielding layer between the underlying metal and the environment. Depending on the application, these properties may include any number of the following: resistance to water and ionic transport, resistance to abrasion, weathering and radiation and good adhesion to the metal surface[50]. In essence, an organic barrier coating is intended to isolate the substrate metal from the environment to prevent the onset of corrosion. However, an organic coating cannot be considered a true barrier to the environment as polymers do allow diffusion of molecular species through them.

Organic coatings, in addition to acting as a barrier, may also incorporate active inhibitor pigments that can act to slow the corrosion process. Corrosion inhibitor pigments are described in more detail in a later section of this report. This allows organic coatings to improve corrosion properties when the barrier is compromised.

Metallic Coatings (Barrier and Sacrificial Protection)

Metallic coatings are also a common way of protecting an underlying material. The coating of a susceptible metal with a thin layer of a metal that is unaffected by the working environment can be a useful way of protecting a metal that is either expensive to replace or structurally important when a viable alternative is unavailable.

A metallic coating may also be capable, if it is more chemically active in a particular environment, of sacrificially protecting the underlying metal if the coating becomes damaged. As previously mentioned, a galvanic corrosion cell is created when electrically connecting two dissimilar metals, leading to the preferential dissolution of the more active metal. Whilst this

can be problematic when occurring unexpectedly[51], by applying the fundamentals of galvanic corrosion, it can also be a useful method of corrosion protection.

Through taking into account the galvanic series, it is generally understood that the metals that with more negative potentials become anodes when forming a galvanic couple with those that are lower in the series. The anodic material will then corrode preferentially, leaving the other material to be free from corrosive attack. In this way, a structure can be protected by attaching a more reactive metal to the surface to form a galvanic couple[51].

An example of a regularly observed sacrificial anode is zinc. Reports of zinc being used for sacrificial protection can be seen in works from as early as the 1800s[52], where it was seen that attaching zinc and copper together was seen to lower the rate of dissolution of copper to undetectable levels. In more recent times, zinc has found common use in protecting steel structures. It has been estimated that around 40% of all zinc produced annually is used to protect steels[53].

Zinc is used as a sacrificial anode due to its high position in the galvanic series, alongside its high anodic efficiency. Anodic efficiency is an important consideration in sacrificial protection, as it determines the current output that is delivered to the cathode when compared to the loss of material (by weight) at the anode over a period of time, as a percentage of the theoretical maximum that the material can provide[53]. The anodic efficiency of zinc is measured at above 90%, whereas other sacrificial anodes such as aluminium (65-90% efficiency) and magnesium (45-55% efficiency) can be significantly lower[53].

Whilst zinc is commonly used as a sacrificial anode, other materials may be more suitable, depending on the final application. For example, cadmium has been used for cathodic protection of steel in military jets, owing to greater anodic lifetime and low activity of

corrosion products. However, the use of cadmium in other applications is limited due to its toxicity[19].

Some work has also been done on increasing the efficiency of sacrificial magnesium anodes for use on underground steels[54]. It is also possible to use carbon steel as a sacrificial anode when connected to copper, with waste steel being utilised to protect copper in marine environments[55]. It is, however, important to note that galvanic protection is not infallible, and cannot protect materials from all forms of corrosive attack. For example, aluminium or lead material that is cathodically protected will still deteriorate due to cathodically produced hydroxide ions causing an alkali environment which dissolves the surface aluminium oxide layer[56].

Electrochemical Protection

Using the same ideas behind protection through the use of sacrificial anodes, protection can be afforded to metals through the direct application of a potential to a metal. As previously seen in the Pourbaix diagram, some metals have areas in which corrosion can be prevented. Knowledge of where these areas are situated within the environment the metal is expected to be exposed to means that there may be a possibility that the metal can be protected[51].

In some cases, a sufficiently negative applied potential can lead to metal immunity. Immunity implies that the metal remains unchanged within the environment. This occurs when the potential of the metal at the surface of the material becomes lower than the potential for the oxidation process[51]. At this point, the oxidation of the metal does not occur and the metal is considered to be thermodynamically stable.

The use of polarisation for cathodic protection requires a counter electrode to act as the anode. This is known as an impressed current anode. In this case, it is useful to use materials that do not take part in anodic dissolution. Examples of inert materials that can be used as

anodes in this way are platinum and graphite. As this does not consume the electrode, another anodic process must occur. An example of this is[12]:

$$2OH^- \rightarrow \frac{1}{2}O_2 + H_2O + 2e^-$$

However, it is not always necessary to use an inert material for protection with impressed current anodes. In some cases, a material that will eventually be consumed is acceptable as an impressed current anode. This occurs when the cost of replacing an expired anode is significantly less than the cost of using an inert anode. The use of scrap steel as an anode to stainless steels to prevent pitting in marine environments is an example of this[56].

Whilst the direct application of a cathodic potential can be useful as a method of protection, there can be some issues that arise. Application of negative overpotentials may lead to significant cathodic activity at the surface. Whilst these are often not directly problematic, the evolution of hydrogen at the surface may encourage hydrogen embrittlement in some materials[57]. There is also the risk of cathodic disbondment of coatings due to increased cathodic activity, which can be problematic in painted samples[58,59].

Alternatively, the application of a sufficiently positive overpotential (anodic polarisation) can lead to passivation. As seen in some areas of some Pourbaix diagrams, this is dependent on both the surrounding environment and particular metal that is being used. Upon passivation with this method, the oxides formed on the metal surface reduce the rate of corrosion[14].

However, sustaining a passive film through anodic polarisation can be dangerous. Slight deviations from the applied potential, or a change in the working environment[60], could result in a shift away from the passivating region, causing severe corrosion to occur as the passive film breaks down.

Corrosion Inhibitors

It is possible to slow the rate of corrosion through the action of certain chemical species when present within the electrolyte. These species are known as corrosion inhibitors, and can be classified as either cathodic or anodic inhibitors, depending on which of these reactions are affected the most.

Cathodic Inhibition

Cathodic inhibitors are species that migrate to the cathodic site and provide coverage, or provide other methods of disrupting cathodic processes.

Positive ions will be attracted to the cathode due to the nature of the surface. In some cases, these ions will react with alkali species that are formed at the cathodic site to form compounds with low solubility. The precipitation of these compounds takes place on the cathode surface and acts as a protective film, limiting the surface area that can take part in cathode reactions[61].

An example of something that can be considered a cathodic inhibitor is cationic zinc. This will interact with the hydroxyl ions produced at the surface to form insoluble zinc hydroxide, which then precipitates and blocks the cathodic sites, resulting in inhibition.

Species can also be added to reduce the rate of the cathodic reaction through other disruptions besides precipitation. An example of the introduction of a species that can disrupt cathodic processes is an oxygen scavenger. An oxygen scavenger is an example of inhibition through environmental modification. Oxygen scavengers work to reduce the concentration of oxygen dissolved within the electrolyte by reacting with it. An example of an oxygen scavenger is hydrazine, which works through the following process[62]:

$$N_2H_4 + O_2 \rightarrow N_2 + 2H_2O$$

The consumption of dissolved oxygen prevents cathodic reactions that rely on the presence of oxygen from taking place, particularly cathodic reduction of oxygen. This reduces anodic activity, and therefore corrosion, by limiting the cathodic reactions that can balance the overall process.

Anodic Inhibition

Anodic inhibition is generally provided by species that aggregate and interact with ions released from the anodic reaction. These species then form insoluble compounds that can form a film on the anode surface. In forming this surface film, the flow of material away from the anodic surface is restricted and thus the rate of anodic dissolution is reduced.

It is considered that the species must be sufficiently oxidising in the particular environment that the material is in to promote surface oxide formation after adsorption to the surface[63]. The presence of oxygen is often required, although strong oxidising agents can promote surface passivation in deaerated solutions. Examples of potential anodic inhibitors include nitrates and silicates[64].

Anodic inhibition can be considered to be fairly dangerous to the material if applied incorrectly. Having an anodic inhibitor that is present in concentrations that are not sufficient to be evenly distributed across the anode surface has the effect of reducing the area of available anodic sites. In these cases, the cathode to anode area ratio becomes unfavourable, causing corrosion to become aggressive at the exposed anodic sites. This generally leads to localised corrosion occurring at the anode[61].

Protection in Coil Coating

Due to the nature of coil coated materials, there must be a multi-faceted approach to corrosion protection. The homogenous nature of the organic coating that is deposited leads to a defect-free organic coating that is generally good as barrier protection. However, as coil

coating is a pre-painting method (i.e. painted before forming into products), product formation must occur after the fact. This can cause inherent defects in the final material.

The cutting of the metal into a workable size is one of the most problematic forming processes. This leads to the inevitable exposure of the substrate to the environment and is known as the cut edge. The cut edge is a site on coil coated materials that is particularly vulnerable to attack by corrosion. As such, coil coated materials must take this into account when considering corrosion protection mechanisms, and is dealt with in a few ways.

Metallic Coatings

One particular method of corrosion protection in coil coated materials is the galvanised layer that is applied to steel substrates before coating. This layer generally comprises of a zinc-based alloy and not only provides an additional barrier layer between the substrate and the environment, but is also capable of providing sacrificial protection at the cut edge, or in the case of general coating damage that exposes the steel.

Process of Galvanising

There are a number of different ways of applying a metallic coating to a substrate. Examples of those that are used for producing zinc and zinc alloys on steel substrates are electroplating, sherardizing, thermal spraying and hot-dipping. For coil coated materials, the substrate is most often hot-dip galvanized.

Hot-dip galvanising is both the oldest and most used process for producing zinc coatings for coil coating, and this is also true generally for zinc coatings[65]. There are two different main methods for hot-dip galvanising, which are batch and continuous processes.

Batch hot-dip galvanising applies a coating to individual parts, and is most applicable when applying metal coatings post-production, or for low quantity work[66]. The size of parts in batch processing is restricted to the size of the available metal bath.

Continuous hot-dip galvanising is more of a large scale process that is applied to wires and sheets, and is more suited to pre-production. A continuous hot dip galvanising line will begin with a cleaning process that removes dirt, oil and other impurities from the substrate surface. There will then be one or several surface preparation steps where the surface is roughened, though processes such as grit-blasting, and chemically fluxed[67]. The substrate will then be immersed into a bath of molten zinc where the zinc coating is attached to the steel. The thickness of this coating is controlled by the use of air knives. The cleaning, pre-treatment and coating processes are done successively in the continuous process. The sheet is then cooled and wound into a coil[65].

Galvanneal

Galvanneal is a zinc-iron alloy coating. It is produced by the heat treatment of an iron or steel substrate that has been galvanized. The heat allows for iron diffusion into the zinc coating to produce the zinc-iron alloy[68]. Therefore the microstructure and properties of the galvanneal coating are determined both by composition of the substrate and by the specifics, the temperature and time exposed, of the heat treatment used[68–70].

Galvanneal was produced to improve coating adhesion to the substrate. It also exhibits greater weldability than other zinc coatings[71]. Galvanneal is also reported to give superior corrosion resistance to coated cold rolled steels[72], although that is unsurprising. A long term SVET experimentation saw a galvanneal coated steel maintain protection for the 12 months that the experiment was run, showing superior corrosion resistance to standard hot dip galvanised material, but with inferior performance to that of the tested zinc-aluminium coatings[73].

Dealloying is reported to occur in some phases present in galvanneal, leaving a porous coating that would lack barrier protection[74]. Galvanneal has also been proven in some environments to not provide adequate corrosion protection. Some tests have observed the presence of red rust, an indication of iron corrosion products and therefore loss of corrosion protection of the

substrate after salt spray tests[71,75]. The presence of red rust is an aesthetic issue that also can affect the galvanneal coating itself due to the iron content, and therefore it is less likely to be used without an organic coating[76]. However, the protective properties of galvanneal have been determined to be superior to that of normal hot dip galvanised materials[73,76,77]

Galfan

Galfan was one of many alloys produced in an effort to improve upon the properties of standard hot dip galvanised steel products. It is a zinc-aluminium binary alloy containing around 5 wt% aluminium, keeping it close to the zinc-aluminium eutectic composition[78], and a small percentage of mischmetal[79]. The mischmetal is a rare earth metal mixture of cerium and lanthanum that is added as it was found to improve fluidity and wettability of the liquid metal, whilst also improving ductility and hindering intergranular corrosion[80,81]. Due to the aluminium content of the Galfan, the formation of iron-zinc intermetallics during the coating of the substrate is supressed and consequently provides the same benefits to adhesion and formability as mentioned previously for minor aluminium additions in the galvanised steel section.

It is difficult to give a definitive microstructure for Galfan as the quoted aluminium weight percentages are variable. It has been reported that Galfan has a microstructure that contains a percentage volume of primary zinc dendrites of around 14%, regardless of cooling rate[82,83]. However, it is suspected that the structure and volume of zinc dendrites can be changed by processing conditions[84]. Furthermore, there have been reports that the surface of the coating is enriched in aluminium, allowing the coating to passivate and improve barrier properties[85,86]. Whilst this claim is disputed[87], it seems likely that it is the case.

Zhang et al[88] have reported that the atmospheric corrosion products present on the Galfan surface contain both zinc and aluminium, such as $Zn_2Al(OH)_6Cl.H_2O$, alongside some products

seen on surface of hot dip galvanised steels. It is also suggested that all aluminium oxide is eventually converted into aluminium-zinc products.

The volume fraction of primary zinc dendrites is reported to have an effect on the corrosion rate of the coating[84]. The cut edge corrosion performance of Galfan coating has been reported to be dependent on the microstructure produced. Barnard and Brown [89] modelled the corrosion rate of Galfan with various cooling rates and determined that faster cooling rate produced a coating with a finer zinc dendrite structure which consequently improved cut edge corrosion. Corrosion of Galfan is reported to initiate through the dissolution of primary zinc phases[90], which supports the previously mentioned hypothesis that the corrosion rate of Galfan is dependent on the volume fraction of zinc dendrites.

Galvalume

Galvalume is a zinc-aluminium alloy containing 55 wt% aluminium and 1.6 wt% silicon developed in the 1970s[91]. The silicon is added to suppress an exothermic reaction between the molten bath and the substrate surface[92] which if left unsuppressed is capable of quickly consuming the substrate.

The microstructure of Galvalume is considered to consist of dendritic areas, which are aluminium dendrites containing zinc rich particles, and interdendritic areas that have small amounts of silicon dispersed within. The interdendritic areas are considered to be aluminium containing zinc and zinc containing aluminium[93].

Galvalume is reported to corrode in chloride containing environments mainly through the zinc-rich constituents of the microstructure, with aluminium corrosion occurring at a low percentage of corrosion activity throughout[94]. This happens as the aluminium oxide surface layer is broken down and replaced with zinc corrosion products. Similarly, McMurray[95] has shown that Galvalume, unlike Galfan, is susceptible to preferential dissolution in some circumstances, with corrosive attack concentrated on zinc-rich phases in the material. It is

theorized that this results in the local enrichment of aluminium which in turn can passivate the area.

However, the corrosion of aluminium can be initiated by the application of a potential to the Galvalume structure[96]. The presence of aluminium in Galvalume is reported to prevent cathodic protection in environments containing low chloride concentrations, which is explained through the presence of an aluminium oxide passivating layer on the surface[97].

Seré et al used[98] compared the corrosion performance of Galvalume coated steel to hot dip galvanized with salt spray, humidity and immersion testing, analysed by observing the corroded area of the material. It was determined that Galvalume showed superior corrosion resistance across all tests. However, weight loss experiments performed by Domínguez-Crespo et al[99] have shown that Galvalume gave worse performance than hot dip galvanised samples when immersed in a sodium chloride solution. Microscopic observation from these tests showed that the corrosion that occurred on the Galvalume was more uniform in nature, and can therefore be considered to be a more controlled corrosion process.

Zinc Magnesium Aluminium Ternary Alloys

A variety of alloys have been produced which introduce both magnesium and aluminium into the zinc coating. Zinc-aluminium-magnesium alloys exhibit a complex microstructure that includes zinc dendrites along with binary and ternary eutectics[58,100–102]. A variety of zinc-magnesium-aluminium alloy compositions are used in industry. There have been some reports that zinc magnesium aluminium alloys are prone to corrosion through dealloying, with the $ZnMg_2$ intermetallic phase dissolving preferentially from the alloy[34,101]. However, an alternative report suggests that initial corrosion attack is instead concentrated close to eutectic phases or close to grain boundaries of primary zinc phases[34], but is otherwise not selective in actual dissolution of phases. The mechanism and site of corrosion initiation is therefore likely to be dependent on the microstructure.

Whilst a general representation of the complex microstructure has been given, the overall organization of the microstructure is different between compositions[75]. The corrosion resistance of the ternary alloys is reported to be superior to that of galvanised steel, regardless of the microstructure. However, as the analysis using 5% red rust time seems like it would be open to interpretation, the overall improvement relative to the original galvanised measurements may not be entirely accurate. It has been reported that zinc-magnesium-aluminium alloys perform better in salt spray than equivalent zinc systems, with no signs of iron oxide corrosion product (red rust) present on the ternary alloy after 600 hours whilst hot dip galvanised coatings show red rusting after just 100 hours[100].

The presence of magnesium within the alloy composition is suggested to make noticeable differences to both the properties of the material and the corrosion products. Zinc oxide based corrosion products are reported to be present at the surface of both hot dip galvanised coatings and Galfan coatings. However, the addition of magnesium to create ternary alloys suppresses the oxidisation of zinc to leave the surface oxides to consist entirely of aluminium and magnesium oxides[103]. This claim is disputed in chloride environments, where XPS measurements have determined that the initial corrosion products consist mainly of a zinc aluminium carbonate hydroxide compound[104]. With this claim, it can be seen that magnesium does not appear to interact with the chloride in the environment.

Chloride is not the only factor that affects the corrosion products of zinc-magnesium-aluminium alloys. The concentration of CO_2 has been reported to have a considerable effect on the corrosion rate of zinc-magnesium-aluminium ternary alloys. The corrosion products found on the surface in conditions with low CO_2 levels were seen to be different to that of CO_2 levels in ambient conditions. It was also seen that in levels of CO_2 found in ambient air, the corrosion products for the ternary alloy were the same as for hot dip galvanised steel[93]. The rate of

corrosion was also notably different for the ternary alloys in low CO_2 concentrations, corroding at a rate approximately 12 times quicker than in normal concentrations.

The microhardness of the coatings is also increased by the addition of magnesium. It has been suggested that due to this increase in hardness of the coating, the resultant material cannot be formed without the development of cracks across the surface. However, despite this, testing has revealed that zinc-magnesium-aluminium ternary alloys provide superior corrosion resistance after forming even with the presence of surface cracking[105].

Corrosion Inhibitors

Chromate

Inhibitors based on hexavalent chromium are commonly used in the coil coating industry. Chromate inhibitors are considered to work well over a large pH range and in the presence of many aggressive species, such as chlorides[106]. They are also noted for the protection that they can afford both the anodic and cathodic surfaces, working on a wide range of substrates[106]. This is because at high concentrations, chromates act as oxidising agents and passivate the surface. At low concentrations, the reduction of chromium (VI) to chromium (III) occurs at the cathodic sites and leads to precipitation which then blocks the site.

The ability to work over a large pH range is down to its solubility over the range, although the actual level of solubility of some chromates (strontium chromate, for example) can be both fairly low, and pH dependant[107,108]. This means that chromates present in the pigment of an organic coating can leach out into the surrounding electrolyte by dissolution[107,108].

The mechanisms of inhibition and paint leaching for chromate species have long been studied and debated. Prosek and Thierry[109] observed the leaching rate for chromates from model primers across a range of different conditions and electrolytes by ion chromatography on

washing to determine the mechanism of release. It was found that the rate of leaching was increased by pH and the presence of chloride ions.

The development of chromate films on steel surfaces was observed through the use of radioactive chromium isotopes. Firstly, the presence of chromium was detected by Brasher[110], who noted the time and pH dependant growth of chromate films on mild steel. Longer immersion times and lower electrolyte pH was noted to improve film growth, whilst chromate concentration was suggested to be ultimately not important to the process. Kubaschewski[111] then proceeded to explain the mechanism as the reduction of chromium (VI) oxides to insoluble chromium (III) oxides at the surface, noted by the film growth rate being limited by the rate of through-film electron transfer.

Clark and McCreery[112] used voltamperometry to explore the mechanism of chromate inhibition on various electrodes. It was determined that the reduction of chromium (IV) to an insoluble chromium (III) monolayer on the electrode surface prevented oxygen chemisorption and prevented the oxygen reduction reaction from taking place. The non-conductive nature of this film also prevents electron transfer through the film and therefore electrochemical reactions cannot take place on the film surface. This theory fits well with the similar findings of other published research[27,107,113,114]

The process in which chromates provide anodic protection is rather less understood. One possible theory is that the reduction of chromium (VI) into insoluble chromium hydroxide ($Cr(OH)_3$) leads to a local increase in pH through either the consumption of hydrogen ions[114] or evolution of hydroxide ions[108]. As a consequence of the reduced pH brought about by the mechanism of chromate inhibition, the ions from anodic dissolution result in insoluble hydroxide products, which are then capable of anodic coverage, resulting in corrosion

inhibition at both the anode and cathode. It is thought that this is possible with zinc anodes[115].

Alternate theories suggest that chromates can act as anodic inhibitors through the same film formation as with cathodic inhibition; however this is only effective at inhibiting the initiation of anodic sites, as opposed to anodic propagation[27]. Prior thoughts on the inhibition of anodic processes by chromates suggested that the formation of chromate films reduced corrosion as it prevented the diffusion of ions away from the anodic site[116].

Formulations containing hexavalent chromium, however, are being phased out. This is due to the inherent health risks, such as carcinogenicity, associated with the handling of those compounds[117]. European legislations have previously placed strong restrictions on the use of hexavalent chromium, particularly in electronics. A sunset date of September 2017 has been given for the use of hexavalent chromium compounds across all applications (REACH Annex XIV-3, Dec 2011). Therefore, effective alternatives for chromate based inhibitors are being sought.

Chromate Replacements

The main issue that is facing the industry for replacing chromate inhibitors is the flexibility of chromates. Chromates act as inhibitors on various metal surfaces, over a range of pHs and are capable of working in both aerated and deaerated conditions[106]. Whilst this flexibility is difficult to replicate without the use of several inhibitors working synergistically, taking into consideration the working environment and particular chemistry of the eventual application allows for some non-chromate inhibitors to be effective.

Phosphates are being considered as a potential replacement for chromates. Naderi and Attar[118] have demonstrated using scanning electron microscopy the presence of a precipitated layer containing phosphates on the surface of steels following exposure to a polyphosphate inhibitor, which is not present after exposure to zinc phosphate. This study

concluded that the inhibition of iron by polyphosphates was much superior to that of monophosphate inhibitors. It was found the polarisation resistance and corrosion current density of monophosphates deviated little from that of blank solutions. This is in good agreement with Bastos et al[119] which also found that the corrosion rate of iron in phosphate inhibited solutions did not differ significantly from the blank solutions until longer exposure times.

It can be suggested that this is the case for phosphate inhibition of iron, however, Simões et al[120] have suggested and observed that the presence of zinc ions, from anodic zinc dissolution, in a solution containing sodium phosphate can result in the precipitation of phosphate at the zinc surface, due to the formation of near-insoluble zinc phosphate. On cut edges, zinc ions would be present mainly around the anode, so precipitation would be seen mainly at the anode site. This precipitate would have the effect of reducing both the current flow and ability for zinc to diffuse away from the surface[120]. However, as zinc diffusion is not completely blocked, over time, zinc ions can migrate to the cathode surface and the presence of phosphates can produce a similar effect[120]. The inhibition efficiency of phosphates also improves with the presence of calcium ions, which has resulted in the use of combined inhibitor systems with phosphate and calcium containing pigments providing synergistic effects[121].

Additionally, Sullivan et al[122] used time-lapse microscopy and scanning vibrating electrode technique to observe the corrosion mechanism of zinc magnesium aluminium alloys. It was seen that the addition of small amounts of sodium phosphate was sufficient to reduce the corrosion of the system significantly, with SVET suggesting an approximate 98% reduction in mass loss, and the shift of the free corrosion potential as observed through polarisation to less negative potentials.

Some success has been had with the introduction of organosilanes. It was proposed that the silane molecules bind to the metal surface, allowing them to form protective cross-linked layers[123]. Some organosilane applications have been reported to exhibit superior corrosion resistance than that of chromate inhibited samples when used in tests containing drying cycles[124]. However, the omission of product line material in this particular test where silanes show better performance is of some concern and could make the results shown in that particular paper questionable. It has also been reported that in-paint tests of a phosphosilicate inhibitor system have shown success with performances comparative to the chromate system tested[125].

Benzotriazole has been considered as an organic replacement for chromate. Research carried out on benzotriazole[126] discovered that it was capable of inhibition on both anodic and cathodic processes, although this was at significantly increased levels of inhibitor than would be realistically possible in a real world scenario.

Alternatives have been researched using ion-exchange as a way of introducing inhibitors. Organic coatings containing yttrium have been used for coating on zinc surfaces where, upon dissolution of the zinc, the yttrium is released and the zinc is captured in the resultant vacancy in the paint matrix. Yttrium then diffuses to the cathodic site where it coats the surface with insoluble hydroxides[127]. This method is reportedly useful in systems where differential aeration pushes one side of the metallic coating anodic to the other.

The use of bentonite clays as a corrosion inhibitor for coil coated materials, particularly on the cut edge, has been researched. In these works, bentonite matrices are produced and modified to change the normal metal cation with others. It was reported that rare earth metals are particularly effective at inhibiting corrosion[128], although the natural composition bentonites also provide corrosion protection close to that of the chromate system that was tested[129].

Molybdates have been proposed as chromate inhibitor replacements. Robertson[130] proposed both molybdates and tungstates as general replacements for chromates in certain applications due to their non-oxidising nature, although this nature has been disputed to claim that they are more accurately mildly oxidising inhibitors[63,131].

Zinc molyphosphate, an industrial non-chromate inhibitor pigment used in the coil coating industry is considered to be a combination of zinc phosphate and molybdate[132]. However, zinc molyphosphate is shown to, when utilised in a common system which also contains calcium ion-exchange inhibitor, and applied to aluminium alloys, that the inhibitor action is mainly composed of phosphates. Therefore, the molybdate part of this inhibitor can be considered a passive part of the inhibition process[133]. Indeed, the usefulness of molybdates as a chromate-replacement inhibitor has been reported to be predominantly as a synergistic part of an overall system[134].

The improved performance of molybdate inhibitors by the presence of zinc cations has been shown by Qian and Turgoose[135], confirmed through the use of weight loss experiments and DC polarisation. The prediction of the production of a porous film at the surface appears to be entirely speculation, however, and should have been confirmed with further analytical techniques such as scanning electron microscopy. The mechanism of inhibition proposed by Monticelli et al[136] suggests that molybdates work through the reinforcement of the oxide film at the metal surface, with additional chemisorption that prevents the ingress of chloride ions to the surface.

Factors Affecting Cut Edge Corrosion

As previously mentioned, corrosion at the cut edge is one of the major points of failure for coil coated materials. There are various factors that can affect how cut edge corrosion proceeds.

The thickness of the metallic coating effects corrosion on the cut edge. Lowering the thickness of the metallic coating leads to a less favourable anode to cathode area ratio, which is already

a concern for corrosion on the cut edge[137]. Similarly, it has been shown that increasing the steel thickness results in an increase of rate of dissolution of the metallic coating[138]. The thickness of coating is also reported to affect the microstructure in Galfan coatings, which also causes differences in corrosion rates[139].

Cut edge corrosion can be affected by the presence of an organic coating. Restrictions placed on the diffusion of ions by the coating can change the mechanism of dissolution from cathodic protection of the steel, to differential aeration between the two sides of metallic coating.

In some applications of coil coated steels, the organic coating is applied at different thicknesses on either side. It has been reported that in this case, as the diffusion of oxygen is less restricted on the thinner coating side, the metallic coating underneath becomes cathodic to the metal coating on the other side. This leads to strong anodic activity occurring, leading to dissolution of one coating side over the other[140]. A similar effect has been reported to take place in the case of two coatings of equal thickness that are cured to different extents, owing to a similar mechanism[141].

The composition and microstructure of the protective metallic coating has also been reported to have a noticeable effect on cut edge corrosion. Upon addition of small amounts of magnesium, the microstructure of Galfan was noted to become increasingly heterogeneous. The heterogeneity is reported to have an effect on the particular site of anodic activity, as dissolution of the zinc phases in heterogeneous microstructures leads to localised corrosion of those phases[142].

1.6 Corrosion Analysis

Gaining an understanding of corrosion processes and behaviours is fundamental to determining suitable materials and additives for particular applications and environments. In this section, an overview of some of the common laboratory and field techniques used to analyse corrosion behaviour will be looked at, touching upon basic theory and some relevant

historical literature, paying particular attention to the techniques used within the experimental sections of this thesis.

1.6.1 Electrochemical Methods

Zero Resistance Amperometry

Zero resistance amperometry refers to the use of a zero resistance ammeter (ZRA) to determine the galvanic current flowing between two metals. By electrically isolating the two metals, and forming a galvanic contact that forces the current flow through a ZRA, the galvanic current of that metallic couple can be measured. The main use of this is to determine the corrosion rate of the system. The relationship between current and corrosion rate can be shown through derivation of Faraday's law of electrolysis. Faraday's law of electrolysis is given by the equation $Q = zFM$, where Q is the charge produced upon ionising *z* moles of material. Taking the derivative of this equation with respect to time, considering that z and F are constant, produces the equation $\frac{dQ}{dt} = zF\frac{dM}{dt}$. Considering that $\frac{dQ}{dt}$ is equivalent to current and $\frac{dM}{dt}$ is equivalent to the flux of substance, the equation can be re-written as $I = zFJ$. Thus, it can be considered that $I \propto J$ and as such the galvanic current is a direct representation of the corrosion rate[3].

Ammeters generally calculate current through the conversion of measured voltage that has been subject to a known resistance through the equation $V = IR$. However, this becomes problematic when dealing with low magnitude currents, such as those that are observed in galvanic couples, as the required resistor becomes large and therefore the voltage drop will interfere with the electrode potential. This necessitates the use of a zero resistance ammeter.

Zero resistance ammeters work by applying a potential across the resistor that is equivalent to the voltage drop from the resistor. By doing this, it can be suggested that any additional voltage measured within the equipment should be as a result of the electrochemical system,

and thus the current can be determined accurately. An example of the circuit diagram for a zero resistance ammeter is given in Figure 1.6.1[143].

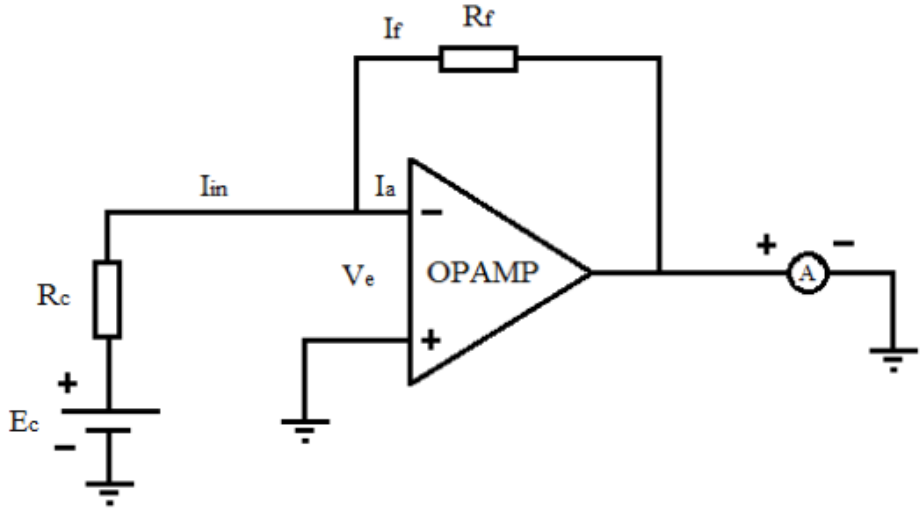

Figure 1.6.1 - An example diagram showing the circuitry contained within a zero resistance ammeter

There is historical literature which reports the use of zero resistance amperometry in analysing the corrosion behaviour of the cut edges of coil coated steels. In order to determine the corrosion current of a cut edge, distinct metals have been electrically isolated, and mounted to be geometrically similar to the configuration seen in a real world cut edge[132,144]. Howard et al[144] used zero resistance amperometry to follow the galvanic current between steel and zinc using this model electrochemical cell with a range of inhibitors to determine the efficiency of each inhibitor. Similarly, Chiba et al[145] observed the change in current of a model cut edge with isolated Galvalume coating during the wet components of a wet-dry-wet corrosion test cycle to follow and determine the effectiveness of chromate inhibition.

Zero resistance amperometry can also been used to study the effectiveness of metallic coating protection. Li et al[91] used zero resistance amperometry to ascertain the galvanic coupling currents galvanising coatings and steel, where it could be seen that zinc coating provides superior sacrificial protection to the two aluminium-containing coatings that were also studied.

The use of zero resistance ammeters has also been seen in the production and validation of models. Jia et al [146] utilised a ZRA array to determine corrosion current density across a range of materials. This was designed to view the effects of separation and electrode areas on the galvanic coupling of steel and magnesium alloys, which produced results that appeared to fit well with the model.

Potentiodynamics

A common and potentially powerful method of analysing electrochemical systems is through the use of potentiodynamics. A potentiodynamic experiment uses a potentiostat apply a linearly-shifting potential to the system, observing and measuring the resultant current. Analysis of the profile obtained of the potential versus the resultant current can give information on elements of a particular system, such as the corrosion potential and any areas of passivation[147].

A number of different processes can be present in a polarisation curve, which is often displayed as a semi-log graph depicting the log of the current against the potential, depending on the particular system being observed, and the direction of the polarisation. Polarisation tends to be driven either cathodically or anodically from a point that is approximately at the open circuit potential of the system so as to gain an understanding of that particular process. Depending on which direction the polarisation is driven, the processes that are evident in these curves are different in each case.

For cathodic region polarisation, an initial drop to zero current is observed at the open circuit potential. This is generally followed by a steady current increase as cathodic reactions begin to occur on the metal surface. The first of these is generally the oxygen reduction reaction. The oxygen reduction reaction is a diffusion limited process, and is therefore kinetically controlled. This means that current flow seen by the system from this reaction will become limited at a point of maximum diffusion rate, seen in the polarisation curve as a current plateau,

independent of the increase in thermodynamic driving force. Further cathodic polarisation will then activate a second reduction reaction which evolves hydrogen at the metal surface.

For polarisations exploring the anodic region, starting at slightly cathodic of the open circuit potential, initially the drop to zero current is seen for the open circuit potential, as in the cathodic polarisation. A steady increase of current is observed as anodic processes begin to occur at the metal surface. This is usually, for non-inert anodes, a metal oxidation process, commonly metal dissolution. With some materials and environments, with further anodic polarisation a current drop can be observed. This is associated with a surface passivation and the production of an adherent metal compound, often oxides, which slow the anodic process. Further anodic polarisation may lead to the breakdown of this passivating layer, and a subsequent sharp increase in the current observed.

The importance of potentiodynamic polarisation to corrosion studies cannot be overstated, and as such, several papers have been published outlining both the uses and particular methods of analysing polarisation curves[147–150].

The use of polarisation to study inhibition mechanisms is well documented. By analysing the shifts in both corrosion potential and current density, the effectiveness and mechanism of an inhibitor can be determined. For example, Baghni et al[115] demonstrated the effects of chromate on the corrosion of steel, showing it to be predominantly cathodically inhibiting through the depression of the corrosion potential and reduction of the current demand. Similarly, Zin et al[151] used polarisation experiments to compare the inhibitor profiles of strontium chromate with various chromate replacement inhibitors and determined similar characteristics for the Shieldex/Actirox mixture when compared to strontium chromate inhibition.

Whilst the understanding of the corrosion behaviour of a system requires more information that can be obtained from merely a polarisation curve alone, they can be used to compare the behaviour of different systems with a reasonable degree of accuracy.

Electrochemical Impedance

Introduction and Basics

An important technique that is used in the investigation of electrochemical reactions is electrochemical impedance spectroscopy (EIS). EIS uses the application of alternating current (AC) to determine the nature of the electrochemical system at the surface of an electrode. Indeed, impedance is the AC analogue of resistance. As such, impedance can be considered to have both a magnitude and a phase.

To understand how impedance spectra can be utilised, the relationships between certain components and impedance values must be known. For a pure resistor, impedance is entirely real and can then be considered to be equivalent to the resistance, R. For a pure capacitor, the impedance is non-real, and the oscillation must be taken into account. For a system with an alternating current, the voltage can be represented by the following equation

$$V = V_1 e^{i\omega t} \text{ where } e^{i\omega t} = \cos \omega t + i \sin \omega t$$

As previously mentioned, impedance is the alternating current equivalent of resistance, and thus can be dictated by the same equations:

$$Z = \frac{V}{I} = \frac{V_1 e^{i\omega t}}{i\omega C V_1 e^{i\omega t}} = -\frac{1}{i\omega C}$$

For a basic system containing a resistor and capacitor in parallel, the overall impedance is the summation of the reciprocal of admittances for both resistors and capacitors. Admittance is the inverse of impedance and can therefore be represented by the following equation:

$$Y_{tot} = \frac{1}{Z_{tot}}$$

Therefore the overall admittance can be given by the following equation:

$$Y_{tot} = Y_R + Y_C \equiv \frac{1}{R} + i\omega C$$

Rearranging the equation that relates current and voltage to impedance can be manipulated to incorporate the admittance as follows:

$$I = \frac{V}{Z_{tot}} \equiv VY_{tot} = V_1 e^{i\omega t}\left(\frac{1 + i\omega CR}{R}\right)$$

$$I \equiv \left(\frac{V}{|Z|}\right) e^{i(\omega t + \propto)} \quad |Z| = \frac{\left(1+\omega^2 C^2 R^2\right)^{\frac{1}{2}}}{\omega C} \quad \propto = \tan^{-1}\frac{1}{\omega CR}\,[152]$$

As a result of manipulation of the complex parts of the equations mentioned above, it can be shown that through fitting data and calculating values for |Z| and the phase angle, α, both R and C can be estimated. To do this effectively, it is important to calculate impedances over a range of frequencies. However, taking consideration of the range of frequencies used is important, as higher frequencies are more likely to contain artefacts, whereas lower frequencies are much more prone to drift and longer term instabilities in the system being measured[152].

Ultimately, it is through these calculations that electrochemical impedance becomes useful. By producing a circuit that is comprised of elements that in effect model the behaviour of the system, the mechanisms can be elucidated and changes in behaviour over time modelled and quantified.

Equivalent Circuit Elements

Combining knowledge of how a system is expected to behave with an equivalent circuit that is similar to the actual behaviour of the system allows mechanistic information of the system to

be retrieved through analysis of the electrochemical impedance spectrum. Each component of an equivalent circuit can be used to model certain behaviours of an electrochemically active system. The following section will briefly explain common elements, and the potential real world implications of including these components within equivalent circuits.

Resistor

In electronics, resistors are devices in which the current flowing is lowered with respect to the applied voltage, and is visually represented in a circuit by the symbol shown in Figure 1.6.2. The equation that represents the effect of a resistor is $I_0 = \frac{V_0}{R_0}$. Due to this, the resistor will have a direct and proportional influence on the current within the system.

Figure 1.6.2 – The equivalent circuit representation of a resistor

Resistors are used to simulate behaviours of processes that are purely resistive in nature, and would respond similarly when subjected to a direct current. Equivalent circuits representations of systems containing coatings or deposited films will normally include resistors. Additionally, solutions themselves also have an inherent resistance which, in most cases, will be represented in the equivalent circuit by a resistor.

Capacitor

A capacitor is an electronic device in which charge is stored following the application of a voltage over time. Current that flows from a capacitor is represented by the equation $I = \frac{dQ}{dt} = \frac{CdV}{dt}$. Consequently, current flow through a capacitor can be considered to be dependent on both the application time and intensity of a voltage.

Figure 1.6.3 - The equivalent circuit representation of a capacitor

Capacitors are a commonly seen element in equivalent circuits developed for analysis of electrochemical impedance spectroscopy, and can be considered to be one of the basic building blocks of equivalent circuits alongside resistors. Elements that are commonly seen in real systems that are capacitive in nature include coatings, which have a degree of capacitance, and the interfacial double layer seen at the surface of electrodes in electrolyte.

Constant Phase Element

In many real situations, the exhibited behaviour of an electrode deviates from standard models that contain resistors and capacitors. Constant phase elements are often used in place of capacitors to ensure that d.c. conductivity is still directly readable. This has been determined to fit well with experimental data and thus is generally considered to be accurate. Constant phase elements are generally characterised through the presence of a depressed semi-circle in the spectrum. A common explanation behind constant phase element behaviour is that of heterogeneity on the surface. This heterogeneity can arise from surface roughness or through other effects, such as ion motion[153], that can cause variation in the capacitive behaviour across the area of the surface. This has been tested by Jorcin et al[154] who used a combination of global and local electrochemical impedance to determine that constant phase element behaviour is due to local variations in resistance.

Warburg Element

The Warburg element is a specific type of constant phase element that models near-infinite linear diffusion of the bulk electrolyte. It is represented by the symbol W in an equivalent

circuit. The presence of a Warburg element is most often characterised by the presence of a linear increase of Z’ vs. Z’’ at progressing at approximately 45˚. This can be seen in Figure 1.6.4. It is most often seen at lower frequencies as this is when diffusion processes begin to become dominant over charge transfer processes.

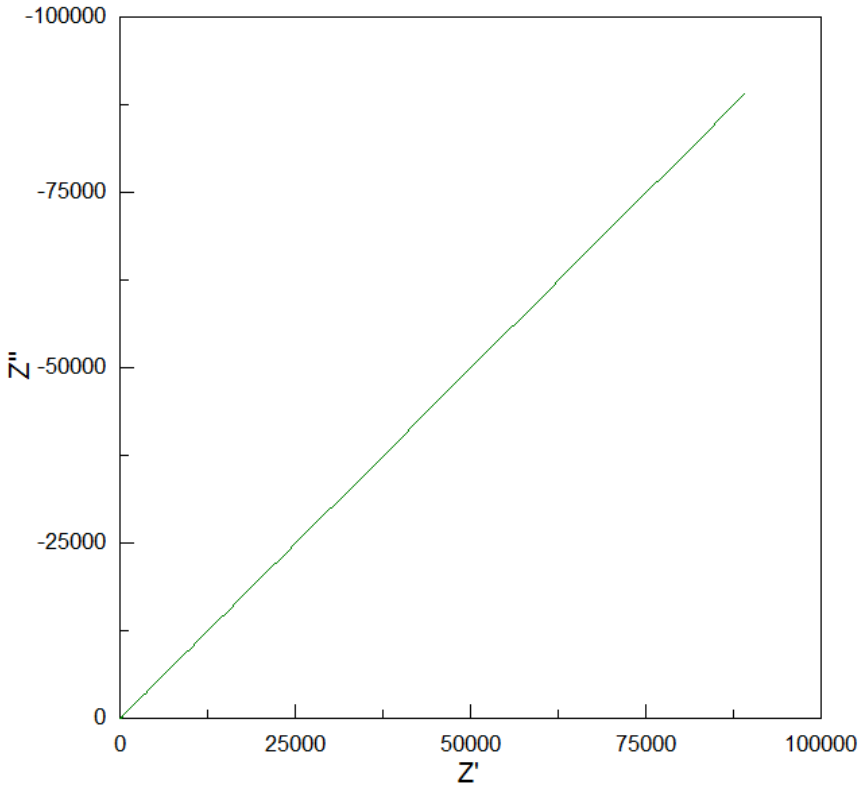

Figure 1.6.4 - A Nyquist plot showin the distinctive appearance of a Warburg element at high frequencies

Inductor

An inductor is generally used to model the effects of adsorbed surface species and their effects on the measured current densities through nature of potentially providing electrons to, or taking electrons from, the electrode surface. The impedance of an inductor increases with increasing frequency, and in this way appears as the opposite of a capacitor. The symbol for an inductor is given in Figure 1.6.5

Figure 1.6.5 - The equivalent circuit representation of an inductor

Randles Circuit

A Randles circuit is an equivalent circuit that was proposed by John Edward Brough Randles[155] and became a common starting point for fitting of EIS data. It consists of a resistor representing the resistance of the solution that is connected in series with a parallel arrangement of a capacitor representing the double layer capacitance in the solution and a resistor representing the charge transfer resistance attached in series with a Warburg element. This arrangement is visually shown in Figure 1.6.6.

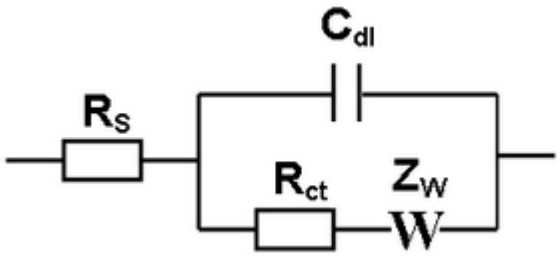

Figure 1.6.6 – A circuit diagram representation for a Randles Circuit

This arrangement is typical of a bare metal in a solution and is therefore frequently observed in many electrochemical systems.

Electrochemical Impedance of Coatings

In theory, an ideal coating is entirely capacitive in nature and can be represented by a resistor and capacitor in series. However, it can be stated that most coatings are realistically imperfect. Thus, a more complicated circuit diagram must be used, which is shown in Figure 1.6.7.

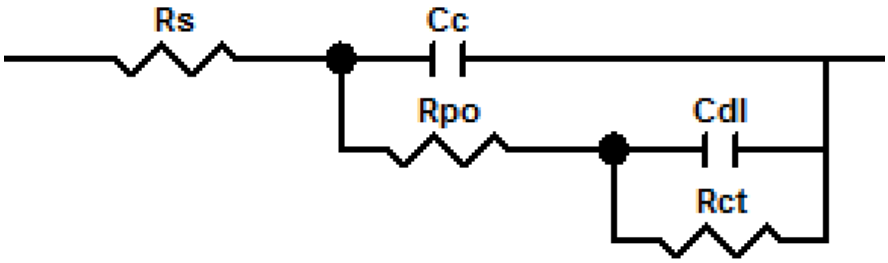

Figure 1.6.7 - Basic electrochemical circuit for an imperfect coating. The physical interpretation of the circuit is as follows: Rs – solution resistance, Cc – coating capacitance, Rpo – pore resistance, Cdl – double layer capacitance, Rct – charge transfer resistance

Using this electrochemical circuit, in cases where the coating capacitance is very large, the obtained impedance spectrum is similar to that of the perfect coating case. However, as the coating fails, two discernible effects can be seen on the values generally obtained. A drop in the coating capacitance is indicative of a reduction in the ability of the coating to shield the underlying substrate from the environment. Additionally, as the electrolyte of the environment ingresses into the coating, the pores within will expand and a resultant drop in the pore resistance will also be observed.

Figure 1.6.8 shows the effect of decreasing the coating capacitance. It can be seen that the second time constant arising from the charge transfer resistance and double layer capacitance segment of the equivalent circuit becomes more easily discernible as the coating capacitance reduces. Figure 1.6.9 shows the effect of decreasing the pore resistance. As the pore resistance drops, the magnitude of the semi-circle representing the first time constant can be seen to reduce in magnitude.

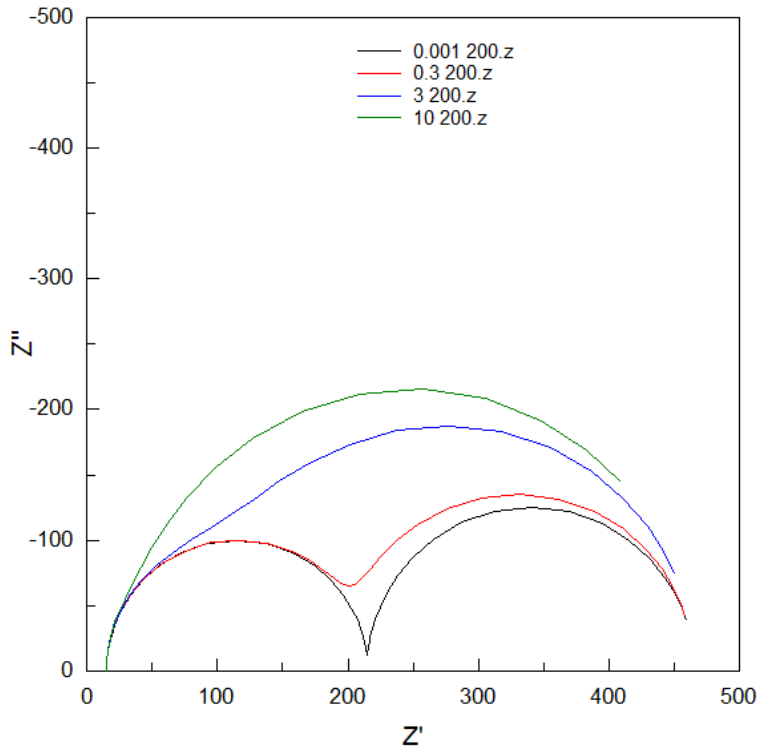

Figure 1.6.8 - A series of Nyquist plots showing the effect of lowering the coating capacitance from green to black (all other parameters remaining the same)

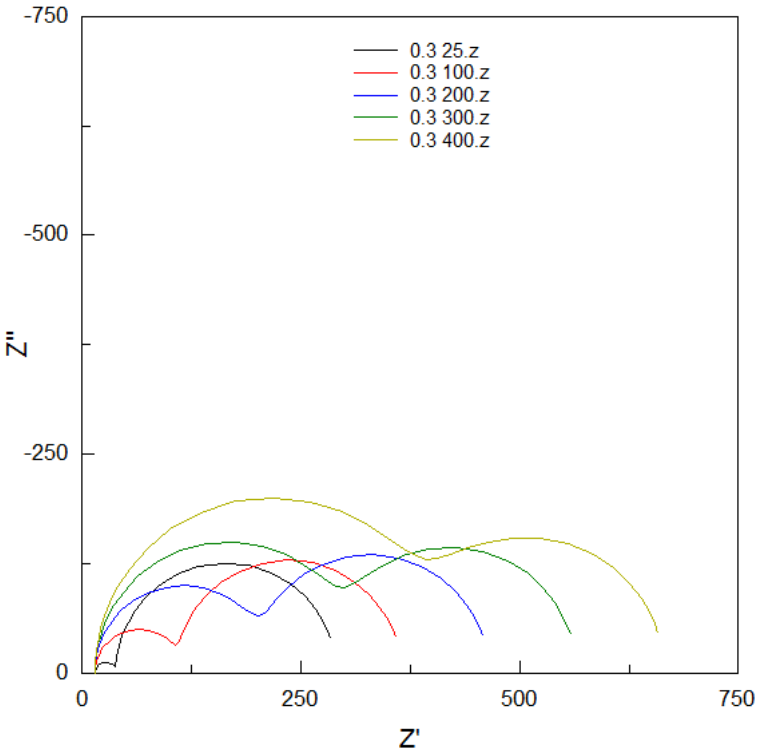

Figure 1.6.9 - A series of Nyquist plots showing the effect of lowering the pore resistance from light green to black (all other parameters remaining the same)

Electrochemical Impedance in Coil Coatings

Research around the area of coil coating has often used EIS as an analytical tool. Naderi and Attar[156] used electrochemical impedance to look at the differences in corrosion inhibition of phosphate based inhibitors. It was shown that zinc orthophosphate hydrate was not an effective inhibitor whilst both strontium aluminium polyphosphate and zinc aluminium polyphosphate were effective, with the polyphosphate inhibitors potentially displaying film-forming behaviour as determined by the equivalent circuits.

Additionally, Pokhmurs'kyi et al[157] used impedance to determine corrosion inhibitor efficiencies of phosphate/calcium ion exchange pigments in comparison to chromates. It was determined that by following the changes in charge transfer resistance of the system with different coatings that whilst the non-chromate inhibition systems did increase corrosion resistance, it did not reach the levels of inhibition found with chromates.

Simões and Fernandes[158] have utilised impedance spectroscopy, combined with scanning vibrating electrode technique to observe corrosion at the cut edge. This allowed them to observe the effects of a phosphate inhibitor on the cut edge, and compare the impedance of the cut edge with that of zinc and steel separately, showing that the impedance spectra gained is similar, but distinct, between zinc and the cut edge, whereas steel is completely different.

Yıldız and Dehri[159] applied EIS to samples following accelerated weathering tests to determine the onset of coating defects from the cut-edge. It was determine through the analysis of the impedance plots that following 120 days exposure the coating resistance reduced significantly suggesting coating deterioration.

Electrochemical impedance is also used in to observe or check the coatings in cut edge corrosion studies without directly observing the cut edge, often prior to using other, localised techniques to observe the cut edge. For example, Worsley et al determined the coating

performance using electrochemical impedance before analysing the cut edge performance with SVET[141].

Impedance Spectroscopy in Other Research

Beyond its uses in coil coating research, electrochemical impedance spectroscopy is used across a wide range of fields for analysis of chemical systems and environments. Of particular importance is its use in analysis of coatings.

Delucchi et al[160] have used impedance spectroscopy to analyse the multiple layers of coatings in a coil coating system following various tests to maximize performance. The information gathered from the impedance spectra allows for reasoned and considered evaluations of performance across a range of tests, and highlights the usefulness of the technique as a quick post-test analytical tool.

Electrochemical impedance has also been utilised to look at local phenomena. Dehri et al[161] isolated sections of a coil coated material following a standard testing procedure using tubes and performed EIS on each tube section individually. The impedance results showed significant deterioration of the coating near the cut edges. Whilst the results make sense, it is important to note that there could be issues caused by the delay required between running sections of the sample.

Mansfield's paper on electrochemical impedance explores the usefulness of electrochemical impedance spectroscopy on the analysis of corrosion protection, showing equivalent circuits that have been used to analyse inhibitors in free solution, conversion coatings and organic coatings, amongst others[162]. However, it is Epelboin et al, whose initial studies showing the usefulness of the charge transfer resistance, readily obtainable from most impedance spectra, and the link it has with the corrosion rate at the metal surface which resulted in the emergence of impedance as a way of monitoring corrosion inhibition[163].

Following the development of inhibitor films is also possible using impedance spectroscopy. Naderi and Attar[156] observed the development of a second time function when following the inhibition of polyphosphates by impedance, which was suggested as the deposition of a thin layer on the surface. Bastos et al[164] also determined the mechanism of inhibition of chromates and phosphates was the deposition of an inhibitive layer on the metal surface through following the impedance of the samples over time.

Scanning Ion-selective Electrode Technique (SIET)

The ion-selective electrode technique is a tool capable of noting small environmental changes with reference to a particular ion, or to localised pH changes. This can be useful, as when cathodic or anodic processes occur on the surface, there is a change in the local pH. This is due to the chemical species that are released or consumed in the electrochemical processes. Knowledge of the particular reactions that may occur on a metal surface, combined with the pH values obtained through pH microsensing can give an idea of whether a particular site on the surface may be anodic or cathodic.

The knowledge of how local environments behave with relation to pH can also be used to develop inhibitor systems that can utilise the local pH changes to become active. Lamaka et al[165] demonstrated the applications of the SIET technique with relation to both pH microsensing for localised acidification and alkalisation reactions, as well as through monitoring the release of ions dissolved from anodic sites.

The quasi-simultaneous use of SVET and SIET was also demonstrated, which would have the potential for observing and analysing the corrosion of complex microstructure if the length scales and resolution could be improved. However, Alvarez-Pampliega et al[166] have shown the usefulness of this combination technique in the determination of mechanisms at the cut edges, using localised pH measurements to understand the movement and inhibition by alloy coating hydroxides. Zdrachek et al[167] have also able to use pH microsensing techniques to

observe and map the localised pH behaviour and corresponding current densities on the cut edge of a zinc magnesium aluminium ternary alloy coated material, so there is potential in this technique for analysing larger scale corrosion and inhibition mechanisms at cut edges.

Other Methods

Scanning Electron Microscopy

Scanning electron microscopy is a useful tool in the field of corrosion. The scanning electron microscope utilises various signals that are produced from the interaction of the sample and a focussed beam of high-energy electrons to produce images. It can be used to obtain topographical detail of corroded surfaces with a good amount of detail. Using scanning electron microscopy allows for greater resolution and depth of field when compared to optical microscopy. This allows a fuller overall picture of localised corrosion structure and potentially allows for dimensions of the phenomena to be obtained.

Whilst scanning electron microscopy ultimately gives no information other than surface corrosion structure, it is commonly combined with energy dispersive x-ray spectroscopy (EDS) to provide chemical information for either the microstructure or the corrosion products. EDS utilises the x-rays that are emitted from the sample as it interacts with the electron beam. The energies of the emitted x-rays are generally characteristic of individual elements and can be used to give an indication of the elemental make-up of a particular site.

SEM is a common analytical tool in corrosion studies, and sees a wide range of uses. For example, Naderi and Attar[156] used SEM to analyse the morphology of corrosion inhibitor pigments, as well as that of the produced inhibitive layer on the surface of the steel, which was capable of being analysed by EDS. In contrast, Bernard et al[168] utilised SEM to show the structures of various zinc corrosion products. Similarly, Muster and Cole[169] used SEM and EDS to observe the structure and confirm the elemental make-up of potentially passivating zinc corrosion product layers.

Duchoslav et al[170] observed both the microstructure and the localised corrosion initiation sites of zinc-magnesium-aluminium ternary alloy coatings using SEM and other techniques. A similar, albeit simplified, version of this experiment was also carried out and analysed by SEM by Palma et al on a Galvalume coating[94].

Scanning electron microscopy finds uses across many areas of coil coating. Combining SEM imaging with EDX analysis allows for greater understanding of alloy coating microstructure, paint structure, corrosion products and inhibition structures. Vu et al[171] used SEM and EDS to follow the corrosion initiation sites at the cut edge of Galvalume coated materials in sulfate and chloride solutions.

X-Ray Photoelectron Spectroscopy

X-Ray photoelectron spectroscopy, or XPS, is a spectroscopic technique that utilises a focussed X-ray beam to determine the elemental composition of a particular surface. When an area of the surface is irradiated with x-rays, the energy from the radiation source is transferred to core-level electrons. This leads to emission of this electron from the sample. The kinetic energy of this electron is dependent on the binding energy of the atomic orbital from which it is released. Therefore, the detected kinetic energy of a released electron can be considered characteristic of coming from a particular orbital of a particular element. In this way, by analysing the quantities and energies of emitted electrons from an irradiated sample, the elemental make-up of the surface may be determined[172].

XPS is a commonly used method of analysis in corrosion. Of particular interest is the utilisation of XPS to analyse inhibitor film formation. Due to the surface resolution of XPS, it can be used for inhibitor films that are too thin to be analysed by SEM/EDS analysis, as XPS observes the top few nanometers (generally considered to be approximately 10 nm) of the surface. For example, Aramaki[173] used XPS to follow the deposition of cationic inhibitor species onto the

surface of zinc, and this allowed for some quantification and analysis of the composition of these surfaces.

The XPS technique is generally found to be unsuitable for cut edge corrosion studies as the required detection area is too large to provide an acceptable direct measurement at the edge. However, studies have been reported that attempt to approximate chemistry on the cut edge. Custódio et al[126] attempted to understand the action of benzotriazole at the cut edge using XPS by producing larger samples that contained a 7:3 steel:zinc ratio. Whilst this may be a reasonable approximation from a chemistry standpoint, it is also worth noting that the steel to zinc ratio of 7:3 is significantly different from the ratio of approximately 40:1 generally observed at the actual cut edge. This may significantly alter the observed chemistry, particularly if there is reliance on dissolved zinc ions. It is possible that this could be an issue as it has been suggested in other research that the inhibitor action of benzotriazole is reliant on the presence of dissolved zinc ions[174].

Weight Loss

One method of characterising the severity of corrosion is to measure the weight difference between the system before and after exposure. Theoretically, as the metal corrodes through anodic processes, weight is lost through the creation and expulsion of corrosion products. By measuring the change in weight as samples corrode, as well as knowing the density and exposed area of the sample measured, the rate of corrosion can be determined[175].

Whilst this can be a useful, and simple, way of deducing corrosion rates, it is prone to errors. Some corrosion products can adhere strongly to the substrate surface and, despite efforts to remove corrosion products, may be included within a weight loss measurement. Similarly, overzealous cleaning of the substrate to remove corrosion products could potentially lead to damaging of unaffected substrate and affect the overall result. Similarly, if looking at rates of

painted surfaces, the uptake of the electrolyte into the paint, as well as the loss of paint throughout the test may affect the overall results.

The use of weight loss as a method of understanding corrosion has been evident for over a century, with Dudley's work published in 1908[176] primarily using the technique to understand the effects of soil on the corrosion of pipes in the presence of gas. More recently, it has been used as a qualitative measure for comparing results[63]. For example, Amadeh et al[177] used weight loss measurement combined with other methods to compare the corrosion rate and profile of galvanised steels with rare earth additions to the zinc layer.

Whilst there are some potential drawbacks to the technique, weight loss studies can be used to form some quantitative results. Ju and Li[178] have attempted to use weight loss measurements to quantify inhibitor efficiency through adapting the equation used with charge transfer resistance. Whilst this is potentially an interesting avenue for calculating inhibitor efficiencies, the previously described issues with the technique could cause problems when comparing calculated results. The most common quantification of weight loss measurements appears to be the aforementioned calculation of the corrosion rate of a sample[179].

1.7 Corrosion Testing

In the aforementioned analytical techniques, some understanding of materials and environments can be gained, including theoretical rates and the particular corrosion processes that may occur. However, whilst this can give a rough idea of the potential uses or drawbacks in particular applications, the link between laboratory analysis and real world results is tenuous. Therefore, it is also important to observe the development of corrosion in more realistic situations. This section will introduce and discuss various methods that have been developed to mimic more realistic corrosion behaviour.

Atmospheric Field Testing

A simple way of testing how materials corrode is to expose them to the environment and observe how corrosion occurs over a period of time. This is often done with a coated panel that has standardised defects introduced, such as scribes and bends. The panel is observed several times over a period of time to analyse the progression of corrosion. Panels are also tested in a variety of different configurations, facing in different directions to vary wind and sunlight exposure, and different angles to change the length of time it takes for rain to wash over the sample.

As it is difficult to accurately measure and characterise the environment in which a particular sample is in over the length of time of exposure, the overall environment of a particular testing site is what is characterised.

Following exposure, a variety of tests can be performed. Many of these involve visual analysis of the test panel as a whole, and potentially measuring corrosion processes that are evident on the surface, such as edge creep and degree of filiform corrosion for comparative purposes. The panels can also be used for mechanical testing to observe the effect of corrosion on the mechanical properties of the material, or be observed under an electron microscope to view smaller scale corrosion processes such as intergranular corrosion[180].

Field testing is the test that is most representative of a material in real service. However, there are some issues with the test. As it is not an accelerated test, it can take a long time to gather useful feedback. The environment also has to be well defined to determine the applicability of the results to other areas of the world, and environmental variability over a long term must be taken into account. However, it is worth noting that the real world environmental variability is not easily replicated in a laboratory environment, which makes this type of testing invaluable.

Accelerated Corrosion Testing

As it takes years to gain a more extensive picture by atmospheric field testing, performing all corrosion testing this way is not feasible. Therefore, the development of tests that cause realistic corrosive damage on an accelerated timescale was vital. Whilst no accelerated test can ultimately provide perfect results[181], some widely-used methods of accelerated corrosion testing have been developed.

Salt Spray

Salt spray testing was one of the first laboratory tests devised for accelerated corrosion testing[180], and is a method that is still commonly used for testing corrosion.

Whilst salt spray testing is mainly dictated by the ASTM B117 standard, this is not the only standard available. Many companies have developed their own standard salt spray tests; for example, Hörnström et al have used a salt spray/humidity test standard that was developed by Volvo in the analysis of paints on Galvalume substrates[124].

The main issue with salt spray testing is that it is performed with conditions that are closely controlled and so there are a limited number of variables. This means that it cannot be truly representative of a real-world environment. To counter this, a comparison standard can be used, which is a sample that is known to show resistances to both atmospheric and accelerated corrosion tests that are acceptable[182].

It has been reported that the standard test solution for salt spray does not provide accurate or reproducible results[49]. Indeed, the applicability of the tests has been doubted in the literature, particularly for testing sacrificial coatings[183]. Static salt spray testing can be considered to be a particularly unrealistic test. It has been recognised that corrosion in atmospheric conditions involves both wet and dry cycles which allows for initial electrolyte deposition on the surface, followed by electrolyte concentration through evaporation which

eventually may lead to solid salt formation on the surface and an eventual washing of the surface. To produce a more realistic result, cyclic salt spray tests were developed[180].

In regards to cut edge corrosion, salt spray testing is not often used to study the cut edge, and tend to seal them instead. This is to prevent effects of having thinner organic coatings at the edges, despite this being the case in real applications.

The sealing of edges can have a noticeable effect on the results obtained from salt spray testing. In one report, the sealing off of edges decreased the time required for the presence of visible iron oxide corrosion product appearing on the sample[75]. This potentially shows a change in corrosion mechanism as a result of the covered edges and brings into question the validity of the results.

Prohesion Testing

The prohesion test was developed following concerns that the standard procedures for salt spray testing (ASTM B117) caused failures in systems which were capable in the real world. The prohesion testing method uses weakened Harrison's solution as opposed to the 5% salt solution in ASTM B117. This less aggressive solution is considered to produce more realistic corrosion results that have a greater reproducibility when used as opposed to the standards set for normal salt spray testing[49]. It is also considered that prohesion testing is more representative of real in-service conditions when compared to normal salt spray testing[134].

Prohesion testing has now become a standard itself, and is dictated by several standard procedures, such as ASTM G85-A5 and ASTM D5894.

Humidity Testing

Testing for corrosion in humidity chambers involves subjecting the material to a high humidity environment. This is generally invokes mild corrosion and is most relevant for observing early onset corrosion. It is commonly used for analysis of metal coatings and inhibitive pre-

treatments[184]. Conditions that can be controlled in humidity chambers are the relative humidity level, which tends to be between 75 and 95 percent, of the chamber and the temperature, which is usually around 25˚C. As with salt spray tests, this can be either static or cyclic in nature. Many standards for humidity testing have been developed, examples of which are ASTM A164-55, A165-55[184] and D227[182].

Immersion

Immersion testing is similar to salt spray testing. However, instead of subjecting the sample to a spray, the sample is immersed in an electrolyte solution. Again, similar to the salt spray testing, immersion testing can be either cyclic or static in nature. It has been reported that cyclic immersion improves the accuracy of corrosion results when compared to field testing. It is thought that this is because the continuous exposure to electrolyte prevents the initiation of local anodic and cathodic sites that can occur in the atmosphere[185].

Immersion testing is reported to become a more accurate test when an external cathode is introduced[186]. However, immersion testing in this way results in fairly slow corrosion, and thus to be considered a reasonable accelerated test, needs a method of further speeding up the tests. It has also been reported that the use of synthetic rainwater solutions in accelerated tests can give more realistic corrosion pathways when corrosion products are compared to field tests[103].

1.8 Final Remarks, Aims and Objectives

This introductory section has attempted to highlight the background behind this project and touch upon the issues that drive it. Corrosion is responsible for substantial global financial losses, as well as injury. Due to the significant losses, industry is taking notice, and gaining a greater understanding of corrosion, alongside the development of corrosion prevention methods, is becoming important.

A major cause of failure in coil coated materials is cut edge corrosion. Inhibition of corrosion at the cut edge is currently done through incorporation of chromate inhibitors. A search for alternatives has been necessitated by the upcoming restrictions placed on chromates in Europe by new safety regulations, owing to its toxicity. The more recent industry push towards complex zinc-aluminium-magnesium alloys increases the difficulty in finding replacements, as these alloys are not as well characterised.

Characterisation of these new alloys presents an issue in attempting to replicate microstructure and particular phases that are present. An overarching approach to this problem would likely require the combination of widely used localised techniques with the application of new methods of isolating electrochemical information for particular phases and chemical information through spectroscopy.

This project specifically aims towards improving the understanding of the mechanism of corrosion inhibitors on multiphase galvanic protection alloy systems. In doing so, it is hoped that effective corrosion prevention systems can be developed that potentially utilise the unique corrosion chemistries of these materials.

To do this, this body of work will be using two main approaches. The first is producing a methodology to observe corrosion inhibitor behaviour on systems containing multiple metals simultaneously whilst maintaining a more realistic electrochemical environment for each of the individual materials. Testing of this methodology will be done on a simplified zinc and steel mimic of galvanised steel using previously characterised industrial inhibitor pigments, concentrating on strontium chromate as a standard, zinc molyphosphate and a calcium exchanged silica pigment.

Once the methodology has been verified, the project will then aim to look at a more recent, newer generation of industrially relevant inhibitor pigments, modified aluminium

polyphosphates, concentrating on the strontium, calcium and magnesium modifications to this pigment.

The second approach will be to, using results obtained from the electrochemical tests, target pigments of interest and apply additional analytical techniques to gain further insight into the mechanism of inhibition. Using surface analysis and imaging, such as scanning electron microscopy, energy dispersive x-ray spectroscopy and x-ray photoelectron spectroscopy, and manipulating the environment, a greater understanding of the nature of the inhibition of these pigments can be sought.

1.9 Chapter References

[1] ISO 8044-1999. Geneve: International Standards Organisation; 2010.

[2] Scully JC. Aqueous Corrosion, in:. The Fundamentals of Corrosion, 2nd ed. Oxford: Pergamon Press; 1975.

[3] Trethewey KR, Chamberlain J. Theory of Aqueous Corrosion, in:. Corrosion for Science and Engineering, 2nd ed. London: Longman Group Limited; 1995.

[4] Piron DL. Basic Electrochemical Concepts and Their Uses, in:. The Electrochemistry of Corrosion. Houston, Texas: NACE International; 1991.

[5] Scully JR. Electrochemical, in:. Baboian R (Ed.). Corrosion Tests and Standards: Application and Interprtation. Philadelphia: ASTM; 1995.

[6] Munger CG. Corrosion as Related to Coatings, in:. Corrosion Prevention by Protective Coatings. Houston, Texas: NACE International; 1984.

[7] Uhlig HH. Corrosion Tendency and Electrode Potentials, in:. Corrosion and Corrosion Control. New York: John Wiley & Sons; 1963.

[8] Wranglen G. Electrochemical Elements, in:. An Introduction to Corrosion and Protection of Metals. London: Chapman and Hall; 1985.

[9] Pourbaix MJN. Thermodynamics of Dilute Aqueous Solutions - With Applications to Electrochemistry and Corrosion. Norwich: Jarrold and Sons; 1949.

[10] Mokaddem M, Volovitch P, Ogle K. Electrochim Acta 2010;55:7867.

[11] Bard AJ, Faulkner LR. Kinetics of Electrode Reactions, in:. Electrochemical Methods: Fundamentals and Applications, 2nd ed. New York: John Wiley & Sons; 2001.

[12] Stewart D, Tulloch DS. Electrode Kinetics, in:. Principles of Corrosion & Protection. London: Macmillan & Co Ltd; 1968.

[13] Bardal E. Electrode Kinetics, in:. Corrosion and Protection. London: Springer-Verlag London; 2003.

[14] Uhlig HH. Passivity, in:. Corrosion and Corrosion Control. New York: John Wiley & Sons; 1963.

[15] Olefjord I, Elfstrom B. Corrosion 1982;38:46.

[16] Bardal E. Passivity, in:. Corrosion and Protection. London: Springer-Verlag London; 2003.

[17] Uhlig HH. Electrochemical Mechanisms, in:. Corrosion and Corrosion Control. New York: John Wiley & Sons; 1963.

[18] Francis R. First Principles, in:. Galvanic Corrosion: A Practical Guide for Engineers. Houston, Texas: NACE International; 2001.

[19] Ketcham S, Pearlstein F, Jankowsky E, Taylor E, Manty B, Snyder W, Hecht R. Metallic Coatings, in:. A Handbook of Protecting Coatings for Military and Aerospace Equipment. Houston, Texas: NACE International; 1983.

[20] Rothwell N, Tullmin M. Corrosion Monitoring Handbook, 1st ed. Oxford: Coxmoor; 2000.

[21] Bardal E. Different Forms of Corrosion, in:. Corrosion and Protection. London: Springer-Verlag London; 2003.

[22] Wranglen G. Some Important Types of Electrochemical Corrosion, in:. An Introduction to Corrosion and Protection of Metals. London: Chapman and Hall; 1985.

[23] Bautista A. Prog Org Coatings 1996;28:49.

[24] Donofrio J. Met Finish 2000;98:57.

[25] Fedrizzi L, Deflorian F, Rossi S, Bonora PL. Mater Sci Forum 1998;289–292:485.

[26] van Ooij WJ, Zhu DQ, Prasad G, Jayaseelan S, Fu Y, Teredesai N. Surf Eng 2000;16:386.

[27] Frankel GS, McCreery RL. Interface 2001;10:34.

[28] Grundmeier G, Schmidt W, Stratmann M. Electrochim Acta 2000;45:2515.

[29] Mercer AD, Jenkins IR. Br Corros J 1968;3:130.

[30] Andrade C, Macias A. Br Corros J 1987;22:162.

[31] Luckeneder G, Fleischanderl M, Steck T, Stellnberger K-H, Faderl J, Schuerz S, Mori G. BHM Berg- und Hüttenmännische Monatshefte 2012;157:121.

[32] Trethewey KR, Chamberlain J. Selective Attack, in:. Corrosion for Science and Engineering, 2nd ed. London: Longman Group Limited; 1995.

[33] Wranglen G. Metallurgical Elements, in:. An Introduction to Corrosion and Protection of Metals. London: Chapman and Hall; 1985.

[34] Sullivan J, Mehraban S, Elvins J. Corros Sci 2011;53:2208.

[35] Volovitch P, Vu TN, Allély C, Abdel Aal A, Ogle K. Corros Sci 2011;53:2437.

[36] Salgueiro Azevedo M, Allély C, Ogle K, Volovitch P. Electrochim Acta 2015;153:159.

[37] Uhlig HH. Iron and Steel, in:. Corrosion and Corrosion Control. New York: John Wiley & Sons; 1963.

[38] Uhlig HH. Iron and Steel, in:. Corrosion and Corrosion Control. New York: John Wiley & Sons; 1963.

[39] Zhang XG. Electrochemical Thermodynamics and Kinetic, in:. Corrosion and Electrochemistry of Zinc. New York: Plenum Press; 1996.

[40] Stanojevic D, Toskovic D, Rajkovic MB. J Min Metall Sect B Metall 2005;41:47.

[41] Uhlig HH. Definition and Importance, in:. Corrosion and Corrosion Control. New York: John Wiley & Sons; 1963.

[42] Trethewey KR, Chamberlain J. Corrosion and Society, in:. Corrosion for Science and Engineering, 2nd ed. London: Longman Group Limited; 1995.

[43] Biezma M V, San Cristóbal JR. Corrosion 2006;62:1051.

[44] Bhaskaran R, Palaniswamy N, Rengaswamy NS, Jayachandran M, Raghavan M. Corros Eng Sci Technol 2005;40:75.

[45] Akinyemi OO, Nwaukocha CN, Asedanya AO. J Eng Sci Technol 2012;7:517.

[46] Bhaskaran R, Palaniswamy N, Rengaswamy NS, Jayachandran M. Mater Corros 2004;55:865.

[47] Drufke R. Met Finish 2006;104:35.

[48] Graziano F. Met Finish 2000;98:175.

[49] Howard RL, Lyon SB, Scantlebury JD. Prog Org Coatings 1999;37:91.

[50] Munger CG. Essential Coating Characteristics, in:. Corrosion Prevention by Protective Coatings. Houston, Texas: NACE International; 1984.

[51] Uhlig HH. Cathodic Protection, in:. Corrosion and Corrosion Control. New York: John Wiley & Sons; 1963.

[52] Davy H. Philos Trans R Soc London 1824;114:151.

[53] Gellings PJ. Prevention and Control of Electrochemical Corrosion, in:. Introduction to Corrosion Prevention and Control. Delft: Delft University Press; 1985.

[54] Kim J, Joo J, Koo S. J Mater Sci Lett 2000;9:477.

[55] Davy H. Philos Trans R Soc London 1825;115:328.

[56] Department of Industry. Cathodic Protection. London: Institute of Corrosion Science and Technology; 1981.

[57] Pourbaix M. Corros Sci 1974;14:25.

[58] Edavan RP, Kopinski R. Corros Sci 2009;51:2429.

[59] Koehler EL. Corrosion 1984;40:5.

[60] Trethewey KR, Chamberlain J. Cathodic and Anodic Protection, in:. Corrosion for Science and Engineering, 2nd ed. London: Longman Group Limited; 1995.

[61] Wranglen G. Corrosion Protection by Corrosive Medium, in:. An Introduction to Corrosion and Protection of Metals. London: Chapman and Hall; 1985.

[62] Fontana MG. Ind Eng Chem 1955;47:81A.

[63] Pryor MJ, Cohen M. J Electrochem Soc 1953;100:203.

[64] Dariva CG, Galio AF. Corrosion Inhibitors – Principles , Mechanisms and Applications, in:. Aliofkhazraei M (Ed.). Developments in Corrosion Protection. InTech; 2014.

[65] Zhang XG. Properties, Products and Processes, in:. Corrosion and Electrochemistry of Zinc. New York: Plenum Press; 1996.

[66] Chen ZW, Kennon NF, See JB, Barter MA. JOM 1992;44:22.

[67] Carter VE. Metallic Coatings for Corrosion Control. London: Butterworth; 1977.

[68] Taniyama A, Arai M, Takayama T, Sato M. Mater Trans 2004;45:2326.

[69] de Oliveira ACL, Rios PR. J Mater Res Technol 2013;2:117.

[70] Chen L, Fourmentin R, Mc Dermid JR. Metall Mater Trans A 2008;39:2128.

[71] Almeida E, Morcillo M. Surf Coatings Technol 2000;124:180.

[72] Bandyopadhyay N, Jha G, Singh AK, Rout TK, Rani N. Surf Coatings Technol 2006;200:4312.

[73] Worsley DA, McMurray HN, Sullivan JH, Williams IP. Corrosion 2004;60:437.

[74] Queiroz FM, Costa I. Surf Coatings Technol 2007;201:7024.

[75] Li F, Lv JS, Yang HG, Zhou F, Zhang L, Wang HK. Appl Mech Mater 2013;442:64.

[76] Lee HH, Hiam D. Corrosion 1989;45:852.

[77] Shibli SMA, Meena BN, Remya R. Surf Coatings Technol 2015;262:210.

[78] Żelechower M, Kliś J, Augustyn E, Grzonka J, Stróż D, Rzychoń T, Woźnica H. Arch Metall Mater 2012;57:517.

[79] Bluni ST, Marder AR, Goldstein JI. Mater Charact 1994;33:93.

[80] Gyurov S, Kostova Y, Parshorov S. J Univ Chem Technol Metall 2012;47:211.

[81] Marder AR. Prog Mater Sci 2000;45:191.

[82] Elvins J, Spittle JA, Worsley DA. Corros Eng Sci Technol 2003;38:197.

[83] Elvins J, Spittle JA, Worsley DA. Corros Sci 2005;47:2740.

[84] Elvins J, Sullivan JH, Spittle JA, Worsley DA. Corros Eng Sci Technol 2005;40:43.

[85] Feliu S, Barranco V. Acta Mater 2003;51:5413.

[86] Rodnyansky A, Warburton YJ, Hanke LD. Surf Interface Anal 2000;29:215.

[87] Shih H., Hsu J., Sun C., Chung S. Surf Coatings Technol 2002;150:70.

[88] Zhang X, Leygraf C, Odnevall Wallinder I. Corros Sci 2013;73:62.

[89] Barnard NC, Brown SGR. Corros Sci 2008;50:2846.

[90] Lin K-L., Yang C-F, Lee J-T. Corrosion 1991;47:9.

[91] Li Y. Bull Mater Sci 2001;24:355.

[92] Selverian JH, Marder AR, Notis MR. Metall Trans A 1988;19:1193.

[93] LeBozec N, Thierry D, Rohwerder M, Persson D, Luckeneder G, Luxem L. Corros Sci 2013;74:379.

[94] Palma E, Puente JM, Morcillo M. Corros Sci 1998;40:61.

[95] McMurray HN. Corrosion 2001;57:313.

[96] Zhang X, Vu T-N, Volovitch P, Leygraf C, Ogle K, Wallinder IO. Appl Surf Sci 2012;258:4351.

[97] Panossian Z, Mariaca L, Morcillo M, Flores S, Rocha J, Peña JJ, Herrera F, Corvo F, Sanchez M, Rincon OT, Pridybailo G, Simancas J. Surf Coatings Technol 2005;190:244.

[98] Seré PR, Zapponi M, Elsner CI, Di Sarli AR. Corros Sci 1998;40:1711.

[99] Domínguez-Crespo MA, Onofre-Bustamante E, Torres-Huerta AM, Rodríguez-Gómez FJ, Rodil SE, Flores-Vela A. Metall Mater Trans A 2009;40:1631.

[100] Schuerz S, Fleischanderl M, Luckeneder GH, Preis K, Haunschmied T, Mori G, Kneissl AC. Corros Sci 2009;51:2355.

[101] Vimalanandan A, Bashir A, Rohwerder M. Mater Corros 2014;65:392.

[102] Arndt M, Duchoslav J, Itani H, Hesser G, Riener CK, Angeli G, Preis K, Stifter D, Hingerl K. Anal Bioanal Chem 2011;403:651.

[103] Salgueiro Azevedo M, Allély C, Ogle K, Volovitch P. Corros Sci 2015;90:472.

[104] Schürz S, Luckeneder GH, Fleischanderl M, Mack P, Gsaller H, Kneissl AC, Mori G. Corros Sci 2010;52:3271.

[105] Kollárová M, Hrabčáková L, Graban J, Šohajová M. Mater Sci Forum 2014;782:623.

[106] Sinko J. Prog Org Coatings 2001;42:267.

[107] Zin IM, Howard RL, Badger SJ, Scantlebury JD, Lyon SB. Prog Org Coatings 1998;33:203.

[108] Baghni IM, Lyon SB. Corros Eng Sci Technol 2005;40:165.

[109] Prosek T, Thierry D. Prog Org Coatings 2004;49:209.

[110] Brasher M. Trans Faraday Soc 1958;54:1214.

[111] Kubaschewski BY, Brasher DM. Trans Faraday Soc 1959;55:1200.

[112] Clark WJ, McCreery RL. J Electrochem Soc 2002;149:B379.

[113] Onuchukwu AI, Lori JA. Corros Sci 1984;24:833.

[114] Kendig MW, Davenport AJ, Isaacs HS. Corros Sci 1993;34:41.

[115] Baghni I., Lyon S., Ding B. Surf Coatings Technol 2004;185:194.

[116] Mayne JEO, Pryor MJ. J Chem Soc 1949;0:1831.

[117] World Health Organization. Chromium and Chromium Compounds, in:. IARC Monographs on the Evaluation of Carcinogenic Risks to Humans - Chromium, Nickel and Welding. Lyon: International Agency for Research on Cancer; 1990.

[118] Naderi R, Attar MM. Electrochim Acta 2008;53:5692.

[119] Bastos AC, Ferreira MG, Simões AM. Corros Sci 2006;48:1500.

[120] Simões AM, Torres J, Picciochi R, Fernandes JCS. Electrochim Acta 2009;54:3857.

[121] Zin IM, Lyon SB, Pokhmurskii VI, Simmonds MC. Corros Eng Sci Technol 2004;39:167.

[122] Sullivan J, Cooze N, Gallagher C, Lewis T, Prosek T, Thierry D. Faraday Discuss 2015;180:361.

[123] van Ooij WJ, Zhu DQ, Prasad G, Jayaseelan S, Fu Y, Teredesai N. Surf Eng 2000;16:386.

[124] Hörnström S, Karlsson J, Van Ooij WJ, Tang N, Klang H. J Adhes Sci Technol 1996;10:883.

[125] Simões AMP, Carbonari RO, Di Sarli AR, Del Amo B, Romagnoli R. Corros Sci 2011;53:464.

[126] Custódio J V., Agostinho SML, Simões AMP. Electrochim Acta 2010;55:5523.

[127] McMurray HN, Powell SM, Worsley DA. Br Corros J 2001;36:42.

[128] McMurray HN, Williams D, Worsley DA. ECS Trans 2006;1:153.

[129] Loveridge MJ, McMurray HN, Worsley DA. Corros Eng Sci Technol 2006;41:240.

[130] Robertson WD. J Electrochem Soc 1951;98:94.

[131] Twite RL, Bierwagen GP. Prog Org Coatings 1998;33:91.

[132] Zin IM, Pokhmurskii VI, Scantlebury JD, Lyon SB. J Electrochem Soc 2001;148:B293.

[133] Zin' IM, Lyon SB, Bilyi LM, Tymus' MB. Mater Sci 2008;44:638.

[134] Walker DE, Wilcox GD. Trans Inst Met Finish 2008;86:251.

[135] Qian YJ, Turgoose S. Br Corros J 1987;22:268.

[136] Monticelli C, Brunoro G, Frignani A, Trabanelli G. J Electrochem Soc 1992;139:706.

[137] Ogle K, Baudu V, Garrigues L, Philippe X. J Electrochem Soc 2000;147:3654.

[138] Ogle K, Morel S, Jacquet D. J Electrochem Soc 2006;153:B1.

[139] Penney D, Sullivan J, Worsley D. Corros Sci 2007;49:1321.

[140] Worsley DA, McMurray HN, Belghazi A. Chem Commun 1997;0:2369.

[141] Worsley DA, Williams D, Ling JSG. Corros Sci 2001;43:2335.

[142] Challis M, Worsley DA. Br Corros J 2001;36:297.

[143] Deshpande P, Deshpande P, Vagge S. UPB Sci Bull Ser B Chem Mater Sci 2013;75:251.

[144] Howard RL, Zin IM, Scantlebury JD, Lyon SB. Prog Org Coatings 1999;37:83.

[145] Chiba A, Muto I, Hara N. J Electrochem Soc 2011;158:C42.

[146] Jia JX, Song G, Atrens A. Corros Sci 2006;48:2133.

[147] Flitt HJ, Schweinsberg DP. Corros Sci 2005;47:2125.

[148] Callow LM, Richardson JA, Dawson JL. Br Corros J 1976;11:123.

[149] Callow LM, Richardson JA, Dawson JL. Br Corros J 1976;11:132.

[150] Hines JG. Br Corros J 1983;18:10.

[151] Zin IM, Lyon SB, Pokhmurskii VI. Corros Sci 2003;45:777.

[152] Christensen PA, Hamnett A. Techniques Giving Mechanistic Information, in:. Techniques and Mechanisms in Electrochemistry. Glasgow: Chapman and Hall; 1994.

[153] Shoar Abouzari MR, Berkemeier F, Schmitz G, Wilmer D. Solid State Ionics 2009;180:922.

[154] Jorcin J-B, Orazem ME, Pébère N, Tribollet B. Electrochim Acta 2006;51:1473.

[155] Randles JEB. Discuss Faraday Soc 1947;1:11.

[156] Naderi R, Attar M. Dye Pigment 2009;80:349.

[157] Pokhmurs'kyi VI, Zin' IM, Lyon SB. Mater Sci 2004;40:383.

[158] Simões AM, Fernandes JCS. Prog Org Coatings 2010;69:219.

[159] Yıldız R, Dehri İ. Arab J Chem 2013;8:821.

[160] Delucchi M, Barbucci A, Cerisola G. Electrochim Acta 1999;44:4297.

[161] Dehri I, Howard RL, Lyon SB. Corros Sci 1999;41:141.

[162] Mansfeld F. Electrochim Acta 1990;35:1533.

[163] Epelboin I, Keddam M, Takenouti H. J Appl Electrochem 1972;2:71.

[164] Bastos AC, Ferreira MGS, Simões AM. Prog Org Coatings 2005;52:339.

[165] Lamaka S, Souto RM, Ferreira MGS. In-Situ Visualization of Local Corrosion by Scanning Ion-Selective Electrode Technique (SIET), in:. Mendez-Vilas A, Diaz J (Eds.). Microsc. Sci. Technol. Appl. Educ. Formatex Research Center; 2010.

[166] Alvarez-Pampliega A, Lamaka SV, Taryba MG, Madani M, De Strycker J, Tourwé E, Ferreira MGS, Terryn H. Electrochim Acta 2012;61:107.

[167] Zdrachek EA, Karotkaya AG, Nazarov VA, Andronchyk KA, Stanishevskii LS, Egorov V V, Taryba MG, Kpoylovich SM, Lamaka S V. Sensors Actuators B Chem 2015;207B:967.

[168] Bernard MC, Hugot-Le Goff A, Phillips N. J Electrochem Soc 1995;142:2162.

[169] Muster TH, Cole IS. Corros Sci 2004;46:2319.

[170] Duchoslav J, Arndt M, Steinberger R, Keppert T, Luckeneder G, Stellnberger KH, Hagler J, Riener CK, Angeli G, Stifter D. Corros Sci 2014;83:327.

[171] Vu AQ, Vuillemin B, Oltra R, Allély C. Corros Sci 2011;53:3016.

[172] Hollander JM, Jolly WL. Acc Chem Res 1970;3:193.

[173] Aramaki K. Corros Sci 2001;43:1573.

[174] Kendig M, Jeanjaquet S, Addison R, Waldrop J. Surf Coatings Technol 2001;140:58.

[175] Arnold CG. Corrosion Testing Techniques, in:. Schweitzer PA (Ed.). Corrosion and Corrosion Protection Handbook. New York: Marcel Dekker, Inc.; 1983.

[176] Dudley WL. J Am Chem Soc 1908;30:247.

[177] Amadeh A, Pahlevani B, Heshmati-Manesh S. Corros Sci 2002;44:2321.

[178] Ju H, Li Y. Corros Sci 2007;49:4185.

[179] Mansfeld F, Tsai S. Corros Sci 1980;20:853.

[180] Lawson HH. Atmospheric Corrosion Test Methods, 4th ed. New York: NACE International; 1995.

[181] Rommal HEG, Lawson KM, Tiburcio AC, Lawson HH. Accelerated Test Development for Coil-Coated Steel Building Panels, in:. Corrosion 98. 1998.

[182] Singleton R. Met Finish 2012;110:12.

[183] Baldwin KR, Smith CJE. Aircr Eng Aerosp Technol 1999;71:239.

[184] Carter VE. Corrosion Testing for Metal Finishing. London: Butterworth Scientific; 1982.

[185] Hosking NC, Ström MA, Shipway PH, Rudd CD. Corros Sci 2007;49:3669.

[186] Howard RL, Lyon SB, Scantlebury JD. Prog Org Coatings 1999;37:99.

2 Chapter 2 - Materials and Methodology

2.1 Introduction

In this section, the methodology behind the experimental results and the materials used throughout this thesis are formally introduced. The details contained within are to be used alongside the experimental sections of the relevant chapters in order to give a full picture of the conditions in which the experiments were undertaken.

The materials section details any chemicals or other materials used either in sample preparation or within the actual experiments. In either case, the name, supplier and any other supplementary information will be given (purities, thicknesses etc.). In the experimental section, the details of any equipment, chemicals and preparation steps will be given. It is hoped that this section may help any person who wishes to perform these experiments by giving the specifics that are likely to differ in any future attempts to either replicate or expand upon these works.

It is important to note that the background theories and workings with regards to the equipment that was utilised throughout this thesis are outlined in the 'Literature Review' section of this thesis. Furthermore, the relevant methodologies, containing more specific details are laid out in the experimental section of each chapter.

2.2 Materials

Metal Substrates

Metal substrates comprise an essential part of all experimentation done throughout this thesis. For the three electrode set-up, the substrates used were mild steel rod (3mm diameter, 0.05% carbon steel), zinc rod (3mm diameter, 99.99+% purity zinc, Goodfellow) and aluminium rod (3mm diameter, 99.95% purity aluminium, Goodfellow). For all other experiments, the

substrates used were mild steel sheet (0.8 mm thickness, Q-Labs, as received) and zinc sheet (20 µm, Goodfellow). All substrates were used as received with no additional heat treatments or other processing, other than those mentioned within the experimental procedures.

Corrosion Inhibitors

The corrosion inhibitors that were used throughout this work were selected to be of future and historical relevance to industrial applications within coil coating. Strontium chromate ($SrCrO_4$) was selected as a readily available hexavalent chromium compound which is known to be an effective corrosion inhibitor. First generation chromate replacements with fairly well understood inhibitor behaviour were selected to be looked at in the initial tests. These were calcium ion-exchanged silica (Shieldex CP4-7394, GRACE) and zinc molyphosphate (Actirox 106, Nubiola), a second generation phosphate pigment. Finally, various modified aluminium polyphosphates, third generation phosphate pigments of industrial relevance, were also selected to be analysed. These were modified strontium aluminium polyphosphate, controlled adjusted modified (HEUCOPHOS® SRPP, Heubach), calcium aluminium polyphosphate silicate hydrate (HEUCOPHOS® CAPP, Heubach) and magnesium aluminium polyphosphate (Novinox® PAM, SNCZ). All inhibitor pigments were used as received with no additional purification or modifications, unless otherwise stated within the methodology.

Metal Chlorides

A number of metal chlorides were used throughout the experimental work given in this thesis. Sodium chloride (NaCl) was used in large quantities to produce the solutions in which all immersion tests were performed. In addition, zinc chloride ($ZnCl_2$), calcium chloride ($CaCl_2$), magnesium chloride ($MgCl_2$) and aluminium chloride ($AlCl_3$) have all been used as solution additions.

2.3 Methodology

Mounting Metal Samples for Electrochemical Testing

The mounting of metal samples was done slightly differently, depending on whether it was for use in the two working electrode system or the three working electrode system.

In the case of the two working electrode system, steel (2 cm x 1 cm x 0.8 mm) and zinc (2 cm x 1 cm x 25 µm) each had a wire attached to the corner of the largest flat face (steel by spot welding, zinc by soldering). Each metal was separately mounted in a small circular mould stood upright with the long, thin face flat at the bottom, allowing the wire to protrude upwards. The wire was surrounded with a thin, plastic tube and the mould was filled with two part epoxy resin (Araldite 3138 and Arudur 3140, in a 10:1 ratio), which was left to set at room temperature for a minimum of 24 hours.

For the cut-edge geometry, the metals were mounted in parallel to each other. Double sided adhesive tape was utilised at the top side (near the wire mounting) to ensure electrical separation of the two metals whilst maintaining close geometry and the wires were surrounded by the same plastic tubing. A diagram showing this configuration is given in Figure 2.3.1

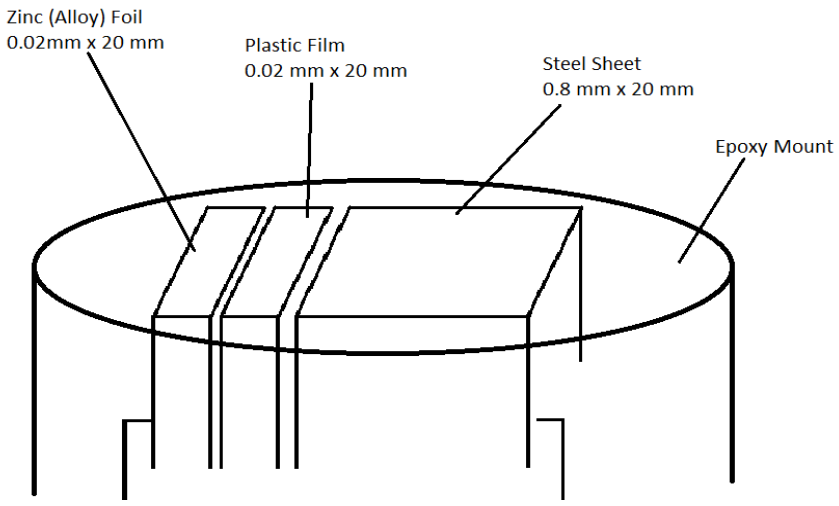

Figure 2.3.1 - Orientation of working electrodes in the secondary segmented electrode impedance tests, designed to mimic an exposed cut edge.

In the case of the three working electrode system, steel, zinc and aluminium rod (3 mm diameter, approx. 10 mm length) each have a wire attached by spot welding, soldering and crimping, respectively. Each metal is surrounded in shrink wrap and then placed in a mould around a piece of tubing in such a way as to produce three points of an equilateral triangle. Each wire in this case is encased in its own individual plastic casing, and the mould is filled using the two part epoxy resin, as previously described. A diagram showing this configuration is given in Figure 2.3.2.

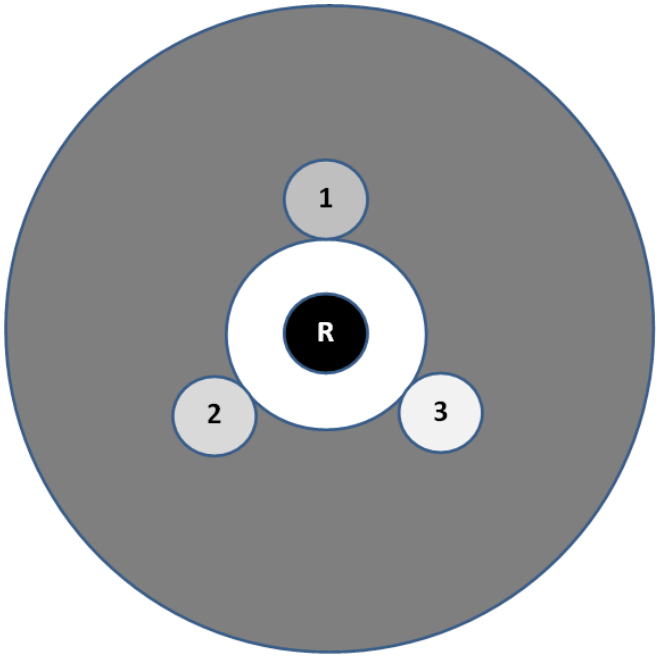

Figure 2.3.2 - Schematic representation of the geometry of the three working electrode setup utilised (1 – steel, 2 – zinc, 3 – aluminium, R – reference)

Preparing Solutions for Immersion

Solution preparation was slightly different, dependant on the experiment. For the electrochemical measurements, sodium chloride was dissolved in deionised water to produce a solution of concentration 0.6 M (3.5 wt%). This concentration is representative of the typical salt concentration in seawater. Into 500 ml of sodium chloride solution, an excess of corrosion inhibitor pigment was added. This mixture was then stirred using a magnetic stirrer and stirrer bar for 24 hours, and then left to settle until cooled to room temperature. The solution was

then transferred to a clean 500 ml volumetric flask through a filter paper to remove any excess solids, a process which was repeated until the solution ran clear (Note: for strontium chromate, this process was repeated until no solid particles could be seen).

For the studies involved SEM-EDX or XPS, sodium chloride was dissolved in deionised water to produce a solution of concentration 0.86 M (5 wt%). 0.1 M solutions of each of the metal chlorides were also produced. A calculated volume of 0.1M metal chloride was added to a 500 ml volumetric flask, and brought up the mark using the sodium chloride solution. Into this solution, an excess of corrosion inhibitor pigment was added. The preparation then proceeded as outlined in the previous paragraph.

Surface Preparations for Electrochemical Studies

For electrochemical studies, firstly the set sample was removed and ground using 80 grit silicon carbide paper until the full area of the metal was exposed to the environment. In the case of the three working electrode set-up, additionally the inner tube circle was also needed to be open and exposed. The sample was then ground using silicon carbide papers of subsequent grades from 160 to 1200 grit. For samples with wires, following surface preparation, the tube encasing the wires was then also heated until flexible and gently bent, allowing for the sample to be exposed vertically during the immersion process.

Electrochemical Measurements (2 Working Electrodes)

For the electrochemical measurements utilising two working electrodes, an ACM Gill AC Weld Tester was used for taking measurements. The ACM Gill AC Weld Tester is a potentiostat with multiple working electrodes connected via zero resistance ammeters. This allows multiple electrodes to be polarised whilst measuring the currents of each electrode independently. An example schematic is shown in Figure 2.3.3.

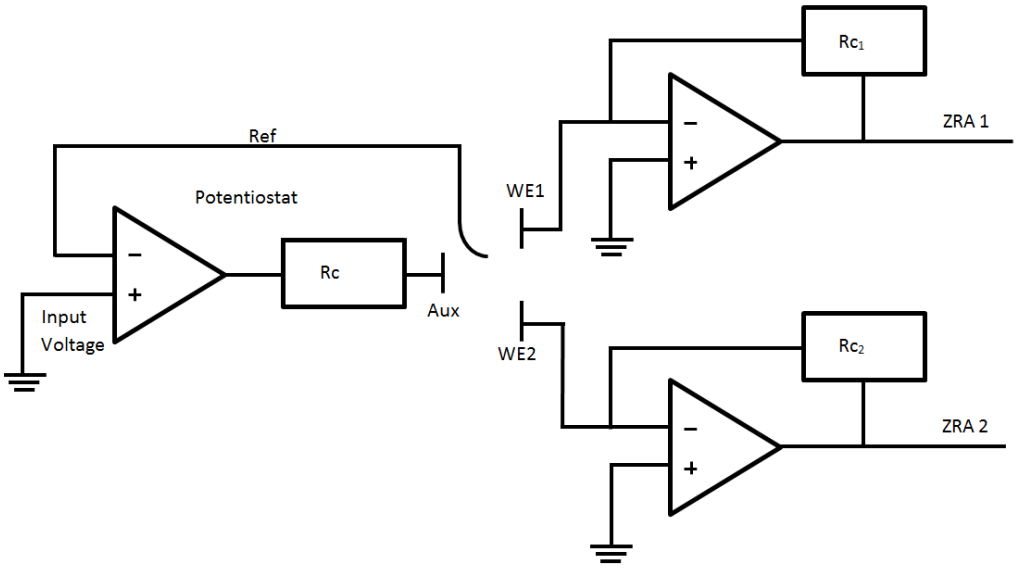

Figure 2.3.3 - An example schematic for the ACM Gill AC Weld Tester utilising two working electrodes

The substrates were attached to the potentiostat intakes denoted as working electrodes 1 and 2. The electrodes were immersed in the relevant solution with a platinum auxiliary electrode and saturated calomel reference electrode. The geometry of the immersion was dependent on the experiment, and a more detailed explanation of the cell geometry is given in the particular chapter section.

The experiment was controlled with the proprietary ACM potentiostat software. The standard experimental procedure in this case used the “Weld Impedance” functionality. An impedance measurement was taken every two hours with the experimental parameters using a frequency range of 0.01 Hz to 10 MHz and perturbation amplitude of 10 mV from the measured coupled corrosion potential. Following an impedance measurement, the procedure used the “current/voltage” functionality to ensure the metals remained at the coupled potential. This was then repeated until the experiment had completed the 72 hour observation period. Selected spectra were then taken and analysed using Scriber’s ZView software.

Electrochemical Measurements (3 Working Electrodes)

For the electrochemical measurements utilising three working electrodes, an ACM Gill AC Weld Tester was used for taking measurements. The substrates were attached to the potentiostat intakes denoted as working electrodes 1, 2 and 3. The electrodes were immersed in the relevant solution with a platinum auxiliary electrode and saturated calomel reference electrode. The geometry of the cell was consistent across all experiments utilising three working electrodes, and this set-up is explained in more details in the relevant chapter.

The experiment was controlled with the proprietary ACM potentiostat software. The standard experimental procedure in this case used the "Weld Impedance" functionality. An impedance measurement was taken every two hours with the experimental parameters using a frequency range of 0.01 Hz to 10 MHz and perturbation amplitude of 10 mV from the measured coupled potential of the system. Following an impedance measurement, the procedure used the "current/voltage" functionality to ensure the metals remained at the coupled potential. This was then repeated until the experiment had completed the 72 hour observation period. Following the observation period, a potentiodynamic sweep was then measured. This was a sweep from -1200 mV to -450 mV at a sweep rate of 0.3 mV s^{-1}. Following the completion of the full experiment, selected spectra were then taken and analysed using Scriber's ZView software. Potentiodynamic polarisation curves were exported as plain text and analysed in Origin.

Immersing Samples for Scanning Electron Microscopy

Following surface preparation, samples were immersed in a small amount of sodium chloride solution saturated with inhibitor pigment, with a small amount of additional metal chloride added if the particular experiment required it. The sample was placed at the bottom of the beaker with the exposed surface facing upwards to ensure the sample did not fall and become

covered or partially covered. Immersion lasted for 72 hours, upon which the sample was removed from the solution and washed gently with deionised water. The sample was then dried and placed under dry conditions until it could be analysed using the electron microscope.

Scanning Electron Microscopy and Energy Dispersive X-Ray Spectroscopy

Samples were attached to a metallic stub using conductive carbon adhesive stickers. For samples that had been exposed to electrochemical tests, wires protruded from the substrate sample through the thickness of epoxy resin mounting material, and therefore these wires produced a conductive pathway. For samples that were not exposed to electrochemical testing prior to electron microscopy, a conductive pathway down to the bottom side of the mounting epoxy was produced using silver containing paint. All scanning electron microscope images and EDX spectra were obtained from a Zeiss Evo 50 scanning electron microscope instrument with EDX attachment. Electron microscope images and EDX spectra used an accelerating voltage of 12 keV.

Ex-situ Sample Preparation for X-Ray Photoelectron Spectroscopy

The x-ray photoelectron spectroscopy measurements were taken on a mild steel substrate. Utilising mild steel panels cut to size (2 cm x 1 cm x 0.8 mm), the samples were ground and polished to a mirror finish, on all faces, utilising silicon carbide paper of subsequent grit grades from 400 to 4000, followed by polishing with 3 µm and 0.25 µm diamond suspension paste. A wire was then spot welded to the corner of the largest face. The wire was encased within a plastic tube which was affixed to the sample using a mixture of beeswax and colophony.

The sample was immersed in a solution containing sodium chloride and inhibitor pigments and/or other metal chlorides as appropriate (the formation of these solutions was outlined earlier in the chapter). The sample was attached to a potentiostat (ACM AC Gill Weld Tester or ACM AC Gill Potentiostat) and potentiostatically polarised to the measured couple potential of

a steel and zinc couple, as measured from the EIS measurements for that particular inhibitor, for a period of time (either 30 minutes, 5 hours or 12 hours, dependant on sample).

Following immersion, the sample is gently washed with deionised water and dried. The wire and wax are then removed by cutting the sample with a guillotine. The remaining sample is then covered in aluminium foil and placed in a desiccator until the sample can be analysed.

X-Ray Photoelectron Spectroscopy

For the initial experiments utilising zinc chloride as the metal chloride additive to the solution, the measurements were carried out on a Kratos AXIS Ultra with a monochromated Al x-ray source at the University of Manchester. Samples were placed on a sample bar and loaded into the instrument chamber. Upon depressurisation of the chamber, each of the samples was focussed using the C1s and O1s peaks. A survey spectrum was taken to determine the presence of elements of interest. Using this, relevant areas for high resolution spectra could be decided and programmed into the scan.

For the samples utilising metal chlorides other than zinc chloride, the measurements were carried out on the Kratos AXIS Nova with a monochromated Al x-ray source at the AkzoNobel site in Sassenheim. Following loading samples onto the sample plate, the process followed was as described for the Kratos AXIS Ultra. In both cases, spectra were analysed using the CasaXPS software package.

Chapter 3

Electrochemical Impedance with Segmented Electrodes for Modelling Zinc Coated Steel

3.1 Introduction

As mentioned previously, in the literature review section, the environmental and legislative issues surrounding hexavalent chromium compounds have resulted in a need for research into chromate replacement inhibitor pigments. Unfortunately, these current chromate replacements do not possess the same level of effectiveness and versatility. Furthermore, the lack of mechanistic knowledge surrounding many of these pigments means the coatings industry relies heavily on anecdotal evidence and long-term tests to determine paint formulations.

One commonly used electrochemical method for analysing inhibitor mechanisms, especially when contained in coatings, is electrochemical impedance spectroscopy (EIS). Through observing the changes in how a system interacts with sinusoidal electrochemical perturbation, various aspects of a system can be interpreted, including mechanistic information through the analysis of time constants[1] and efficiency or effectiveness of each mechanism through comparison of the analysed numbers[2]. However, by its nature EIS can only provide a representation of the macroscopic system. Of particular concern, when dealing with complex multiple metal systems, is that any areas where the impedance is lower will dominate the obtained spectra, producing results that are not fully representative of the whole system. Therefore developing an understanding of the electrochemistry of multi-phase alloys and multiple metal systems necessitates an alternative approach.

One such approach that can be proposed is the use of spatially separated electrodes that are attached to individual zero-resistance ammeters and then coupled through an overarching potentiostat. Dawson et al[3] have previously described the use of multiple zero resistance ammeters grounded through a singular potentiostat as a method capable of measuring the response of individual electrodes as part of an overall coupled system. A simplified schematic for this electrochemical set-up can be seen in Figure 2.3.3[4] (Methodology, Page 94) . This particular methodology allows a number of different electrochemical experiments to be

performed on a set of segmented electrodes in order to determine information about each individual segment in the system.

However, whilst this spatially separated electrode set up has been known for some time, literature describing the practical application of this technique is scarce. Woollam et al[4] have used the technique to determine the differences seen in erosion corrosion between electrode surfaces that were are nominally identical. Segmented electrode electrochemical techniques have also found use in the analysis of welded materials [5–9], whereby the weld is segmented into its component parts (i.e. parent metal, heat affected zone and fusion zone) and the influence of the corrosive environment as well as inhibition can then be studied on the individual components of the welded system.

Much previous literature in this domain mainly concentrates on weld materials or nominally similar materials and does not touch on the potential application of the technique for use in macro-galvanic cells with distinct metals, such as galvanised steel.

This chapter will concentrate on analysing the applicability of using electrochemical impedance with segmented electrodes within a macro-galvanic system. It will aim to verify the use of this methodology by utilising inhibitor systems in which the mechanism of action is better understood. Electrochemical impedance with segmented electrodes will then be applied to modified aluminium polyphosphate corrosion inhibitors, a prevailing class of chromate replacement pigments, in an attempt to understand better their mode of action.

3.2 Verification of Technique

3.2.1 Introduction

The aim of this preliminary study was to determine the feasibility of investigating corrosion inhibition on complex multiple metal systems through a novel application of a previously developed segmented electrode technique designed for observing welds. This was to be done through testing inhibitor pigments which have behaviours that have previously been reported

in the literature for galvanised steel with a simple zinc coating. To obtain results in these tests that were indicative of zinc coated steel, a simplified model was devised. The simplifications to the model were as follows:

- Separate electrodes of pure steel and pure zinc were to be used as an analogue for the components of galvanised steel
- The steel and zinc electrodes were of the same size and geometry to minimize any geometrical effects
- The steel and zinc electrodes were to be spatially separated on the macro scale to minimize interference through local chemistry effects.

In doing this, it was hoped that the use of electrochemical impedance with segmented electrode could be verified as a potential method for understanding the inhibition process on various components of a complex multiple metal system.

3.2.2 Experimental

Experiments concentrated on following the effects of dissolved corrosion inhibitors on the anodic (zinc) and cathodic (steel) electrodes simulating the cut edge of a galvanised steel sheet. 1 cm^2 samples of mild steel (Q-Labs, as received) and zinc (Goodfellow, as received) were separately mounted in epoxy resin, and ground using incremental grades of silicon carbide abrasive discs, up to and including 1200 grade, so as to leave a single flat surface exposed to the environment.

The zinc and steel were then immersed in a 3.5 weight % (approximately 0.6M) sodium chloride solution containing leached species from an inhibitor pigment. Thus, saturated solutions of relevant inhibitors were prepared by introducing approximately 2 g of solid into 1 L of electrolyte, and stirred continuously for 24 h. The solution was then filtered to remove any remaining excess solid from the solution. The concentrations of inhibitive species in solution were not measured in this work as the solubility comparison between pigments was not

deemed to be of interest at this stage as the differences are likely to be similar from real world pigment leaching.

A four-electrode cell was used and attached to an ACM AC Weld Test instrument, utilising steel and zinc as two working electrodes, a saturated calomel reference electrode and a platinum counter electrode. The electrode arrangement was as displayed in Figure 3.2.1. The system was at laboratory temperature (18-21°C) monitored for 72 h, with electrochemical impedance measurements taken every 2 h for the duration of the experiment. The impedance measurements were taken in the frequency range of 10,000 Hz to 0.01 Hz with a signal amplitude of 10 mV. These measurements were taken at the mixed potential of the iron and zinc couple. This was determined automatically by the potentiostat immediately before the spectrum was taken.

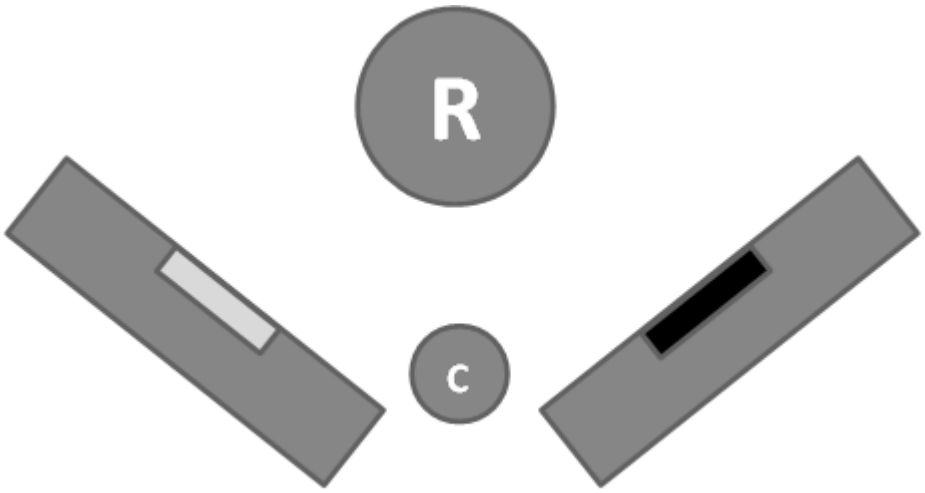

Figure 3.2.1 - The orientation of electrodes as used in the segmented electrode impedance tests (R - saturated calomel reference electrode, C - platinum counter electrode)

3.2.3 Results

EIS data for uninhibited steel and zinc are shown in Figure 3.2.2, while Figure 3.2.3 shows similar data for steel and zinc in saturated strontium chromate, Figure 3.2.4 in saturated calcium ion-exchanged silica, Figure 3.2.5 in saturated zinc molyphosphate and Figure 3.2.6 in a mixture of saturated calcium ion-exchanged silica and zinc molyphosphate. It is re-stated

here that these measurements are carried out at the overall mixed couple potential and the steel is therefore polarised net cathodically and the zinc polarised net anodically. The graphs shown are from representative data that are, post processing, shown to have approximately median values once anomalous results have been removed.

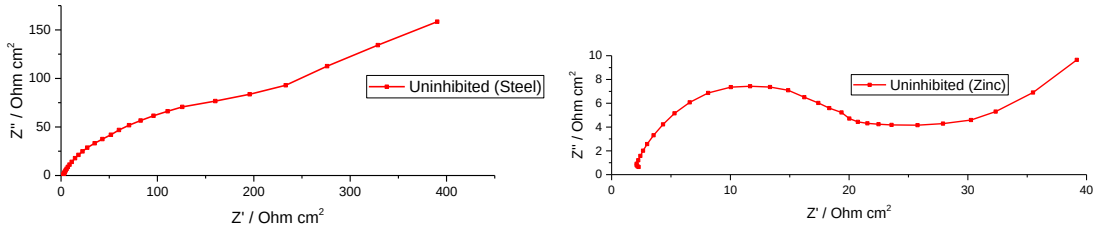

Figure 3.2.2 - Nyquist plots obtained for the blank, uninhibited 0.6M sodium chloride solution for steel (cathodic, left) and zinc (right) electrodes of equal area.

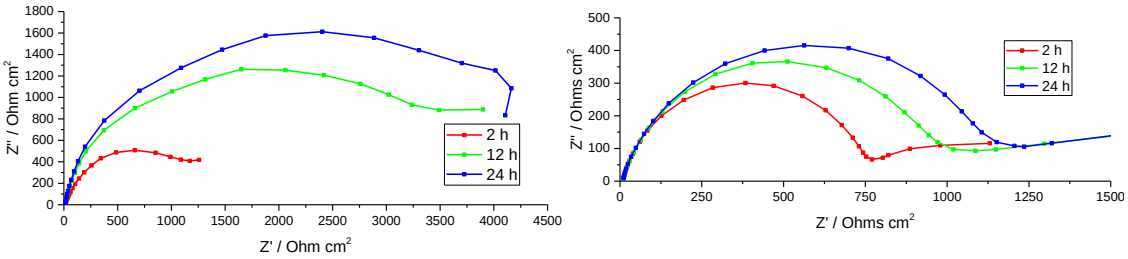

Figure 3.2.3 - Nyquist plots obtained for the strontium chromate inhibited 0.6M sodium chloride solution for steel (cathodic, left) and zinc (right) electrodes of equal area.

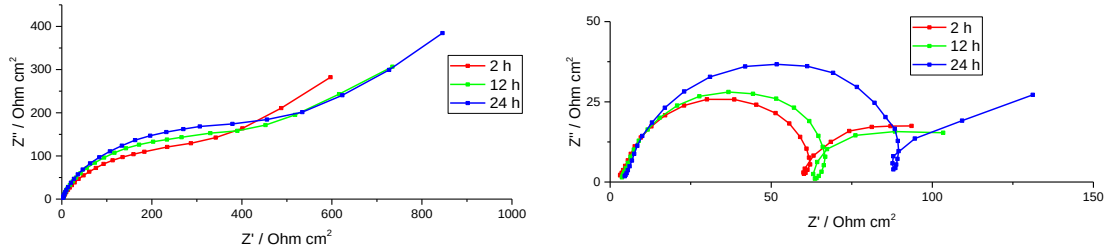

Figure 3.2.4 - Nyquist plots obtained for the calcium exchanged silica inhibited 0.6M sodium chloride solution for steel (cathodic, left) and zinc (right) electrodes of equal area.

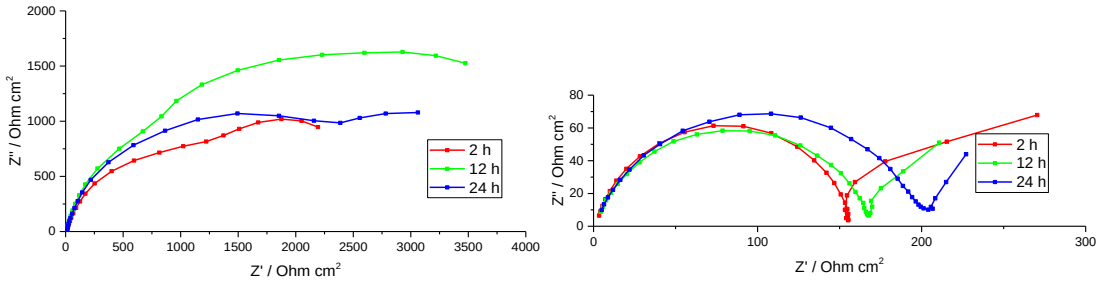

Figure 3.2.5 - Nyquist plots obtained for the zinc molyphosphate inhibited 0.6M sodium chloride solution for steel (cathodic, left) and zinc (anodic, right)

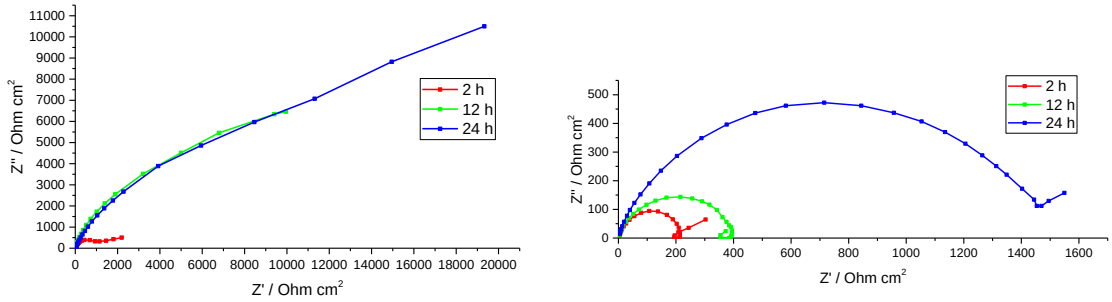

Figure 3.2.6 - Nyquist plots obtained for the calcium exchanged silica/zinc molyphosphate mixture inhibited 0.6M sodium chloride solution for steel (cathodic, left) and zinc (anodic, right)

3.2.4 Discussion

Interpretation of Results

The charge transfer resistance was obtained through the use of equivalent circuit analysis of the impedance plots. The equivalent circuit analysis utilised a number of equivalent circuits to determine the values of the particular elements of each time constant. A justification of the utilised equivalent circuits for the steel and zinc electrodes is presented later in the discussion. Where two time constants are evident in the spectra, the higher frequency element is taken as a simple analogue of the corrosion process. By assuming that the charge transfer resistance is approximately inversely proportional to the corrosion rate, the inhibitor efficiency (IE) can be estimated from the ratio of the charge transfer resistance of the inhibited sample (R_{CT}) to that of the uninhibited sample (R_{CTo}), equation 1:

$$IE\ (\%) = (1 - \frac{R_{CT_0}}{R_{CT}}) \times 100 \quad \ldots. (1)$$

Table 3.2-1 gives the charge transfer resistances obtained through the equivalent circuit analysis of the obtained impedance spectra. Table 3.2-2 gives the calculated inhibitor efficiencies for all inhibitor pigments studied in this section.

		Charge Transfer Resistance (R_{ct}) / Ohm cm^2				
	Time	*Uninhibited*	*Zinc Molyphosphate*	*Calcium Exchanged Silica*	*Mixture*	*Strontium Chromate*
Steel	*2 h*	650	1900	690	2200	3800
	12 h		3400	1600	3600	3500
	24 h		2600	1700	3800	4500
Zinc	*2 h*	45	63	46	130	760
	12 h		71	43	140	980
	24 h		98	45	150	1100

Table 3.2-1 - Obtained charge transfer resistances at selected time intervals for inhibited samples, and the value obtained for the initial uninhibited sample. Fitting errors for the values given were plus/minus less than 3%.

		Inhibitor Efficiency / %			
	Time	*ZMP*	*CES*	*MIX*	*CRO*
Steel	*2h*	65	5	71	83
	12h	81	59	82	81
	24h	75	62	83	85
Zinc	*2h*	29	3	65	94
	12h	37	-5	68	96
	24h	55	1	71	96

Table 3.2-2 - Calculated inhibitor efficiency percentages for each inhibitor system tested at selected time intervals (ZMP – Zinc molyphosphate, CES – calcium exchanged silica, MIX – mixture of calcium exchanged silica and zinc molyphosphate, CRO – strontium chromate)

In previous studies[10,11], chromate has been found to provide corrosion protection through a mixed-action inhibitor mechanism, acting as an anodic inhibitor for zinc dissolution and as a cathodic inhibitor for steel. The results obtained in this set of experiments show high inhibitor efficiency on both steel and zinc that begins at the earliest time frame analysed (2 hours). The

relatively high initial anodic inhibition is consistent with a proposed mechanism that requires chromate conversion to Cr (III) for cathodic inhibition.

Calcium exchanged silica is known to act on the cathodic process by precipitation of a solid film[12] and this is shown clearly here where only the steel component of the couple is inhibited, which is consistent with previous evidence in the literature [13], Notably, this inhibition was very limited after only 2 h exposure but increased to a more reasonable value after 24 h. Zinc molyphosphate shows significant cathodic inhibition with a low level of anodic inhibition also evident. The reports of cathodic inhibition are consistent with observations made by previous reports[13,14]. The polarisation curves presented by Zin et al[14] also appear to be shifted in the positive direction, suggesting that a degree of anodic protection may be evident. This, again, would be consistent with the data obtained in the current study.

A mixture of calcium exchanged silica and zinc molyphosphate inhibitor pigments has been previously researched as a potential chromate replacement. Studies have determined that synergistic interactions between the two produce an inhibition mechanism which affects both anodic and cathodic processes[13,15]. Experiments carried out on the pigment mixture in this study showed a noticeable improvement in inhibitor efficiency over the component parts. This is particularly evident when looking at the anodic inhibition of the zinc surface, where the inhibitive efficiency approaches that of the steel.

Comparing these results, it is clear that chromate exhibits superior inhibition to all of the other inhibitor systems studied. The zinc molyphosphate/calcium exchanged silica mixture shows inhibition levels that approach the efficiency of chromate. Both of these comparative observations can be considered to be consistent with the previous work of Zin et al[13]. Furthermore, the inhibition exhibited by zinc molyphosphate, when compared to calcium exchanged silica, is greatly superior. This observation is also consistent with previously published works[14].

Notably this novel experimental methodology, using EIS at the coupled potential of the mixed metal system, produces the same relative findings as other approaches but does so more rapidly. It has also been shown that, even with relatively crude analysis of the data, this technique can correctly and quantitatively identify whether the inhibitor species of interest affects only the anode, only the cathode, or both anode and cathode.

Justification of Equivalent Circuits

As mentioned in the introductory chapters, the interpretation of electrochemical impedance spectra requires the utilisation of equivalent circuits with sufficient fitting parameters to determine the overall meaning of the spectra. Furthermore, the makeup of the equivalent circuits must also be justifiable, in that the components and structure of the circuit must be representative of physical processes that could be, and are likely to be, taking place on the surface.

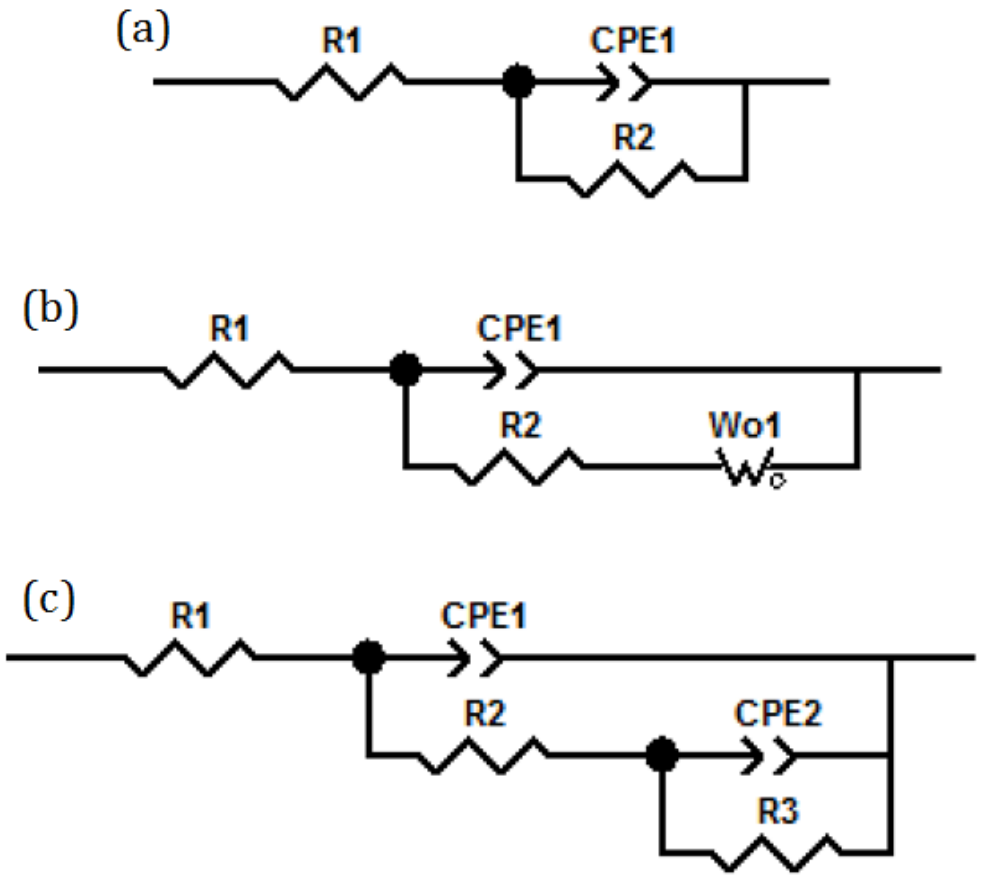

Figure 3.2.7 - Representative equivalent circuits used for the analysis of electrochemical impedance obtained on the surface of steel – (a) a simplified Randles circuit, (b) modified Randles circuit and (c) an equivalent circuit containing two time constants

In Figure 3.2.7, the representative equivalent circuits that were utilised across this study (and further studies presented in this chapter) for the analysis of the surface of steel samples are shown. These are the simplest possible circuits that are consistent with the expected electrochemistry. In all of the circuits, an initial resistor, R_{sol} (R1) can be seen. This is the resistance that arises due to the resistive solution that is situated between the working and reference electrodes, and is therefore more indicative of the set-up as opposed to the system itself.

The first time constant, which is, again, present across all samples measured, is that which represents the corrosion process. The elements seen in Figure 3.2.7 (a) are those which are representative of the corrosion process, where the resistor (R2) represents the charge transfer

resistance, whereas the constant phase element represents the capacitive double layer (normally C_{DL}, seen in the diagrams as CPE1). The use of the constant phase element over the more traditional capacitor represents the imperfect nature of the system response.

Another time constant also appears in several of the spectra, and is dealt with using the addition seen in Figure 3.2.7 (b). This is the Warburg impedance (Wo1) which is used in the circuit to denote diffusion related phenomena. In the case of the cathode, the oxygen reduction reaction is expected to a dominant pathway, and therefore this can be rate limited by the diffusion of oxygen toward the system surface, and hence the presence of Warburg behaviour.

A secondary, non-diffusion related time constant is seen in some of the observed spectra. This is seen as a second parallel set containing a resistor (R3) and a constant phase elements (CPE2). These elements are representative of a deposited layer, and are also often seen in the analysis of coated materials. It can therefore be suggested that the resistor is indicative of the coating resistance of the deposition, whereas the constant phase element is representative of the capacitive behaviour of the deposit. Whilst this is a useful distinction in determining the mechanism and deposition kinetics of the inhibitors, it is not an important consideration for the calculation of the inhibitor efficiency.

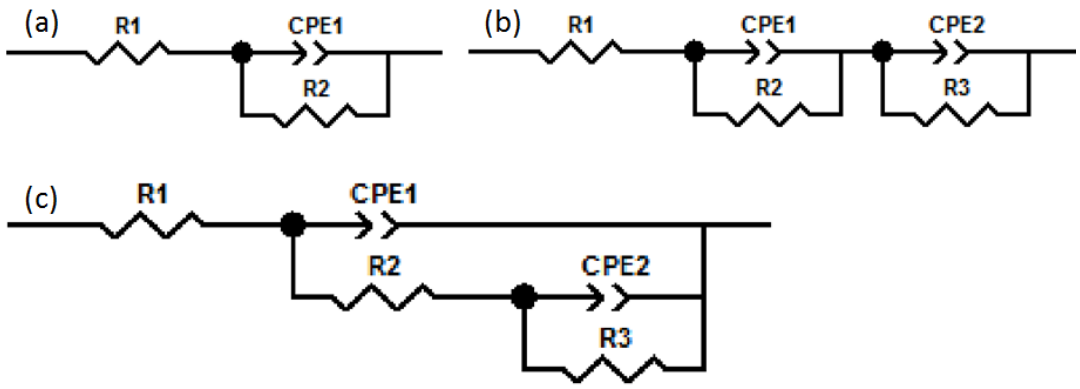

Figure 3.2.8 - Representative equivalent circuits used for the analysis of electrochemical impedance obtained on the surface of zinc.

Figure 3.2.8 shows each of the equivalent circuits that have been utilised for the analysis of zinc surfaces throughout this body of work. Circuits b and c represent the simplest representations of two discrete homogeneous layers and one heterogeneous layer respectively[16]. A constant phase element has been used in place of a capacitor to allow for non-ideal behaviour. The calculated n-values ranged from 0.78 to 0.91

The electrochemical impedance study presented herein initially showed the presence of two time constants, where the time constant present at lower frequencies is suggested to correspond to zinc polyphosphate deposition. We propose that this layer is subsequently broken down, leading to the suppression of that time constant. For longer exposure times, another second time constant becomes evident at lower frequencies, indicating further coverage.

The presence of an inductive loop in some of the spectra can be modelled, however, it is considered to be more likely that this is due to shifts in the mixed electrode potential that can have a large effect on some values obtained, particularly in the low frequency areas.

3.2.5 Conclusions

The action of various inhibitors was determined using a segmented electrode technique. The observed behaviour was then compared with that which has been previously reported. Through equivalent circuit analysis of the electrochemical impedance spectra obtained, the following conclusions could be drawn:

- Strontium chromate acts as a mixed action inhibitor with an initial efficiency superior to that of the other inhibitors tested
- Calcium exchanged silica shows low initial inhibitor efficiency, with cathodic inhibition evident in later tests.
- Zinc molyphosphate shows mainly cathodic inhibition, with evidence of anodic inhibition possible
- Mixing zinc molyphosphate and calcium exchanged silica inhibitors results in mixed inhibition that is superior to the component parts, and approaches the inhibitor efficiency shown by chromate.
- The results obtained for each of the inhibitor pigments studied appears consistent with the behaviours as previously described in the literature

With this, it can be suggested that the segmented electrode technique may have potential for following the corrosion of complex multiple metal systems. Furthermore, the ability to determine processes occurring separately on both the cathodic and anodic surfaces of a macro-galvanic cell allows for a simple and rapid classification of inhibitor actions and mechanisms.

3.3 Application of Segmented Electrode Technique to Chromate Replacement Pigments - Polyphosphates

3.3.1 Introduction

The aim of this study was to utilise electrochemical impedance with segmented electrodes, a technique verified in the previous section of this chapter, to determine the behaviour of anti-corrosive pigments that are proposed as potential replacements for hexavalent chromium compounds. Anecdotal evidence provided by the industrial sponsors of this project suggested that the modified aluminium polyphosphate inhibitors show differing levels of corrosion performance depending on the composition of the underlying substrate.

By using the technique in this way, it was suggested that the inhibitor behaviour over the two distinct areas can be measured, leading to a greater understanding of how the pigments work with a simple zinc and steel couple mimicking galvanised steel. This would form the beginning steps toward the fundamental understanding of the inhibitors that would be required to explain the changes in behaviour when used on different alloy systems.

3.3.2 Experimental

The set-up for this experiment was identical to that as described in section 2.1.2. using modified aluminium polyphosphate pigments. The pigments that were leached to form saturated solutions were modified strontium aluminium polyphosphate (SAPP, Heubach, as received), calcium aluminium polyphosphate (CAPP, Heubach, as received) and magnesium aluminium polyphosphate (MAPP, SNCZ, as received). Concentrations were not measured during this study as the study was designed to determine the effects of inhibitors at high concentrations, similar to what would be expected with pigment leaching into a small volume (e.g. a raindrop).

3.3.3 Results

Strontium Aluminium Polyphosphate

The charge transfer resistance was obtained through the use of equivalent circuit analysis of electrochemical impedance plots. The equivalent circuit analysis employed a simplified

Randles circuit, shown in Figure 1.6.6 (Introduction, Page 65), to determine the values of the particular elements of each time constant. In cases where two time constants appear, the element situated within the higher frequencies is taken to be a simple analogue of the corrosion process. The inhibitor efficiency can be estimated by assuming that the charge transfer resistance is approximately inversely proportional to the corrosion rate. The inhibitor efficiency (IE) can be estimated from the ratio of the charge transfer resistance of the inhibited sample (R_{CT}) to that of the uninhibited sample (R_{CT_0}). The data for an uninhibited sample is taken from the previously presented work in section 3.1.2.

A numerical value can be assigned to the inhibitor efficiency through the application of Equation 1 to the obtained charge transfer resistance[17].

$$IE\ (\%) = \left(1 - \frac{R_{CT_0}}{R_{CT}}\right) \times 100 \qquad (1)$$

Figure 3.3.1 and Figure 3.3.2 show a selection of the Nyquist plots that were obtained on steel and zinc sides respectively following exposure to SAPP saturated salt solutions for 72 h.

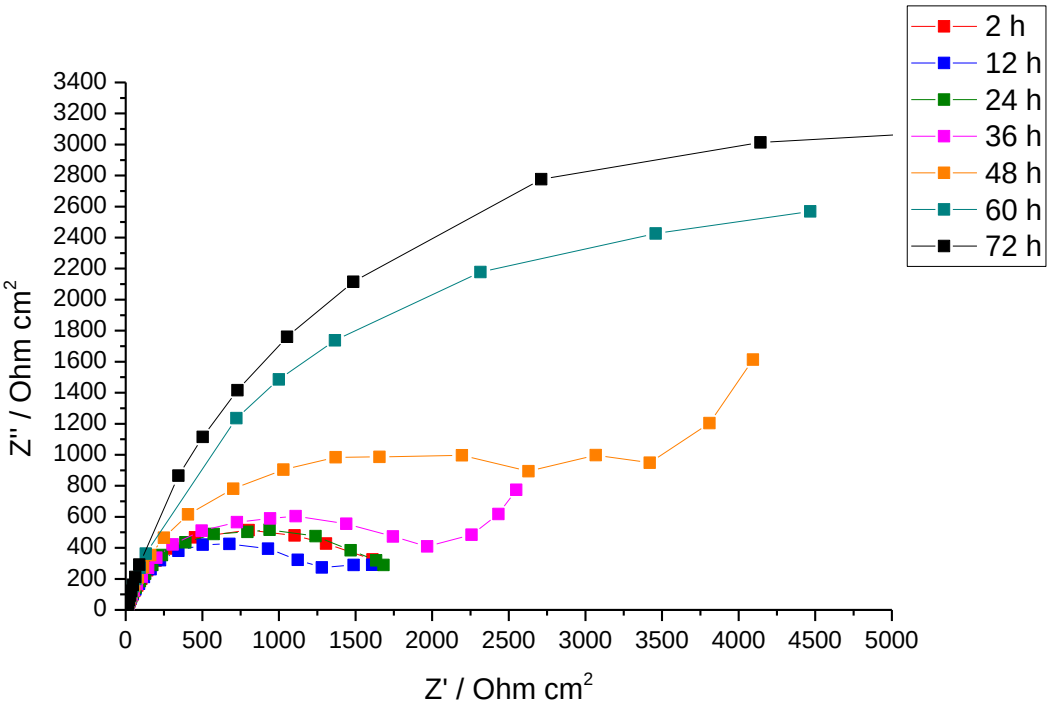

Figure 3.3.1 - Selected Nyquist plots obtained for the strontium aluminium polyphosphate inhibited 0.6M sodium chloride solution immersed steel sample when coupled to zinc over a 72 hour period

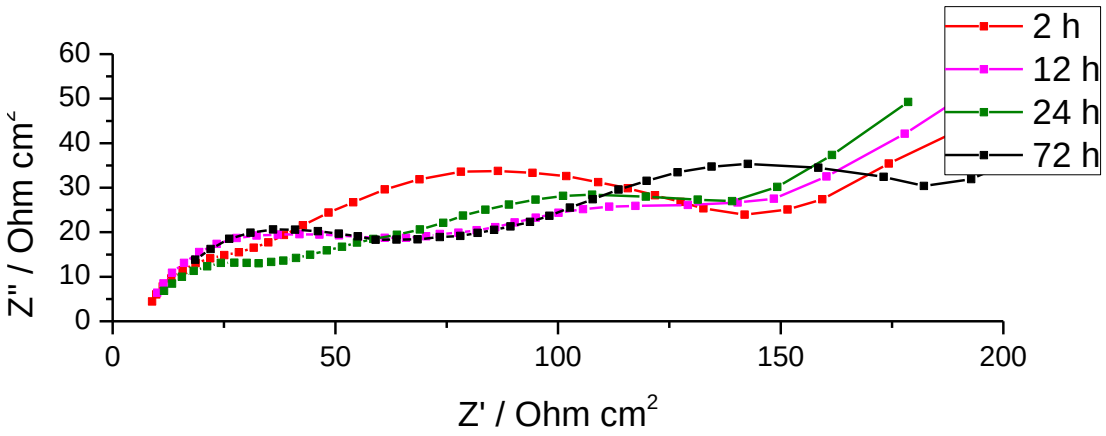

Figure 3.3.2 - Selected Nyquist plots obtained for the strontium aluminium polyphosphate inhibited 0.6M sodium chloride solution immersed zinc sample when coupled to steel over a 72 hour period

From Figure 3.3.1, it can be seen that the steel electrode exhibits only a single time constant, as expected due to the extent of cathodic polarisation. An initial reduction in the magnitude of this time constant, visible as the major semi-circle within the Nyquist plot, indicates a reduction in the charge transfer resistance and thus a reduction in the observed inhibitor efficiency. This is followed by a recovery and then increase of the charge transfer resistance, consistent with an improvement in corrosion inhibition following an induction period, this is clearly observed by comparison of the 12 and 24 hour exposure plots. This effect is clearly evident for the steel electrode, and whilst it is discernible on the zinc electrode, after a later onset, the effect is less prominent.

Calcium Aluminium Polyphosphate

Figure 3.3.3 and Figure 3.3.4 show a selection of the Nyquist plots that were obtained on steel and zinc sides respectively following exposure to CAPP saturated salt solutions for 72 h.

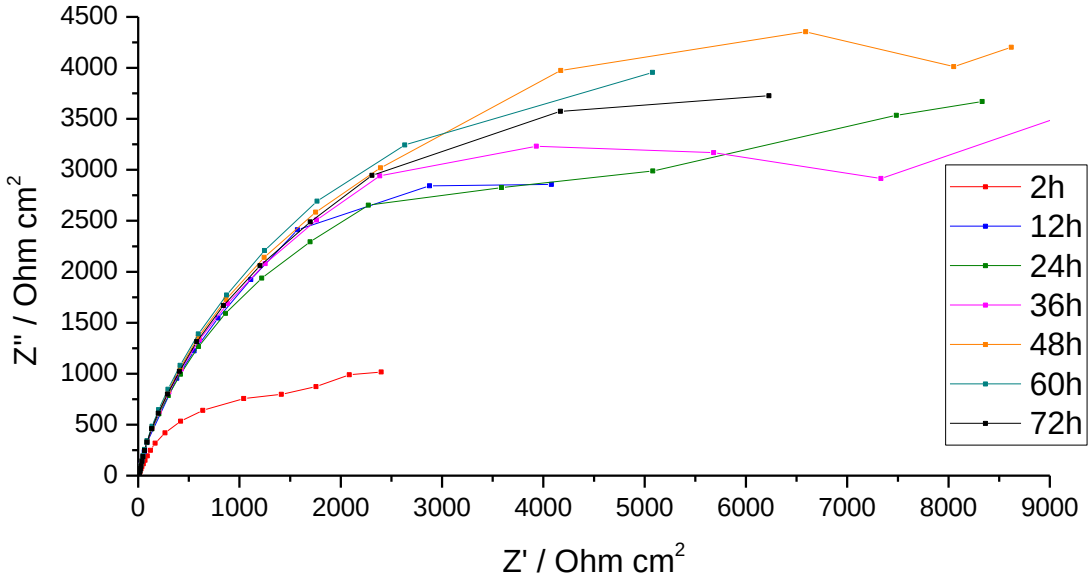

Figure 3.3.3 - Selected Nyquist plots obtained for steel in the electrochemical impedance with segmented electrodes experiment when coupled to zinc over a 72 hour period

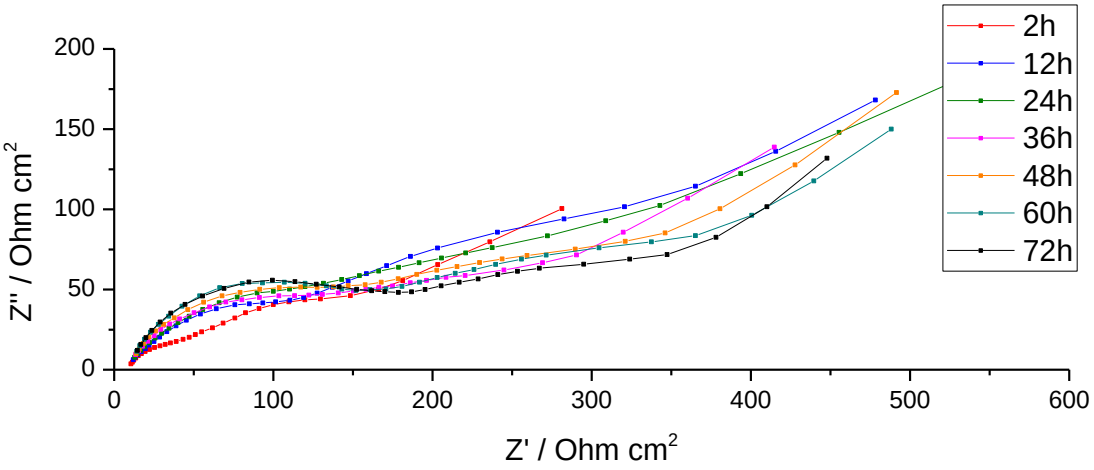

Figure 3.3.4 - Selected Nyquist plots obtained for zinc in the electrochemical impedance with segmented electrodes experiment when coupled to steel over a 72 hour period

From Figure 3.3.3, it can be seen that the steel electrode exhibits only a single time constant, as expected due to the extent of cathodic polarisation. A second time constant is possibly visible in the lower frequency regions, with a tail-like feature present. However, this secondary time constant is too small for any meaningful interpretation. Unlike what is seen with the strontium aluminium polyphosphate inhibitor pigment, the magnitude of the time constant seen in the Nyquist plot shows an immediate increase, suggesting that the action of the inhibitor is nominally immediate. A minor drop in the measured charge transfer resistance is seen following a maximum value at around 48 hours.

Similarly, Figure 3.3.4 shows that the zinc electrode appears to display an inhibition profile that increases consistently from the initial measurement through the final measurement. This suggests that the calcium aluminium polyphosphate pigment is inhibiting the zinc surface, with the efficiency in which this inhibition occurs improving consistently throughout the exposure time. The extent of inhibition, or the overall improvement in inhibition throughout the test, appears to be more significant for the steel surface than that of the zinc surface.

Magnesium Aluminium Polyphosphate

Figure 3.3.5 and Figure 3.3.6 show a selection of the Nyquist plots that were obtained on steel and zinc sides respectively following exposure to PAM saturated salt solutions for 72 h.

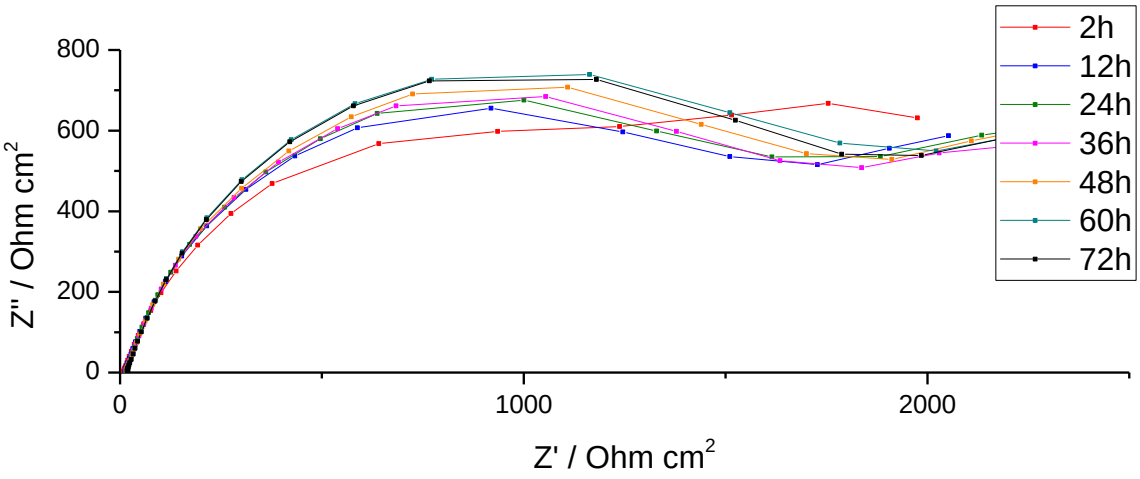

Figure 3.3.5 - Selected Nyquist plots obtained for steel in the electrochemical impedance with segmented electrodes experiment when coupled to zinc over a 72 hour period

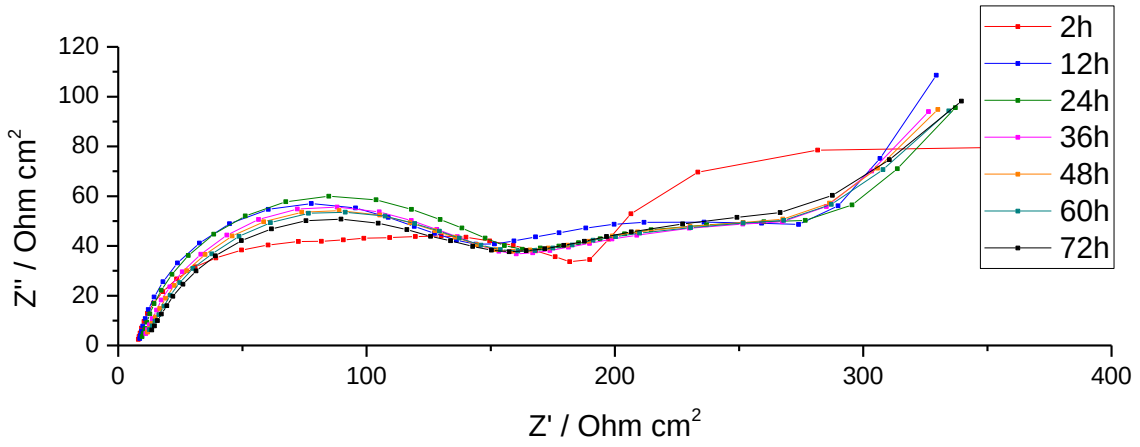

Figure 3.3.6 - Selected Nyquist plots obtained for zinc in the electrochemical impedance with segmented electrodes experiment when coupled to steel over a 72 hour period

From Figure 3.3.5, it can be seen that the steel electrode exhibits only a single time constant, as expected due to the extent of cathodic polarisation. A second time constant is possibly

visible in the lower frequency regions, with a tail-like feature present. However, much like the impedance measurements for the previously analysed inhibitor pigments, this secondary time constant is too small for any meaningful interpretation.

The Nyquist plots for the magnesium aluminium polyphosphate inhibitor pigment show similarities to the inhibition profile exhibited by calcium aluminium polyphosphate, where a constant increase is evident from the initial measurement taken after 2 hours of exposure. Therefore, it is suggested that the inhibition proceeds from the initial exposure. The increase in calculated charge transfer resistance appears to halt following the 60 hours exposure measurement, suggesting that the inhibition on the steel surface hits a maximum value after this length of exposure. Overall, the difference between the initial and final impedance measurements taken appears to be significantly lower than that of the other two inhibitor pigments observed.

Figure 3.3.6 shows that the zinc electrode appears to display an inhibition profile that has initial increases from the initial measurement for the first 24 hours of exposure, which is followed by small decreases throughout the remaining measurements. This suggests that whilst the magnesium aluminium polyphosphate pigment is inhibiting the zinc surface, the effectiveness of this inhibition declines in longer exposure times. The extent of inhibition, or the overall improvement in inhibition throughout the test, appears to be more significant for the steel surface than that of the zinc surface, which has been a consistent observation across all polyphosphate inhibitors examined in this set of experiments.

The impedances obtained from the zinc electrodes show two measurable time constants. Of these, the lower frequency process appears to be stable, with very little effect shown from the inhibition process. However, this time constant is seen to be different for the 2 hour exposure spectra, which may suggest that the system has not have reached equilibrium following this length of exposure.

3.3.4 Discussion

Initial Findings

From initial observations of the obtained impedance plots, some information can be gathered regarding the behaviour of the inhibitor pigments. Calcium aluminium polyphosphate exhibits an immediately prevalent, and relatively consistent, efficiency on both the zinc and steel surface. Similarly, magnesium aluminium polyphosphate also exhibits inhibition which is noticeable within the earliest exposure times measured and remains relatively consistent throughout the test.

Strontium aluminium polyphosphate shows a delay before it provides a levels of inhibition that matches that of the other two inhibitor pigments, particularly on the steel surface. This is seen as an initial drop of inhibitor efficiency between the 2 hour and 12 hour exposure times, and is followed by substantial increases in the calculated inhibitor efficiency after 24 hours exposure. This phenomenon is also demonstrable in the measurements obtained on the zinc surface too.

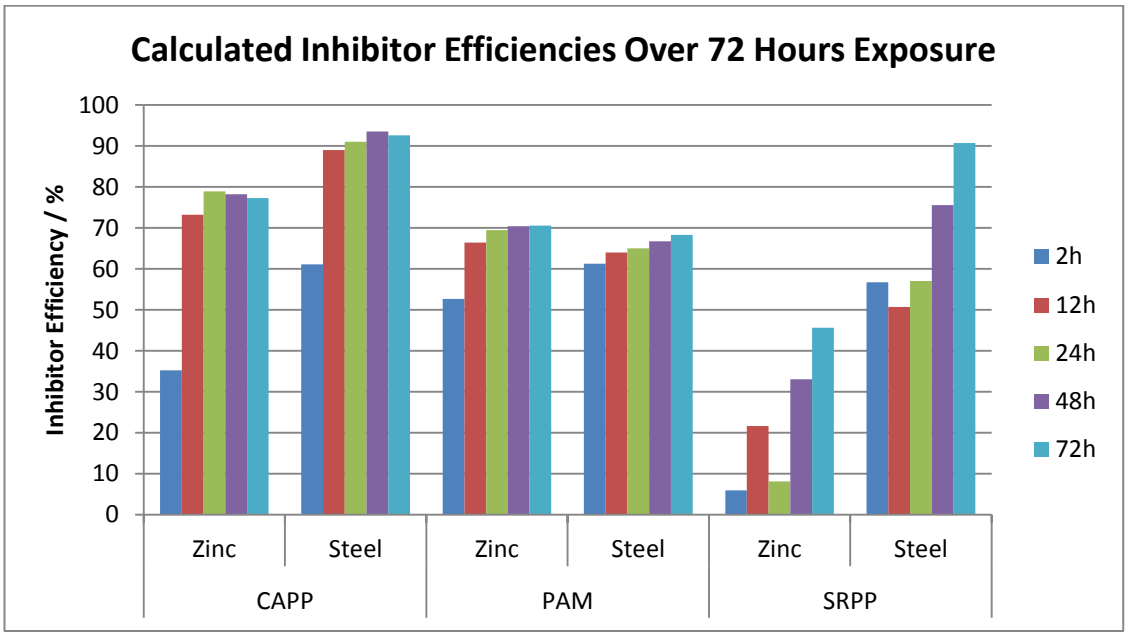

Figure 3.3.7 - Graph displaying calculated inhibitor efficiencies for the modified aluminium polyphosphate inhibitors on the surfaces of coupled steel and zinc

A comparison of the inhibitor efficiencies, on both the steel and zinc surfaces, at a number of different exposure times for each of the polyphosphate inhibitor pigments observed is shown in Figure 3.3.7.

In the initial inhibition stages, taken in these experiments as following 2 hours exposure, it can be seen that magnesium aluminium polyphosphate is the most effective inhibitor measured, with a notable superiority in inhibiting the zinc surface over the other two inhibitor pigments. Calcium aluminium polyphosphate exhibits near identical levels of corrosion inhibition for the steel surface, when compared to magnesium aluminium polyphosphate, but lower zinc surface inhibition, at approximately 30% efficiency. Strontium aluminium polyphosphate shows lesser, but similar, steel surface inhibition at early stages of exposure. Initially, the results also suggest that it does not exert any notable inhibitive action on the zinc surface.

The calculations suggest that magnesium aluminium polyphosphate is the pigment which is the quickest to reach the maximum inhibitor efficiency, with only minor increases visible on the steel surface after the initial results, and the same seen on the zinc surface following 12 hours exposure. Calcium aluminium polyphosphate appears to be roughly consistent after 12 hours exposure across both surfaces, whereas strontium aluminium polyphosphate does not give an indication of reaching the highest level of inhibition it is capable of within the 72 hour exposure time.

This suggests that magnesium aluminium polyphosphate has the quickest mechanism of action of the three polyphosphate pigments measured, with strontium aluminium polyphosphate being the slowest, and even showing negative inhibition trends in the earlier exposure times. The reasons behind this will be discussed later in this section. However, whilst magnesium aluminium polyphosphate can be considered to be the fastest, both calcium aluminium polyphosphate and strontium aluminium polyphosphate are capable of providing greater inhibition to the steel surface over longer exposure periods. Calcium aluminium polyphosphate

is also capable of providing superior zinc surface corrosion inhibition, but strontium aluminium polyphosphate displays relatively weak zinc inhibition throughout the test period when compared to the other pigments tested.

Strontium Aluminium Polyphosphate Inhibition Profile

As mentioned previously, exposure to solutions saturated with the strontium aluminium polyphosphate inhibitor pigment exhibited corrosion behaviour that was distinctly different than those measured for the other polyphosphate inhibitor pigments that were used. A reproducible and not insignificant delay in the increasing of the calculated charge transfer resistance was observed in the electrochemical impedance for both the steel and zinc electrodes, suggesting a delay in inhibitor action. It was also noted that the delay in inhibition was not equal between the two electrodes, with inhibition on the steel surface proceeding before it is observed on the zinc surface.

One theory for the observed delay of inhibition on the steel surface relates to the secondary counter ion in the pigment. If the “metallic aluminium polyphosphate” pigment exists as a modified aluminium polyphosphate, meaning that upon dissolution, this is released as aluminium polyphosphate and the secondary counter ion is released as the metallic cation. In the case of the three polyphosphate inhibitors, this would be as Sr^{2+}, Ca^{2+} and Mg^{2+}. It could be suggested that ion exchange between the aluminium polyphosphate and the metallic cationic species could occur in solution. It has been previously reported in the literature[18] that the presence of divalent cationic species in solution improves the inhibition of mild steel by polyphosphates.

In the case of these polyphosphate inhibitors, it is suggested that presence of a secondary species is essential for an effective inhibitor action. In analysing the results from lower exposure times, it can be proposed that calcium and magnesium are divalent cationic species

that can produce effective polyphosphate inhibition. Conversely, the results suggest that the presence of strontium is not sufficient to provide the same effect.

However, this alone does not explain the significant improvement in the inhibitor efficiency that is observed following longer exposure times, as it is unlikely that inhibition of this effectiveness would begin after a delay without another process occurring. It is therefore suggested that the presence of another cationic species, namely Zn^{2+} produced by anodic dissolution of the zinc electrode, acts with the polyphosphate to produce effective inhibition. In this case, the delay between first exposure and the action of the inhibitor can be explained through firstly the extended diffusion pathway between the two working electrodes, and secondly a minimum concentration requirement of the cation at the surface of the steel for noticeable inhibitor efficiency.

The Usage of Polyphosphates in Galvanised Steel

The usage of hexavalent chromium compounds in galvanised steel can be considered to be driven by the attributes that those compounds are known to have. As previously mentioned in the literature review chapter, the main benefits of using chromium based anticorrosive pigments can be considered to be a high efficacy, unrivalled flexibility and a rapid onset of inhibition. Additionally, with zinc coated steel being a galvanic couple, the mixed inhibition action of hexavalent chromium is also an important consideration where distinct areas of cathodic and anodic activity will be present.

Phosphates are primarily referred to as non-oxidizing anodic inhibitors[13,19]. However, this is not the behaviour that was observed in this set of experiments. Indeed, inhibition on the cathodic steel surfaces is seen at higher percentage efficiencies in all cases. It can therefore be suggested that the pigments examined in this study can be considered as mixed action inhibitors in this case. However, it is also important to consider what processes may be

occurring on each of the surfaces to gain a greater understanding in the usefulness and limitations of these inhibitor pigments.

As was previously mentioned, the inhibition provided by phosphate species in solution is improved by the presence of certain divalent cationic species. It has also been reported that the presence of calcium cations is an essential component in producing a cathodic inhibitor response from phosphates[20]. The chemical process which produces the inhibitive species in orthophosphates is as given by the following chemical equation:

$$2HPO_4^{2-} + 2OH^- + 3Ca^{2+} \rightarrow Ca_3(PO_4)_2 + 2H_2O$$

This, alongside a reduction in the solubility due to the local increase in pH from the release of hydroxide at the cathodic site resulting in surface deposition, explains the strong cathodic inhibition exhibited by the calcium aluminium polyphosphate inhibitor pigment, as it is capable of providing the calcium cations required for the mechanism of inhibition shown for the cathode.

In the discussion taking into consideration the distinct inhibitor behaviour of the strontium aluminium polyphosphate inhibitor, it was suggested that strontium does not have the capability of producing an inhibitive film in this way. It is possible that this is due to greater solubility in the local alkaline environment of the strontium phosphate compound. From the results obtained, it would be suggested that the influence of cationic species on the efficacy of inhibition, without taking into account any possible effects with regards to the strontium aluminium polyphosphate inhibitor, would be Ca > Mg > Sr.

Corrosion protection by phosphate containing inhibitors on the zinc surface has been more extensively studied, with Simões et al[20] indicating the incorporation of the anodically produced zinc ions into a zinc phosphate deposit on the surface. The electrochemical impedance study presented showed initially the presence of two time constants. The time

constant present at lower frequencies is suggested to be due to the deposition of a polyphosphate-based layer. Subsequent damage or break down of this layer leads to the suppression of that time constant. For longer exposure times, another second time constant becomes evident at lower frequencies, indicating further surface coverage.

Experimental Limitations

In the previous chapter section, the ability of electrochemical impedance utilising segmented electrodes to determine inhibition on metallic systems containing multiple components showed that the site of inhibitor action could be determined quickly using only crude analysis of the impedance data. In this work, the segmented electrode technique was utilised to determine the effectiveness of three modified aluminium polyphosphate inhibitor pigments and has been able to determine some differences between pigments which nominally would have been expected to work similarly on the analysed system. It is clear, therefore, that the technique has potential for more explorative studies in the inhibition of complex systems

However, despite this potential, it is also important to call attention to possible limitations of the technique moving forward.

Electrochemical impedance spectroscopy is, in most cases, performed at the open circuit potential. As the segmented electrochemical impedance experiments are run at the mixed corrosion potential, it is unlikely to fall over the individual open circuit potential of any of the constituent components of the model. This appears to often result, particularly for the steel surface in the case of the steel and zinc couple, in the lowering of time constants visible within the spectrum.

It is suspected that this is due to the dominance of a particular electrochemical reaction following polarisation away from the open circuit potential. Indeed, many of the spectra obtained contain low frequency tails that could potentially be the embryonic stages of a

further time constant. However, there are not enough data points present for any meaningful analysis. Consequently, many of the mechanistic traits that can be, in the normal situations, elucidated through the application of model electrochemical circuits and comparing simulations to the real data are unobtainable. However, as this technique is used to look at galvanic cells, the loss of the information can be considered to not be a significant drawback.

3.3.5 Conclusions

The inhibition of modified aluminium polyphosphate pigments on a steel and zinc metallic couple has been measured. From the results obtained and the subsequent analysis, the following conclusions could be made:

- Calcium aluminium polyphosphate and magnesium aluminium polyphosphate show inhibition profiles that are distinctly different from that of strontium aluminium polyphosphate, potentially suggesting alternative inhibition mechanisms between the different modified aluminium polyphosphate inhibitor pigments.
- It was indicated that magnesium aluminium polyphosphate is the inhibitor pigment measured with the quickest inhibitor onset, with the highest inhibition efficiency at initial stages of experiments, but with the lowest effectiveness in the latter stages.
- Calcium aluminium polyphosphate is a highly effective mixed corrosion inhibitor, with the highest measured inhibition efficiency of the polyphosphate inhibitors on both the steel and zinc electrodes in the latter stages of exposure.
- Strontium aluminium polyphosphate is the weakest inhibitor in the initial stages of exposure, with inhibition improving at a high rate following longer periods of exposure.
- Overall trends in inhibitor efficiency do not appear to fit well with trends in other parameters such as solubility of the suspected compound deposits.

3.4 Effects of Changing Spatial Geometry

3.4.1 Introduction

In the previous section, the experiments utilising electrochemical impedance spectroscopy on segmented zinc and steel electrodes showed an unusual inhibition profile for the strontium aluminium polyphosphate inhibitor pigment. This profile can be summarised as the inhibitor remaining inefficient on the cathodic surface for the initial period of the test, followed by a sustained period of increasing efficiency.

It was suggested that this phenomenon occurs due to the time taken for anodically dissolved zinc ions to diffuse to the cathode surface. If the presence of zinc, in sufficient concentrations, is a major component of the inhibitor mechanism, then the previously observed delay in inhibition could be explained by the presence of a diffusion pathway.

Therefore, the aim of this study was to examine the proposed cause of the inhibition profile through the modification of experimental parameters. This was done through employing a previously devised geometrical model of the cut edge of galvanised steel which maintains the segmentation of the incorporated metals. In using this geometric set up, the diffusion pathway for the zinc ions released into the solution through anodic dissolution to the steel surface is significantly reduced. Therefore, if the proposed explanation is true, a change in the inhibition profile for the strontium aluminium polyphosphate inhibitor pigment would be observed, foregoing the initial period of lessened inhibitor efficiency.

3.4.2 Experimental

The experimental set-up for this experiment followed the same sample preparation and solution preparation methodology as given in the section 2.1.2., whilst utilising modified working electrode geometry. The working electrodes were mounted so as to attempt to geometrically mimic the cut edge of galvanised steel. This set-up was based on a model electrochemical cell that has been previously shown in the literature, and is shown in Figure 2.3.1[13] (Methodology, Page 91).

The system was maintained at the laboratory temperature (18-21°C), and monitored for a 72 hour period. Electrochemical impedance measurements were taken for each individual electrode at 2 hour intervals for the observation period. Impedance measurements were taken at the measured system coupled corrosion potential in the frequency range of 10,000 to 0.01 Hz with a signal amplitude of 10 mV.

3.4.3 Results

The proposed mechanistic change being studied in this particular section was prevalent in the results obtained for the strontium aluminium polyphosphate pigment inhibited samples. Therefore, it is with this pigment that this particular study concentrates on. Figure 3.4.1 and Figure 3.4.2 show a selection of the Nyquist plots that were obtained utilising the model cut edge electrochemical cell with the SAPP inhibitor pigment, for the steel and zinc electrodes respectively.

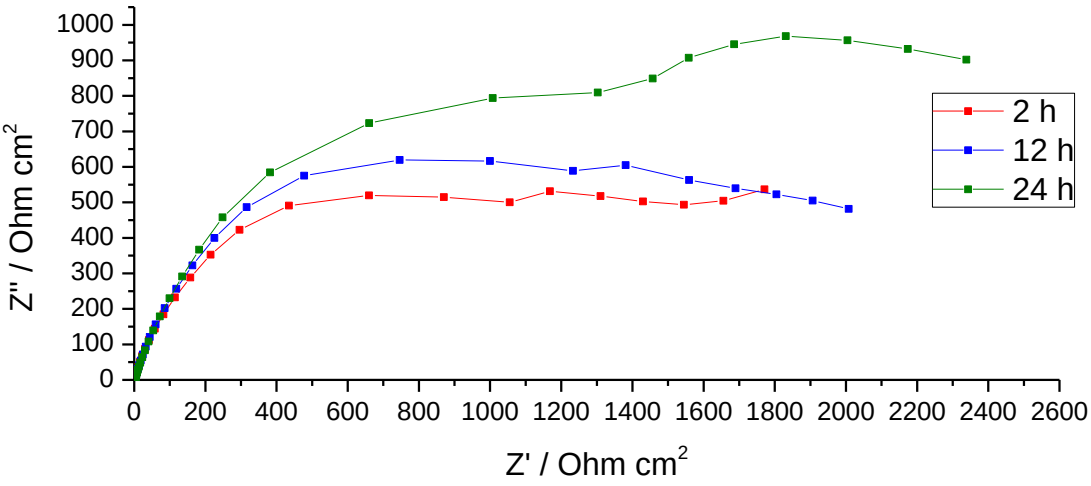

Figure 3.4.1 - Selected Nyquist plots obtained for steel in the electrochemical impedance with segmented electrodes experiment when coupled to zinc over a 24 hour period in the model cut edge geometry cell

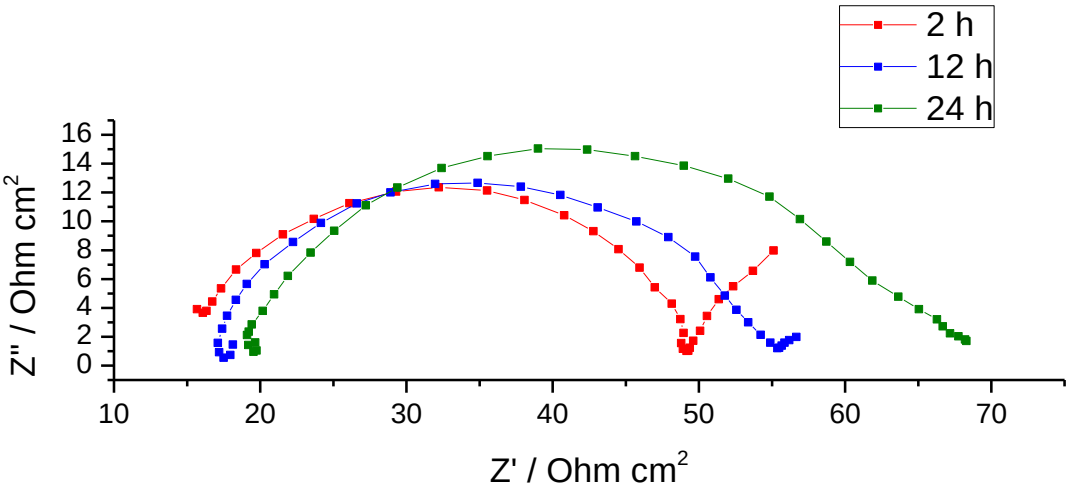

Figure 3.4.2 - Selected Nyquist plots obtained for zinc in the electrochemical impedance with segmented electrodes experiment when coupled to steel over a 24 hour period in the model cut edge geometry cell

The plots for both the steel and zinc electrodes only exhibit one fully analysable time constant. Whilst some of the samples appear to show tails at low frequencies that may imply the presence of a secondary time constant, it is suggested that no meaningful analysis could be taken from these.

Each plot appears to show consistent increases in the size of the visible semi-circle within the Nyquist plot. In contrast to the original geometry, the plots from the model cut edge show no evidence of a delay in inhibitor performance improvement, with an apparent instantaneous increase in charge transfer resistance observed. This effect is observed on both the zinc and steel surfaces, with the effect being more pronounced on the steel electrode.

3.4.4 Discussion

The hypothesis given in the previous section proposed that the inhibition delay observed in the SAPP inhibited samples for the original working electrode geometry was due to mechanistic changes that lead to improved phosphate deposition on the surface when a sufficient concentration of zinc cations are available at the steel surface. Figure 3.4.3 shows a comparison of the development of the calculated inhibitor efficiencies over time, calculated from the electrochemical impedance spectra that were obtained on the steel electrode, for the

strontium aluminium polyphosphate inhibitor pigment utilising both working electrode geometries.

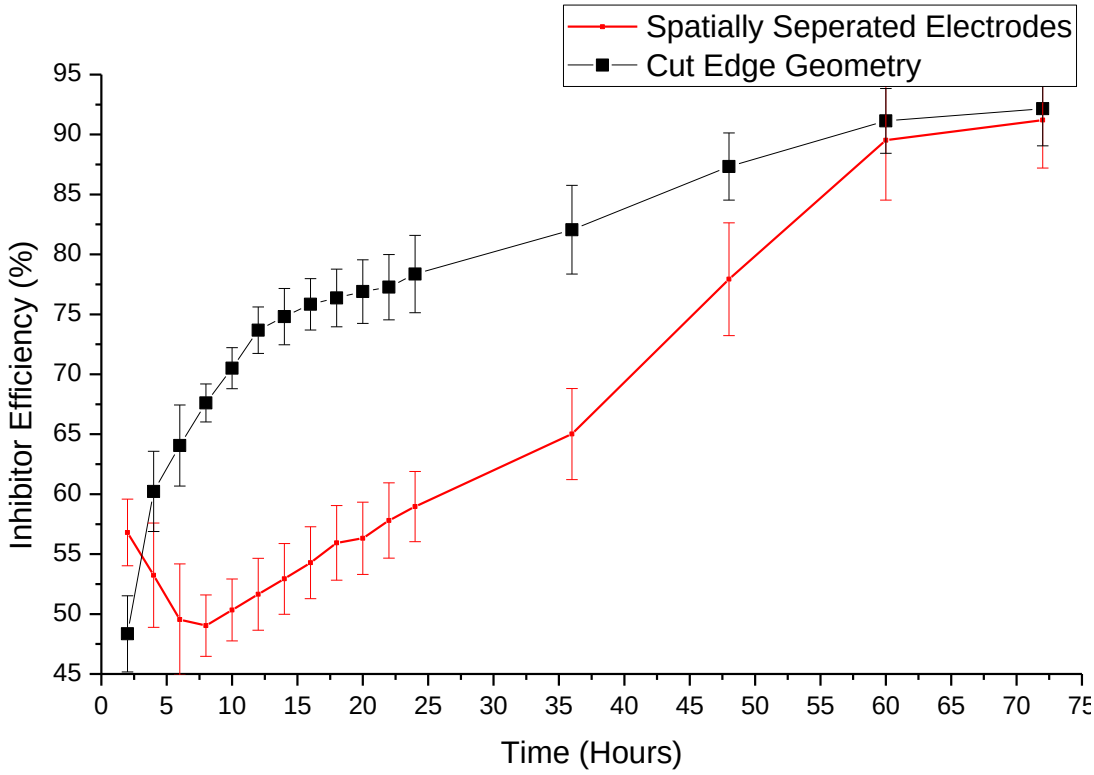

Figure 3.4.3 - Scatter graph showing the progression of inhibitor efficiency on the steel surface over time for both the original cell geometry and the cut edge mimic

In looking at the comparison between the two electrode geometries, it was observed that reducing the distance between the steel and zinc electrodes resulted in the absence of a delay in inhibitor action. The extent of corrosion protection at the initial stages of the experiments can also be seen to be approximately equivalent for both geometries. Additionally, upon the conclusion of the observation period, it can be seen that the extent of inhibition is approximately the same for both geometries. This observation is consistent with what would have been an expected result with the suggested hypothesis.

A greater rate of corrosion inhibition improvement is also seen in the initial stages of the cut edge geometry measurements. There are two potential explanations for this finding. One is that the surface of the steel electrode is cleaner due to the lesser exposure times required before the inhibitor and anodically dissolved zinc can interact, in which the deposition mechanism is more effective with a cleaner substrate. Alternatively, despite the lower area of zinc used in the geometry used for the cut edge mimic, the initial anodic reaction results in a local enrichment of zinc ions at the surface of the steel sample that is of sufficient concentration to result in a large improvement in the inhibitor efficiency.

However, it is clear that whilst the results can be explained by the hypothesis presented, the current results are insufficient to confirm it. One suggestion is that in the case of the presence of zinc being important in surface deposition mechanisms, the surface deposition structure and composition could be different between samples exposed to inhibited solutions in zinc-free and zinc-rich environments.

3.4.5 Conclusions

In this study, the effects of changing the spatial separation between zinc and steel electrodes on the inhibition by strontium aluminium polyphosphate were analysed. From these results, the following conclusions could be made:

- The reduction in distance between the steel and zinc electrodes results in the absence of any notable delays in increasing inhibitor efficiency with the strontium aluminium polyphosphate inhibitor pigment
- The strontium aluminium polyphosphate pigment appears to require additional elements to be present before it can act as an effective inhibitor. It is suggested from these experiments that the presence of anodically released zinc ions is one particular change that can result in inhibitor improvements
- Modifying the spatial geometry of the electrochemical cell is sufficient to change the obtained results, suggesting that this may be an experimental parameter that can be changed with this technique for greater understanding of how a particular system may work

3.5 Chapter Summary and Conclusions

In this chapter, the inhibition of galvanised steel was explored through the use of an electrochemical set-up which utilises segmented electrodes of distinct composition. From the work presented in this chapter, the following conclusions have been made:

- Electrochemical impedance utilising segmented electrodes is capable of quickly producing results that can indicate inhibition on dissimilar metals which represent the cathodic and anodic materials of a galvanic couple
- Consistency was seen between the analysis of inhibitor behaviours reported in the literature and the results obtained using the segmented electrode electrochemical impedance technique in Chapter 2.1
- The electrochemical impedance plots obtained through the segmented electrode technique are somewhat limited as they appear to be mostly limited to single time constants, reducing the amount of information that can be gathered from the results
- The three aluminium polyphosphate based inhibitors tested during these studies appear to show non-identical behaviour, potentially indicating differences in the inhibition mechanisms
- Strontium aluminium polyphosphate shows distinct behaviours between different electrode geometries. Changing the cell geometry is therefore an option for looking at obtaining information of the corrosion inhibition of the overall system.

3.6 Chapter References

[1] Tan YJ, Bailey S, Kinsella B. Corros Sci 1996;38:1545.

[2] Bastos AC, Zheludkevich ML, Ferreira MGS. Port Electrochim Acta 2007;26:47.

[3] Dawson JL, Gill JS, Al-Zanki IA, Woolam RC. Dechema Monogr 1985;101:235.

[4] Woollam RC, Gill JS, Dawson JL. Mater Sci Forum 1986;8:53.

[5] Alawadhi K, Robinson MJ. Corros Eng Sci Technol 2011;46:318.

[6] Rebak RB. Preferential Weld Corrosion: Effects of Weldment Microstructure and Composition, in:. Corros. 2005. 2005.

[7] Mok WY, Gamble CG, Jenkins AE, Keenan SR. Control of Localized Corrosion Using Green Corrosion Inhibitors, in:. Corros. 2005. 2005.

[8] Winning IG, Bretherton N, McMahon A, McNaughtan D. Evaluation of Weld Corrosion Behavior and the Application of Corrosion Inhibitors and Combined Scale/corrosion Inhibitors, in:. Corrosion 2004. 2004.

[9] McNaughtan D, Winning IG, Clariant Oil Services. Comparison of Segmented Weld Corrosion Tests with Short and Long Pre-Corrosion and The Influence of Synergist in Corrosion Inhibitors, in:. 1st Int. Symp. Oilf. Corros. 2004.

[10] Stern M. J Electrochem Soc 1958;105:638.

[11] Zin IM, Howard RL, Badger SJ, Scantlebury JD, Lyon SB. Prog Org Coatings 1998;33:203.

[12] Deflorian F, Fedrizzi L, Rossi S. Corros Sci 2000;42:1283.

[13] Zin IM, Pokhmurskii VI, Scantlebury JD, Lyon SB. J Electrochem Soc 2001;148:B293.

[14] Zin IM, Lyon SB, Pokhmurskii VI. Corros Sci 2003;45:777.

[15] Pokhmurs'kyi VI, Zin' IM, Layon SB, Bilyi LM. Mater Sci 2003;39:153.

[16] Jüttner K. Electrochim Acta 1990;35:1501.

[17] Epelboin I, Keddam M, Takenouti H. J Appl Electrochem 1972;2:71.

[18] Lahodny-Ŝarc O, Kaštelan L. Corros Sci 1976;16:25.

[19] Pryor MJ, Cohen M. J Electrochem Soc 1953;100:203.

[20] Simões AM, Torres J, Picciochi R, Fernandes JCS. Electrochim Acta 2009;54:3857.

Chapter 4

Analysis of Polyphosphate Inhibitor Film Formation

4.1 Introduction

The formation of films on the surface of a metal is a commonly observed action for inhibitive species. Understanding the nature of this film can be important in determining how to produce, or formulate, the most effective inhibitor or inhibitor mixture for a particular scenario or environment.

In the previous chapter, it was shown that the spatial separation between steel and zinc electrodes had an effect on the measured effectiveness of inhibition when using the SAPP inhibitor pigment. A potential explanation was provided for this effect in the interaction of zinc ions released from the anodic process with the inhibitor to produce a different inhibiting species. In this chapter, the potential effects of the presence of cationic species within the inhibited solution on the produced surface deposits.

This chapter will initially aim to look at the effects of dissolved zinc ions on the corrosion behaviour and surface structure on exposure to bare steel substrates by utilising scanning electron microscopy and combining this with energy dispersive x-ray spectroscopy. The effect of dissolved zinc ions on the surface composition and deposit thickness will then be analysed for exposure on cathodically polarised steel substrates through the use of x-ray photoelectron spectroscopy. Finally, further x-ray photoelectron spectroscopy analysis will be obtained for the surfaces of cathodically polarised steel samples exposed to modified aluminium polyphosphate inhibitor pigment solutions containing alternative cationic species to determine any further synergistic or antagonistic relationships.

4.2 Scanning Electron Microscopy and Energy Dispersive X-Ray Spectroscopy

4.2.1 Introduction

The first part of this chapter will be dealing with initial experiments that concentrated on observing the interaction of dissolved commercial “modified aluminium polyphosphate” inhibitor pigments on the surface of mild steel. Modified aluminium polyphosphates are considered to be a promising set of corrosion inhibitors for replacing hexavalent chromium based corrosion inhibitors in coil coated applications. However, as they are available as industrially produced pigments, they are ultimately poorly defined, comprised of a mixture of components, as opposed to a well-defined single chemical component. As such, when studying these materials, it is important to take into consideration the possibility that the nominal composition and structure of these pigments may differ from the reality.

Therefore, the intentions of this set of experiments were to initially scope and qualitatively understand the differences in morphology and elements which comprise the surface deposits on steel for each of the pigments. A secondary aim was to determine the effects, if any, of the addition of zinc ions to the solution to these properties.

To do this, the surfaces of steel samples were exposed to polyphosphate inhibitor solutions without electrochemical perturbation. These samples were then initially analysed optically, observing the formation, colour and general cohesive and adherence properties of the overlying corrosion products and surface deposits. Scanning electron microscopy was used to discern the morphology of the deposited layer, whilst energy dispersive x-ray spectroscopy was utilised to determine the elemental composition of the layer.

4.2.2 Experimental

Steel specimens of approximate dimensions 1 cm x 2 cm were cut from a mild steel Q panel and mounted in two part epoxy. The steel surface was exposed and ground using silicon carbide paper down to a 1200 grade. Samples were immersed for 72 hours, without any external electrochemical perturbation, in a solution of 0.62M sodium chloride either uninhibited or containing an inhibitor pigment added to saturation. In samples that were to be exposed to a zinc-rich environment, zinc chloride was added until a concentration of 2 mM was achieved.

Following exposure, the samples were dried and washed gently with deionised water, with images taken before and after washing for comparison. Samples were then analysed using a Zeiss Evo 50 Scanning Electron Microscope with Energy Dispersive X-Ray Spectroscopy addition. EDX spectroscopy was performed at an accelerating voltage of 12 keV. This particular accelerating voltage was chosen to reduce the interaction volume of the electron beam whilst maintaining a sufficient energy to excite the generation of x-rays.

4.2.3 Results

To first understand the effect of the presence of zinc ions on the general corrosion of steel, initial experiments were done on steel samples exposed to salt solutions containing no inhibitor with and without the addition of zinc chloride.

No Inhibitor/ Blank Samples

Visual Inspection

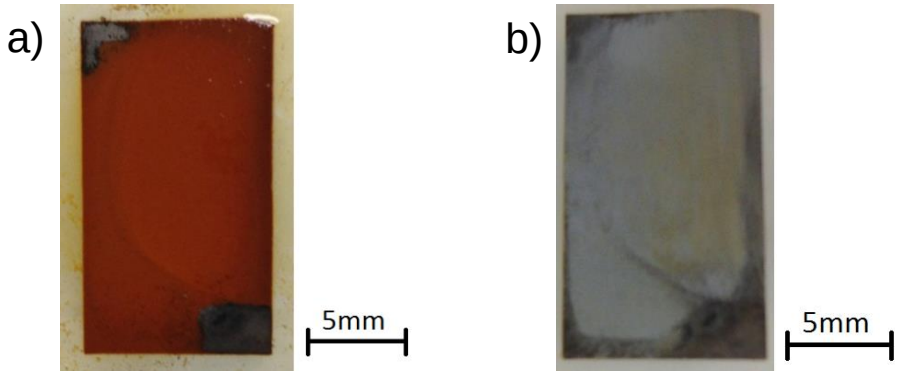

Figure 4.2.1 - Images of steel surfaces following exposure to an uninhibited solution. a) - Pre-wash, b) - Post-wash

Visual inspection of the uninhibited sample, Figure 4.2.1, observed that the majority of the steel surface was covered with a thick layer of a red-orange layer, assumed to be rust. It was also noted that the exposure solution had been significantly yellowed during the test, likely due to the release of iron ions into the solution. The rust layer showed little-to-no adhesion to the underlying substrate and was removed easily with gentle washing, leaving a grey-silver exposed steel surface.

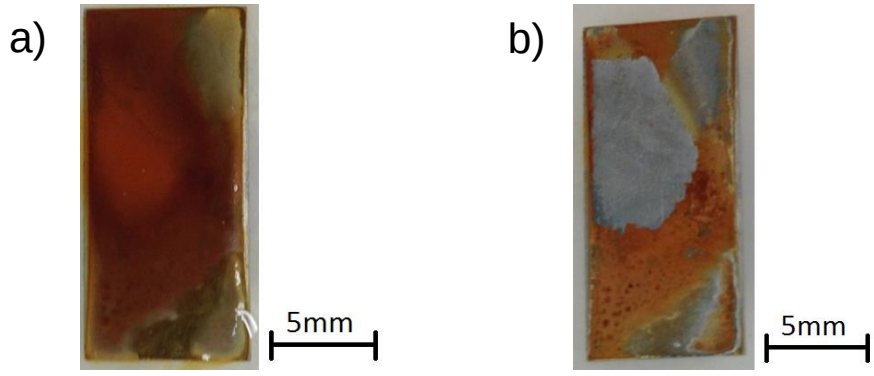

Figure 4.2.2 - Images of steel surfaces following exposure to a zinc-rich uninhibited solution. a) - Pre-wash, b) - Post-wash

In the case of the zinc-containing environment, as seen in Figure 4.2.2, the steel surface was partially covered with an inconsistent orange rust layer with evidence of some white corrosion products. Unlike in the sample without zinc chloride, no significant yellowing of the exposure

solution was observed. Loss of some of the covering material was observed on gentle washing of the surface; however some orange, yellow and white products were seen to maintain adhesion to the steel surface.

a)

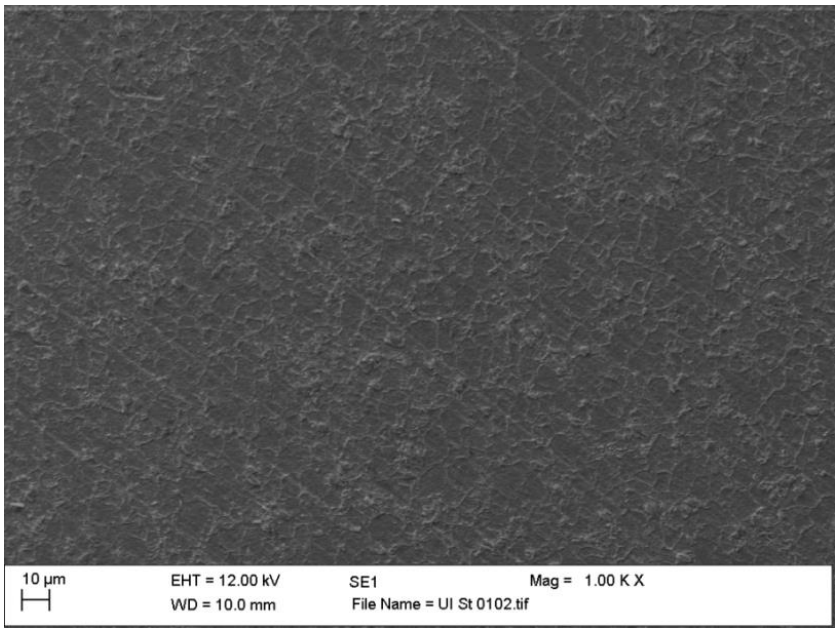

b)

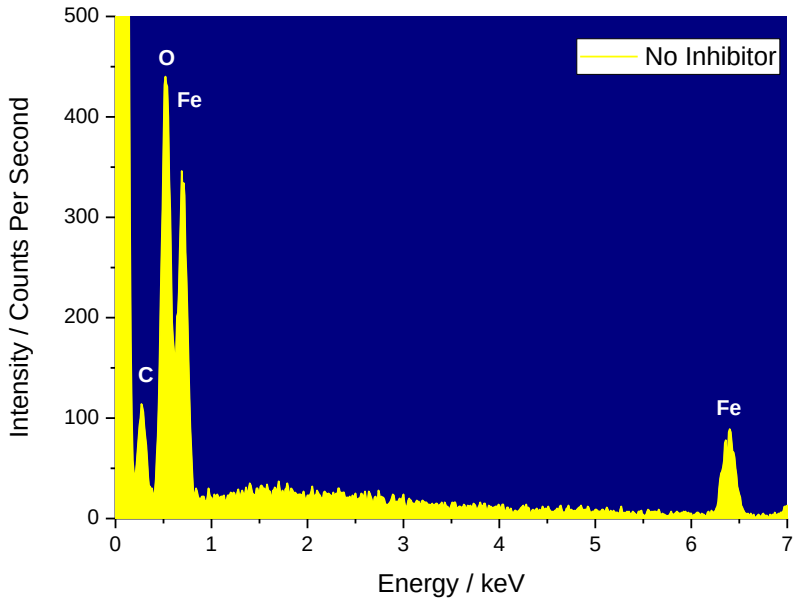

Figure 4.2.3 – a) - A representative image of the steel surface after washing from the electron microscopy. b) - A measured EDX spectrum representative of the surface shown on SEM, cut to show observed elements

The scanning electron microscope images of post-washed uninhibited samples exposed to a sodium chloride solution without any additions, shown in Figure 4.2.3, appears to show a

rough surface morphology. This could potentially be from corrosion occurring at the surface. EDX analysis was only able to detect iron and traces of carbon at the surface, which is consistent with the steel composition. This suggests that any potential corrosion products deposited on the surface, and still remaining following the washing procedure, would be too thin to be detectable through this technique, due to the penetration depth of EDX.

Electron microscope images and the EDX spectrum obtained from the sample exposed to the environment containing zinc chloride with no inhibitors are shown in Figure 4.2.4. Two distinct structures were evident, a rough surface morphology, similar to that observed for the non-zinc exposed sample and a rougher morphology with apparent porosity that was not present within the other uninhibited sample. EDX analysis determined that the surface composition appears similar to that of zinc-free environment sample. However, the areas displaying the porous-like surface structure gave EDX spectra as in Figure 4.2.4. As such, it can be considered that these areas may be zinc-rich, which implies that this is likely an area of zinc oxide or zinc hydroxide deposition. On the sample, this may be due to activity at cathodic sites, where the local pH would be increased due to the development of the hydroxide species. In the presence of zinc ions, this could produce zinc oxide and zinc hydroxide species that have low solubility and therefore deposit on the surface.

The peak seen at approximately 1 keV is labelled as both zinc and sodium, which will be seen as a consistent label throughout this chapter. The Kα for sodium is situated at 1.041 keV, whilst the Lα for zinc is situated at 1.012 keV, and therefore the peaks are overlapping within the spectrum and unlikely to be distinct. Usually, the presence of zinc will be confirmed through the presence of a Kα peak (8.630 keV), however the selected excitation energy of 12 keV means that this peak is generally only detected when the Lα is seen at high intensity. Therefore, the presence of zinc is assumed in spectra without the zinc Kα peak in examples where zinc has been shown to be present in later experiments.

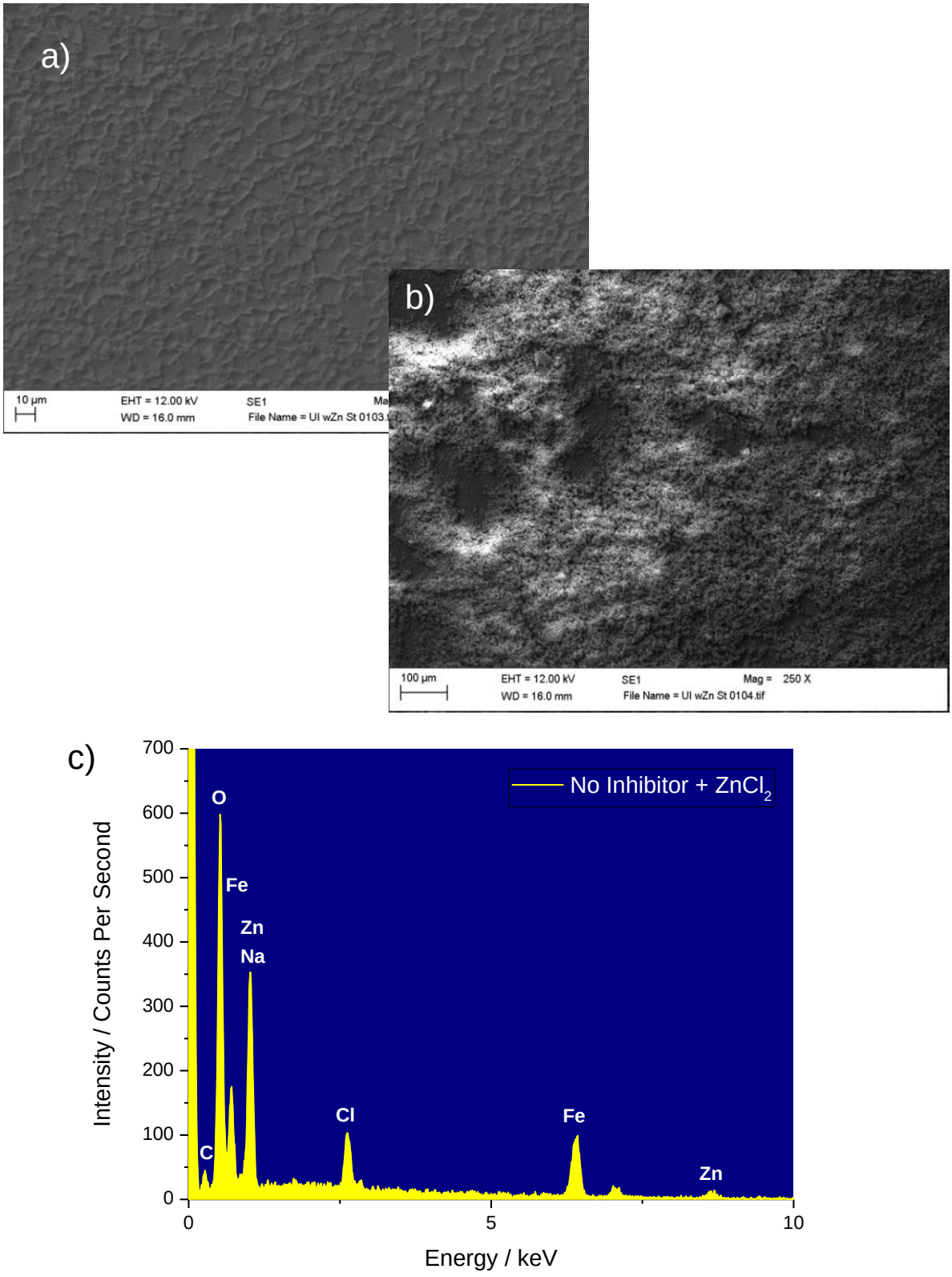

Figure 4.2.4 – Results obtained from exposure to electrolyte containing sodium chloride and zinc chloride. a) - Electron microscope image showing the general structure of the surface without visually detectable adhered deposits. b) - Electron microscope image showing the general structure of the surface containing adhered deposit. c) – EDX spectrum showing the detectable species in the adhered deposit.

Strontium Aluminium Polyphosphate (SAPP)

Visual Inspection

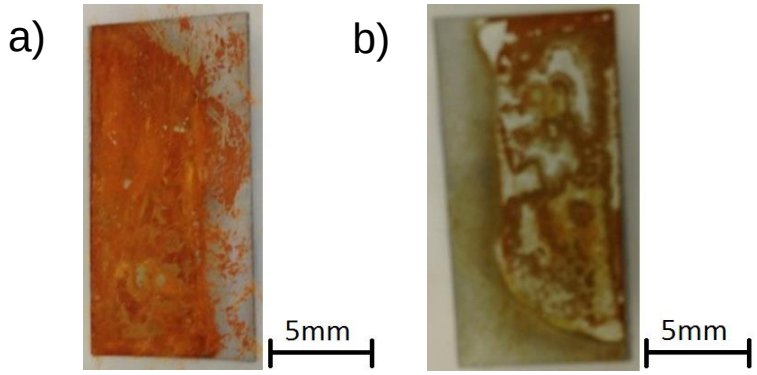

Figure 4.2.5 - Images of steel surfaces following exposure to SAPP inhibited solution. a) - Pre-wash, b) - Post-wash

Through visual inspection of the zinc-free environment exposure to SAPP inhibited solution, it can be seen that a dark orange deposit is present on the surface, albeit with incomplete coverage, meaning some steel surface is still exposed. Yellowing of the solution during the experiment was also noted. Following gentle washing, it can be seen that the orange substance has been removed, and was therefore poorly adherent. The washing process left further exposed steel segments surrounded by an adherent brown-red product.

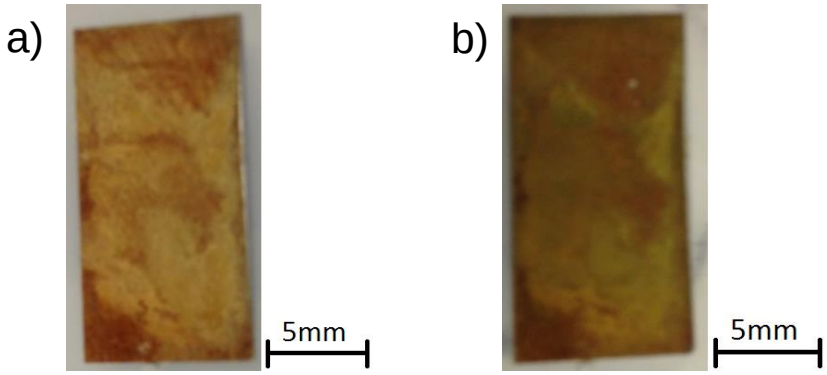

Figure 4.2.6 - Images of steel surfaces following exposure to SAPP inhibited solution containing zinc. a) - Pre-wash. b) - Post-wash

Inspection of the sample exposed to the zinc-containing SAPP inhibited solution showed a thick yellow to orange surface layer that had developed on the surface of the steel, suggesting that the inhibition of the surface is poor. Gentle washing of the sample implied that this layer was adherent to the surface as no visual change could be observed. Therefore, it can be suggested that whilst the inhibition is poor, there is an effect of the inhibitor and zinc combination that results in changes to the nature of the corrosion product.

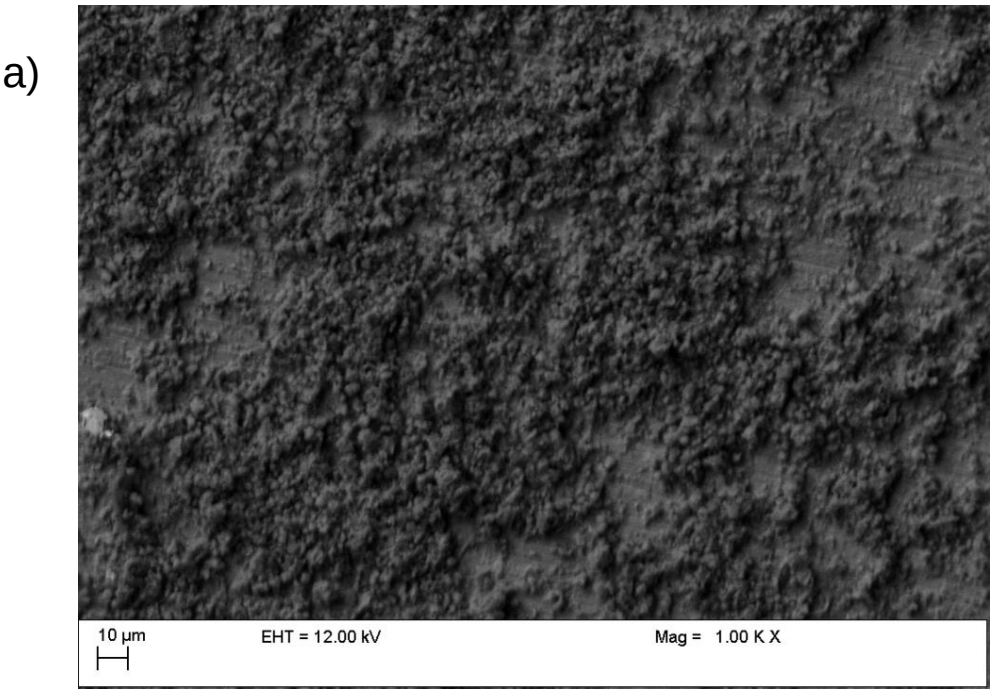

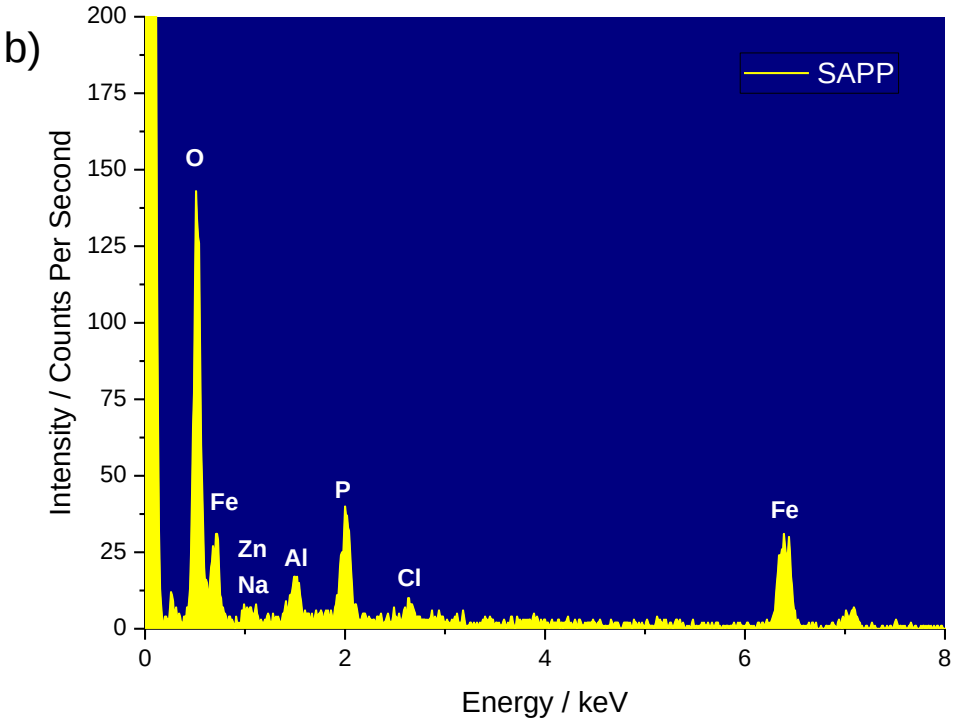

Figure 4.2.7 – a) - A representative electon microscopeimage of the steel surface exposed to a sodium chloride solution containing strontium aluminium polyphosphate inhibitor pigment, after washing. b) - A measured EDX spectrum representative of the surface shown on SEM, with the observed element peaks labelled

EDX of the surface from the sample exposed to a sodium chloride environment containing the SAPP inhibitor pigment showed the presence of aluminium and phosphorus, but an absence of strontium. This gives an indication that in this particular test, the deposited layer on the steel surface is most likely to be comprised of aluminium and phosphorus, with no involvement from the strontium component of the inhibitor pigment. No quantification analysis was carried out at this stage to determine the likely chemistry of this mixture. A weak signal referring to zinc was also detected. This suggests that zinc may be present as an inclusion within the SAPP inhibitor pigment, and may also imply that this also plays a role in the deposition. The morphology of the deposit as seen in the SEM images can be described as appearing as a particulate as opposed to the formation of a thin film.

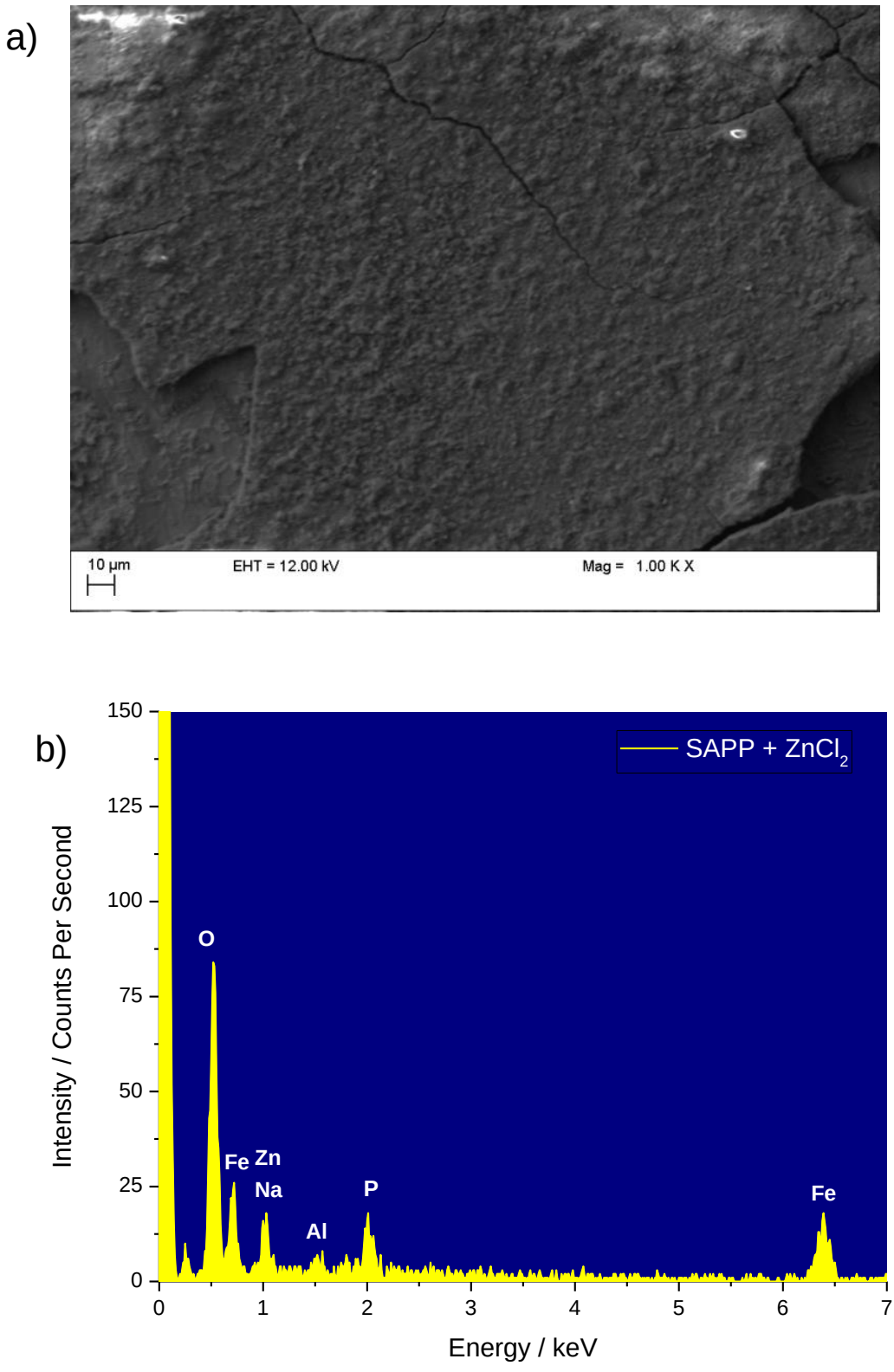

Figure 4.2.8 – Results obtained for the sample exposed to an electrolyte containing sodium chloride, SAPP inhibitor pigment and zinc chloride. a) - A representative image of the steel surface after washing from the electron microscopy. b) - A measured EDX spectrum representative of the surface shown on SEM, cut to show observed elements.

In comparison, the results obtained from exposure to the solution containing both zinc chloride and SAPP also show an absence of strontium, with aluminium also dropping to low-to-undetectable levels. A strong zinc peak is present in the EDX spectra. It can be suggested that the deposited is comprised of a structure that contains zinc and phosphorus, with some evidence of aluminium. This is somewhat different to what is observed when zinc chloride is not present within the environment.

Additionally, a change in the morphology observed on the surface is also observed. The structure of the surface deposit is seen to be more plate-like in nature, compared to the particulate nature of the deposit seen previously. These observations put forward the possibility of a working hypothesis regarding the inhibition mechanism of the SAPP inhibitor pigment, namely that the presence of a concentration of zinc ions within the solution changes the final structure and composition of the deposition. However, the full nature of this effect cannot be discerned using these results alone.

Calcium Aluminium Polyphosphate (CAPP)

Visual Inspection

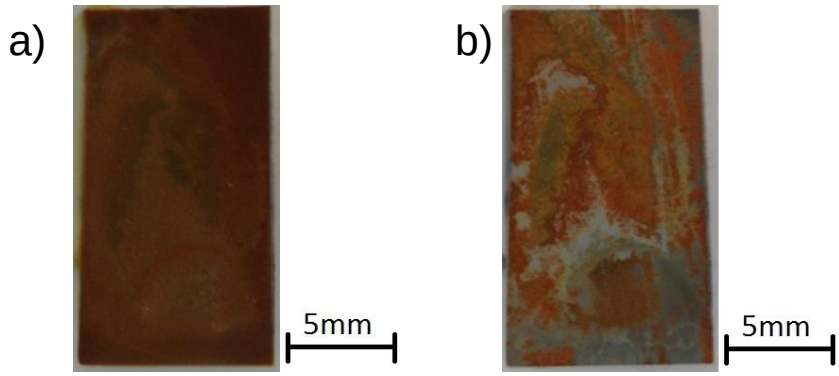

Figure 4.2.9 - Images of steel surfaces following exposure to CAPP inhibited solution. a) - Pre-wash, b) - Post-wash

Through visual inspection of the zinc-free environment exposure to CAPP inhibited solution, it can be seen that a brown deposit appears with near-to-full coverage of the steel surface, with

some steel surface still exposed. Following gentle washing, it can be seen that some of the deposit had been removed, leaving a small proportion of the steel surface exposed, surrounded by remaining adherent orange-brown product.

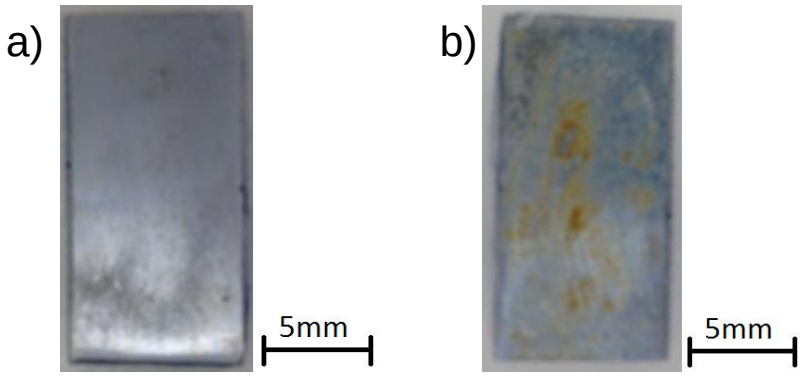

Figure 4.2.10 - Images of steel surfaces following exposure to CAPP inhibited solution containing zinc. a) - Pre-wash, b) - Post-wash

In the case of the zinc-containing CAPP solution, a shiny steel surface was evident upon removal from the electrolyte, suggesting effective inhibition of the surface However, upon cleaning there was some evidence of corrosion spots. It is possible that this is due to flash corrosion of the steel when exposed to the air during the cleaning procedure. Alternatively, this could be due to residual anodic activity that becomes evident following the cleaning procedure.

a)

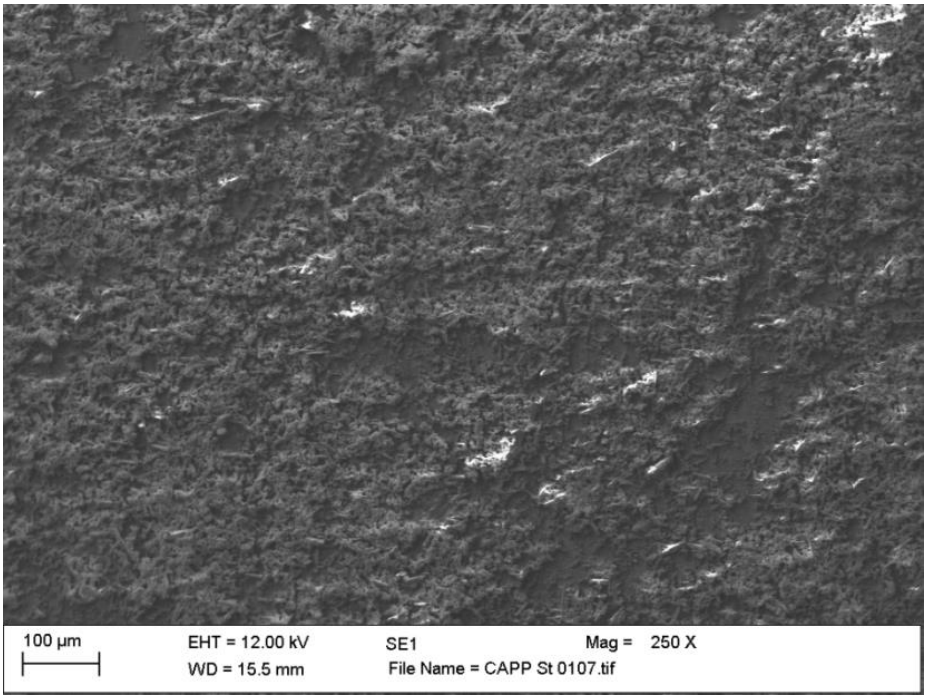

b)

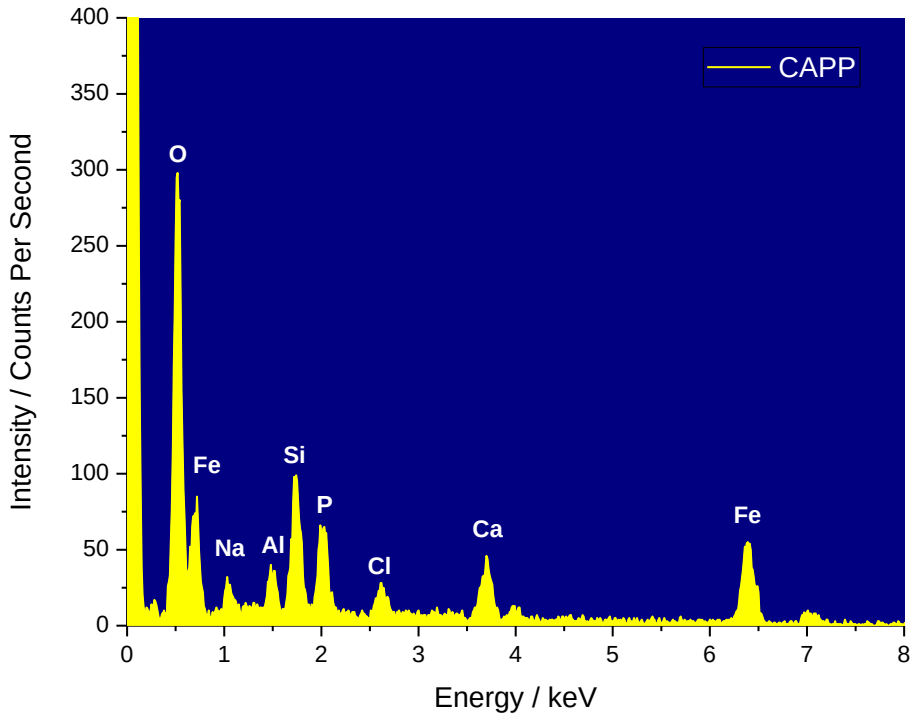

Figure 4.2.11 – Results obtained for steel exposed to a sodium chloride solution containing the CAPP inhibitor pigment. a) - A representative image of the steel surface after washing from the electron microscopy. b) - A measured EDX spectrum representative of the surface shown on SEM, cut to show observed elements

EDX results from the zinc-free environment showed the presence of aluminium, phosphorus, calcium and silicon. As the industrial pigment used for this test is referred to as calcium aluminium polyphosphate silicate, the presence of silicon is not unaccountable for. However, with some presence within the surface deposit, it can be considered likely that the silicon component of the pigment is a component with an active role to play in the inhibition mechanism. From literature around inhibition on coil coated materials, there is a possibility that this calcium and silicon containing species would be a type of ion-exchanged silica, which are well known for use as inhibitors, alongside use in the coil coating industry[1].

With calcium aluminium polyphosphate showing a similar, albeit less extreme, time-dependant inhibition profile to that of strontium aluminium polyphosphate within the electrochemical results, it is suspected that the inhibitor layer formed may be similar. However, the presence of aluminium in the zinc containing x-ray spectrum for the CAPP inhibitor shows that there is certainly a difference in the way the inhibitor is deposited from solution in the presence of zinc chloride.

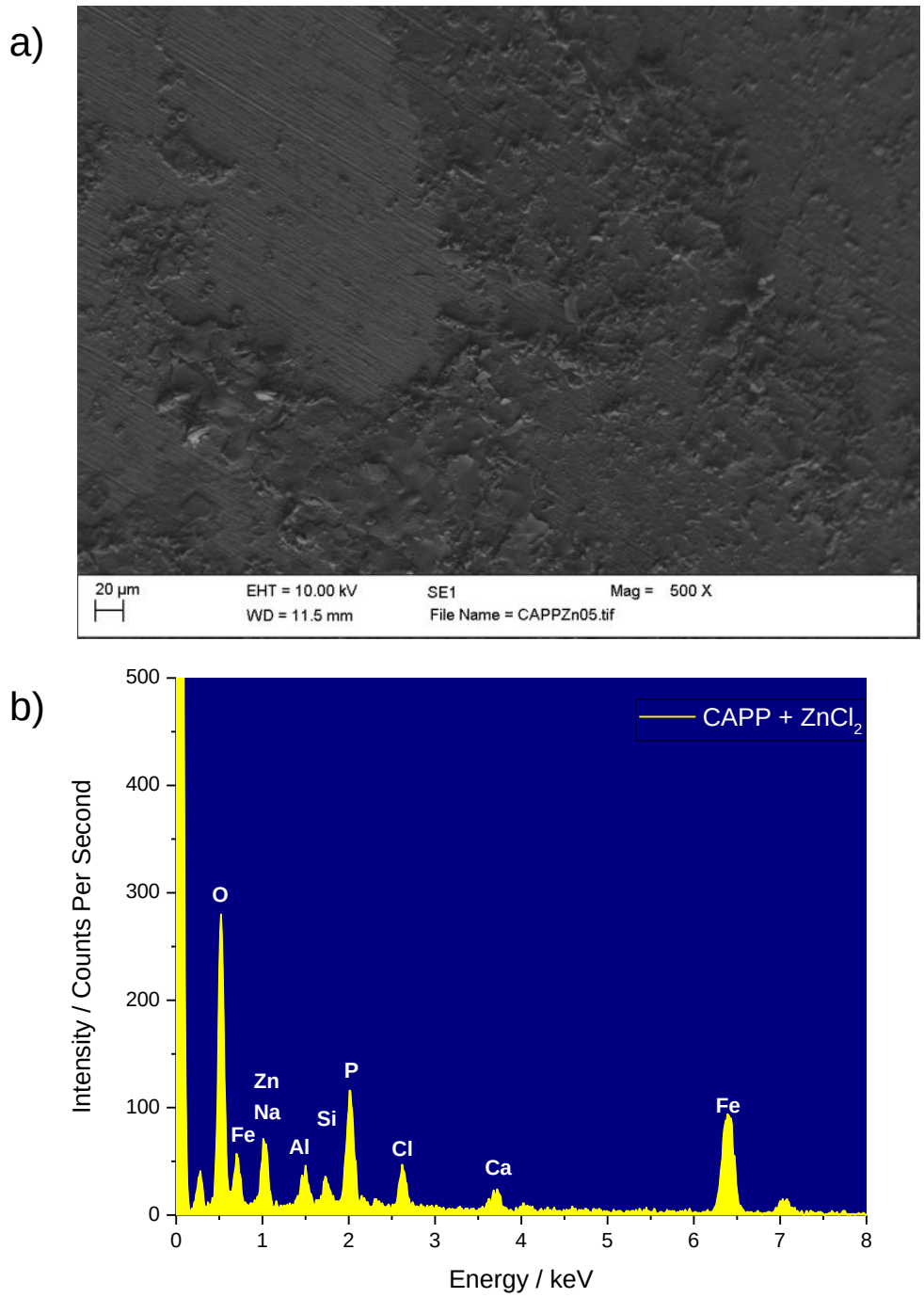

Figure 4.2.12 – Results obtained for steel exposed to a sodium chloride solution containing the CAPP inhibitor pigment and zinc chloride. a) - A representative image of the steel surface after washing from the electron microscopy. b) - A measured EDX spectrum representative of the surface shown on SEM, cut to show observed elements

Magnesium Aluminium Polyphosphate (MAPP)

Visual Inspection

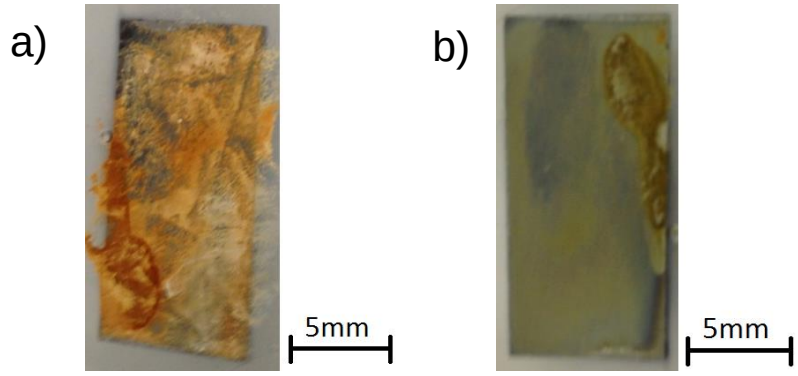

Figure 4.2.13 - Images of steel surfaces following exposure to MAPP inhibited solution. a) - Pre-wash, b) - Post-wash

Through visual inspection of the sample exposed to the MAPP inhibited solution containing no zinc chloride, it can be seen that an orange-to-white deposit appears with inconsistently coverage of the steel surface. It was clear from initial inspection that this product was not adhered to the underlying steel. This was confirmed as, following gentle washing of the sample, it could be seen that the majority of the covering material had been removed, leaving a yellowed surface, suspected to be an inhibitor deposit alongside a small area of residual anodic activity which is covered by a yellow-brown corrosion product.

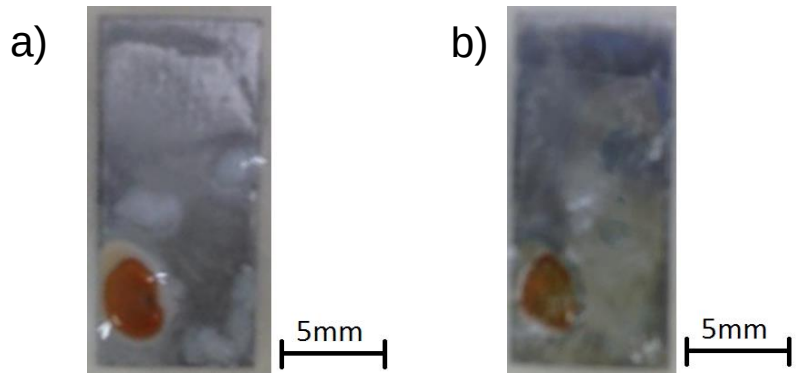

Figure 4.2.14 - Images of steel surfaces following exposure to MAPP inhibited solution containing zinc. a) - Pre-wash, b) - Post-wash

Analysing the zinc-containing environment for MAPP inhibited solution, it can be seen that there is a prominent corrosion spot alongside some white deposits seen on the unwashed sample. Following gently washing, a miscoloured steel surface can be seen in the absence of the white deposits. The orange-brown corrosion spot appears to have maintained adherence to the surface.

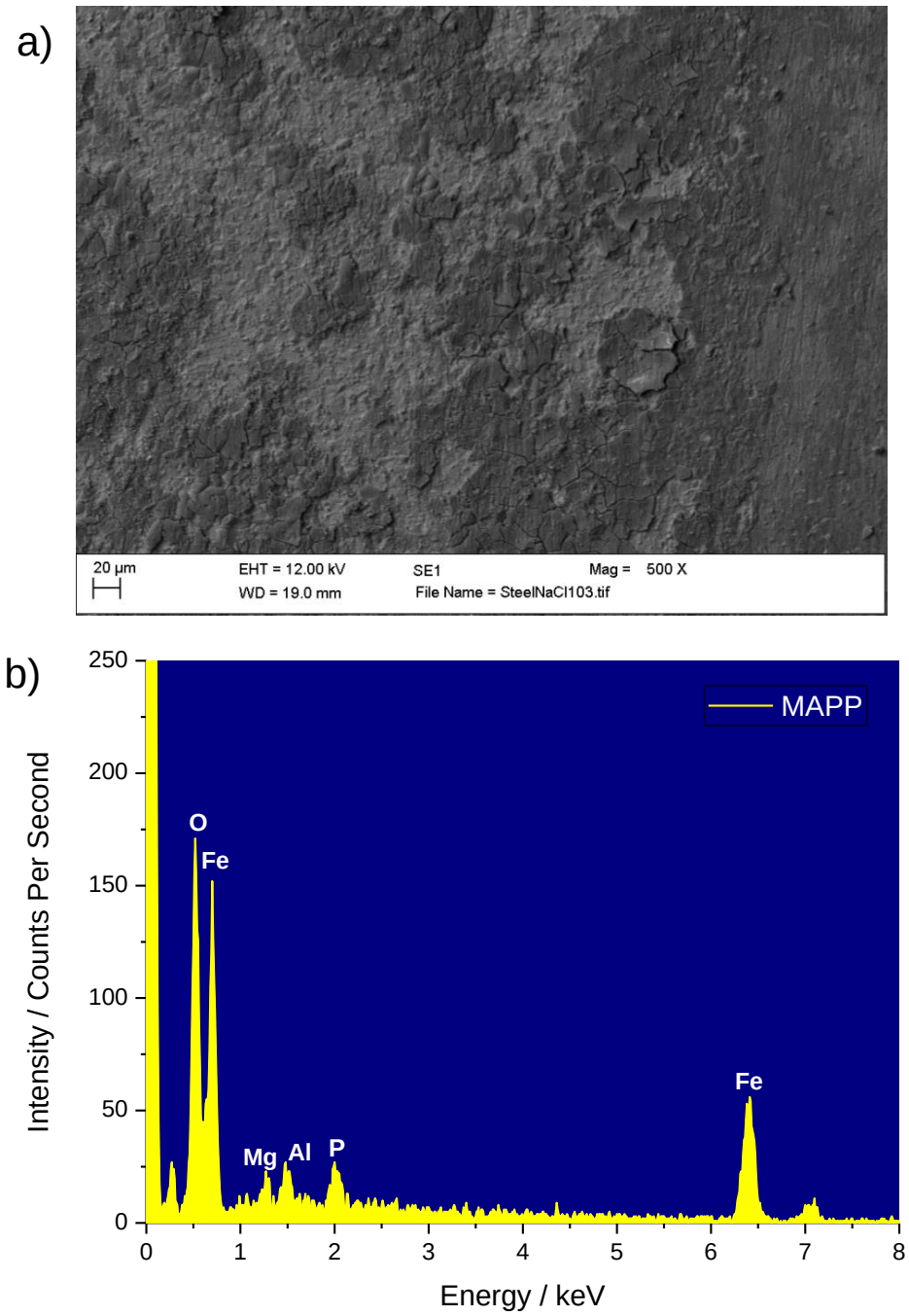

Figure 4.2.15 – Results obtained for steel exposed to a sodium chloride solution containing the MAPP inhibitor pigment in the absence of zinc chloride. a) - A representative image of the steel surface after washing from the electron microscopy, showing a deposit (darker areas) alongside areas where only iron and oxygen could be observed. b) - A measured EDX spectrum representative of the surface shown on SEM, cut to show observed elements

Figure 4.2.15 shows a representative SEM image and EDX result from the zinc-free MAPP inhibited sample. In this, it can be seen that the surface is coated by layer that appears to be somewhat cracked and removed in the image. The EDX of the darker regions show the presence of magnesium, aluminium and phosphorus, whereas the elemental analysis of the lighter regions is only able to detect iron, oxygen and carbon, suggesting a bare steel surface, or alternatively deposits that are of a thickness below the detection limit of the technique. It is difficult to fully understand the structure of the inhibitor layer deposited in this particular case; however, it is suspected that both the magnesium and aluminium are incorporated in a layer containing magnesium/aluminium phosphate/polyphosphate type character.

In the presence of zinc, the presence of the MAPP inhibitor layer appears to be difficult to notice with the electron microscope images alone, with the visible morphology being similar to that of polished steel. Some darker areas appear as either pits or particulates on the surface, and the EDX spectra obtained for each area appear to be distinct in regards to observed element intensity. Within the two contrasting regions (appearing lighter and darker within the electron microscope image), the elemental make-up is similar, with oxygen, magnesium, zinc and phosphorus present. Whilst there is notable differences in the intensities of the elements shown, with the lighter areas having less pronounced oxygen peaks and more pronounced zinc peaks seen across the sample, quantitative analysis was not done to determine whether this was an actual effect.

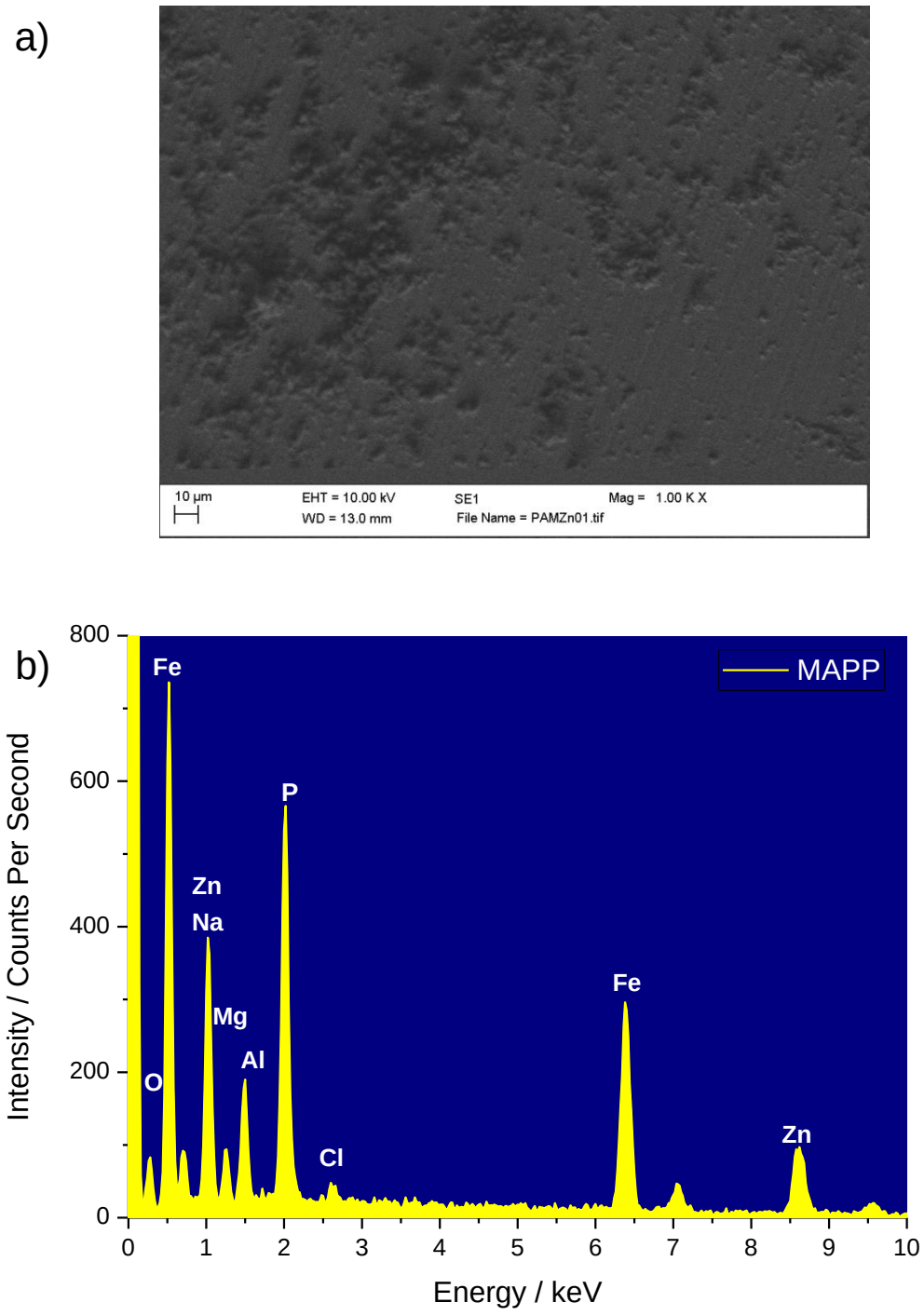

Figure 4.2.16 - Results obtained for steel exposed to a sodium chloride solution containing the MAPP inhibitor pigment and zinc chloride. a) - A representative image of the steel surface after washing from the electron microscopy. b) - Measured EDX spectra representative of the particulate surface shown on SEM.

Strontium Aluminium Polyphosphate (SAPP) with Cathodic Polarisation

In each of the studies seen so far in this chapter, the effect of the inclusion of zinc on the visual corrosion, surface morphology and elemental composition of deposit has been noted on a steel surface. However, it is worth noting that the behaviour of the inhibitor systems is likely to differ in a situation where the metal surface is coupled, such as in galvanised steel. Therefore, a further experiment was added to look at the effects of strontium aluminium polyphosphate on steel when a cathodic potential is imparted during the immersion period.

Figure 4.2.17 shows a representative image obtained through electron microscopy, and an EDX spectrum obtained from the surface. Outside of the surface imperfection seen within the image provided, there appears to be little of interest with regards to surface morphology. Indeed, much of the surface seems to have an appearance similar to that of ground steel. Additionally, the peaks present on the EDX are mainly iron, with potentially a low intensity peak present for zinc. This is consistent with what would be expected for a cathodically protected steel sample.

In this case, it can be suggested that there is no evidence within these results for the deposition of any material from the inhibitor in solution. However, the penetration depth of EDX is high, and there is certainly the potential for thin layer deposition which would be at concentrations and thicknesses beyond the detection limit for this technique. Therefore, it is suggested that a more sensitive technique may need to be employed to gain any meaningful insight into the cathodically polarised systems.

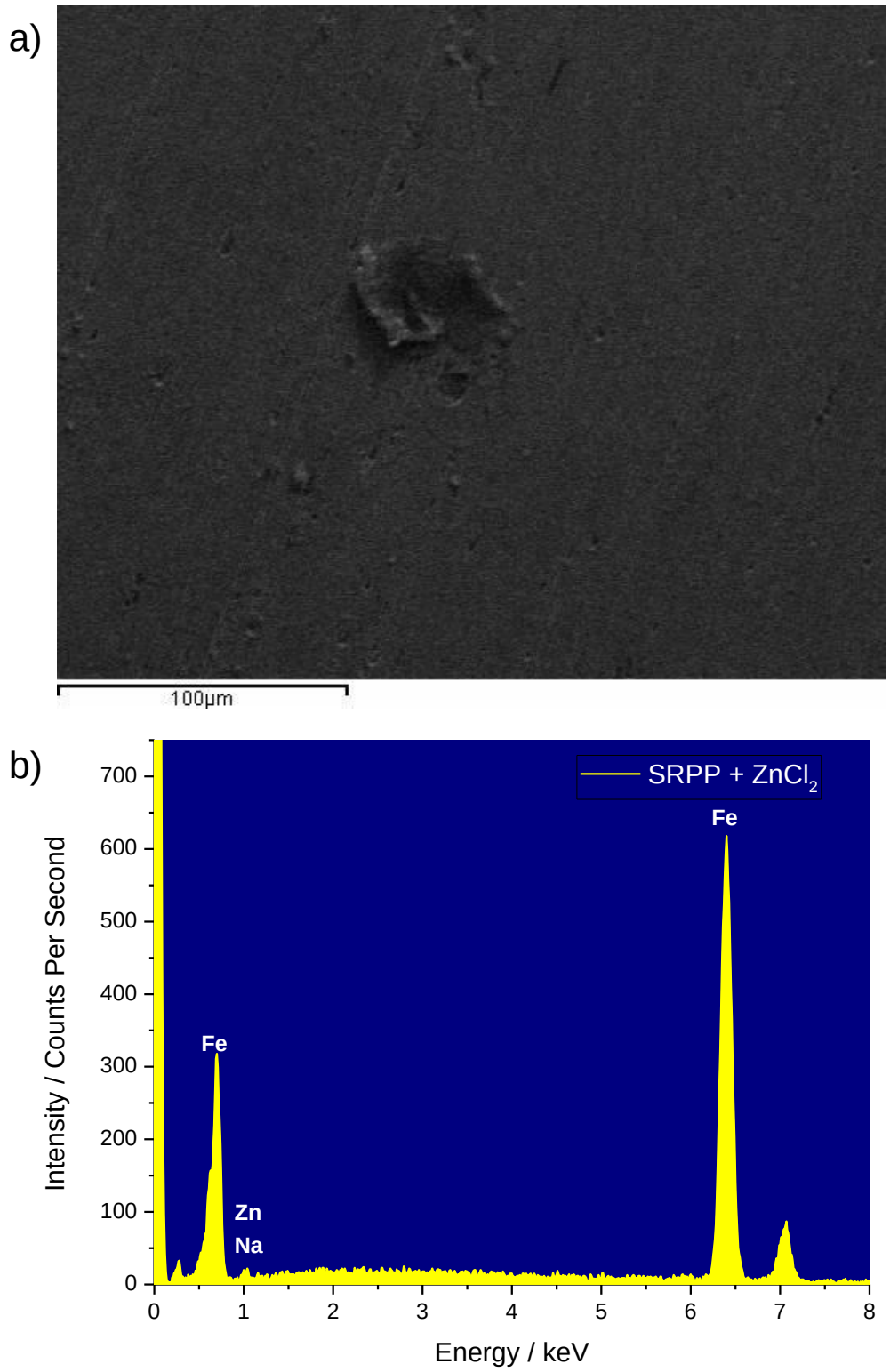

Figure 4.2.17 - Results obtained for steel exposed to a sodium chloride solution containing the SAPP inhibitor pigment and zinc chloride. a) - A representative image of the steel surface, after washing, from the electron microscopy. b) - Measured EDX spectra representative of the surface shown on SEM.

4.2.4 Discussion

In the results presented, differences between the deposited layers, with and without the presence of zinc, can be seen. The effect of zinc on these three polyphosphate inhibitors, and the overall way that these inhibitors appear to work, is seen to be different.

Strontium aluminium polyphosphate shows noteworthy changes when zinc has been introduced to the solution. The adherence of the corrosion products to the surface appear to have improved, with a morphological change of the overlying layer also evident, shifting from a particulate structure to a plate-like structure.

Analysing the elemental composition measured at the surface, a few points of interest can be discerned. Firstly, the absence of strontium from the spectra of both samples suggests that strontium is not incorporated into the surface inhibitive film and therefore plays no part in the anti-corrosion mechanism for SAPP. Secondly, the addition of zinc to the solution also has an effect on the SAPP deposits beyond the detection of zinc at the surface, which may be an expected outcome. The peak attributed to aluminium within the EDX spectra is seen to become lower in intensity, potentially suggesting less incorporation of aluminium into the surface deposit.

One potential explanation for this occurrence is a reaction or ion-exchange with aluminium polyphosphate producing a zinc phosphate or zinc polyphosphate that is the major contributing species to the inhibitor mechanism. In this case, it is important to understand why deposition of these materials may occur.

Through the visual observations laid out in this chapter, and linking back to the electrochemical results presented in the previous chapter, it can be suggested that the main action of the inhibitors is at the cathodic sites. At the cathodic sites, it would be expected that the oxygen reduction reaction would predominantly occur, particularly as the tests were carried out in aerated conditions. Therefore, the local microenvironment at the metal interface

would be subject to an increase in pH which would subsequently lead to the solubility product of the deposited species being exceeded within this microenvironment. With the inhibitors that have been observed, it is likely that the formation of calcium phosphate and zinc phosphate based deposited are due to low solubility and therefore have an increased likelihood to deposit earlier.

The visual inspection of the samples exposed to solutions containing calcium aluminium polyphosphate suggested that there was a reduction in the presence of corrosion at the steel surface with zinc present. This potentially indicates an improvement in corrosion inhibitor efficacy. When using electron microscopy to analyse the morphology of the surface, a change can be seen between the two samples. With the zinc free environment, a thick deposit with a rough morphology forms on the surface. Whereas when zinc is present, the surface deposit morphology appears both thinner and more compact, lacking the roughness of the other specimen.

Elemental analysis of the CAPP exposed steel sample surfaces showed a secondary set of elements, with silicon being easily detectable on the surface. This suggests that the CAPP corrosion inhibitor pigments include an active silicon-based compound alongside the polyphosphate component. One suggestion is that this species is a calcium exchanged silica inhibitor, similar to Shieldex, giving this inhibitor pigment a secondary method of inhibition.

In contrast to the observations made with SAPP, CAPP shows no significant reduction in the levels of aluminium seen at the surface when zinc is incorporated. This suggests that the inhibitor interaction with the zinc species in solution is likely to be different to that of SAPP, where aluminium is not detected on the surface. It is possible that this is indicative of a mechanistic difference overall with the inhibitor action between the two species, but it is impossible to say that for certain with just these results.

Magnesium aluminium polyphosphate, in the absence of zinc chloride, is seen to corrode slightly, with the electron microscope images following cleaning showing a thin surface deposit with a tendency to crack. However, similar to CAPP, the MAPP inhibitor shows a reduction in the level of visible corrosion products on the surface in the presence of zinc, suggesting an improvement in the corrosion resistance of the system.

Electron microscopy showed the presence of thin surface layers on top of the steel substrate in both cases. However, subtle differences between the two environments were evident. Inclusion of the zinc species appears to either improve the adherence properties or reduce the tendency to cracking of the thin deposited layer, as there was no evidence of the clear cracking of the deposited layer that was present on the zinc free sample. Additionally, the zinc containing sample included some particle structures within the deposit layer which were absent on the zinc free surface, suggesting that the presence of zinc may promote the agglomeration of deposits as opposed to producing a simple layer.

Elemental analysis of the two surfaces suggests that the overall layer composition is relatively unchanged, besides the addition of levels of zinc, with no obvious reductions in levels of aluminium or magnesium compared to the sample exposed to magnesium aluminium polyphosphate inhibitor only. However, analysis of the particles present on the zinc exposed surfaces suggests that the particles are enriched in magnesium and phosphorus.

One potential drawback of this experiment is the well-known behaviour of the zinc cation as a cathodic corrosion inhibitor. By incorporating the zinc cation, the behaviour of the solution can be considered to have changed, independent of any interactions the polyphosphate may have with the zinc. Certainly, differences can be seen between the two samples without polyphosphate incorporated, suggesting an effect of zinc.

However, the differences observed between the two uninhibited samples and the pairs of samples containing polyphosphate pigments are distinctly dissimilar. The addition of zinc improves the adhesion of the corrosion products inconsistently on the surface, meaning that whilst the adhesion of the corrosion product to the surface is improved, there were still areas in the tests done within this chapter where the corrosion product is still removed during gentle washing.

Whilst this behaviour is observed in the case of SAPP, albeit with a more consistent film, the same cannot be said for the other polyphosphate inhibitors. Other behaviours, such as the aggregation of magnesium into particles and the reduction of surface aluminium concentration for SAPP, are occurrences in which the presence of zinc, and the interaction of this species with the polyphosphate inhibitor, can be considered to be a major contributor.

Whilst these results suggest differences in deposition structure and elemental composition when zinc is added to the solution, the experimental methodology means that these results may not be directly applicable. By exposing a steel sample to the environment without electrochemical perturbation, the local environment and reactivity of the surface is likely to be different to that of the cut edge of galvanised steel, where the steel will be polarised cathodically by the sacrificial anode.

However, as it was shown in the final experiment in this section, the techniques used in this section may not be suitable for observing the behaviour of these inhibitors on a surface which has been polarised cathodically away from open circuit potential, as neither electron microscopy nor energy dispersive x-ray spectroscopy are able to detect morphological or elemental deposits.

4.2.5 Conclusions

The results shown in this section have shown that the addition of zinc makes changes to the phosphate-substrate interactions above and beyond the differences observed rom the addition of zinc by itself. Notably, this includes changes in the colour and adherence properties of the corrosion products present on the surface. Analysis of the surface has also determined changes in both the elemental composition and structure of the deposits on the surface in which the polyphosphate inhibitor pigments are incorporated.

Behaviour of three polyphosphate inhibitors is distinct, and the following conclusions could be made:

- The presence of some residual anodic activity suggests that the observed inhibitors are predominantly cathodic in nature.
- SAPP, CAPP and MAPP all show changes to the overall surface deposit structure, when compared with the uninhibited samples, with varying degrees of changes to the elemental composition of those deposits
- Elemental analysis of the surfaces determined the presence of aluminium and phosphorus, as well as calcium and silicon for CAPP and magnesium for MAPP
- Strontium was not detected in either SAPP sample, suggesting that it is does not play a significant role in the inhibition mechanism of SAPP.
- Zinc was detected on the surface for CAPP and MAPP following exposure to the solutions containing both the inhibitor and zinc chloride, with little effect noted to other elements present.
- Zinc appears to be an additive constituent in the CAPP deposition layers, with no significant changes observed to the intensity of peaks for other elements measured on the surface

- The surface of the MAPP sample appears to show a secondary particulate deposit in the presence of zinc, which was determined as a magnesium-rich phosphate-containing particle through EDX.
- The addition of zinc improves the corrosion inhibition properties of CAPP and MAPP, as seen by corrosion product coverage on the surface.
- A reduction in the intensity of the aluminium peaks detected on the surface of the SAPP samples to near-zero levels was seen, suggesting a change to the elemental composition of the deposits on the steel surface when zinc chloride is present.

These results give insight into some of the ways in which the polyphosphate inhibitors interact with the steel surface. However, it is clear that, whilst they do give some insight into the behaviour of these polyphosphate inhibitors, they are not directly applicable to the real-world scenario of galvanically coupled zinc and steel, where the couple corrosion potential is cathodic to that of the open circuit potential of mild steel.

In the case of exposing cathodically polarised steels to polyphosphate containing solutions, the deposition on the surface was not visible through SEM and was not detectable by EDX. This suggests that the deposit on a cathodic surface is of a thickness below the detection limit of the EDX, and therefore a technique with greater resolution would be required.

4.3 X-Ray Photoelectron Spectroscopy – The Effect of Zinc on Inhibitor Film Formation

4.3.1 Introduction

In the previous section of this chapter, the morphology and elemental composition of surface deposits on steel arising from corrosion inhibition were shown to be changed by the presence of zinc chloride in polyphosphate inhibitor containing solutions through the use of scanning electron microscopy and energy dispersive x-ray spectroscopy. However, this combination of techniques was not able to determine unambiguously the film compositions that deposited on a cathodically polarised steel sample, presumably because the interaction depth of the incident electron beam at 12 keV (approximately 1 micron) greatly exceeded the deposited film thickness.

Therefore, in this section, the surfaces of cathodically polarised steel samples exposed to polyphosphate inhibitor saturated salt solutions were analysed using x-ray photoelectron spectroscopy, which has both the ability to analyse quantitatively and a specific surface sensitivity, to understand the elemental composition of the inhibitor films deposited, alongside any structural information that may also be concluded from the data gathered. It was therefore anticipated that the effect of zinc cations have on the modified aluminium polyphosphate inhibitors could be ascertained.

4.3.2 Experimental

Samples for x-ray photoelectron spectroscopy analysis were created from mild steel of approximate dimensions 1 cm x 2 cm and given a consistent surface finish using incremental grades of silicon carbide abrasive discs up to and including 4000 grade, followed by subsequent polishing utilising diamond suspensions of size 3 micron, 1 micron and ¼ micron successively. Samples were immersed in the relevant inhibitor-saturated sodium chloride solution and polarised cathodically to the potential of the zinc and steel couple, which was measured during the electrochemical impedance measurements, which is shown in the table below.

Inhibitor System	Measured Mixed Corrosion Potential
Strontium Aluminium Polyphosphate	- 1035 mV
Calcium Aluminium Polyphosphate	- 1050 mV
Magnesium Aluminium Polyphosphate	- 1045 mV

Table 4.3-1 - Measured mixed corrosion potentials that were used as the polarisation values for steel in the XPS study.

In order to mimic the effects of the changing composition of the microenvironment caused by dissolution of zinc in a genuinely coupled sample, zinc chloride was added to the inhibitor containing solution at a concentration of 2 mM. Control samples, without zinc chloride added, were also ran and analysed. Following exposure, the samples were air dried and washed with deionised water. The preparation and exposure of XPS samples was completed ex-situ. Samples were then analysed using Kratos Axis Ultra X-Ray Photoelectron Spectroscope with a monochromated aluminium X-ray source.

4.3.3 Results

The surfaces of steel samples were polarised cathodically and exposed to polyphosphate saturated solutions for periods of time. Spectra were calibrated against charging to the C 1s peak of adventitious carbon, introduced to the sample surface upon contact with air, at 284.8 eV.

Strontium Aluminium Polyphosphate

A representative example survey spectra is shown in Figure 4.3.1, highlighting major elements detected on the surface – zinc, oxygen, phosphorus and carbon. As with the EDX study, the presence of strontium was not detected in any of the obtained XPS spectra. Additionally, none of the spectra showed levels of aluminium that could be considered significant. This is directly contradictory of the EDX study, and will be discussed later in the chapter.

The presence of the iron 2p peak was detected for the samples without zinc chloride added, and the 30 minutes exposure time with added zinc chloride. This is suspected to be due to the low thickness or inconsistent deposition of the phosphate inhibition layer in these samples.

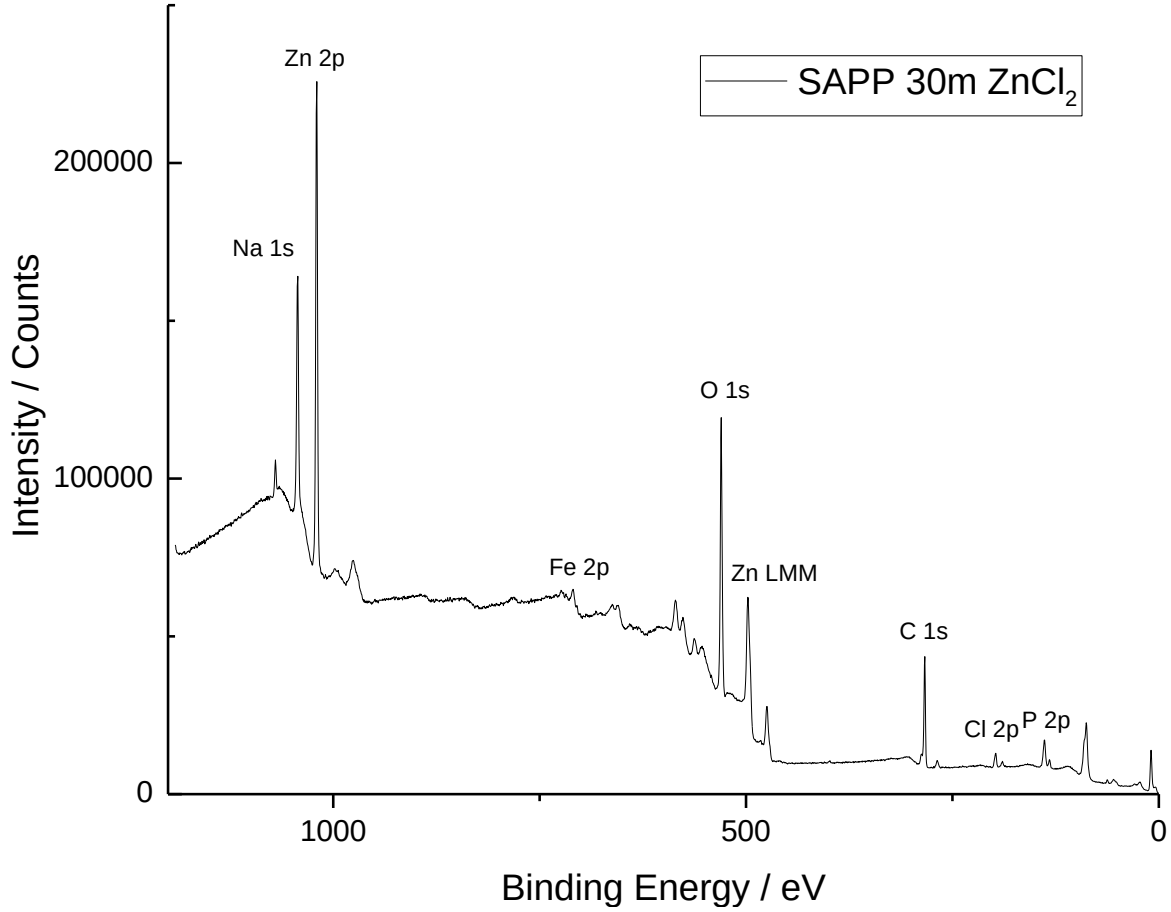

Figure 4.3.1 - An example wide scan XPS spectrum for a steel surface cathodically polarised and exposed to a sodium chloride solution containing SAPP and 2 mM zinc chloride.

The phosphorus content on the surface was followed by taking high resolution spectra across the range of binding energies in which the phosphorus 2p band is located. This is shown in Figure 4.3.2

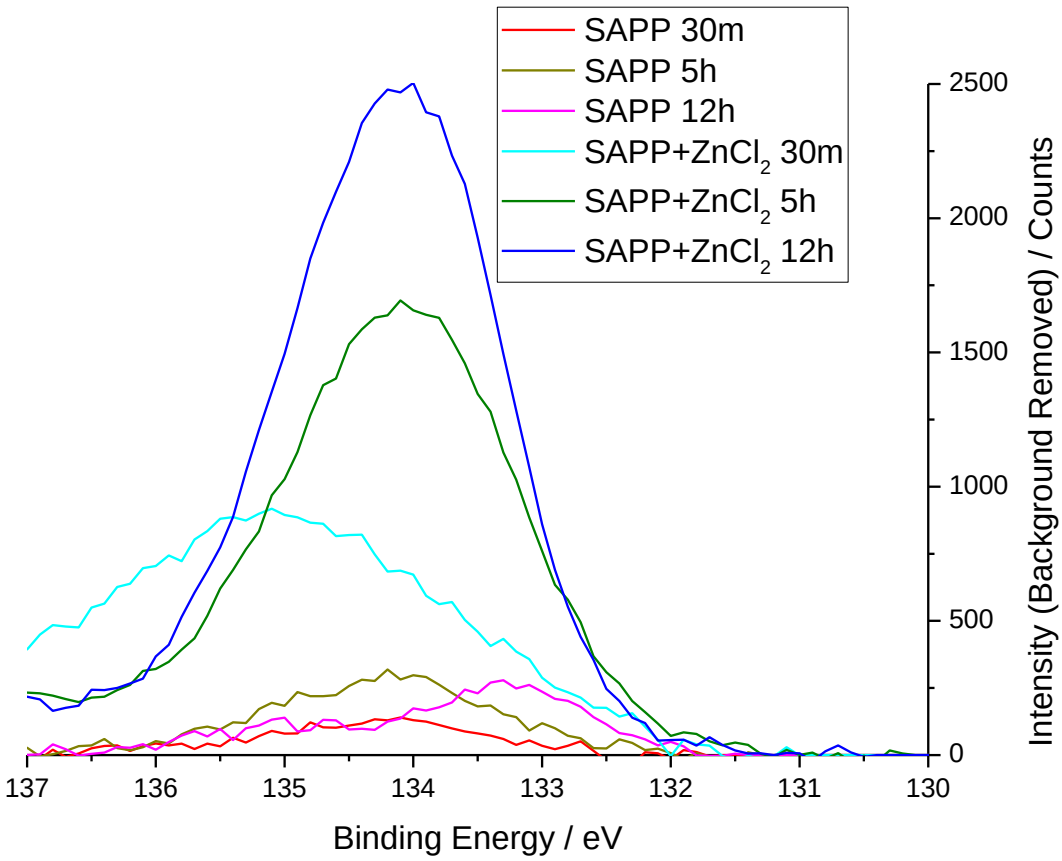

Figure 4.3.2 - High resolution, background-subtracted XPS spectrum of the region containing the phosphorus 2p peak, showing samples obtained with and without zinc chloride. Spectra are shown as obtained, i.e. without smoothing by deconvolution summation.

In this study, the intensity of the phosphorus 2p peak is used as a quantitative measure of the surface coverage and thickness of deposited phosphate layer. As can be seen, the peaks obtained for samples exposed to zinc chloride are all larger than those without zinc chloride present, even after short exposure times. The difference in detected phosphorus between the 12 hour zinc chloride free and 30 minute zinc chloride containing samples is significant, with calculated atomic concentrations of phosphorus of 3 at% and 9 at% respectively.

Low levels of phosphorus, likely from a phosphate source, are consistently observed on the surfaces of samples without the presence of zinc chloride. However, the XPS spectra for non-zinc chloride exposed samples also shows the presence of peaks around 500 eV binding energy, characteristic of the Zn LMM auger peak, which indicates the presence of zinc on the

surface, albeit this has been calculated at low levels (between 0.9 and 1.8 at%). It is therefore possible that zinc impurities within the industrially produced SAPP pigment are a contributing factor to the presence of phosphorus on the surface. Indeed, whilst the structure may not be exactly the same, the binding energies associated with the results link well with previously reported values for zinc phosphate glasses[2].

Deconvolution of the phosphorus peak suggested only a single binding state was present in each spectrum, with peak positions of the P 2p 3/2 and P 2p 1/2 peaks generally lying within 0.5 eV of 133.7 eV and 134.6 eV respectively. However, the sample with 30 minutes exposure to the zinc chloride containing solution was shifted by around 1 eV with respect to these values, which implies that the phosphorus was present with differing chemistry. The discussion section of this chapter will deliberate over the exact composition for these, and those determined in the coming segments.

Calcium Aluminium Polyphosphate

A representative example survey spectra is shown in Figure 4.3.3, highlighting major elements detected on the surface – calcium, zinc, oxygen, phosphorus and carbon. Aluminium was not observed at noteworthy concentrations.

The presence of the iron 2p peak was detected for three samples, both 30 minute samples, and the 5 hour sample without zinc chloride. Again, this is suspected to be due to either thin or incomplete deposition of the phosphate inhibition layer in these samples.

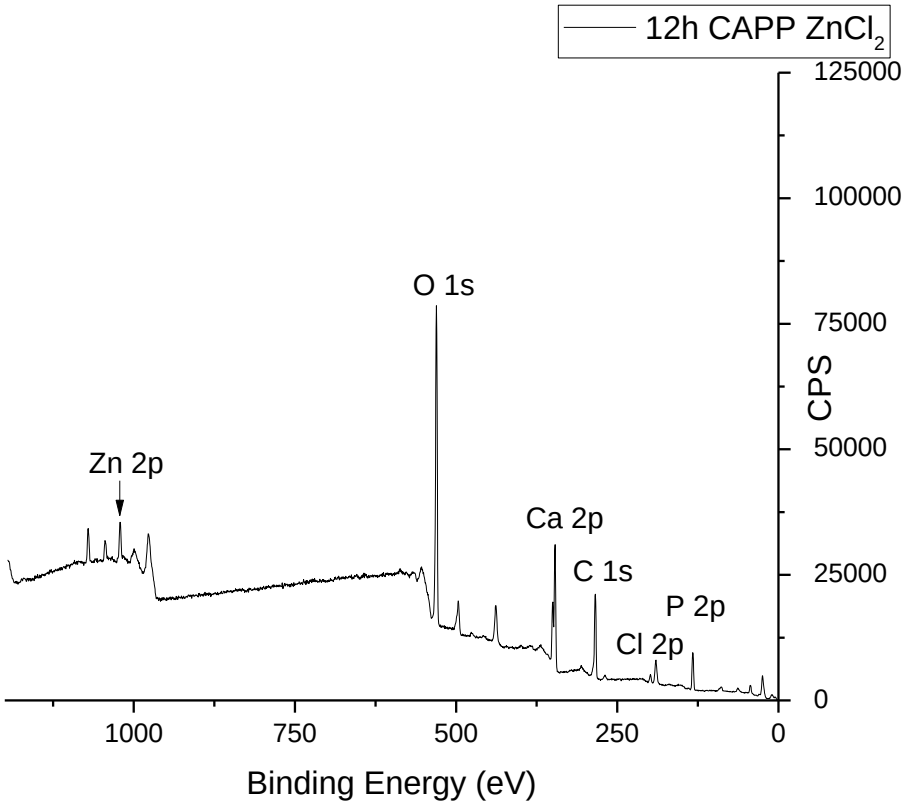

Figure 4.3.3 - An example survey scan XPS spectrum for a steel surface cathodically polarised and exposed to a sodium chloride solution containing CAPP and 2 mM zinc chloride

The phosphorus content on the surface was followed by taking high resolution spectra across the range of binding energies in which the phosphorus 2p band is located. This is shown in Figure 4.3.4.

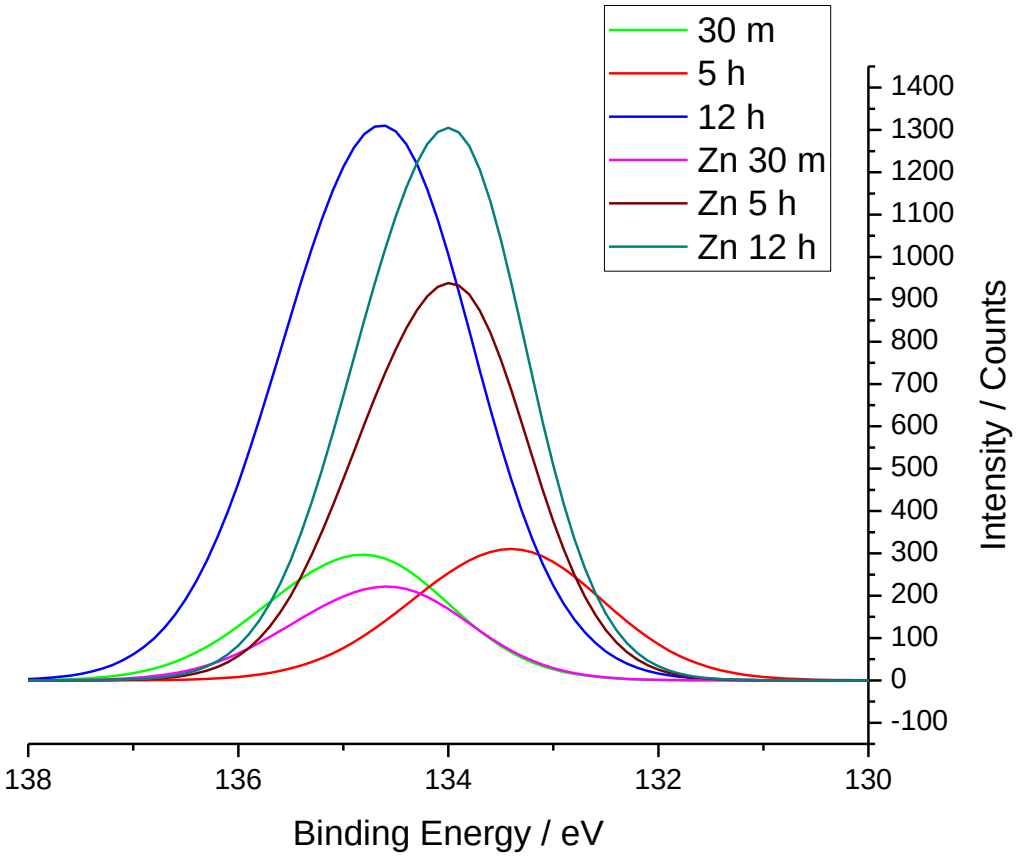

Figure 4.3.4 - High resolution, background-subtracted XPS spectrum of the region containing the phosphorus 2p peak, showing CAPP samples obtained with and without zinc chloride. Spectra shown are summations of the deconvoluted spectra.

The phosphorus profile for CAPP differs to that of SAPP. The phosphorus deposition on the surface for both 30 minute exposures and 12 hour exposures are similar. A difference between the two environments can be seen by comparing the 5 hour exposure peaks, in which the zinc containing sample displays a significantly higher concentration (20 at%) of phosphorus than that of the zinc free sample (5 at%).

Deconvolution of the CAPP P 2p peaks suggests a single binding state present for all samples for the phosphorus 2p peak. The analysed binding states showed a P 2p peak with a binding energy at approximately 133.9 eV for each sample in this set of experiments, within a 0.5 eV tolerance. This binding energy fits well with the understood value for a metallic phosphate.

Magnesium Aluminium Polyphosphate

A representative example survey spectra is shown in Figure 4.3.5, highlighting major elements detected on the surface – magnesium, oxygen, phosphorus and carbon. Aluminium was not observed at noteworthy concentrations in any of the obtained spectra.

The presence of the iron 2p peak was detected for only one sample, the 30 minutes exposure time with added zinc chloride, an indication of low or poor surface coverage.

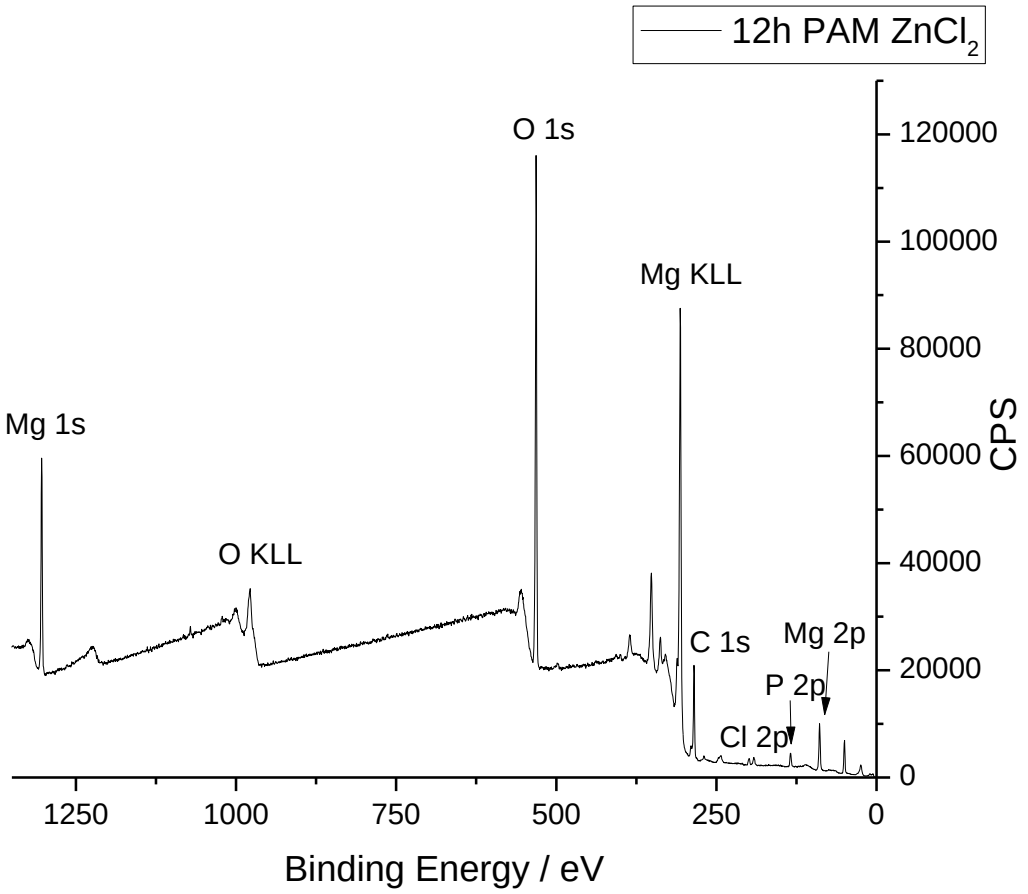

Figure 4.3.5 - An example wide scan XPS spectrum for a steel surface cathodically polarised and exposed to a sodium chloride solution containing MAPP and 2 mM zinc chloride

The phosphorus content on the surface was followed by taking high resolution spectra across the range of binding energies in which the phosphorus 2p band is located. This is shown in Figure 4.3.6.

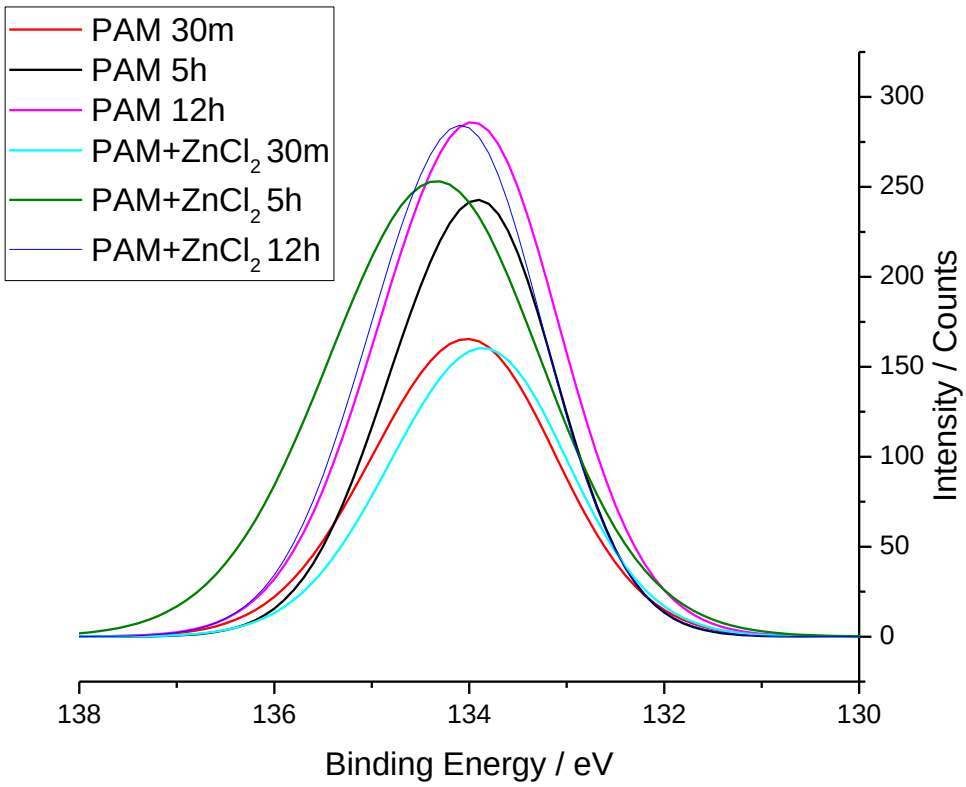

Figure 4.3.6 - High resolution, background-subtracted XPS spectrum of the region containing the phosphorus 2p peak, showing MAPP samples obtained with and without zinc chloride. Spectra shown are summations of the deconvoluted spectra.

The results show approximately equivalent phosphorus peak intensities on the surface, with minor differences in peak binding energy that can be considered to be subtle differences in overall chemistry within the surface chemistry over the observation area that is unlikely to be significant. This will be discussed in more detail in the next section.

The presence of zinc was noted at between 0.1 and 0.4 at% as measured by the stronger Zn 2p peaks, which were seen at just above the noise threshold. Therefore, whilst a zinc peak (Zn 3s) would be expected close the P 2p peak, it is not observed due to the low concentration of zinc.

4.3.4 Discussion

Initial Discussions

In this set of experiments, the detected concentration of phosphorus at the surface using x-ray photoelectron spectroscopy was used as an indicator of both the thickness and degree of surface coverage following exposure. This gives an indication of the overall effect of the presence of zinc ions in solution on the deposition kinetics of phosphate species.

The strontium aluminium polyphosphate samples showed consistently low levels of phosphorus in the samples free of zinc ions. Upon the addition of zinc ions, the detected levels of phosphorus on the surface are noticeably increased. One important observation in this sample set is that the detected phosphorus levels are higher after 30 minutes exposure with zinc than any samples detected throughout 12 hours exposure in the zinc free environment. This suggests that the presence of zinc is important to the mechanism in which phosphate deposits on the surface from the strontium aluminium polyphosphate inhibitor pigment.

Additionally, trace levels of zinc have been detected in the inhibitor pigment itself, suggesting that the samples without added zinc chloride may still contain low levels of zinc within the solution. It is possible that this background level of zinc is a contributing factor into why phosphorus is detectable at the surface at all in the nominally zinc free environments.

One further observation of interest is seen through analysing the binding energy of the phosphorus peak when fitting the constituent 2p components. Only one sample, the 30 minute exposure with zinc chloride sample, had a peak binding energy outside of a deviation of approximately 0.5 eV from the mean value. This potentially suggests a slightly different chemistry of the phosphate layer in the initial stages of deposition.

For the calcium aluminium polyphosphate inhibitor pigment, it can be seen that the phosphorus levels are similar for both the short term and long term exposure samples. This is

true in terms of both the corrected area and overall peak intensity of the P 2p peak. This suggests that the overall deposition is unaffected by the presence of zinc in the solution.

However, there is a notable difference seen between the samples with and without added zinc chloride for the samples exposed to the environment for a period of 5 hours. In this case, the zinc chloride containing solution is shown to have greater phosphorus deposition than the zinc chloride free sample. One potential explanation for this observation is that the phosphate deposition on the steel surface has a distinct, faster mechanism involving zinc which results in a chemically similar deposit.

Surface zinc levels are relatively consistent, in terms of concentration detected by XPS, for the CAPP exposed sample, staying at approximately 2 at%. The suggestion being that zinc is not a major constituent of the deposited phosphate layer. One possible suggestion is that zinc, in this case, acting as more of a catalyst for the phosphate layer, improving speed of uptake but having no effect on the maximum levels deposited. Indeed, Rangel et al determined that the presence of both calcium and zinc ions produces a more compact film which would be consistent with a greater overall phosphate concentration, as seen in the spectra obtained[3]. However, there is some evidence to suggest that zinc is capable of substituting for calcium within calcium phosphate structures (hydroxyapatite), and thus there is the potential for a chemical structure similar to that with a relatively low level of zinc uptake[4].

Despite being noted as present when analysing the surface through EDX, the presence of silicon was also absent from the XPS spectrum. The presence of silicon within the steel would appear a likely source for these peaks within the EDX spectra, however, that would be expected within all spectra and wasn't observed. The most likely explanation for the presence of silicon within the EDX spectra, therefore, is pigment encapsulation within the corrosion product formed on the surface.

Unlike the other two pigments examined within this study, magnesium aluminium polyphosphate appears to show little difference between the two environments. When considering the phosphorus peak, it can be seen that the detected concentration at the surface shows little change. Similarly, the difference in the binding energies can be considered to be insignificant.

Indeed, analysis of any peaks not considered to be affected by external contamination (carbon is suspected to be entirely adventitious, some oxygen may also be) shows that the difference between samples with and without zinc chloride added is minimal across most elements. Even in the case of the spectral peak for zinc, where the difference might be expected to be most pronounced, only trace levels are observed on the surface. This suggests that the role of zinc in the phosphate deposition for the MAPP inhibitor pigment is insignificant, with seemingly zero overall effect on the surface.

In all cases, the XPS spectra lacked the presence of aluminium, suggesting a considerable modification to the proposed aluminium polyphosphate structure of the inhibitor pigments. In the cases of CAPP and MAPP, this finding is in direct contrast to that observed in the SEM-EDX study that has been reported in the previous section of this chapter. There are two possible explanations for this observation. One suggestion could be that the aluminium content measured by EDX was from pigments that have been incorporated within the corrosion product as opposed to ones which have acted on the surface, and therefore would not be present on a sample which has been cathodically polarised. Alternatively, the aluminium containing part of the industrial pigments may have a mode of action on anodic sites, which would also result in a discrepancy between XPS and EDX data.

XPS Quantification and Suggested Structures

The calculations to determine the quantities of the elements on the surface, as obtained by x-ray photoelectron spectroscopy, dismissed elements that were likely to be not included in the surface deposits of interest, such as adventitious carbon. Figure 4.3.7 shows the calculated atomic percentages of the detected phosphate, oxygen, and major secondary element (zinc, calcium or magnesium.)

By analysing the atomic ratios, a structure of each of the deposited phosphates can be suggested. For this, it is expected that the samples with the longest exposure time (12 hours) will be the most representative of the final composition, and thus it is for this exposure time that the composition will be predicted.

In the case of the strontium aluminium polyphosphate inhibitor pigment, even without the addition of zinc chloride, the zinc/phosphorus ratio is around 0.6, suggesting a chemical formula that contains approximately one zinc atom for every two phosphorus atoms present. However, the overall percentage of oxygen seen at the surface is very high, so it is impossible for the oxygen detected to be entirely from deposited phosphates. It is likely that much of the oxygen is incorporated into metal hydroxides on the surface.

The oxygen to phosphorus ratio is maintained at too high a level to realistically be appropriated to entirely phosphate, with a large proportion likely to be attributed to surface hydroxides. However, with the addition of zinc chloride, the oxygen to phosphorus ratio reduces over time from 7:1 to closer to 4:1 and a reduction of the secondary O 1s peak to zero area. This suggests that the oxygen has a greater proportion of phosphate character.

Over the test period, the P 3p 3/2 peak is seen to shift from 134.7 to 133.9, suggesting a shift towards a less positively charged phosphorus environment. It is thought that this coincides with an increased influence of the zinc counter ion on the phosphate.

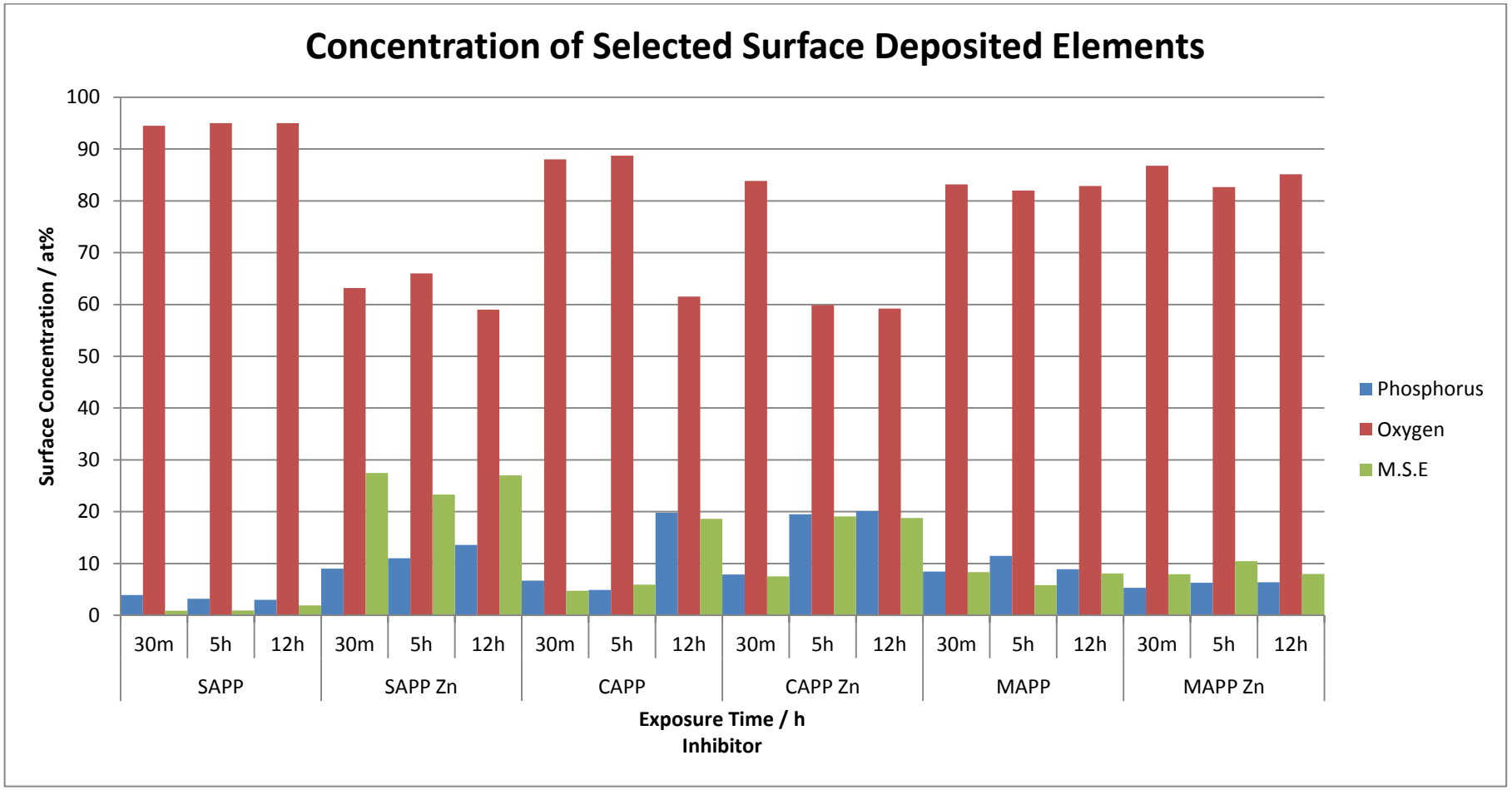

Figure 4.3.7 - Graph showing the concentrations of selected elements deposited on the steel surface, as determined by X-ray photoelectron spectroscopy (M.S.E. – major secondary element(s) including zinc, calcium and magnesium)

With this data, the general chemical formula of the deposit from strontium aluminium phosphate and zinc chloride has been calculated to be most likely zinc metaphosphate ($Zn(PO_3)_2$), as this fits best with the behaviours and results as observed and mentioned in this section.

For calcium aluminium polyphosphate, the calcium/phosphorus ratio sits at approximately 1. However, there is a slight deviation from this in the early exposure times for samples containing zinc chloride, where there is a significant presence of zinc observed. In this case, the addition of the concentrations of zinc and calcium in this case maintains the 1:1 ratio of phosphorus and potentially significant counter ions (in this case, zinc and calcium).

In the earlier exposure times, similar to what is observed with strontium aluminium polyphosphate, the oxygen concentration is seen to be in excess of what could realistically be incorporated into the inhibitor deposits. However, the oxygen/phosphorus ratio for longer exposures (and the middle exposure for the zinc chloride containing solution) tends to an approximate value of 3.

The phosphorus 3p 3/2 peak is seen to shift from approximate values of 134.5 to 133.8, again suggesting a shift to a less positively charged environment, which again coincides to a greater influence of the calcium and/or zinc counter ions in the phosphate environment over time.

Following this analysis, the composition of the surface deposit appears to be something approaching that of calcium pyrophosphate ($Ca_2(P_2O_7)$), as this most fits with the results as presented. However, for the early stages of the samples exposed to the zinc chloride containing solution, it is likely that this may be somewhat substituted. A potential suggested structure of the deposit in this case may well be along the lines of $Ca_{1.3}Zn_{0.7}(P_2O_7)$. However, the implications of this structure are not necessarily clear, albeit with the results presented, it

is possible this is an intermediate stage for the catalyst-like effect that the presence of zinc ions has on the calcium aluminium polyphosphate inhibition.

An alternative theory may be presented in the literature. It has been reported that hydroxyapatite, $Ca_{10}(PO_4)_6(OH)_2$, a common calcium-phosphorus compound, undergoes an ion-exchange process in the presence of zinc to produce zinc exchanged calcium hydroxyapatite[5]. In this case, the structure would approximate to $Ca_{6.5}Zn_{3.5}(PO_4)_6(OH)_2$, although the secondary element (zinc, calcium) to phosphorus ratio would be away from the calculated ratio in this case.

In the case of magnesium aluminium polyphosphate, the magnesium/phosphorus ratio has a sample to sample variation between 1 and 1.5. It was observed that the composition ratio tends towards 1 in the absence of zinc chloride, whilst the presence of zinc chloride tends towards 1.5. Unfortunately, the concentration of oxygen maintains a value above that which could be considered useful for determining the composition using the ratio of this and phosphorus.

In analysing the phosphorus 3p 3/2 peak, it does not appear to change much over the course of the experiment, and maintains a value around 133.8 eV. This suggests that there isn't much change to the phosphorus environment throughout the tests, or that any changes to the chemical environment that phosphorus is exposed to are similar.

With the variation in results over the test period, and few notable trends, it's difficult to ascertain a likely composition of the deposits. However, the one realistic composition suggestion for the deposit in this case is magnesium phosphate ($Mg_3(PO_4)_2$), as this has been previously reported in phosphate inhibition[6]. It could be suggested from the obtained data that the presence of zinc stabilises this particular form. In the case of the zinc chloride free environment, it could be considered that a suggested chemical composition of $Mg_2P_2O_7$

would be more likely. However, the progression of the energy profile for the P 3p 3/2 peak seen in the obtained data does not really fit with this suggestion.

4.3.5 Conclusions

In conclusion, it is clear that the effect of the addition of zinc chloride to a polyphosphate saturated inhibitor solution is dependent on the original composition of the polyphosphate. In each of the three modified aluminium polyphosphates examined in this study, the effect that the presence of zinc in solution had on the deposition of a phosphate layer on the surface of cathodically polarised steel was different. The main conclusions from this set of experiments are:

- Strontium aluminium polyphosphate shows low levels of phosphate deposition on cathodically polarised steel surfaces that do not significantly increase over the 12 hour observation period.
- The presence of zinc results in a greater level of phosphate deposition when paired with the strontium aluminium polyphosphate inhibitor pigment, with phosphate on the surface observed at levels greater than seen throughout the zinc-free samples following low exposure times.
- Calcium aluminium polyphosphate shows significantly increased phosphate deposition levels compared to that of SAPP in the absence of zinc.
- Zinc chloride appears to increase the rate of phosphate deposition for CAPP. However, the maximum level of deposition observed after 12 hours of exposure appears to be the same, suggesting a mechanistic change that is more catalytic in nature.
- Magnesium aluminium polyphosphate appears to show no significant changes between deposition behaviour when exposed to zinc containing or zinc free solutions.

The results suggest that the composition of the solution, and the cationic species contained within, can potentially be manipulated to improve the efficiency of the polyphosphate inhibition through producing a thicker or more coherent phosphate layer.

4.4 Surface Analysis – The Effects of Competing Cationic Species on Inhibitor Film Formation

4.4.1 Introduction

In the previous section of this chapter, the addition of zinc chloride was shown to have varying degrees of effectiveness on improving the deposition characteristics of modified aluminium polyphosphate inhibitor pigments. Strontium aluminium polyphosphate showed a clear increase in the overall phosphate deposition observed when zinc chloride was present. Conversely, magnesium aluminium polyphosphate was shown to be relatively unaffected by the presence of zinc chloride in solution, with phosphate deposition observed to be similar in terms of concentration, and surface uptake of zinc was determined to be low.

Following these observations, it can be suggested that the addition of a secondary species could be utilised to improve the corrosion inhibitor efficiency of these pigments. In this chapter section, the initial steps towards understanding the effects of the addition of several different metallic chlorides on the composition of surface depositions on cathodically polarised steel samples were taken, by observing the behaviour using x-ray photoelectron spectroscopy.

4.4.2 Experimental

Samples for x-ray photoelectron spectroscopy analysis were created from mild steel of approximate dimensions 1 cm x 2 cm and given a consistent surface finish using incremental grades of silicon carbide abrasive discs up to and including 4000 grade, followed by subsequent polishing utilising diamond suspensions of size 3 micron, 1 micron and ¼ micron successively. Samples were immersed in an inhibitor saturated sodium chloride solution and polarised cathodically to the potential of the zinc and steel couple, which was measured during the electrochemical impedance measurements.

For the specimens requiring a zinc-rich environment, zinc chloride was added to the solutions, prior to exposure, until a relative zinc ion concentration of 2 mM was obtained. Following exposure, the samples were air dried and washed gently with deionised water. The preparation and exposure of XPS samples was completed ex-situ. Samples were then analysed using Kratos Axis Nova X-Ray Photoelectron Spectroscope with a monochromated aluminium X-ray source.

4.4.3 Results

The initial experiments for this section looked at replacing the zinc chloride addition from the previous chapter section with equal concentrations of other metal chlorides to determine the differing effects, if any. This concentrated on two of the inhibitor pigments observed previously, strontium aluminium polyphosphate and calcium aluminium polyphosphate.

Effect of Calcium

Strontium Aluminium Polyphosphate

A representative example survey spectra is shown in Figure 4.4.1, highlighting major elements detected on the surface – zinc, oxygen, phosphorus, calcium and carbon.

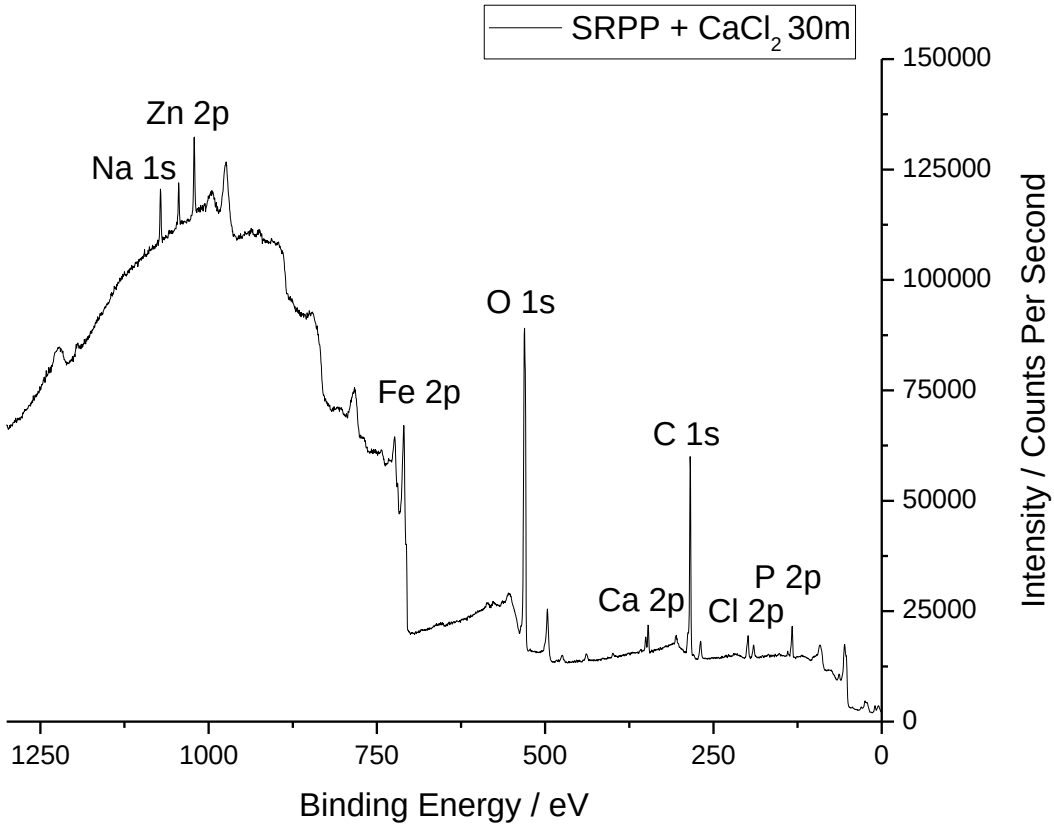

Figure 4.4.1 - An example wide scan XPS spectrum for a steel surface cathodically polarised and exposed to a sodium chloride solution containing SAPP and calcium chloride.

The presence of a peak associated with metallic iron within the spectra is used to determine the depth and surface coverage of the deposited layer. With the penetration depth of the XPS technique being approximately 10 nm, and the spot size being on the order of mm, the detection of metallic iron can be considered to show either incomplete coverage or thin layer deposition. In this case, iron was observed only on the short exposure time sample.

For these samples, the high resolution spectra for the calcium 2p and phosphorus 2p peaks were followed to determine the development of the surface layer.

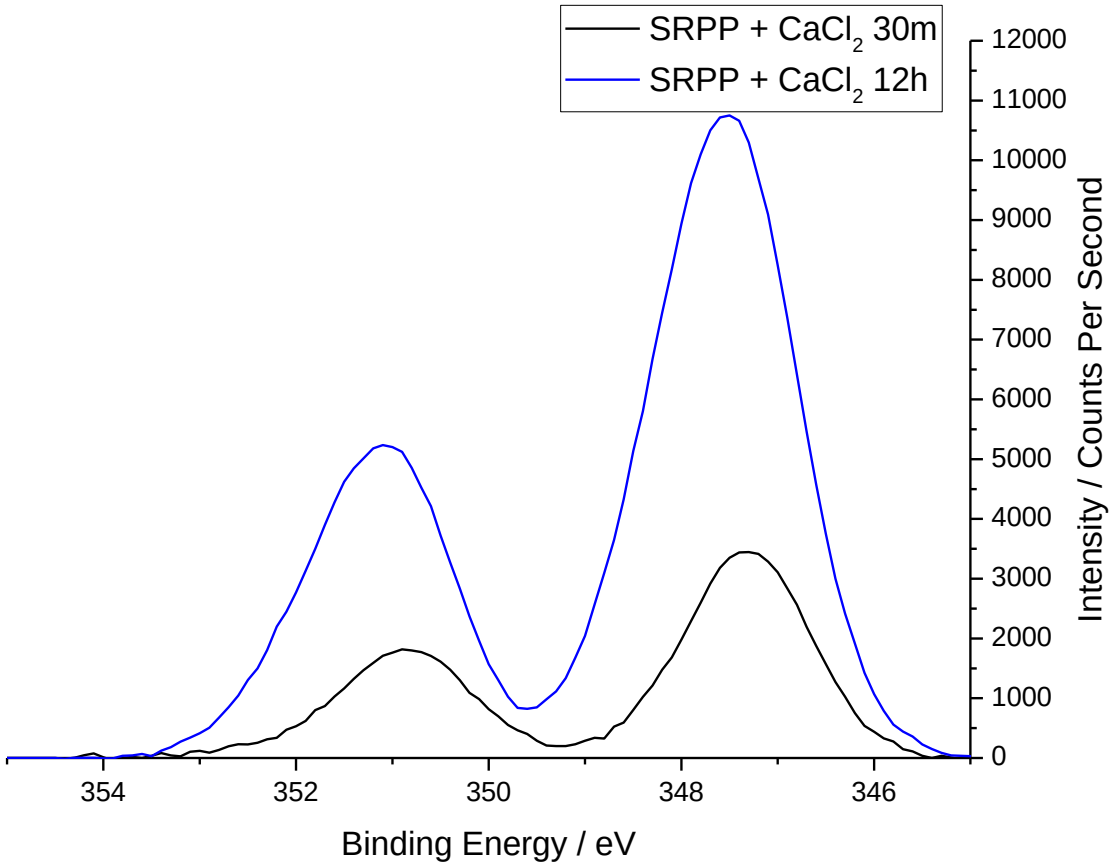

Figure 4.4.2 - High resolution, background-subtracted XPS spectrum of the region containing the calcium 2p peak. Spectra shown are summations of the deconvoluted spectra.

Figure 4.4.2 shows the XPS spectra over the region of binding energies in which the calcium 2p peak is situated. In these spectra, calcium was shown to exist in a single binding state over both the exposure times examined, with the observed concentration increasing from 3.8 at% to 6.2at% at the longer exposure time. It was also noted that there was only a small shift in the observed binding energies for this peak between the two exposure times.

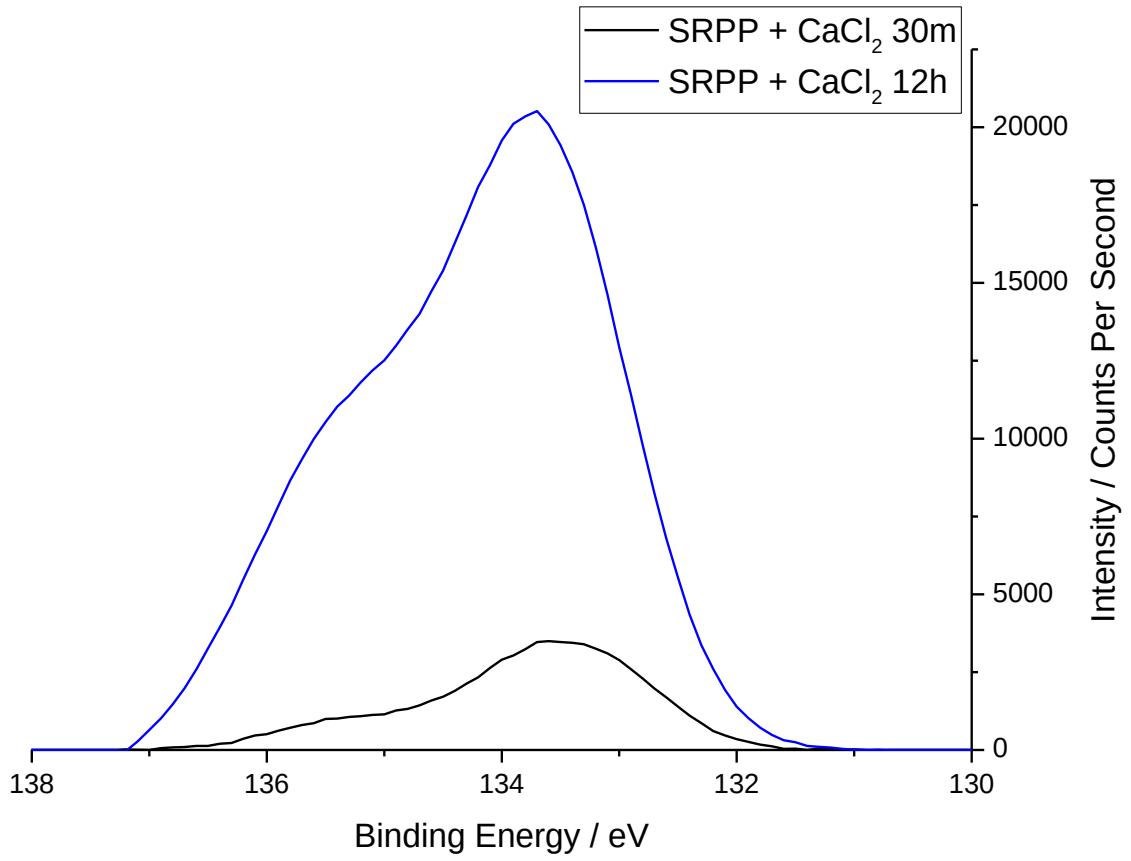

Figure 4.4.3 - High resolution, background-subtracted XPS spectrum of the region containing the phosphorus 2p peak. Spectra shown are summations of the deconvoluted spectra.

Figure 4.4.3 shows the observed XPS spectra for the phosphorus 2p peak. In this case, a large increase in concentration between the short exposure time and longer exposure time is observed. Component fitting for this peak showed two binding states present for the phosphorus peak. In the fitting, the phosphorus 2p 3/2 peaks are observed at binding energies of 133.3 eV and 135.3 eV, with a peak splitting of approximately +0.87 eV to the relevant 2p 1/2 peak. The area ratio between the two binding states changes from 6:1 in the short exposure time sample to 3:1 in the longer exposure time sample.

Calcium Aluminium Polyphosphate

A representative example survey spectra is shown in Figure 4.4.4, highlighting major elements detected on the surface – oxygen, phosphorus, calcium and carbon.

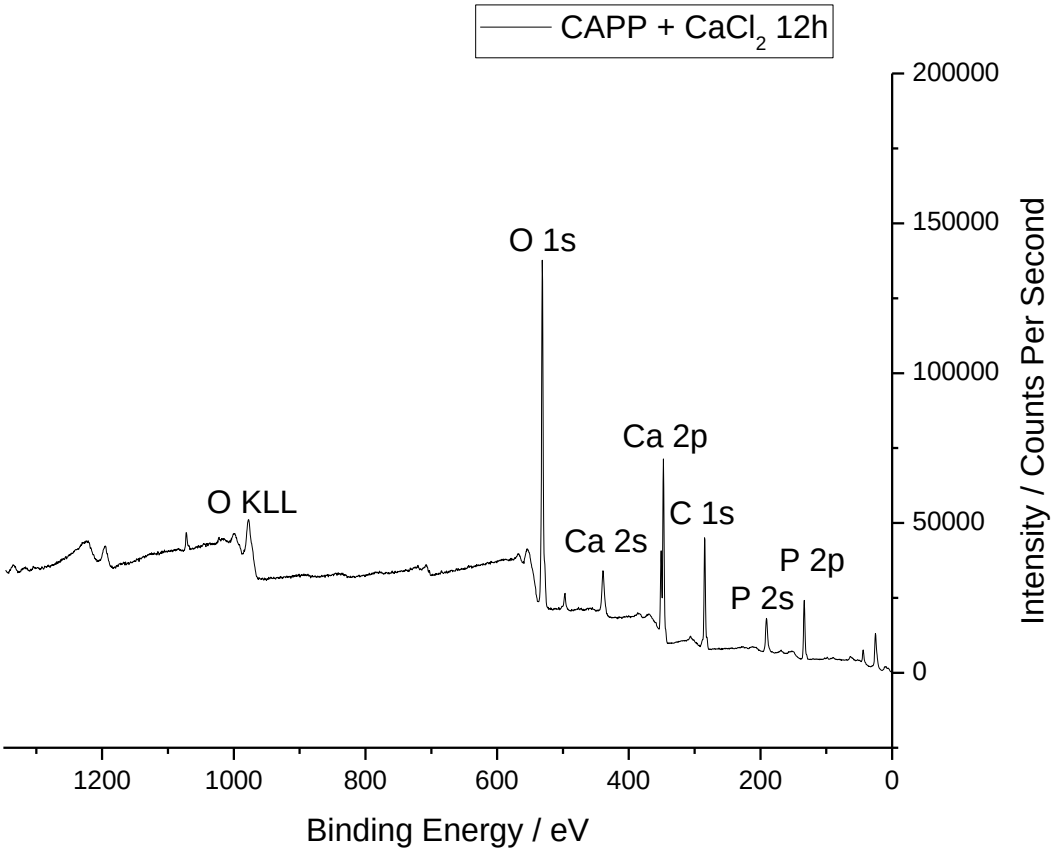

Figure 4.4.4 - An example wide scan XPS spectrum for a steel surface cathodically polarised and exposed to a sodium chloride solution containing CAPP and calcium chloride.

The iron 2p peak, which is used as an indicator for deposition thickness and surface coverage, is present only at the lowest exposure time sample, and is only present at a low concentration. This suggests that the deposition layer on the steel surface is relatively quick.

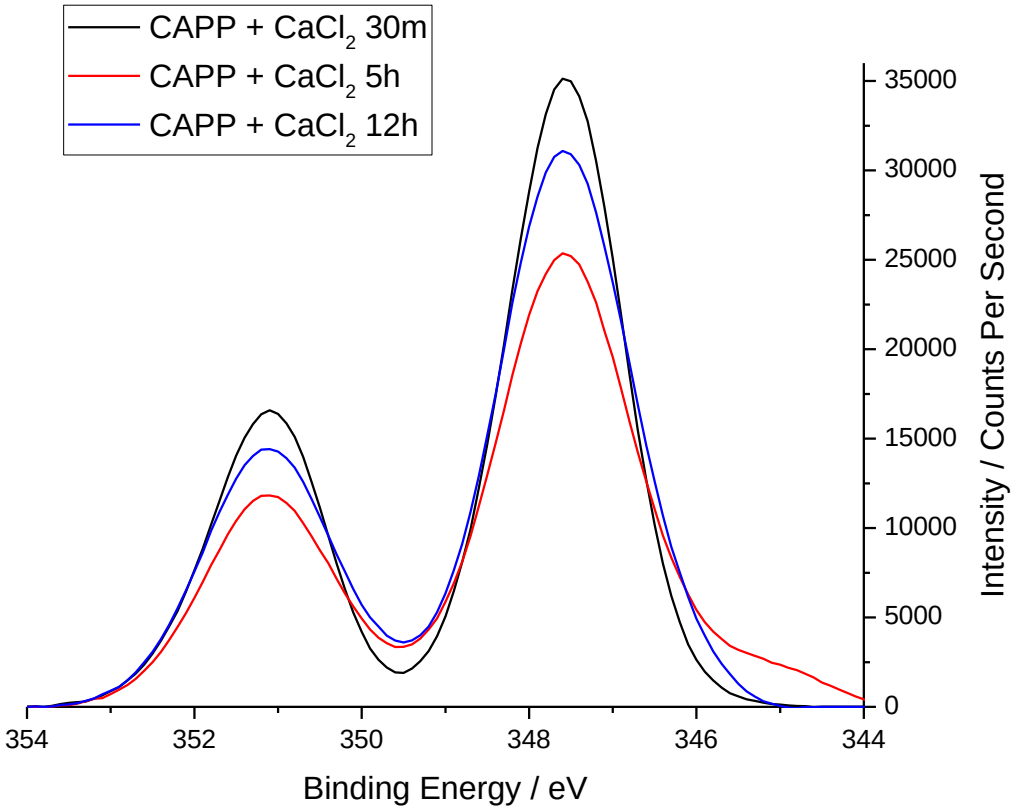

Figure 4.4.5 - High resolution, background-subtracted XPS spectrum of the region containing the calcium 2p peak. Spectra shown are summations of the deconvoluted spectra.

Figure 4.4.5 shows the calcium 2p XPS spectra. Calcium is observed in a singular binding state across all observed samples at a consistent binding energy throughout. No clear trend in surface calcium concentration could be determined from the XPS spectra.

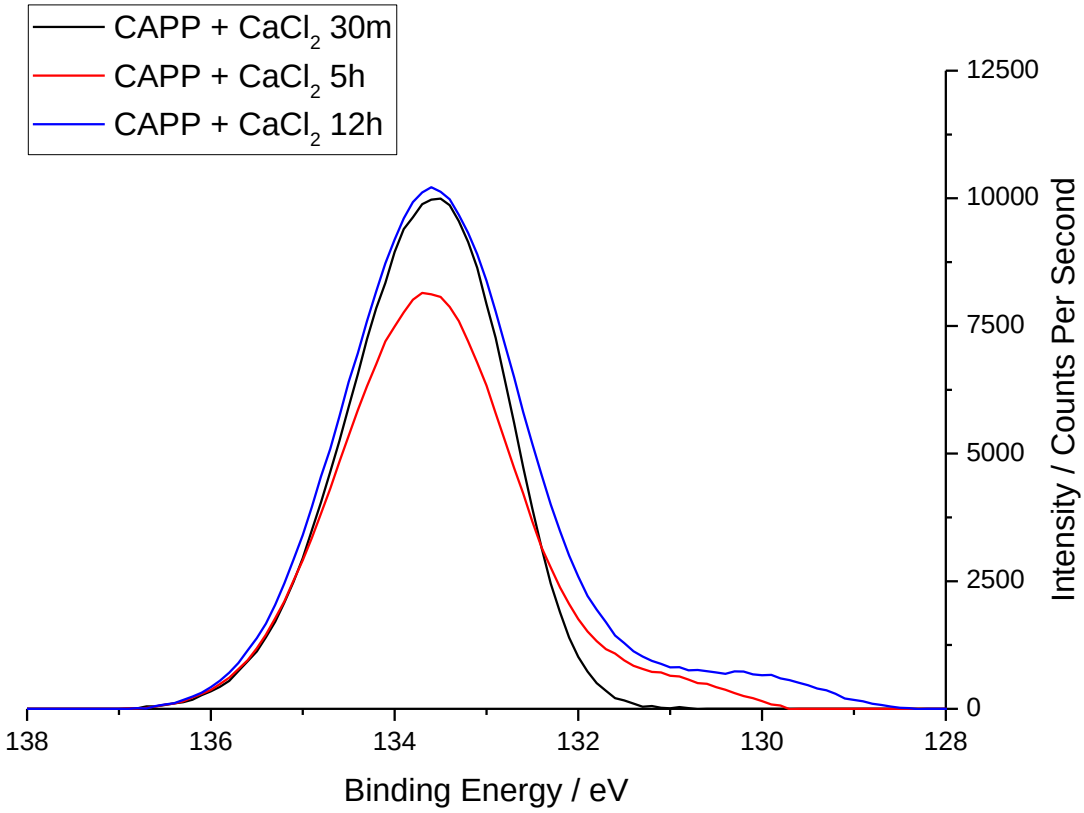

Figure 4.4.6 - High resolution, background-subtracted XPS spectrum of the region containing the magnesium 1s peak. Spectra shown are summations of the deconvoluted spectra.

Figure 4.4.6 shows the XPS spectra for the phosphorus 2p peak. A single binding state was observed throughout the exposure period, with the P 2p 3/2 peak presiding at a binding energy of 133.3 eV. Following quantification calculations, it can be seen that whilst the intensities at first glance appear inconsistent, the concentration of phosphorus detected on the surface increases from around 18 at% to 22 at% throughout the observation period.

Effect of Magnesium

Strontium Aluminium Polyphosphate

A representative example survey spectra is shown in Figure 4.4.7, highlighting major elements detected on the surface – magnesium, oxygen, phosphorus, and carbon.

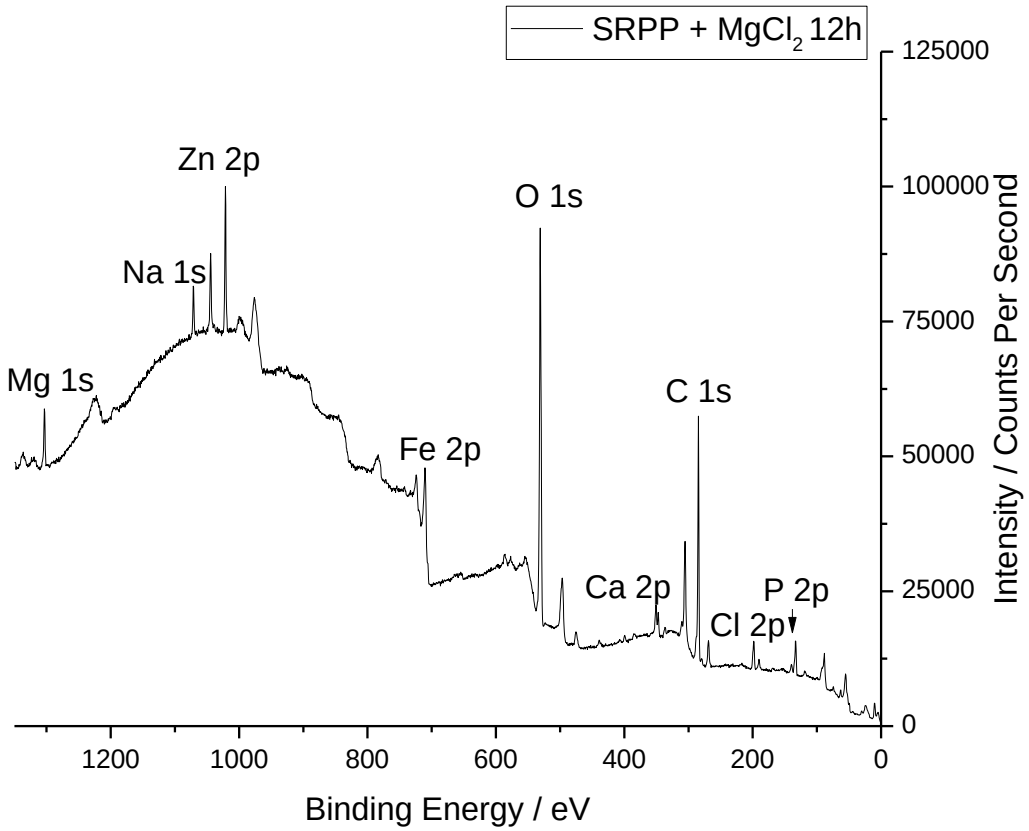

Figure 4.4.7 - An example wide scan XPS spectrum for a steel surface cathodically polarised and exposed to a sodium chloride solution containing SAPP and magnesium chloride.

The overall quality of deposition in this system is suggested to be poor. Iron detected in the XPS spectra for these systems is assumed to be from the substrate surface, and a strong iron peak is observed across all exposure times tested for this particular environment.

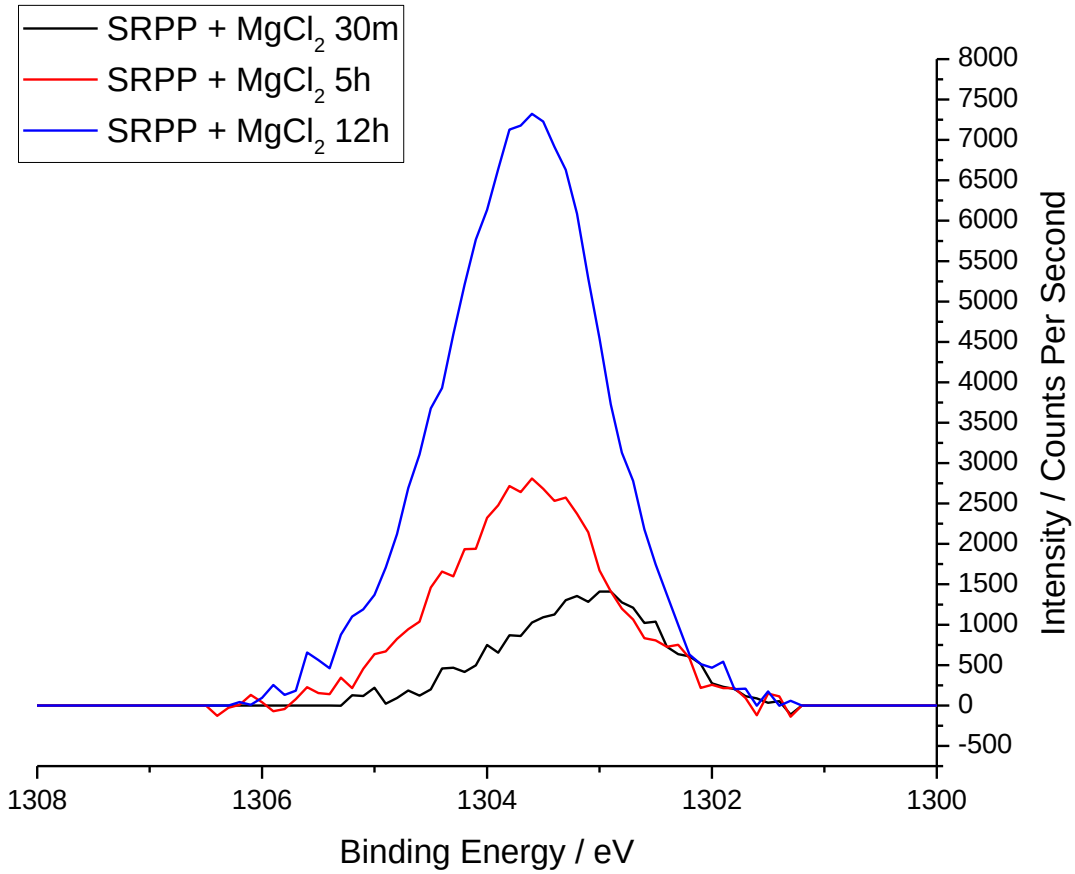

Figure 4.4.8 - High resolution, background-subtracted XPS spectrum of the region containing the magnesium 1s peak. The spectra displayed in this figure are as obtained without additional processing.

Figure 4.4.8 shows the XPS spectra for the magnesium 1s peak. The peak has a single binding state across all measured exposure times at approximately 1303.6 eV. This peak appears to increase consistently across the exposure times, suggesting an uptake of magnesium on the substrate surface.

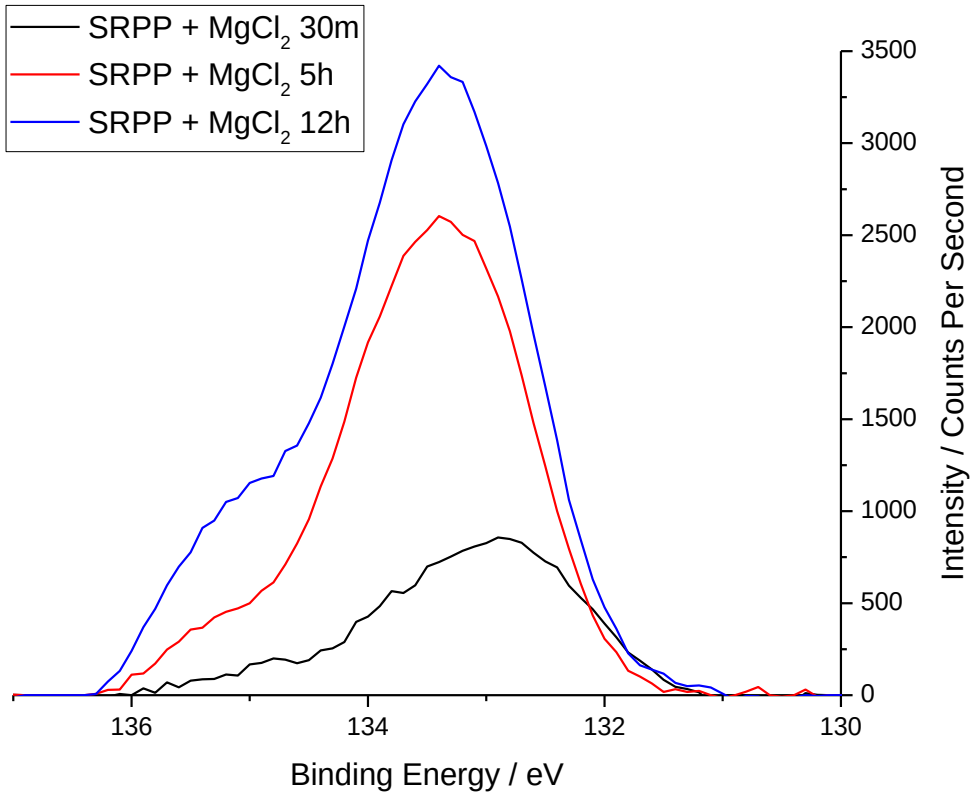

Figure 4.4.9 - High resolution, background-subtracted XPS spectrum of the region containing the phosphorus 2p peak. The spectra displayed in this figure are as obtained without additional processing.

Figure 4.4.9 shows the XPS spectra for the phosphorus 2p peak. There are two observed binding energies for this peak over the observation period, with the 2p 3/2 peak situated at 133.1 eV and 135.1 eV. A clear trend for the area ratio between the phosphorus bound in these states is not apparent, with the ratio proceeding from 6:1, to 11:1 and finalising at 4:1 at the longest exposure time. There is, however, a clear increase in the observed concentration from the shortest to the longest exposure times observed.

Within this set of experiments, a large calcium impurity was observed. It is suspected that this may have been an inherent impurity within the magnesium chloride that was used. It is noted that this impurity was most prominent on the 30 minute sample. Therefore, it is possible that this accounts for the secondary binding state and overall movement of the binding energy.

Calcium Aluminium Polyphosphate

A representative example survey spectra is shown in Figure 4.4.10, highlighting major elements detected on the surface – magnesium, oxygen, phosphorus, calcium and carbon.

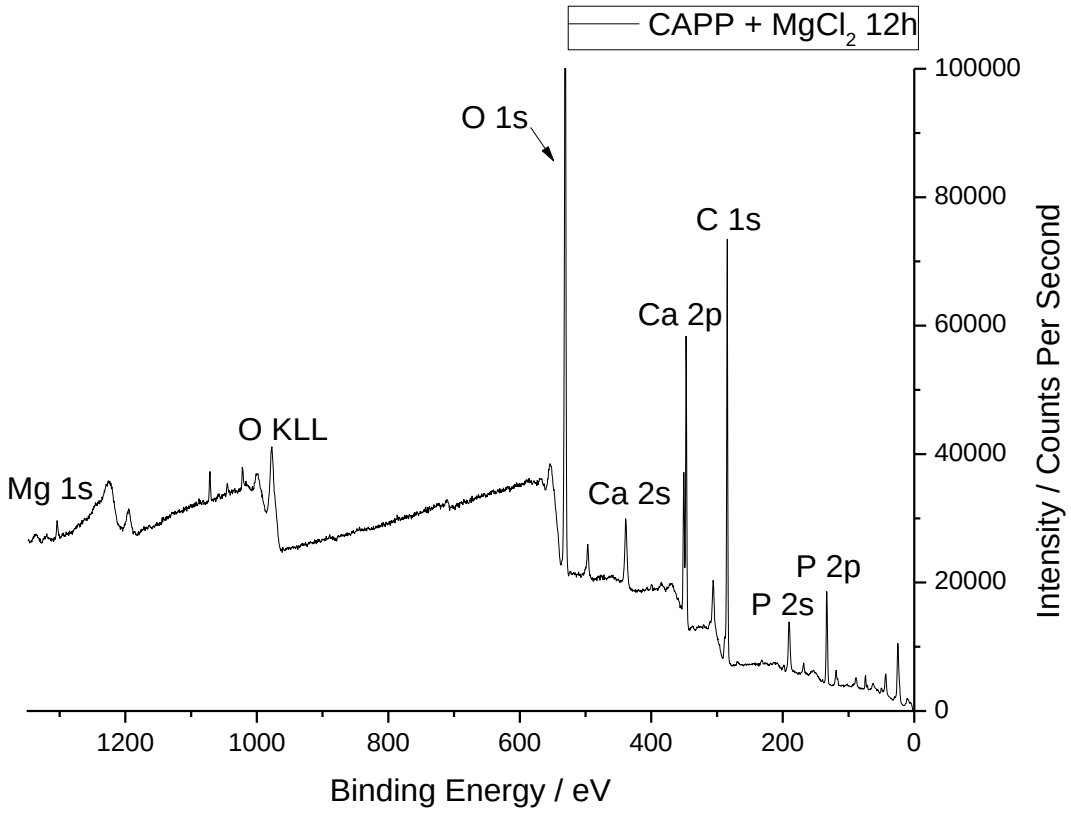

Figure 4.4.10 - An example wide scan XPS spectrum for a steel surface cathodically polarised and exposed to a sodium chloride solution containing CAPP and magnesium chloride.

The presence of iron within the spectra is used to determine the depth and surface coverage of the deposited layer. In this case, iron was observed on the short exposure time sample only. For this system, high resolution spectra were obtained for the regions containing magnesium, calcium and phosphorus peaks to determine the nature of the deposited layer.

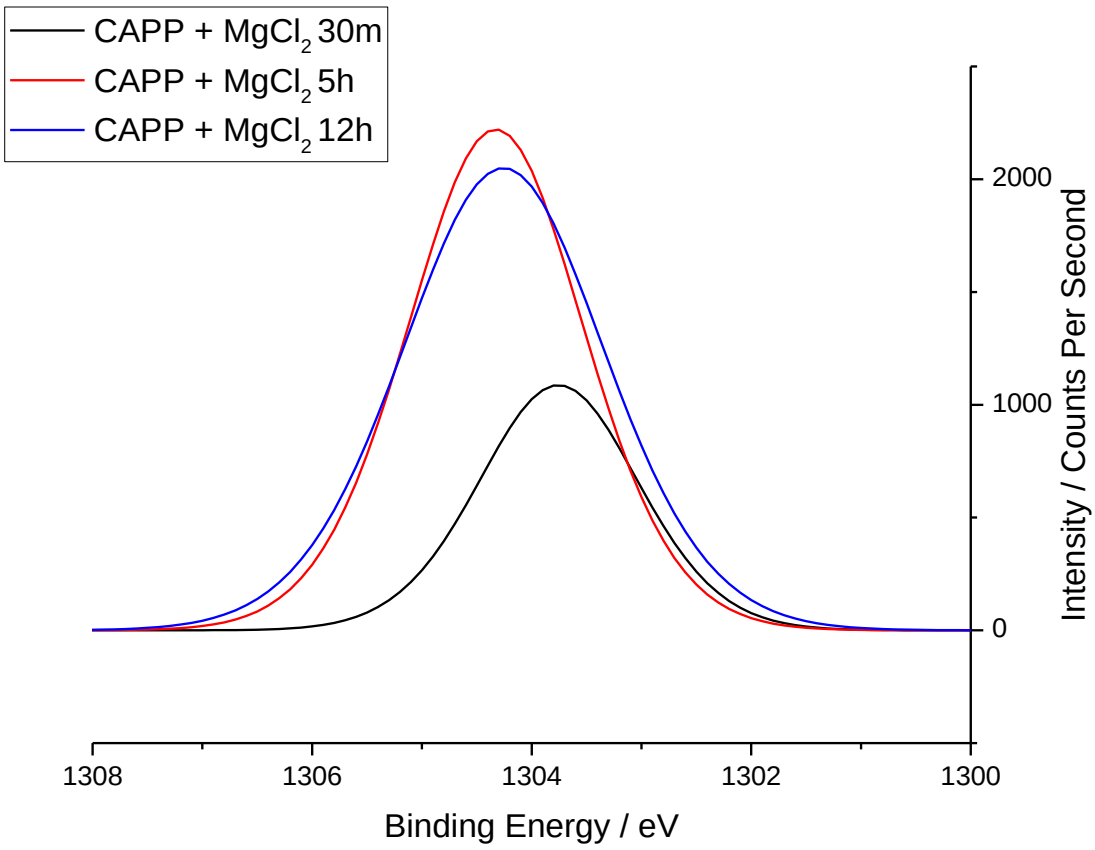

Figure 4.4.11 - High resolution, background-subtracted XPS spectrum of the region containing the magnesium 1s peak. Spectra shown are summations of the deconvoluted spectra.

Figure 4.4.11 shows the magnesium 1s peak at the selected observation times. This peak exhibits a singular binding state, which shifts to higher binding energies between the early and mid-length exposure times. This suggests molecular bonding with an electronegative species, potentially greater phosphate character. At this point, the level of magnesium detected at the surface can be considered to be approximately consistent throughout the remainder of exposure.

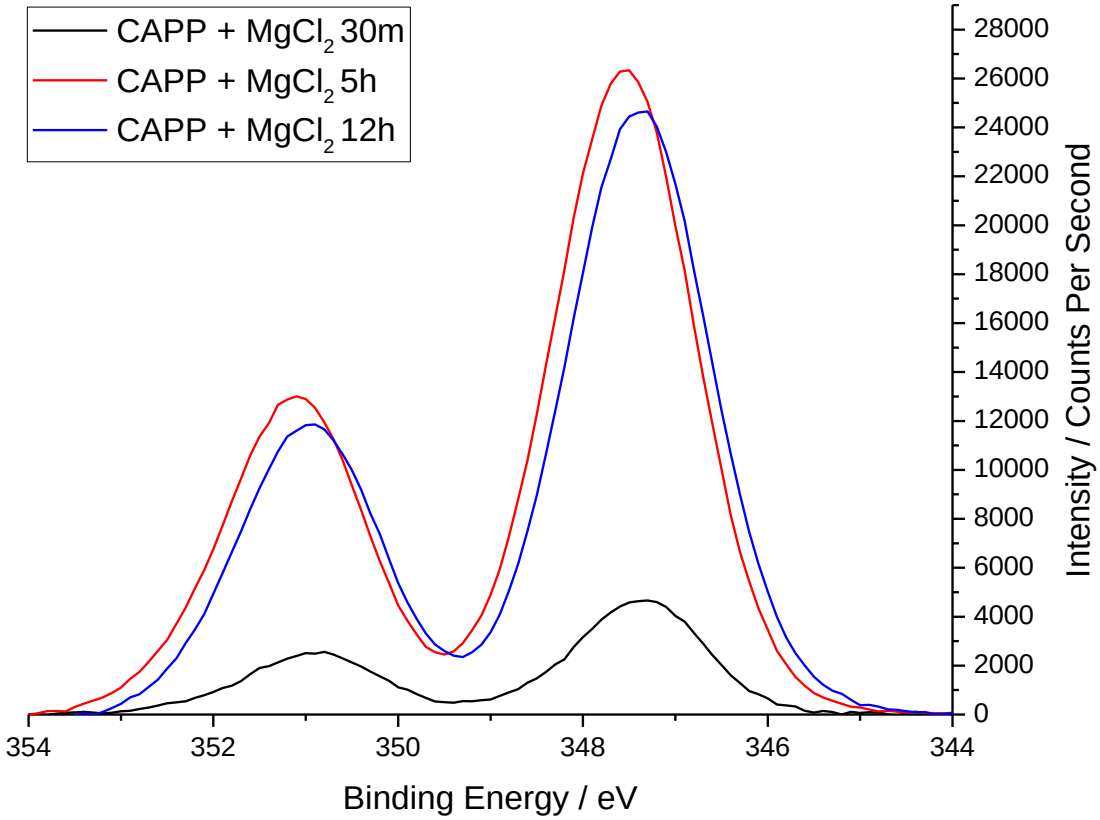

Figure 4.4.12 - High resolution, background-subtracted XPS spectrum of the region containing the calcium 2p peak. Spectra shown are summations of the deconvoluted spectra.

Figure 4.4.12 shows the high resolution spectra for the calcium 2p peak. The calcium peak contains a singular binding state at approximately 347.4 eV and is relatively consistent at this value throughout the test. With regards to the concentration levels of calcium on the surface, the profile follows similar to that of the magnesium peak.

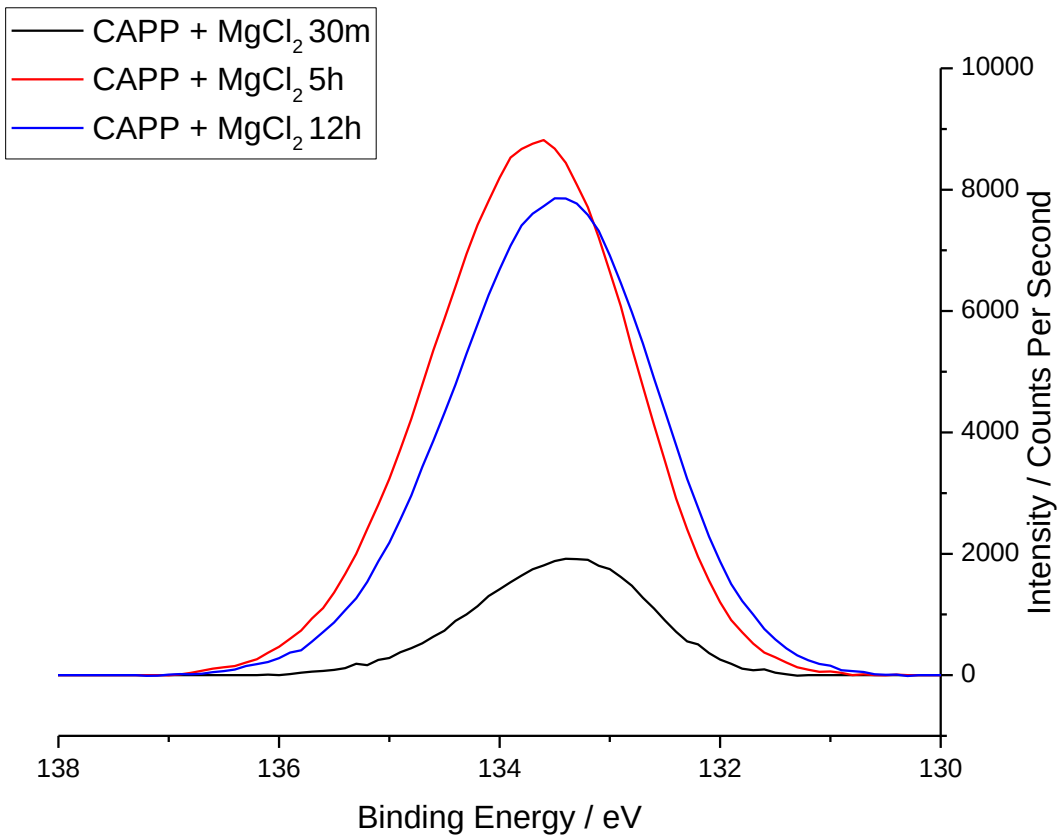

Figure 4.4.13 - High resolution, background-subtracted XPS spectrum of the region containing the phosphorus 2p peak. Spectra shown are summations of the deconvoluted spectra.

Figure 4.4.13 shows the high resolution spectra for the phosphorus 2p peak. The phosphorus peak also exhibits a singular binding state that can be considered to be situated at a consistent binding energy of 133.4 eV, within experimental error. This peak also follows the same trends with regards to concentration levels as the other elements mentioned within this sample environment.

Effect of Aluminium

Strontium Aluminium Polyphosphate

A representative example survey spectra is shown in Figure 4.4.14, highlighting major elements detected on the surface – zinc, oxygen, phosphorus and carbon.

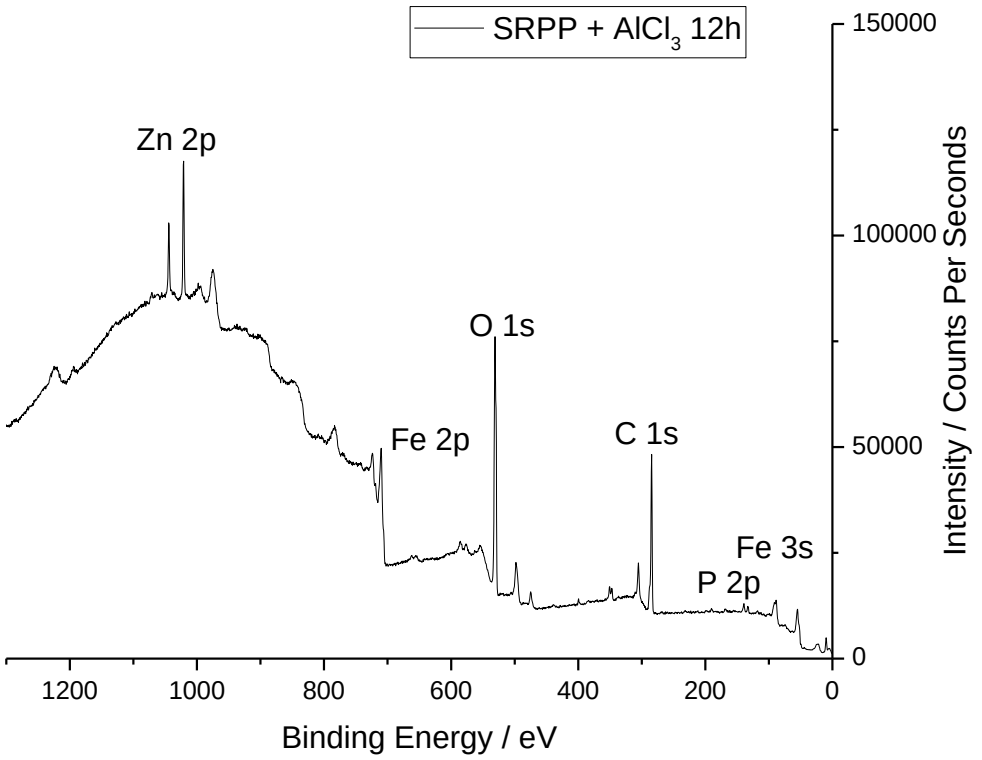

Figure 4.4.14 - An example wide scan XPS spectrum for a steel surface cathodically polarised and exposed to a sodium chloride solution containing SAPP and both aluminium chloride.

The presence of iron within the spectra is used to determine the depth and surface coverage of the deposited layer. In this case, iron was observed on all measured spectra. This suggests poor surface coverage of phosphate in this system. For this system, high resolution spectra of the phosphorus 2p area, including the zinc 3s area, was followed to determine the quality and composition of surface deposits.

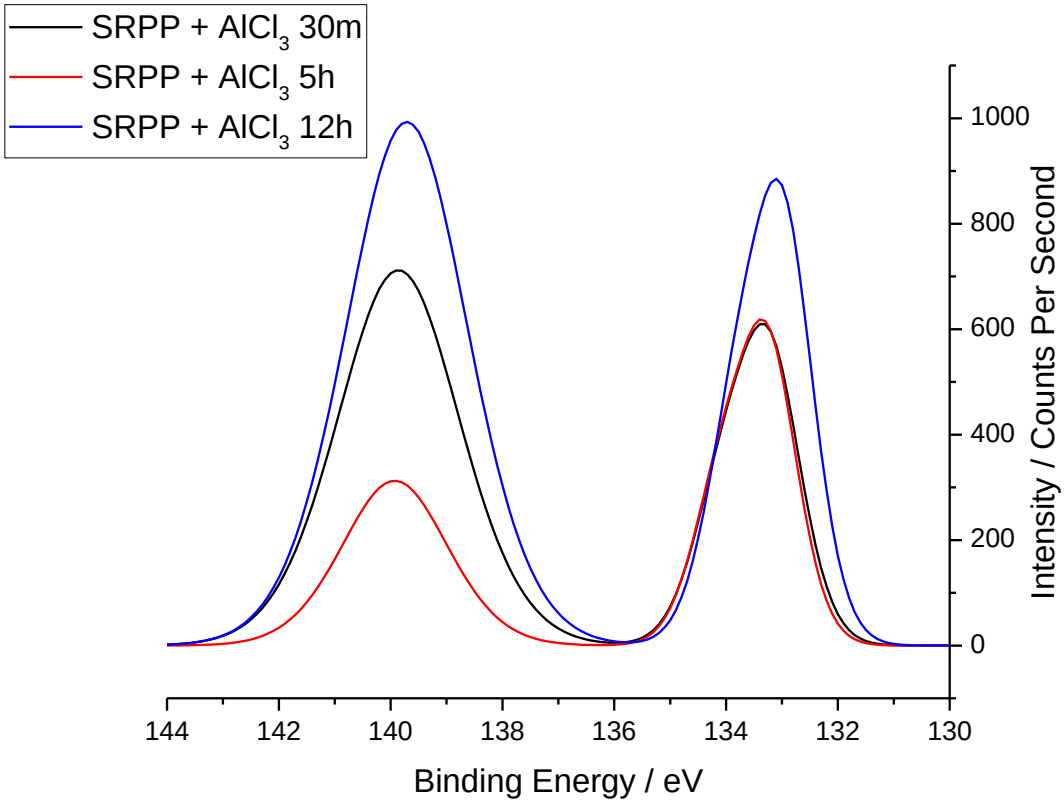

Figure 4.4.15 - High resolution, background-subtracted XPS spectrum of the region containing the phosphorus 2p and zinc 3s peaks. Spectra shown are summations of the deconvoluted spectra.

Figure 4.4.15 shows the high resolution spectra containing the phosphorus 2p and zinc 3s peaks. Both show singular binding states, with the phosphorus peak situated at around 133.5eV and the zinc peak situated at around 140.1 eV. It can be considered that, with regards to the levels of phosphate, an initial deposition may be present that is unaffected within mid-term exposure times. A small increase is evident for the longest exposure time.

The levels of zinc on the surface appears to show no logical progression throughout the test, with the measured concentrations initially dropping from 5.1 at% to 1.7 at% and then raising to 7.2 at% in the longest exposure time. This observation could suggest that there is an inconsistent surface deposition and the 5 hour exposure sample spectra obtain positions have taken place on areas of poor surface coverage.

One other possible explanation can be suggested from the presence of aluminium on the surface, at 3.1 at% for the 5 hour exposure compared to 1.7 at% for the 12 hour exposure and none noted at 30 minutes. In this case, it could be considered that whilst the presence of aluminium appears to aid the deposition of phosphate overall compared to the no additives strontium aluminium polyphosphate, there is a competitive nature between aluminium and zinc based surface deposits.

Calcium Aluminium Polyphosphate

A representative example survey spectra is shown in Figure 4.4.16, highlighting major elements detected on the surface – oxygen, phosphorus, calcium and carbon.

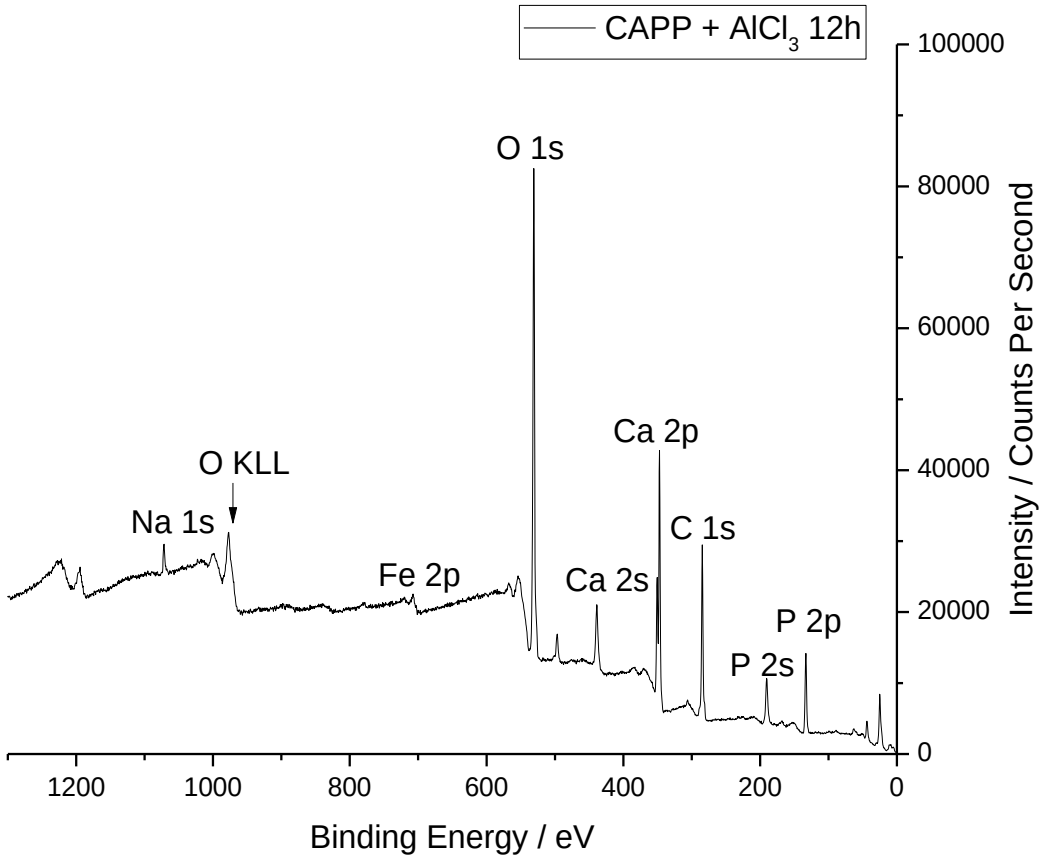

Figure 4.4.16 - An example wide scan XPS spectrum for a steel surface cathodically polarised and exposed to a sodium chloride solution containing CAPP and both aluminium chloride.

.

The presence of iron within the spectra is used to determine the depth and surface coverage of the deposited layer. In this case, iron was observed on all measured spectra, albeit at low levels for the longest exposure time. This suggests poor, or slow, surface coverage of surface deposits in this system. For this system, the major components followed in high resolution were calcium and phosphorus.

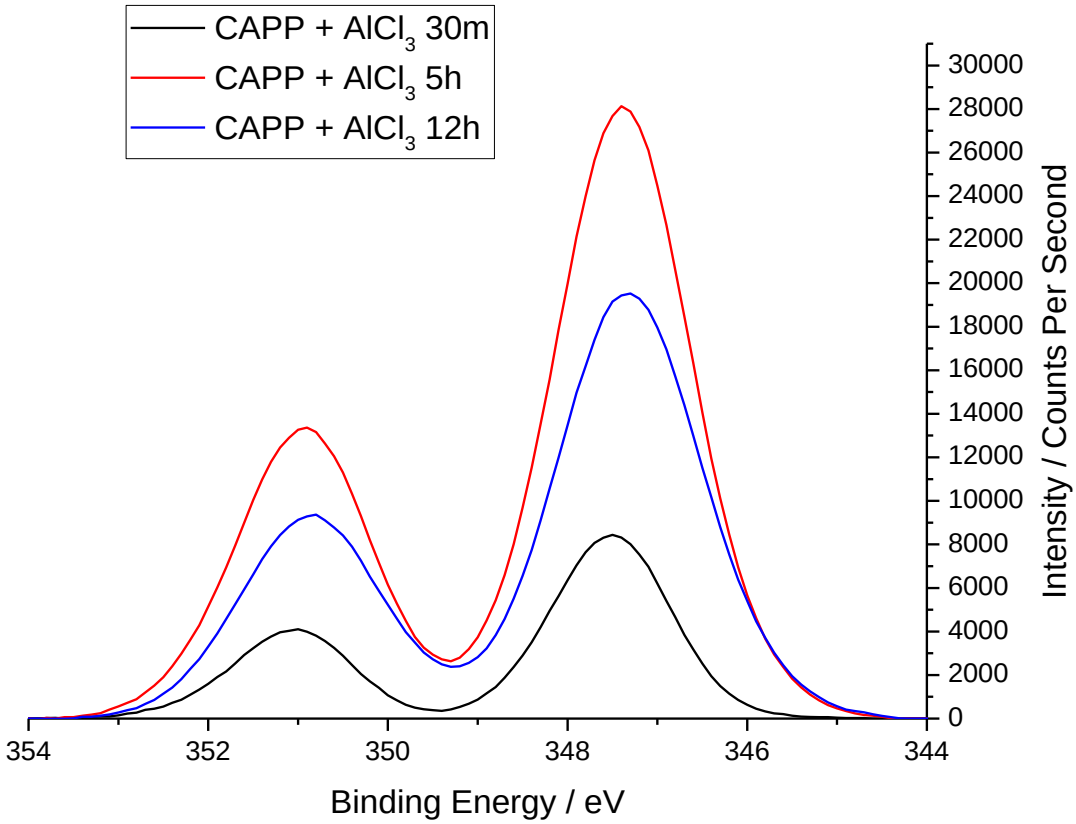

Figure 4.4.17 - High resolution, background-subtracted XPS spectrum of the region containing the calcium 2p peak. Spectra shown are summations of the deconvoluted spectra.

Figure 4.4.17 shows the high resolution spectra for the region containing the calcium 2p peak. The calcium peak exhibits a singular binding state, in which the 2p 3/2 peak has a binding energy of approximately 347.3 eV, which remains consistent within experimental error throughout the exposure period. With regards to the measured concentration of calcium at the surface, it can be see that there is some inconsistency, however, it can be suggested that there are significant increases from the initial measurement. This observation can be

considered to be somewhat consistent with expectations arising from the analysis of the presence of iron.

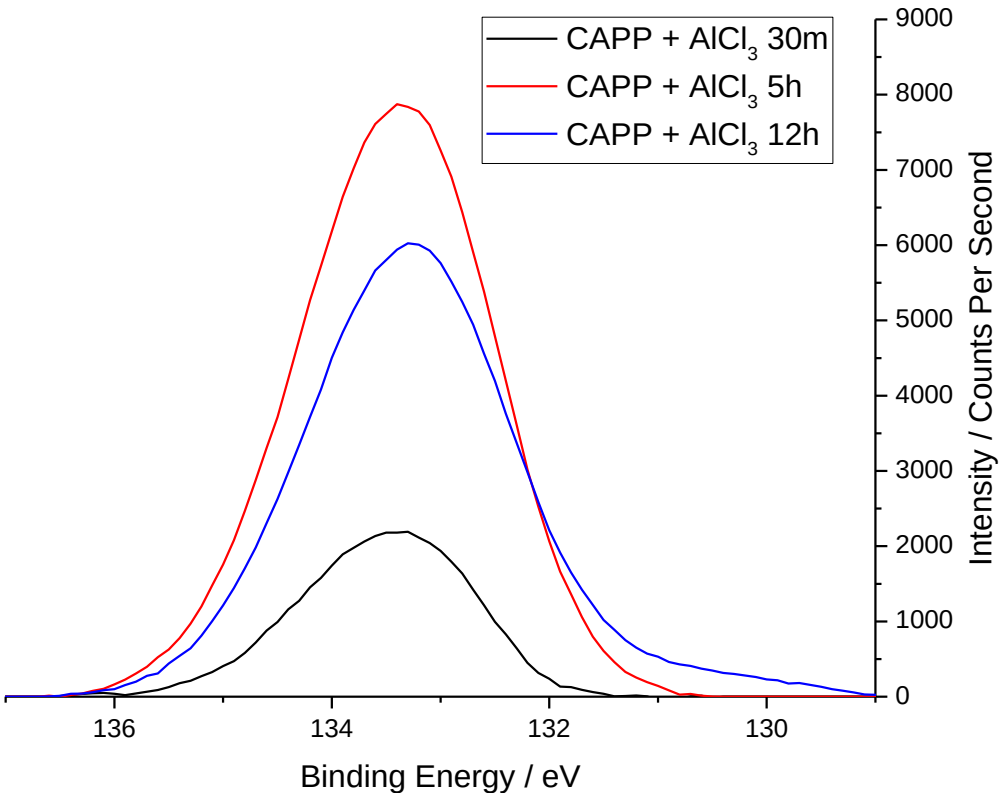

Figure 4.4.18 - High resolution, background-subtracted XPS spectrum of the region containing the phosphorus 2p peak. Spectra shown are summations of the deconvoluted spectra.

Figure 4.4.18 shows the high resolution spectra for the region containing the phosphorus 2p peak. The phosphorus peak contains a singular binding state in which the binding energy is consistent between exposure times, with the binding energy of the 2p 3/2 peak situated at approximately 133.1 eV, suggesting a metallic phosphate.

Similarly to the observations on the calcium peak, the phosphorus peak is again inconsistent with the calculated concentrations or peak areas. This result may be consistent with a relatively heterogeneous surface which could lead to discrepancy within the results.

Effect of Calcium and Zinc Combination

Strontium Aluminium Polyphosphate

A representative example survey spectra is shown in Figure 4.4.19, highlighting major elements detected on the surface – zinc, oxygen, phosphorus, calcium and carbon.

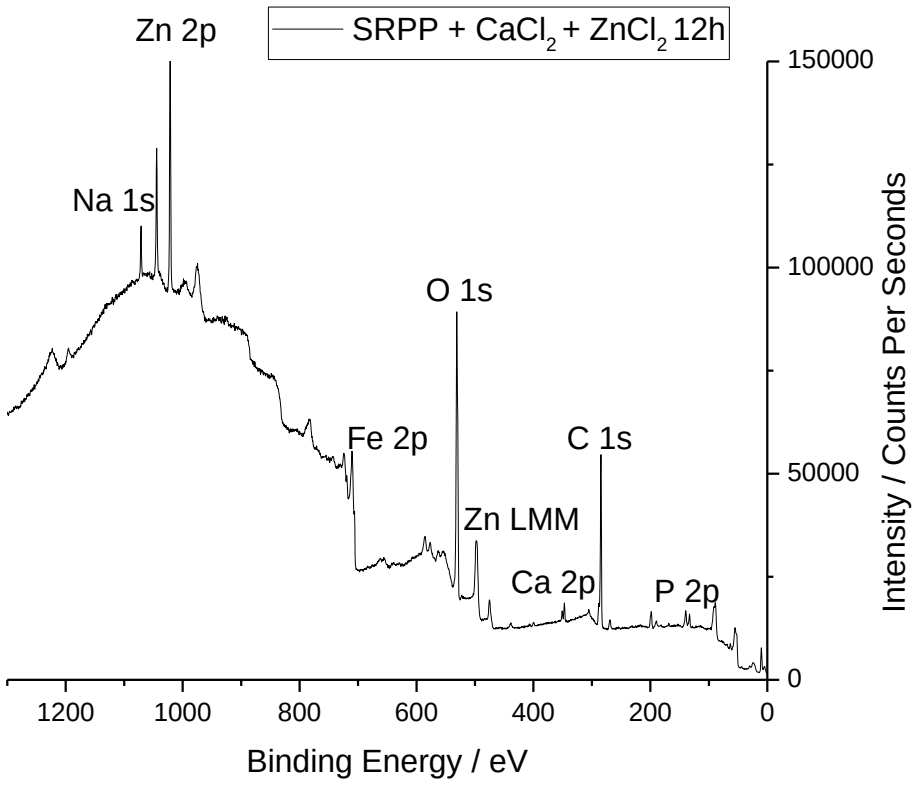

Figure 4.4.19 - An example wide scan XPS spectrum for a steel surface cathodically polarised and exposed to a sodium chloride solution containing SAPP and both calcium chloride and zinc chloride at 1mM concentration.

The presence of iron within the spectra is used to determine the depth and surface coverage of the deposited layer. In this case, iron was observed on all measured spectra. This suggests poor coverage of surface deposits in this system.

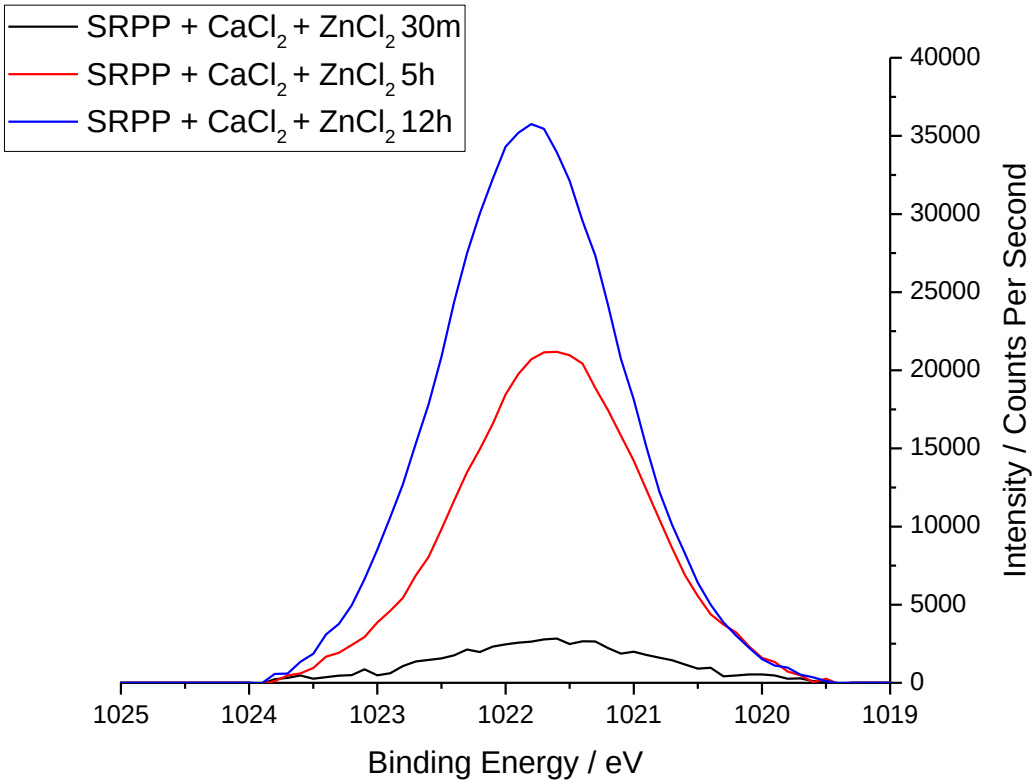

Figure 4.4.20 - High resolution, background-subtracted XPS spectrum of the region containing the zinc 2p (3/2) peak. Spectra shown are summations of the deconvoluted spectra.

Figure 4.4.20 displays a high resolution XPS spectra for the region containing the zinc 2p 3/2 peak. It can be seen that this peak displayed a singular binding state, which has a binding energy situated at around 1021.7 eV, with a small trend towards higher binding energies following longer exposure times. A consistent increase in the levels of zinc present on the surface is seen throughout the testing period.

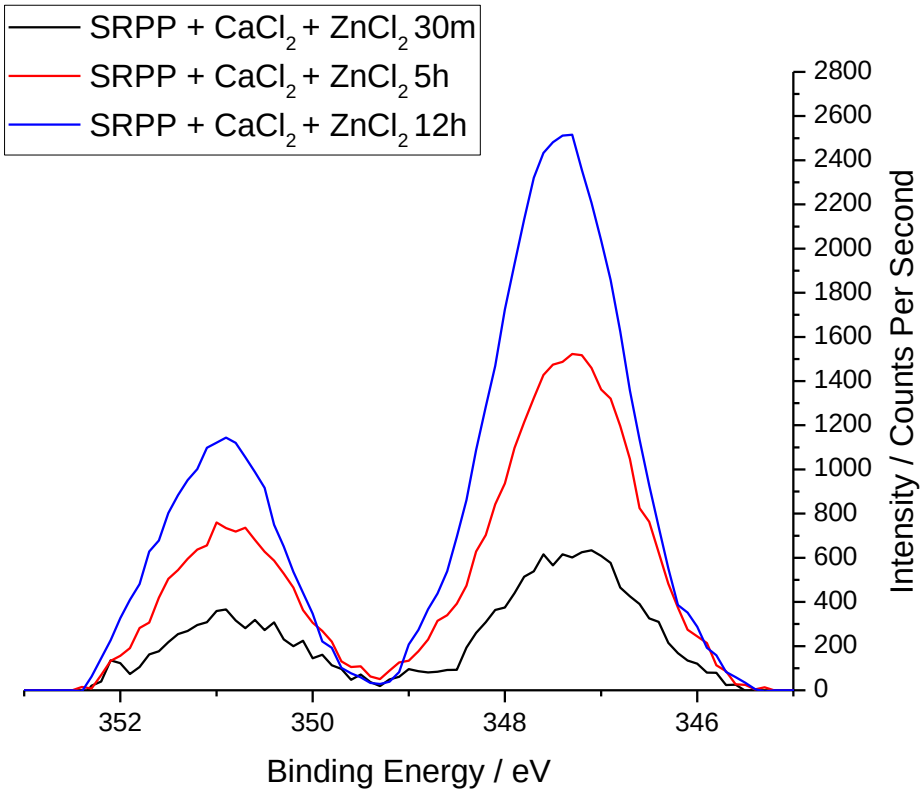

Figure 4.4.21 - High resolution, background-subtracted XPS spectrum of the region containing the calcium 2p peak. The spectra displayed in this figure are as obtained.

Figure 4.4.21 displays a high resolution XPS spectra for the region containing the calcium 2p peak. Component analysis suggested that calcium exhibited a singular binding state, with the 2p 3/2 peak being situated at a binding energy of approximately 374.5 eV. Similarly to the trend observed with zinc, the levels of calcium on the surface are seen to increase consistently across the observation period, albeit at relatively low intensities.

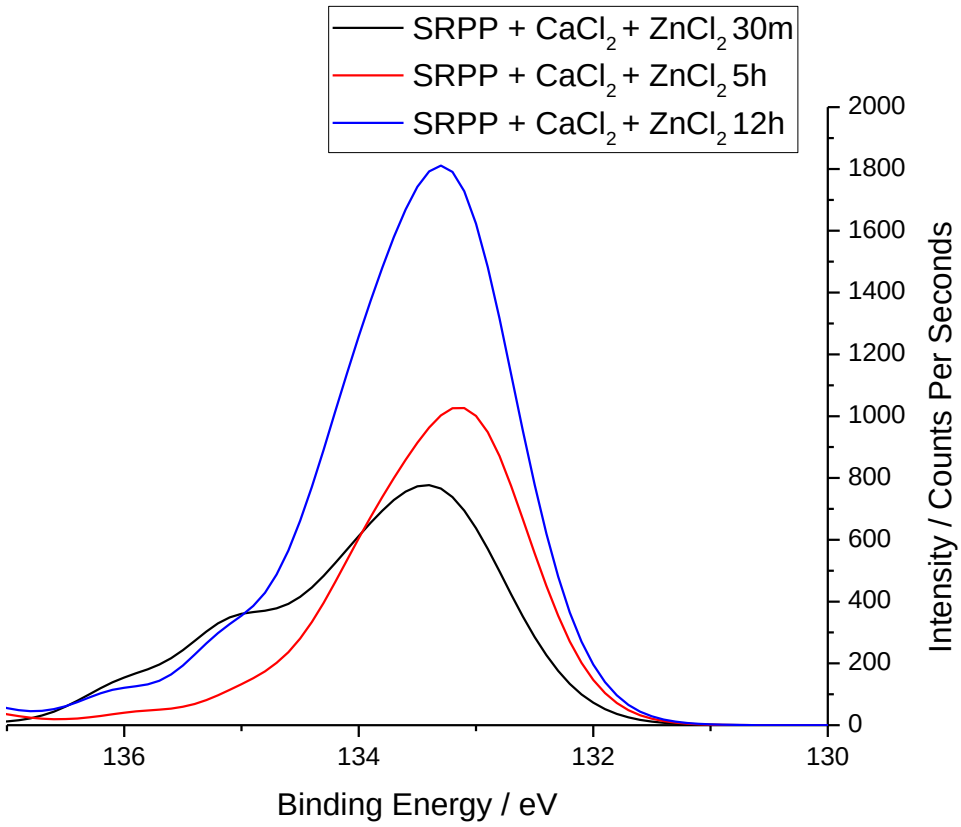

Figure 4.4.22 - High resolution, background-subtracted XPS spectrum of the region containing the phosphorus 2p peak. Spectra shown are summations of the deconvoluted spectra.

Figure 4.4.22 shows a high resolution spectra for the region containing the phosphorus 2p peak. With component fitting, two binding states are evident, with the 2p 3/2 peaks of these components situated at approximate binding energies of 133.1 eV and 135.1 eV. The possible sources of these multiple binding states will be discussed in detail later. The area ratios for these two binding energies vary throughout the measurements, with 5 hours exposure showing a large ratio difference of approximately 16:1, whereas the 12 hour exposure sample exhibits a smaller ratio of approximately 12:1. However, one distinction within this system can be suggested, with the concentration of phosphate at the surface clearly increasing over the observation period.

Calcium Aluminium Polyphosphate

A representative example survey spectra is shown in Figure 4.4.23, highlighting major elements detected on the surface – zinc, oxygen, phosphorus, calcium and carbon.

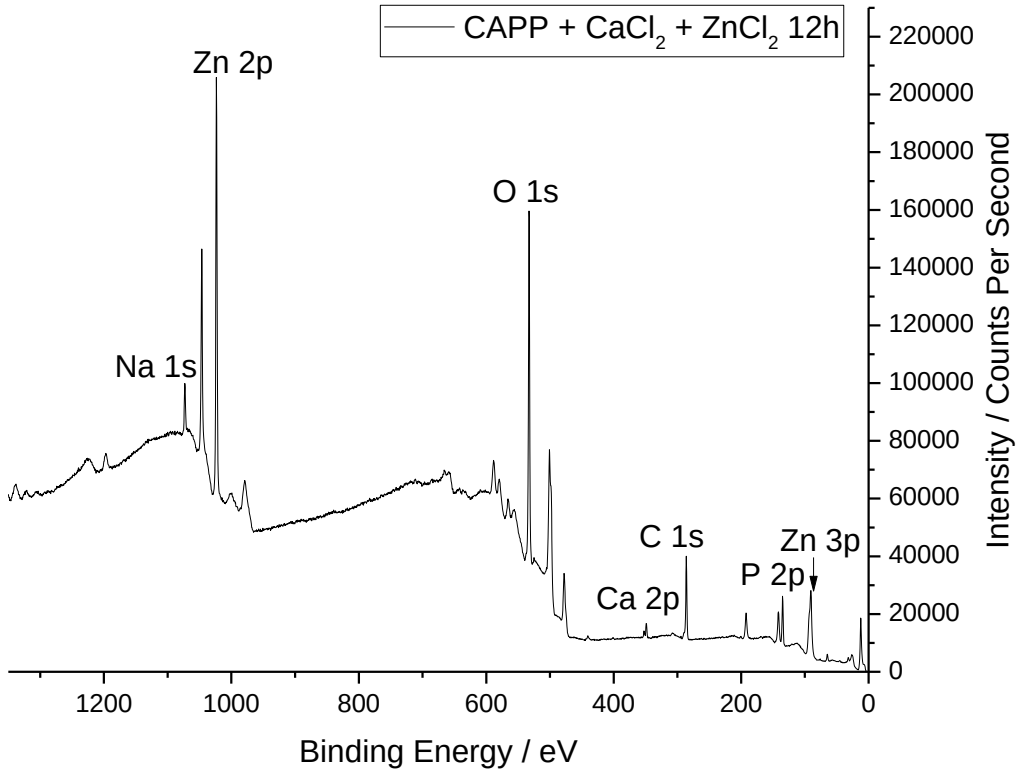

Figure 4.4.23 - An example wide scan XPS spectrum for a steel surface cathodically polarised and exposed to a sodium chloride solution containing CAPP and both calcium chloride and zinc chloride at 1 mM concentration.

The presence of iron within the spectra is used to determine the depth and surface coverage of the deposited layer. In this case, iron was observed at only low concentrations in the earliest spectra. This suggests that this system has a mechanism of surface deposition which has a quick mode of action. High resolution spectra of areas containing calcium and phosphorus are were taken to determine the properties of the surface deposits in this system.

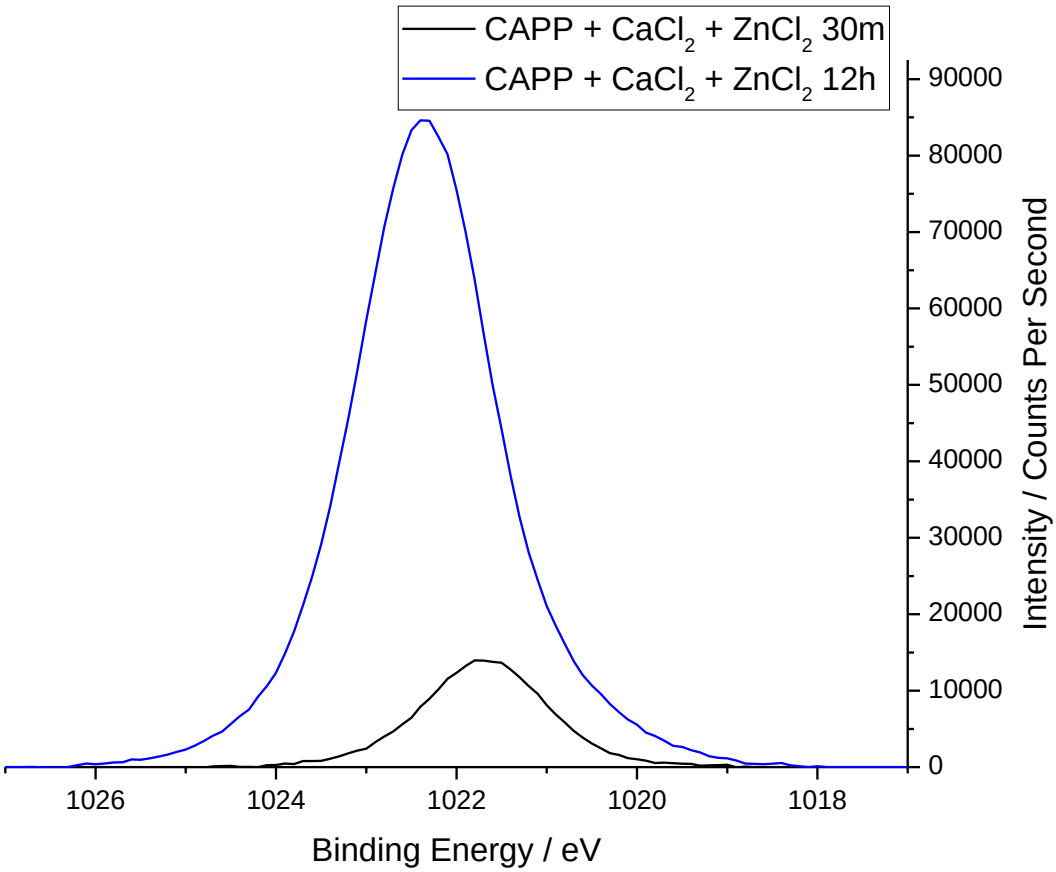

Figure 4.4.24 - High resolution, background-subtracted XPS spectrum of the region containing the zinc 2p 3/2 peak. Spectra shown are summations of the deconvoluted spectra.

Figure 4.4.24 shows the high resolution spectra showing the zinc 2p 3/2 peak. This shows a singular binding state which shifts to higher binding energy over time, from 1021.8 eV to 1022.4 eV, suggesting a greater degree of phosphate binding to the zinc in this case.

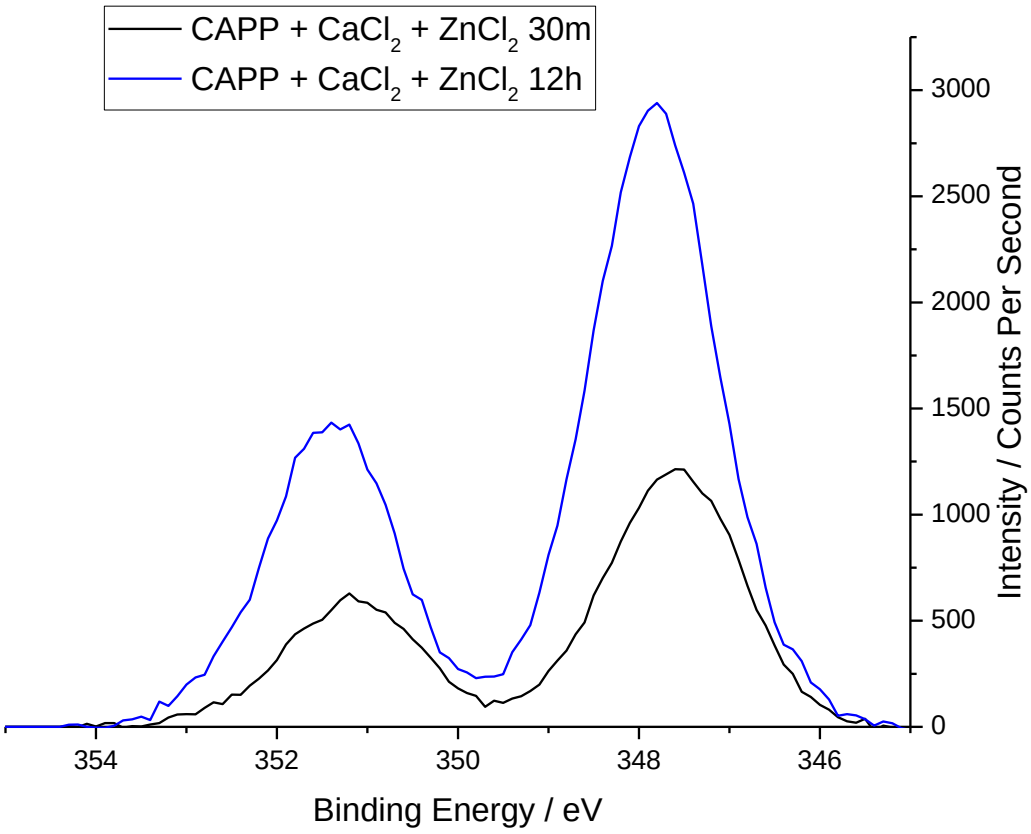

Figure 4.4.25 - High resolution, background-subtracted XPS spectrum of the region containing the calcium 2p peak. The spectra displayed in this figure are as obtained without additional processing.

Figure 4.4.25 shows the high resolution spectra for the area containing the calcium 2p peak. A singular binding state was determined to be present follow component analysis, with the 2p 3/2 peak situated at approximately 347.5 eV binding energy, which moves to a higher binding energy of 348.0 eV upon completion of the test. The overall concentration of calcium seen within the sample remains approximately the same throughout the test (3 at%).

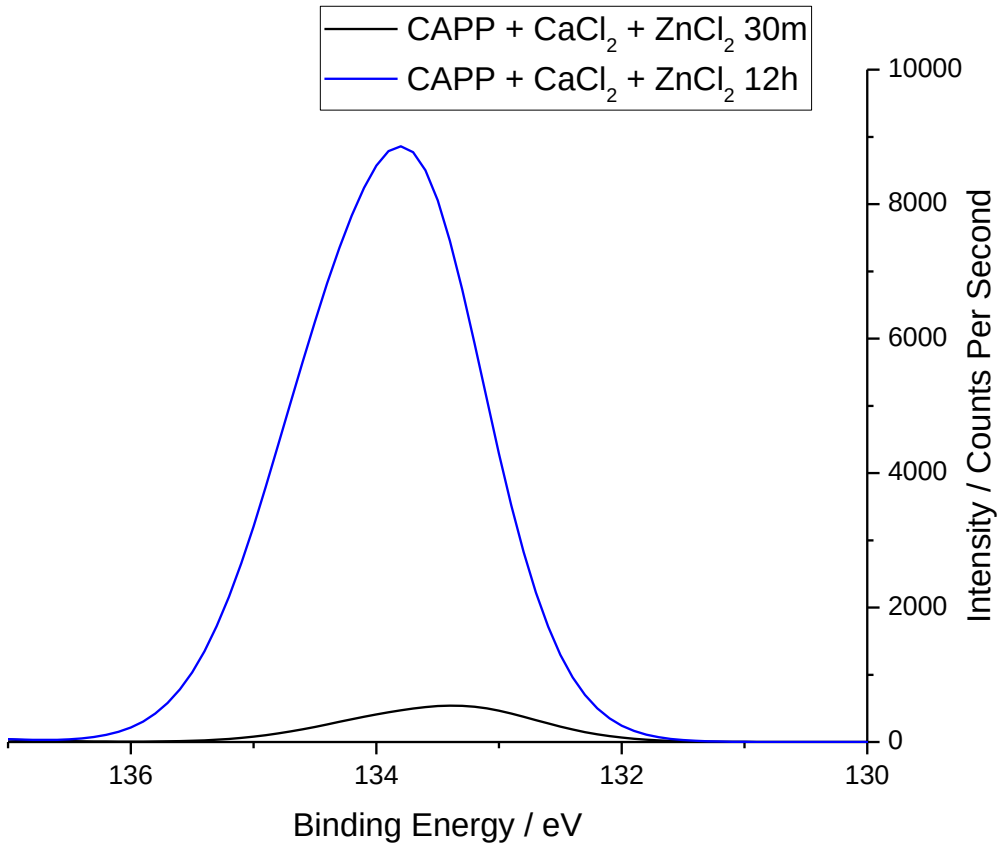

Figure 4.4.26 - High resolution, background-subtracted XPS spectrum of the region containing the phosphorus 2p peak. Spectra shown are summations of the deconvoluted spectra.

Figure 4.4.26 shows the high resolution spectra for the area containing the phosphorus 2p peak. Component fitting of the peak determined that there was a singular binding state present, with the 2p 3/2 peak being situated at approximately 133.4 eV, with this value shifting to 133.9 eV throughout the test, suggesting a change in the overall chemistry of the deposited layer. The calculated concentration of phosphorus at the surface is seen to increase from approximately 4 at% at earliest times to 17 at% at the final exposure time. This is comparable to that seen with CAPP with no additional ionic species present, and therefore it can be suggested that with CAPP the 1 mM addition of both calcium and zinc chlorides does not result in the same behaviour that is seen with 2 mM of either.

4.4.4 Effect of Zinc Ion Concentration

One additional effect which was looked at in this set of experiments was the effect of the secondary ion concentration on phosphate deposition. In experiments shown in the previous chapter, the addition of 2 mM of zinc chloride was shown to improve the extent of surface deposition significantly in the case of the strontium aluminium polyphosphate inhibitor pigment. Therefore, a number of different concentrations of zinc chloride addition were looked at to investigate whether the addition of further zinc ions would result in further improvements to the surface deposition, and if lower concentrations of zinc addition could produce similar results.

Figure 4.4.27, Figure 4.4.28, Figure 4.4.29 and Figure 4.4.30 show the XPS spectrum region for the phosphorus 2p and zinc 3s peaks for the environments containing 0.1 mM, 0.5 mM, 1 mM and 4 mM respectively.

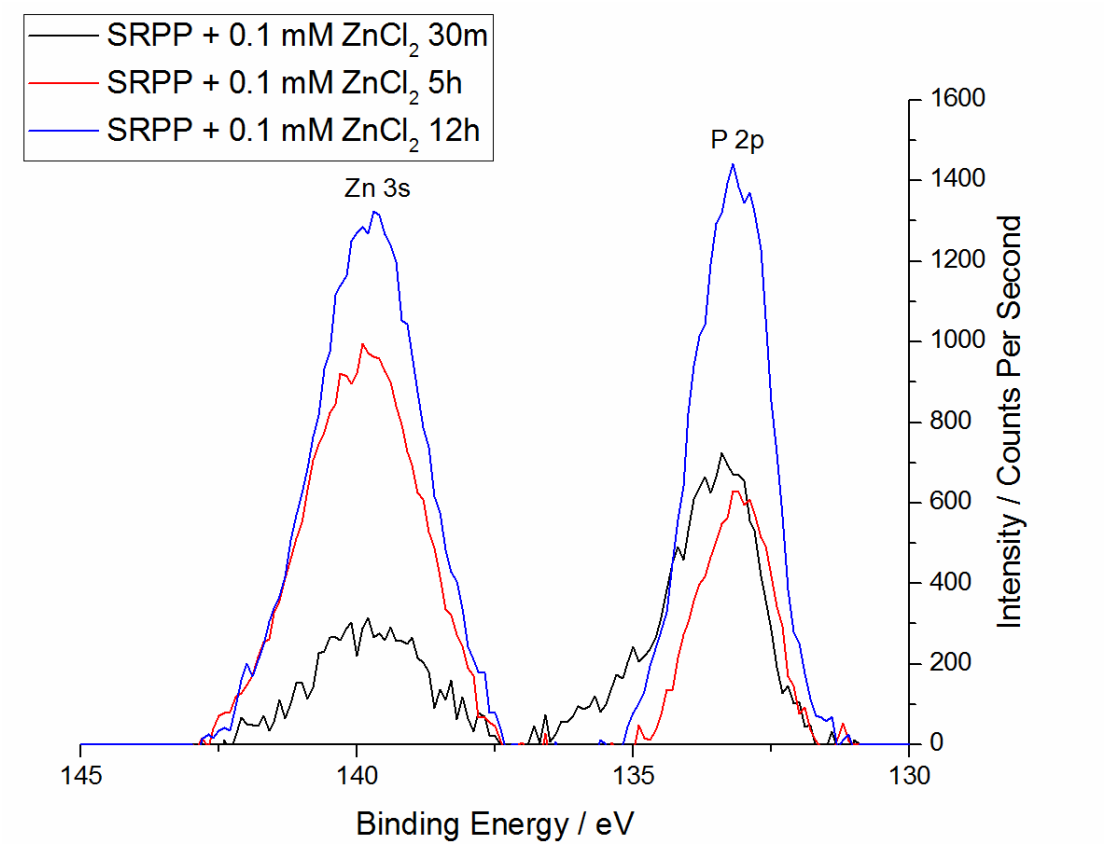

Figure 4.4.27 - High resolution, background-subtracted XPS spectrum of the region containing the zinc 3s (left, 140 eV)) and phosphorus 2p (right, 133 eV) peaks for the solution containing 0.1 mM zinc chloride. The spectra displayed in this figure are as obtained.

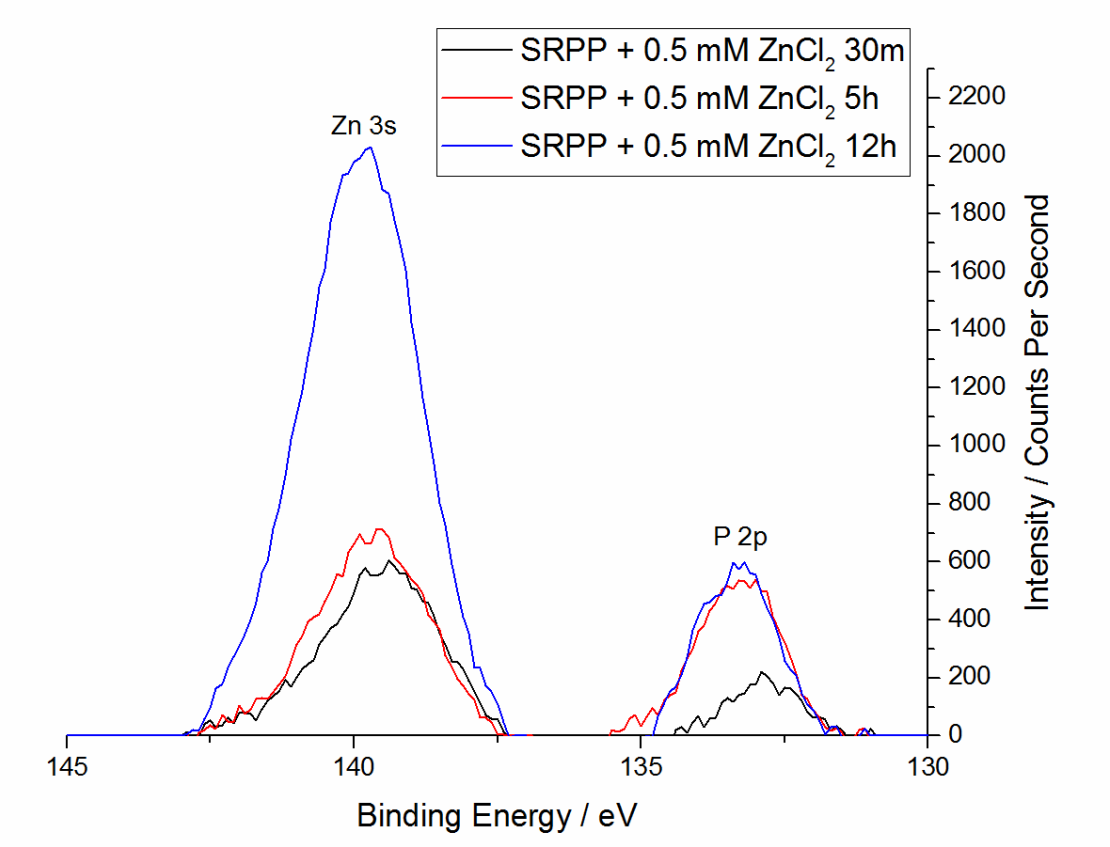

Figure 4.4.28 - High resolution, background-subtracted XPS spectrum of the region containing the zinc 3s (left, 140 eV)) and phosphorus 2p (right, 133 eV) peaks for the solution containing 0.5 mM zinc chloride. The spectra displayed in this figure are as obtained

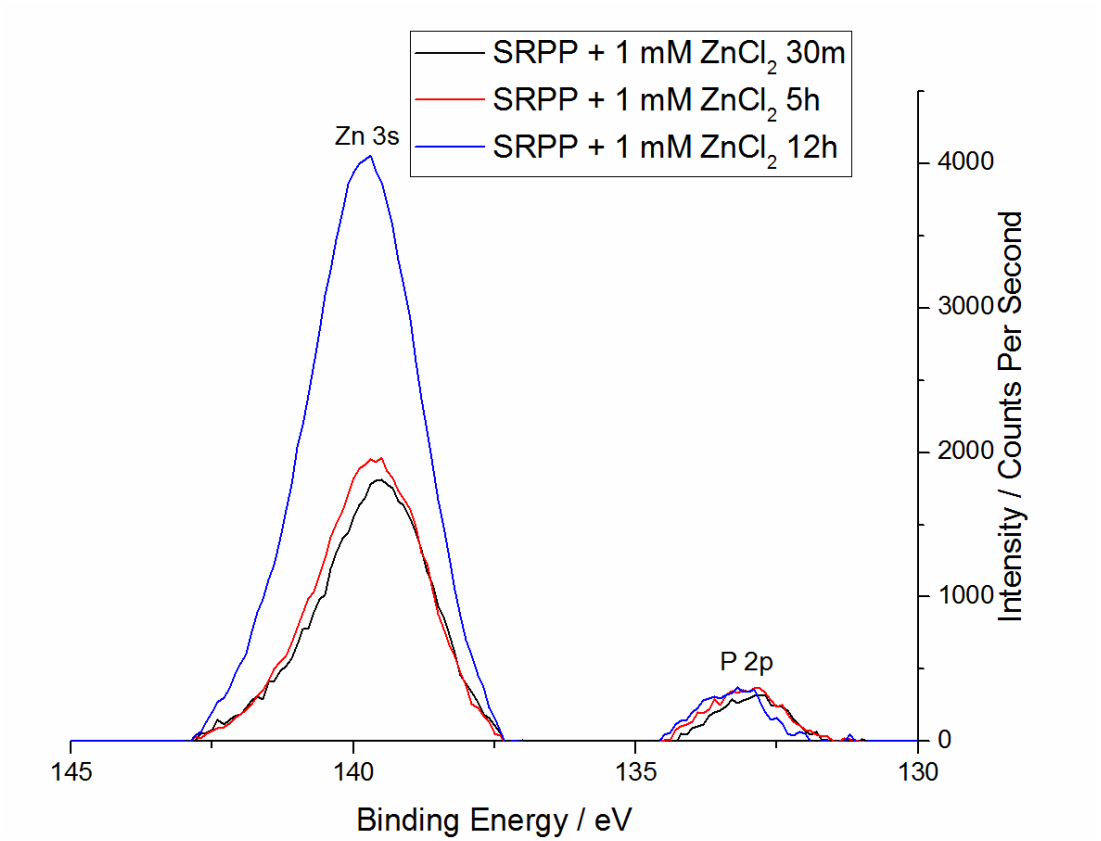

Figure 4.4.29 - High resolution, background-subtracted XPS spectrum of the region containing the zinc 3s (left, 140 eV)) and phosphorus 2p (right, 133 eV) peaks for the solution containing 1 mM zinc chloride. The spectra displayed in this figure are as obtained.

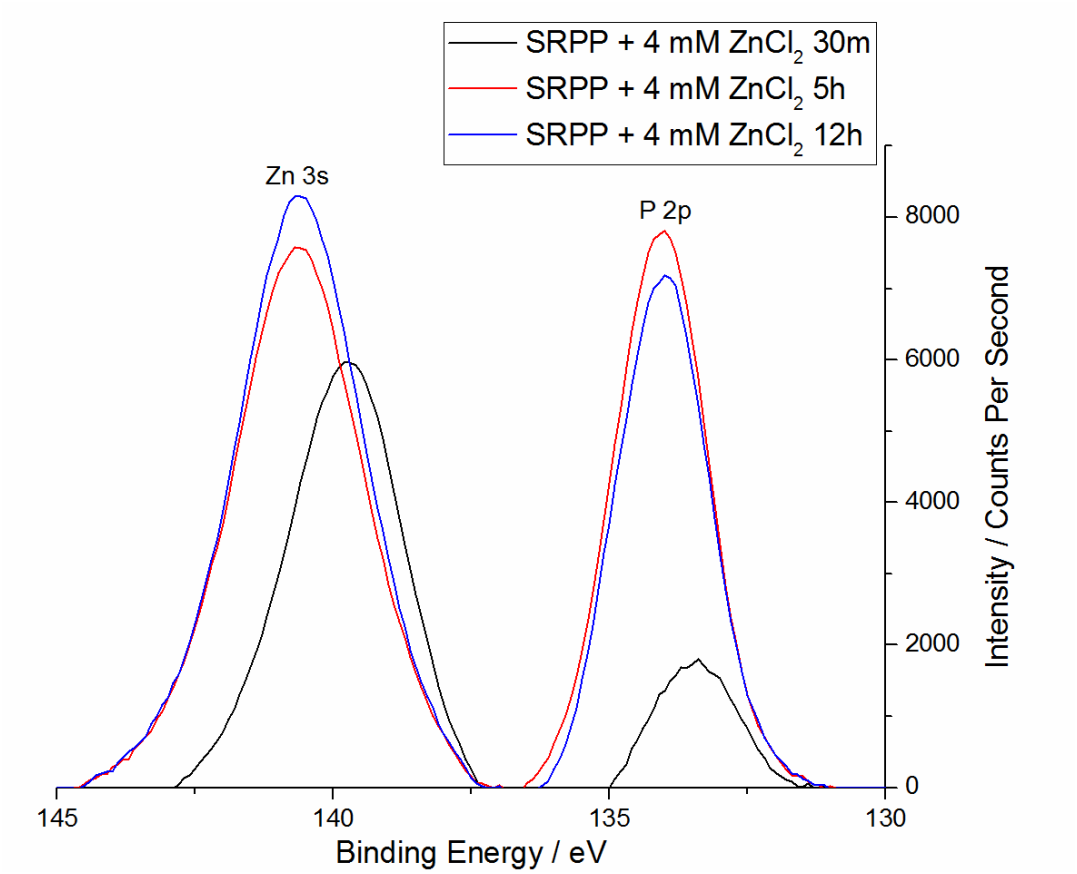

Figure 4.4.30 - High resolution, background-subtracted XPS spectrum of the region containing the zinc 3s (left, 140 eV)) and phosphorus 2p (right, 133-134 eV) peaks for the solution containing 4 mM zinc chloride. The spectra displayed in this figure are as obtained.

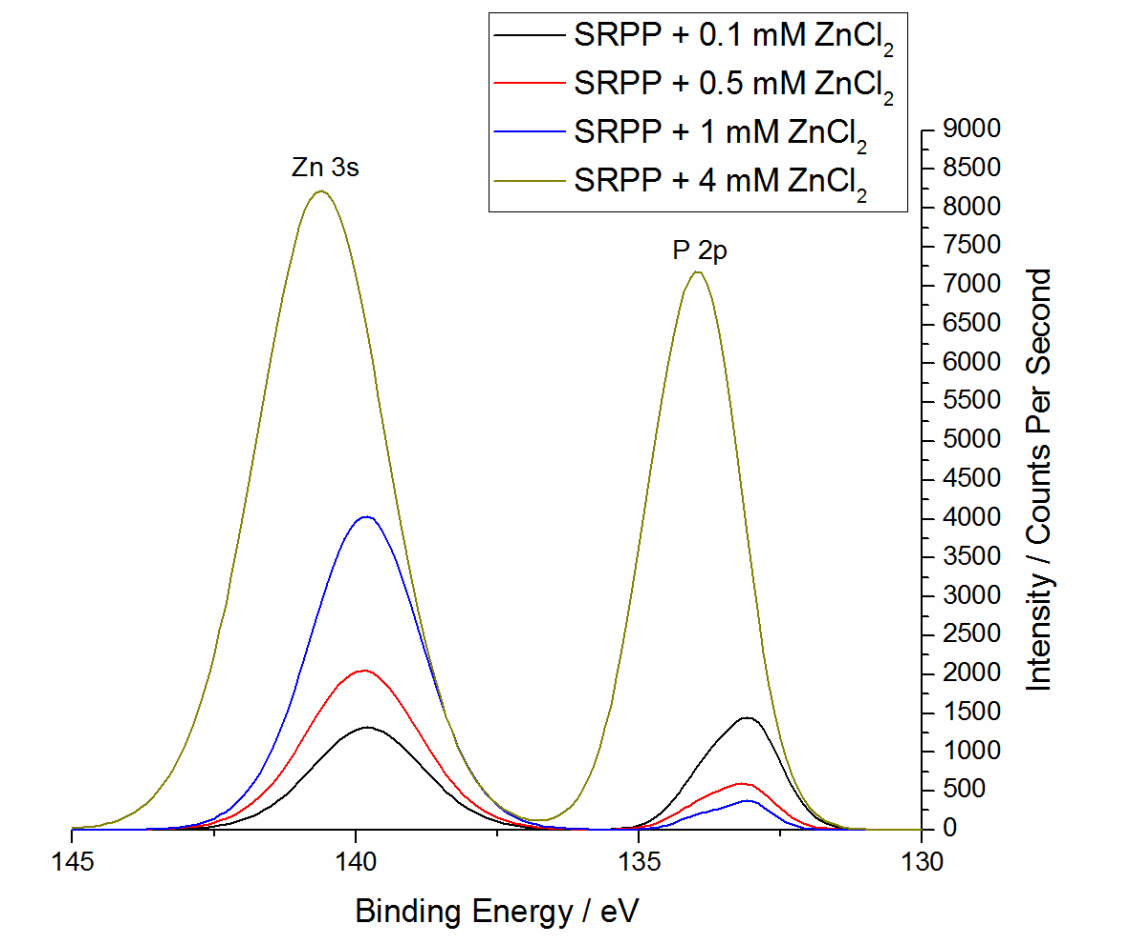

Figure 4.4.31 - High resolution, background-subtracted XPS spectrum of the region containing the zinc 3s (left, 140 eV)) and phosphorus 2p (right, 133 eV) peaks, showing a comparison of the 12 hour exposure times for each of the zinc concentrations measured. The spectra displayed in this figure are

Figure 4.4.31 shows the comparison of the zinc 3s and phosphorus 2p peaks for the different concentrations observed in this study following 12 hours exposure. Both zinc and phosphorus show singular binding states across all measured concentrations, which are slightly shifted to higher binding energies for the highest concentration of zinc chloride The concentration of zinc is seen to increase consistently with greater concentrations of added zinc chloride. However, the same does not apply to the phosphorus concentration, which is seen to drop from 5.3 at% for the 0.1 mM zinc chloride addition down to 0.9 at% for the 1 mM zinc chloride addition. This will be discussed in more detail in the next section.

4.4.5 Discussion

Initial Observations

The effects of the metal cationic species magnesium, calcium and aluminium, alongside a combination of zinc and calcium cations, introduces as concentrations of the relevant metal chloride on the surface deposits of strontium aluminium polyphosphate and calcium aluminium polyphosphate were determined using XPS.

In the case of the addition of magnesium, there were distinct differences present between the two polyphosphate inhibitor pigments. In the case of strontium aluminium polyphosphate, the quality of the surface phosphate deposits can be considered to be fairly poor. The presence of the Fe 2p peak was clearly observable throughout the tests, which for these experiments is an indication that the incident x-ray beam is able to penetrate through the deposit down to the underlying substrate. It is possible that this is a thin but well protecting layer. However, this is unlikely to be the case if taking into consideration the properties of the phosphate layers deposited in the initial SAPP study and the corresponding electrochemical impedance.

Whilst the addition of magnesium cations to strontium aluminium polyphosphate containing solutions appears to make no significant improvements to the rate or overall quality of surface deposition, the effect of magnesium on calcium aluminium polyphosphate is minimal. Calcium aluminium polyphosphate can be considered to be fairly effective without the addition of additional cationic species, and in this case the addition of magnesium appears to make little difference to the overall composition or rate of deposition compared to that of the magnesium free sample shown in the previous chapter.

With the calcium aluminium polyphosphate pigment, the addition of calcium chloride exhibits an acceleration in deposition kinetics, with phosphorus content after 12 hours being similar to that of what is seen without additions (as shown in the previous chapter). However, after 30

minutes exposure, the spectra for samples exposed to this environment are also exhibiting deposition at similar levels (18 at% phosphorus vs. approximately 20 at% after 12 hours exposure).

The addition of additional calcium cations to the inhibitor solutions appears to also have a positive effect on the deposition of the SAPP pigment exposed sample, with a notable increase in the phosphorus content at the surface and a suppression of the metallic iron peaks within the spectra. This suggests a thicker phosphate deposition on the surface. However, it is also worth noting that the phosphorus 2p peak also displays peak multiplicity, which suggests that there are two phosphorus binding states, likely arising from the presence of both calcium and zinc within the deposition structure. The presence of zinc within the spectra is noted, and that is most likely due to the previously mentioned zinc impurities that are within the SAPP inhibitor pigment.

The addition of lower levels of both calcium and zinc chlorides to the SAPP pigment shows the same peak duplicity within the spectra. There are suggestions within the literature that a mixture of zinc and calcium cations with a phosphate deposition system will result in a more effective and more compact film production[7]. This will be discussed in more detail later in the following section.

SAPP Peak Multiplicity

SAPP shows phosphate peak multiplicity (i.e. more than one P 2p 3/2 peak present) in all solutions besides those containing just zinc chloride as the solution dopant, at binding energies of approximately 133.3 eV, consistent with metallic phosphate, and 135.1 eV. One explanation for this observation would be that the presence of a secondary metallic cation that is active within the mechanism of deposition, as it has been previously reported that strontium shows no significant inhibitive actions[8]. It has been previously mentioned that zinc is observed

within the SAPP pigment and thus can be considered to not be a “secondary metallic cation” in this case.

However, with this explanation, it would have been expected that phosphate peak multiplicity would have been observed in the calcium aluminium polyphosphate and magnesium aluminium polyphosphate. This is not the case, with neither exhibiting multiple binding states in the phosphorus peak in the previous study with zinc chloride. Additionally, in the present study, none of the cationic additions to calcium aluminium polyphosphate result in the presence of further binding states.

This means that alternative explanations have to be sought. One potential alternative theory is that the structure of strontium aluminium polyphosphate is different to that of the other two polyphosphate inhibitors, potentially due to the higher solubility of strontium, which facilitates a secondary binding state when alternative cationic species, such as zinc or calcium, are present.

Another theory is that the initially presented hypothesis is correct, however, the overall stability of the calcium and magnesium complexes with polyphosphates is of a magnitude that is sufficiently greater than that of zinc, resulting in an inability for zinc to displace either calcium or magnesium in this case. In the case of strontium aluminium polyphosphate, the zinc content of the pigment itself is sufficient to initially form the zinc phosphate.

Chemical formula of aluminium polyphosphate is suspected to be $Al_5(P_3O_{10})_3$. A source in the literature[9] suggests that in the case of sodium polyphosphate ($Na(PO_3)_x$) that the presence of calcium facilitates the conversion of the polyphosphate to calcium orthophosphate, $Ca_3(PO_4)_2$. This opens up another possible explanation for the behaviour seen on the strontium aluminium polyphosphate inhibitors.

The primary phosphorus binding states for the P 2p 3/2 peak are situated at around 133.3 eV binding energy. This is consistent with metallic phosphate XPS peak values. Examples are available in the literature for both calcium orthophosphate[10] and zinc orthophosphate[11]. No literature values regarding a magnesium orthophosphate or other likely compositions containing magnesium and phosphorus were available at the time of writing.

With the secondary binding state for this peak having a binding energy at approximately 135.1 eV, this suggests that the strength of attraction of the internal electrons to the phosphorus nucleus has increased. This would be consistent with the reduction in the ratio of oxygen to phosphorus in the molecule. High binding energies for phosphorus compounds in the literature that are somewhat likely to be similar in composition to realistic deposits from the available solution could be considered to be a polyphosphate[12] that either contains, or is stabilised by, the presence of zinc. It is possible that the polyphosphate component of strontium aluminium polyphosphate is more stable than that seen in calcium aluminium polyphosphate or magnesium aluminium polyphosphate, and thus the secondary binding state can be in this case considered to be a polyphosphate.

For any of these cases, literature on the composition of deposited layers is scarce, and thus most of the assumptions made previously rely on literature values from materials that can be considered significantly different to that which would be situated on the steel surfaces measured.

Effect of Zinc Chloride concentration

The study in the previous chapter showed that doping an SAPP saturated solution with zinc chloride, providing a nominal zinc concentration within the solution of 2 mM, was sufficient to improve the surface phosphate deposition on the cathodically polarised steel surface. This study was designed to determine a few parameters. Firstly, the minimum concentration of

additional zinc required, above that which is provided by the SAPP pigment, for notable improvements in phosphate deposition compared to blank solutions. The second is to determine whether an increase in the level of zinc above the 2mM level from the previous study provides further improvements in phosphate deposition.

Results suggest that the presence of zinc ions in solution at concentrations of 1 mM appear to have little effect on the phosphate deposition with SAPP, with an overall deposition of 0.9 at% measured in this case. From the results, it would appear that there is some argument to suggest that there is some correlation to suggest that the effectiveness of the phosphate deposition improves with lower zinc content below the 1 mM level, with a phosphate concentration observed of approximately 5 at% with 0.1 mM zinc chloride added.

Despite this, there is a strong argument to make the suggestion that the minimum concentration of zinc ions required in solution for efficient polyphosphate inhibition by strontium aluminium polyphosphate can be determined to be at a value between 1 mM and 2 mM. Indeed, the chemical nature of the phosphorus peak can be suggested to change significantly with a binding energy shift detected from approximately 133.0 mV for lower zinc content samples to approximately 134.0 mV for samples containing 2 mM or more zinc chloride. Potential future experimentation may be able to more accurately define the required zinc level for effective phosphate deposition.

For the sample that was prepared at 4 mM concentration of zinc chloride, the suggestion from the results is that the increase in zinc concentration in solution does improve the ability for the polyphosphate inhibitor to deposit on the steel surface, compared to the result obtained for the 2 mM concentration that was given in the previous chapter section.

With this preliminary study showing further increases are possible with greater addition of zinc beyond the initially selected 2 mM level, one worthwhile future study may look at the impact

of further increases in the zinc content of the solution. This could then be expanded to determine at what point increased zinc loading becomes less effective for improved phosphorus deposition.

4.4.6 Conclusions

In this section, the effects of the addition of several different cationic species on the surface deposits on cathodically polarised steel were analysed through the use of x-ray photoelectron spectroscopy. Additionally, the effect of the concentration of metal chlorides was also studied by varying the amount of zinc chloride present in solutions containing strontium aluminium polyphosphate inhibitor pigment. Despite the absence of some results, due to either machine malfunction or restricted machine time, several tentative conclusions can still be made with the reported results:

- The addition of metallic cationic species into solution can be seen, in some cases, to improve phosphate deposition on the cathodic steel surface.
    - The addition of calcium chloride shows a large increase in the presence of phosphorus (to approximately 45 at%) for SAPP, and an acceleration when added to CAPP (phosphorus at approximately 18 at% following 30 minutes exposure).
    - The addition of magnesium chloride shows similar phosphate deposition kinetics to the same concentration addition of zinc chloride, albeit slower at earlier exposure times for SAPP (4.4 at% at 30 minutes to 13.6 at% at 12 hours exposure, compared to 9 at% and 13.6 at% for zinc chloride), and a similar acceleration effect as seen with zinc chloride on CAPP.
- The extent of the improvement appears to be dependent both on the particular metallic species and initial inhibitor pigment used.
    - The acceleration effect shown on CAPP pigment by zinc chloride is also displayed with aluminium chloride. However, the effect of aluminium chloride

on SAPP is less evident (surface phosphorus concentration of 3.5 at% following 12 hours exposure).

- Strontium aluminium polyphosphate is the only inhibitor pigment which exhibits multiple phosphorus binding states, but insufficient evidence is currently presented to determine the reasoning behind this observation beyond doubt.
    - It has been suggested that the structure or chemical composition of the strontium aluminium polyphosphate pigment differs sufficiently from that of calcium aluminium polyphosphate or magnesium aluminium polyphosphate to allow stabilisation of a polyphosphate component as a surface deposit.
- The minimum concentration of zinc ions required for a notable improvement in the rate and concentration of phosphorus deposited at the surface appears to be between 1 and 2 mM.
    - It is suspected that this will likely be closer to 2 mM as a concentration of 1 mM zinc chloride appeared to be ineffective in producing phosphate deposition.
    - However, there is also an apparent improving of deposition when reducing the level of zinc chloride from 1 mM (0.9 at% surface phosphorus) down to 0.1 mM (5.3 at% surface phosphorus), suggesting there may be an inhibition improvement curve that has a minima around 1 mM zinc chloride.
- The addition of further zinc chloride beyond the 2 mM level appears to have little-to-no beneficial effect to the phosphate deposition.

4.5 Chapter Summary and Conclusions

The main points to take away from the results shown in this chapter are as follows:

- The addition of dissolved zinc cations was shown to alter the composition and structure of surface deposits on the steel surface by the strontium aluminium polyphosphate inhibitor pigment, utilising SEM-EDX and XPS analysis
- Surface deposition was not detectable by SEM-EDX for cathodically polarised steel samples. The detection of phosphorus and other elements related to the inhibitor pigment at the surface was possible on cathodically polarised samples using XPS analysis, suggesting that the deposited layer is sub 1 micron in thickness, most likely on the scale of 10 to 100 nm in thickness.
- The presence of strontium on the surface was not detected in any method. This means that strontium appears to have no influence on the mechanism of inhibition on steel for the strontium aluminium polyphosphate inhibitor pigment, regardless of potential shift.
- A minima for externally introduced concentrations of zinc ions to make a discernible difference on the deposition mechanics of the strontium aluminium polyphosphate inhibitor pigment was determined to be between 1 and 2 mM bulk zinc cation concentration
    - Some evidence was shown for a range of concentrations where the effect of zinc is substantially reduced, as the 0.1 mM zinc chloride solution showed a much greater concentration of phosphorus (5.25 at%) than that of either 0.5 mM (2.7 at%) or 1 mM (0.9 at%) during the test period.
- The effects of zinc cations on cathodically polarised depositions are less pronounced for the calcium aluminium polyphosphate inhibitor pigment, where it appears to be catalytic, and for magnesium aluminium polyphosphate, where there appears to be an absence of any real effects.

4.6 **Chapter References**

[1] Zin IM, Lyon SB, Hussain A. Prog Org Coatings 2005;52:126.

[2] Brow RK. J Non Cryst Solids 1996;194:267.

[3] Rangel CM, De Damborenea J, De Sá AI, Simplício MH. Br Corros J 1992;27:207.

[4] Zin IM, Lyon SB, Pokhmurskii VI. Corros Sci 2003;45:777.

[5] Zin IM, Lyon SB, Pokhmurskii VI, Simmonds MC. Corros Eng Sci Technol 2004;39:167.

[6] Phuong N Van, Lee K, Chang D, Kim M, Lee S, Moon S. Met Mater Int 2013;19:273.

[7] Zeng R, Lan Z, Kong L, Huang Y, Cui H. Surf Coatings Technol 2011;205:3347.

[8] Baghni I., Lyon S., Ding B. Surf Coatings Technol 2004;185:194.

[9] Koudelka M, Sanchez J, Augustynski J. J Electrochem Soc 1982;129:1186.

[10] Demri B, Muster D. J Mater Process Technol 1995;55:311.

[11] Franke R, Chassé T, Streubel P, Meisel A. J Electron Spectros Relat Phenomena 1991;56:381.

[12] Onyiriuka EC. J Non Cryst Solids 1993;163:268.

Chapter 5

Electrochemical Experiments Utilising Segmented Electrode for Modelling a High Percentage Aluminium Alloyed Zinc Coated Steel

5.1 Introduction

In a previous chapter, the utilisation of segmented electrochemical impedance for looking at the inhibition of galvanised steel, using a pure steel and zinc model, was explored. The results obtained showed that the results can be rapidly analysed to quickly understand sites of action for inhibitor molecules. In addition to this, it was determined that some basic mechanistic information can be obtained through observation of electrochemical changes that occur upon changing of experimental parameters.

However, the composition of the sacrificial galvanising layer has been modified and made increasingly more complex. Common alloying additions include aluminium and magnesium, meaning that the local chemistries and overall electrochemistry of the coating is changed significantly. It can be considered, therefore, that the effects of the inhibitor pigments on these galvanising alloys will be significantly different to that of the simpler steel and zinc system explored previously.

As such, in this chapter, the potential for utilising modifications to the initial testing of segmented electrode electrochemical impedance experiments as a method of understanding inhibition on complex alloys was explored.

A three electrode segmented cell, comprising of zinc, aluminium and mild steel rods arranged in a circle was devised to best ensure consistent distance between each working electrode and the reference electrode. The overall system was to be exposed to each of the inhibitor systems that have been previously used in this body of work in an attempt to understand the influence of aluminium on the inhibition of the metallic sacrificial protection layer.

5.2 Experimental

Experiments concentrated on following the effects of dissolved corrosion inhibitors on the triple working electrode cell utilising zinc, aluminium and mild steel electrodes. 3 mm diameter rods of mild steel (0.05% carbon steel), zinc (99.99+% purity zinc) and aluminium (99.95%

purity aluminium) were mounted in epoxy resin and ground using incremental grades of silicon carbide abrasive discs up to and including 1200 grade so as to leave a single flat surface exposed to the environment.

The mounted metals were then immersed in a 3.5 weight % (approximately 0.6M) sodium chloride solution containing leached species from an inhibitor pigment. Thus, saturated solutions of relevant inhibitors were prepared by introducing approximately 2 g of solid into 1 L of electrolyte, and stirred continuously for 24 h. The solution was then filtered to remove any remaining excess solid from the solution. The following inhibitor pigments and combinations were utilised in this work, and were added as received:

- Strontium Chromate ($SrCrO_4$)
- Zinc Molyphosphate (ZMP)
- Calcium-exchanged Silica (CES)
- Zinc Molyphosphate and Calcium-exchanged Silica Mixture
- Strontium Aluminium Polyphosphate Hydrate (SAPP)
- Calcium Aluminium Polyphosphate (CAPP)
- Magnesium Aluminium Polyphosphate (MAPP)

A five-electrode cell was used and attached to an ACM AC Weld Test instrument, utilising steel, zinc and aluminium as three working electrodes, a saturated calomel reference electrode and a platinum counter electrode. The electrode arrangement was as displayed in Figure 5.2.1. The system was at laboratory temperature (18-21 °C) monitored for 72 h, with electrochemical impedance measurements taken every 2 h for the duration of the experiment. Impedance measurements were taken at the measured system coupled corrosion potential in the frequency range of 10,000 to 0.01 Hz with a signal amplitude of 10 mV.

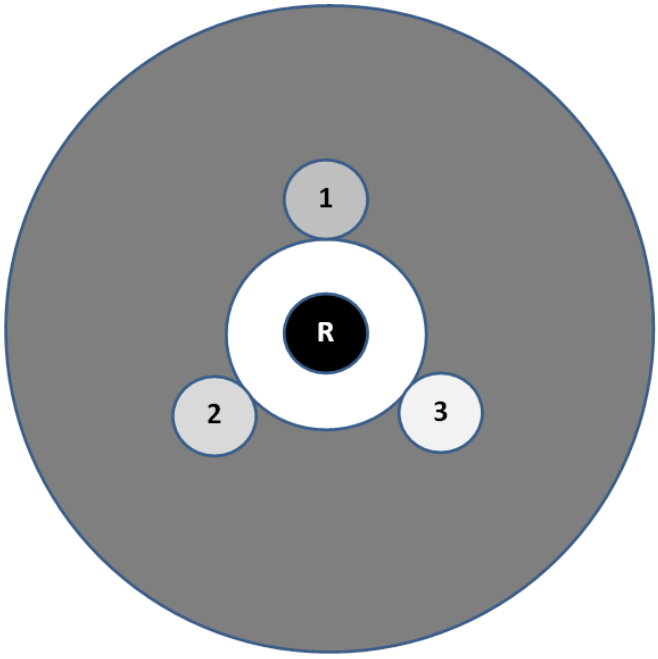

Figure 5.2.1 - Schematic representation of the geometry of the three working electrode setup utilised (1 – steel, 2 – zinc, 3 – aluminium, R – reference)

Following the electrochemical impedance measurements, the samples were then subjected to potentiodynamic polarisation. The measurement began at a potential cathodic to the overall system, chosen to be at -1200 mV, and was swept to a potential value of -400 mV, with an overall sweep rate of 20 mV per minute.

5.3 Results

Potentiodynamic Polarisation

Potentiodynamic polarisation curves were obtained for each of the inhibitor systems that were measured in Chapter 2 for the three electrode set-up following an exposure period of 72 hours. The obtained polarisation curves for each individual component, along with the overall responses, are presented overlaid for each inhibitor are shown from Figure 5.3.1 through Figure 5.3.8.

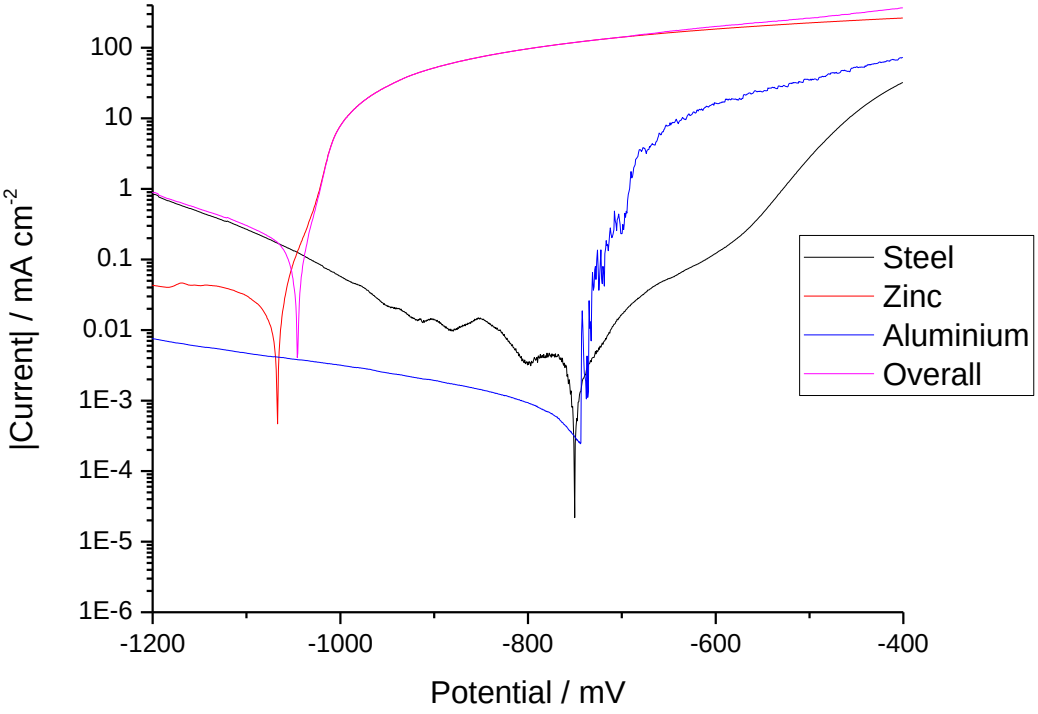

Figure 5.3.1 - The split cell potentiodynamic polarisation graph for the three electrode system in an uninhibited solution

In Figure 5.3.1, it can be seen that potential of the overall system sits close (within 50 mV) to the corrosion potential of zinc, suggesting that the overall system is anodically controlled. Both steel and aluminium are shown to be cathodes in this environment, with the magnitude of oxygen reduction occurring on the steel being roughly two orders of magnitude more than on the aluminium. At an approximate potential of -730 mV, aluminium is seen to pit, which is behaviour not observed on the steel surface.

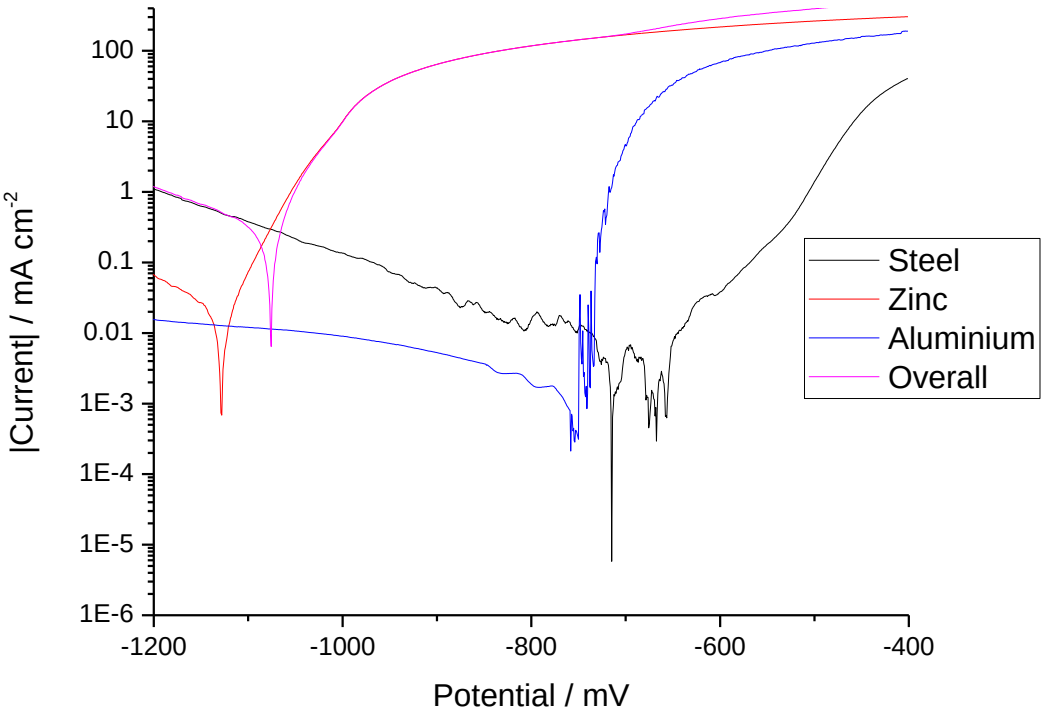

Figure 5.3.2 - The split cell potentiodynamic polarisation graph for the three electrode system in a zinc molyphosphate inhibited salt solution

In Figure 5.3.2, it can be seen that potential of the overall system sits close (within 50 mV) to the corrosion potential of zinc, suggesting that the overall system is anodically controlled. Both steel and aluminium are shown to be cathodes in this environment, with the magnitude of oxygen reduction occurring on the steel being roughly one and a half to two orders of magnitude more than on the aluminium. At an approximate potential of -750 mV, aluminium is seen to pit, which is behaviour not observed on the steel surface, although some unstable events do appear to be occurring around that potential range.

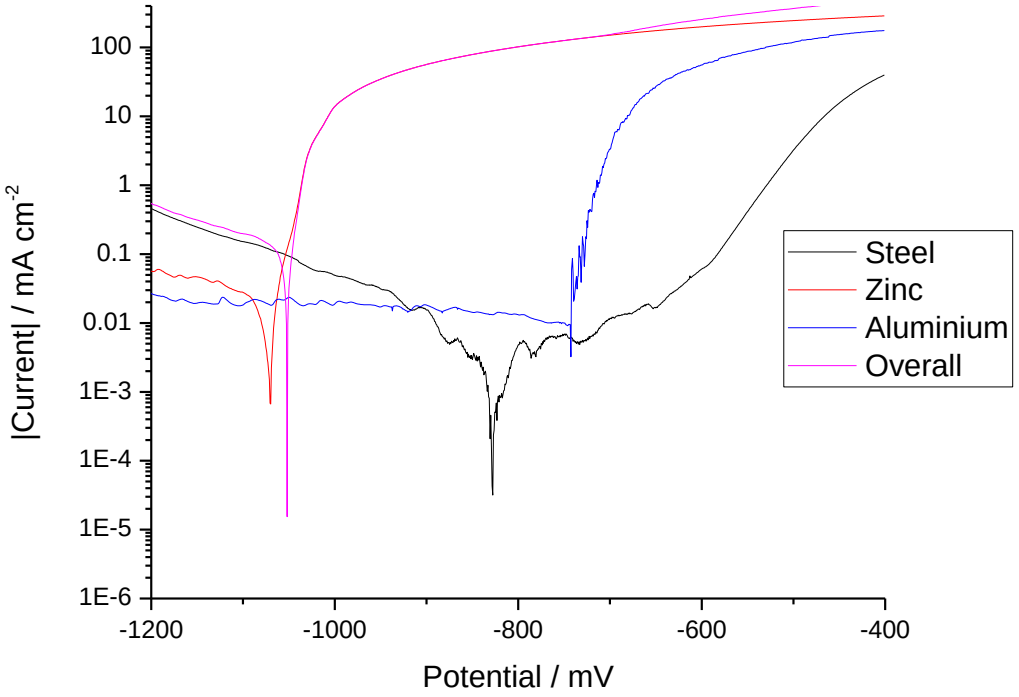

Figure 5.3.3 - The split cell potentiodynamic polarisation graph for the three electrode system in an calcium exchanged silica inhibited salt solution

In Figure 5.3.3, it can be seen that potential of the overall system sits close (within 50 mV) to the corrosion potential of zinc, suggesting that the overall system is anodically controlled. Both steel and aluminium are shown to be cathodes in this environment, with the magnitude of oxygen reduction occurring on the steel being roughly an order of magnitude more than on the aluminium. At an approximate potential of -730 mV, aluminium is seen to pit, which is behaviour not observed on the steel surface.

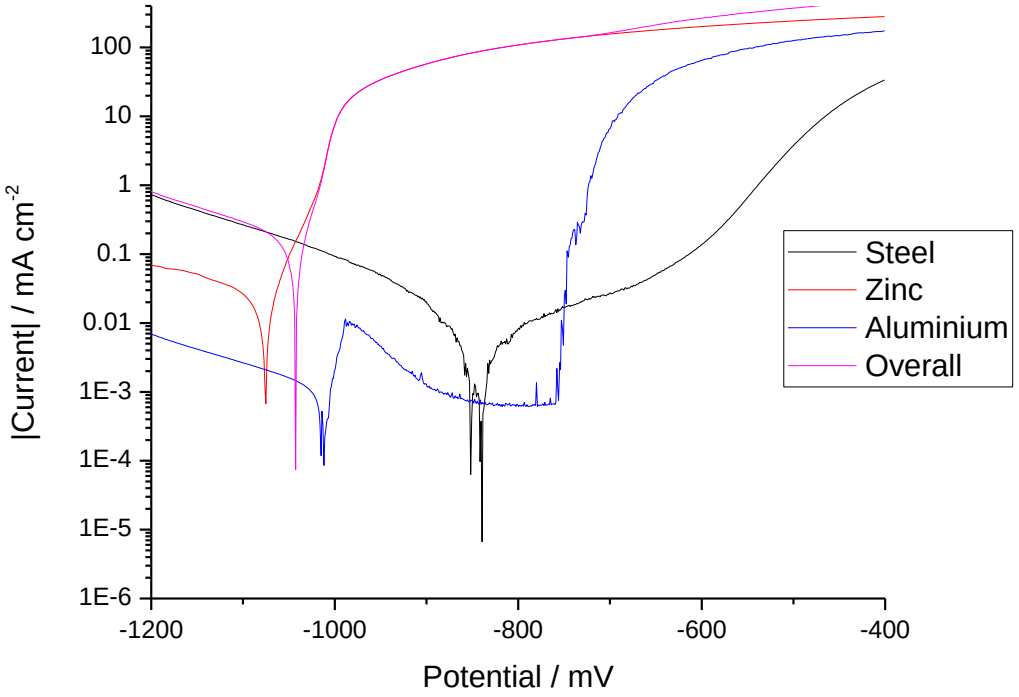

Figure 5.3.4 - The split cell potentiodynamic polarisation graph for the three electrode system in a zinc molyphosphate and calcium exchanged silica mixed inhibitor salt solution

In Figure 5.3.4, it can be seen that potential of the overall system sits close (within 50 mV) to the corrosion potential of zinc, suggesting that the overall system is anodically controlled. Both steel and aluminium are shown to be cathodes in this environment, with the magnitude of oxygen reduction occurring on the steel being roughly two orders of magnitude more than on the aluminium. Metastable pitting of aluminium is seen to occur at potentials slightly more positive than the mixed potential. At an approximate potential of -730 mV, aluminium is seen to begin an unstable pitting process, which is behaviour not observed on the steel surface.

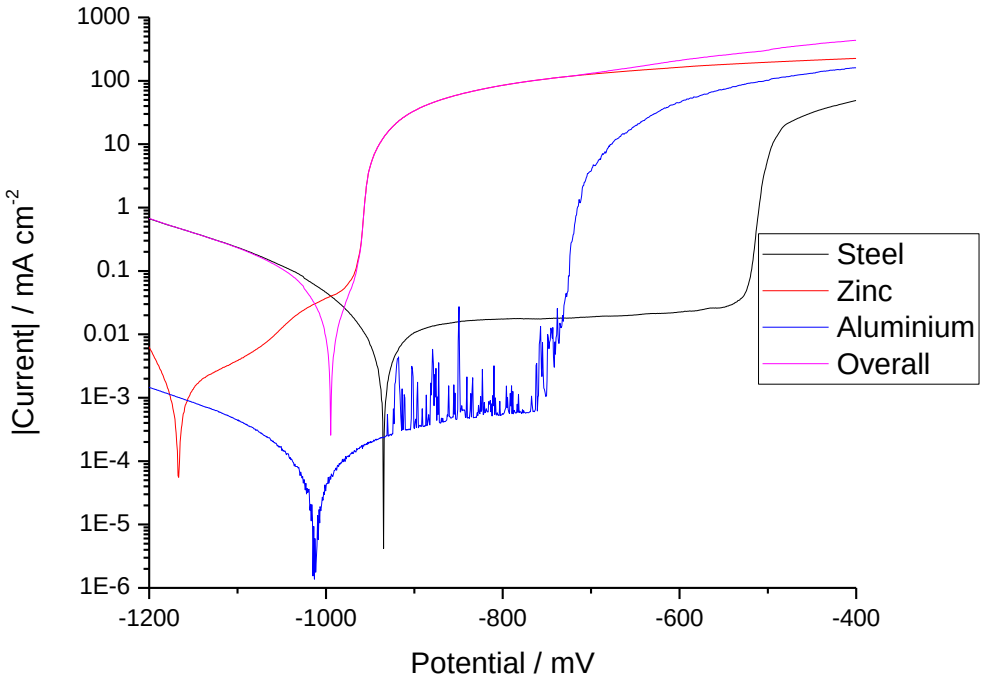

Figure 5.3.5 - The split cell potentiodynamic polarisation graph for the three electrode system in a strontium chromate inhibited salt solution

In Figure 5.3.5, it can be seen that potential of the overall system is relatively far positive (around 150-200 mV) to the corrosion potential of zinc, particularly when compared to the samples shown so far. This suggests that the overall system is not as strongly anodically controlled. Indeed, it appears that the mixed potential sits at around the potential in which aluminium begins metastable pitting (approximately -1000 mV).

In the cathodic environment, aluminium is shown to participate in oxygen reduction approximately three orders of magnitude less than steel. The steel surface is shown to become passive until around -500 mV. At an approximate potential of -730 mV, aluminium is seen to pit, which is behaviour not observed on the steel surface.

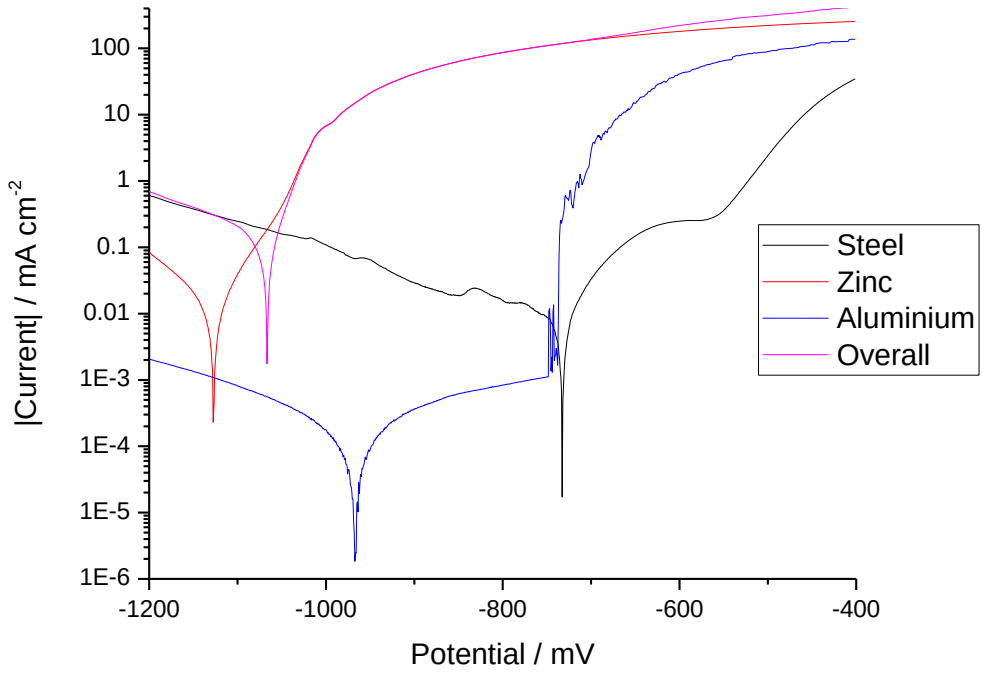

Figure 5.3.6 - The split cell potentiodynamic polarisation graph for the three electrode system in a strontium aluminium polyphosphate inhibited salt solution

In Figure 5.3.6, it can be seen that potential of the overall system sits close (within 100 mV) to the corrosion potential of zinc, suggesting that the overall system is anodically controlled. Both steel and aluminium are shown to be cathodes in this environment, with the magnitude of oxygen reduction occurring on the steel being roughly two and a half orders of magnitude more than on the aluminium. Aluminium is shown to passivate at around -950 mV, and is seen to begin pitting at an approximate potential of -730 mV. No pitting behaviour is observed on the steel surface.

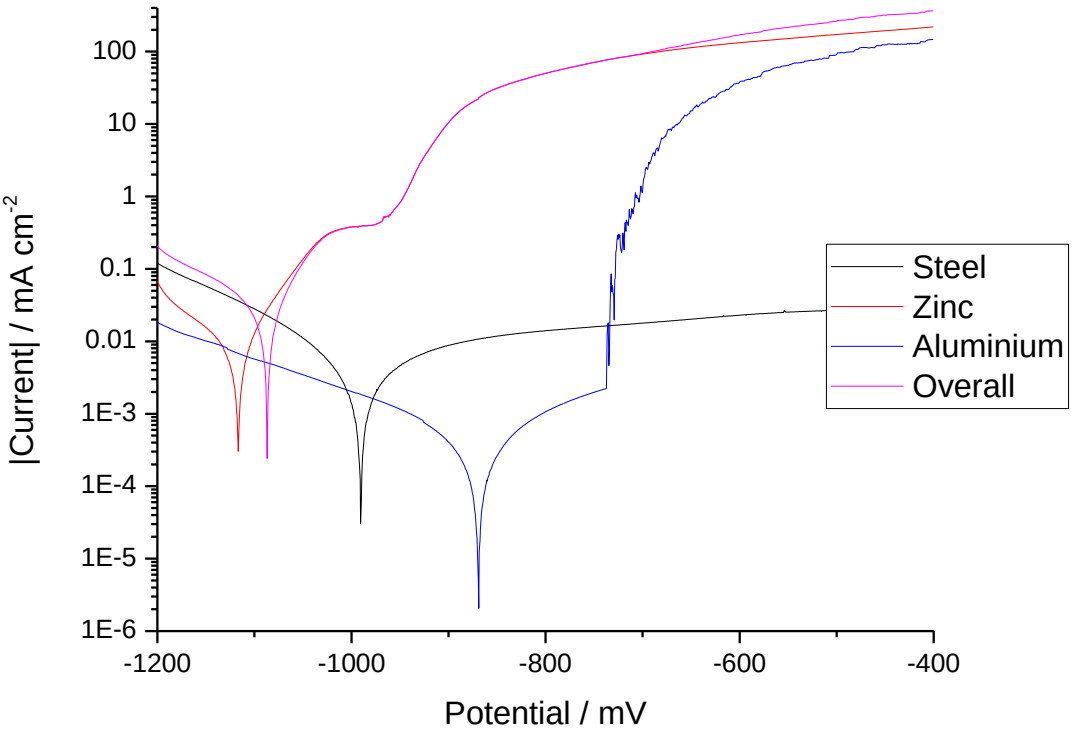

Figure 5.3.7 - The split cell potentiodynamic polarisation graph for the three electrode system in a calcium aluminium polyphosphate inhibited salt solution

In Figure 5.3.7, it can be seen that potential of the overall system sits close (within 50 mV) to the corrosion potential of zinc, suggesting that the overall system is anodically controlled. Both steel and aluminium are shown to be cathodes in this environment, with the magnitude of oxygen reduction occurring on the steel being roughly one order of magnitude more than on the aluminium. At an approximate potential of -730 mV, aluminium is seen to pit. Steel appears to become passive at a potential around -1000 mV, and this passive layer was not shown to break down during this test.

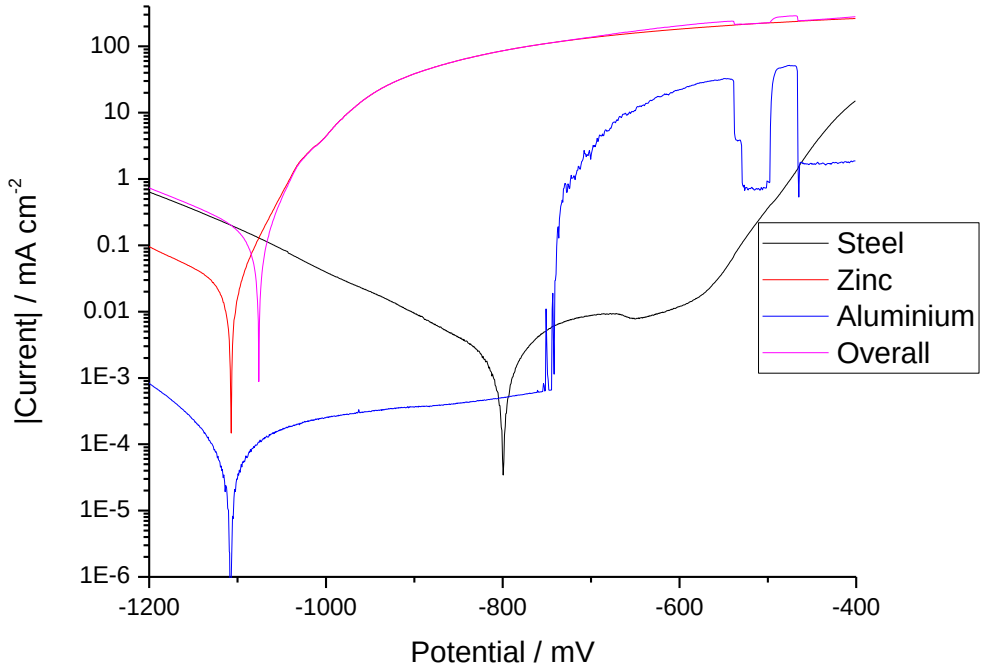

Figure 5.3.8 - The split cell potentiodynamic polarisation graph for the three electrode system in a magnesium aluminium polyphosphate inhibited salt solution

In Figure 5.3.8, it can be seen that potential of the overall system sits close (within 50 mV) to the corrosion potential of zinc, suggesting that the overall system is anodically controlled. It is also seen that the passivity region of aluminium is shown to be shifted to values more negative than that of the mixed potential, an observation which is unique to this particular inhibitor system within the current study. However, at an approximate potential of -730 mV, the passivity breaks down and aluminium is seen to pit, which is behaviour not observed on the steel surface.

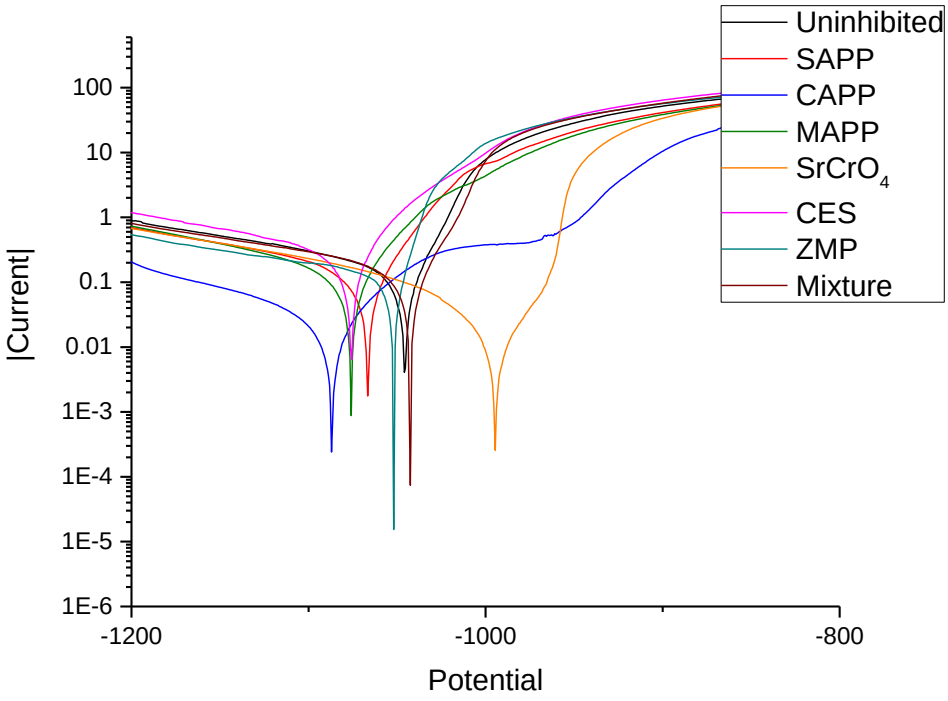

Figure 5.3.9 - A comparison of the potentiodynamic polarisation measurements for overall system in each of the inhibitor solutions measured

Electrochemical Impedance

All electrochemical impedance plots within this section are taken at the measured mixed galvanic potential. The potential in which this sits is likely to be cathodic of steel and anodic of zinc. With regards to aluminium, it is suspected that the potential will be anodic to aluminium metal, but cathodic to the pitting/passivating potential of aluminium oxide.

Uninhibited System

As in Chapter 2.1, the first experiments undertaken involved obtaining results for the three electrode cell for an uninhibited system, as this is required for the inhibitor efficiency calculations. Selected Nyquist plots acquired from these initial experiments are shown in Figure 5.3.10, Figure 5.3.11 and Figure 5.3.12 for steel, zinc and aluminium respectively. As in the previous cases, the impedance plots were taken at the measured mixed galvanic potential of the system.

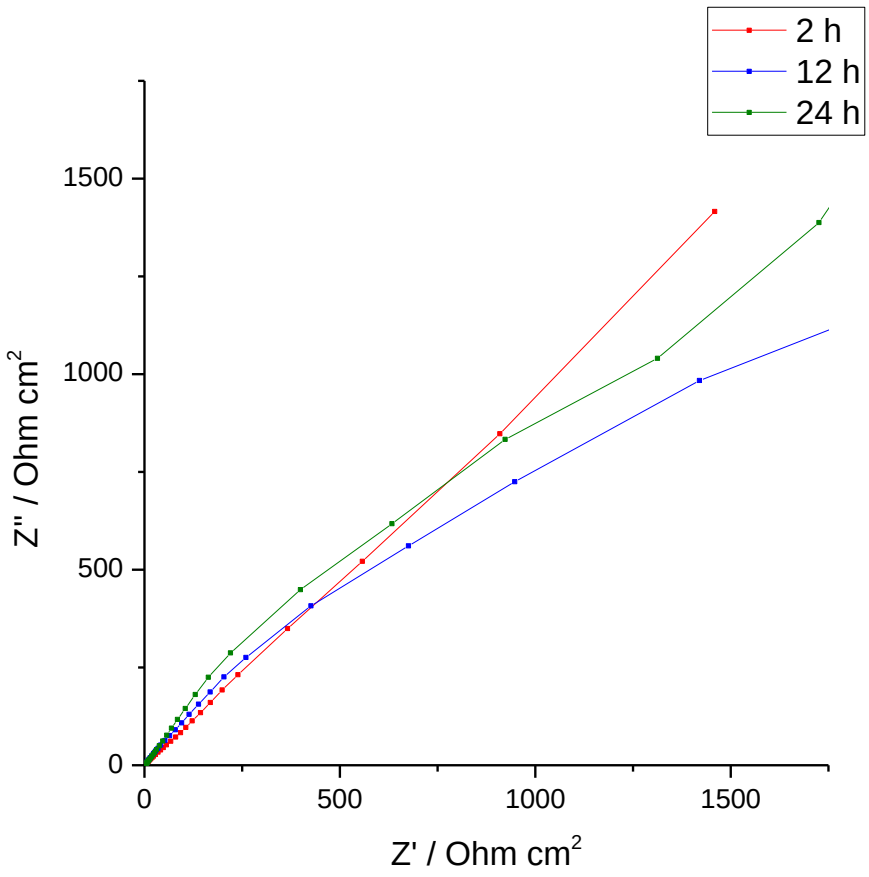

Figure 5.3.10 - Selected Nyquist plots obtained for the steel surface in an uninhibited 0.6M sodium chloride solution for the three electrode system

The impedance appearing on the steel shows a bias towards diffusion based kinetics, with the Warburg element being a large part of the overall spectrum for each of the shown exposure times, although the influence is shown to wane in the latter stages of exposure.

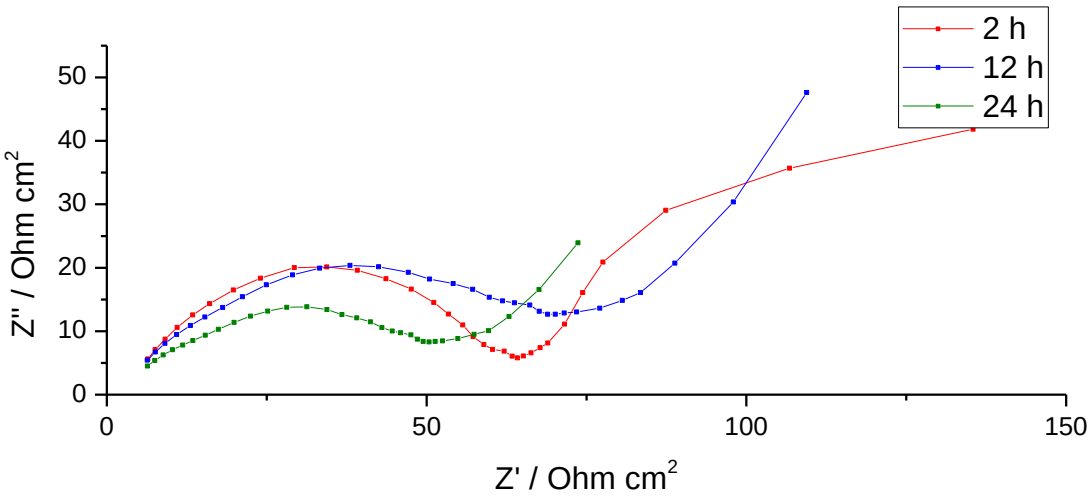

Figure 5.3.11 - Selected Nyquist plots obtained for the zinc surface in an uninhibited 0.6M sodium chloride solution for the three electrode system

The impedance obtained on the zinc surface shows relatively low impedance, consistent with the anodic nature of the electrode within this particular arrangement. The depression of the capacitive semi-circle suggests that the electrode tends toward less ideal behaviour. It is also suggested that the corrosion rate on the zinc electrode increases with longer exposure times.

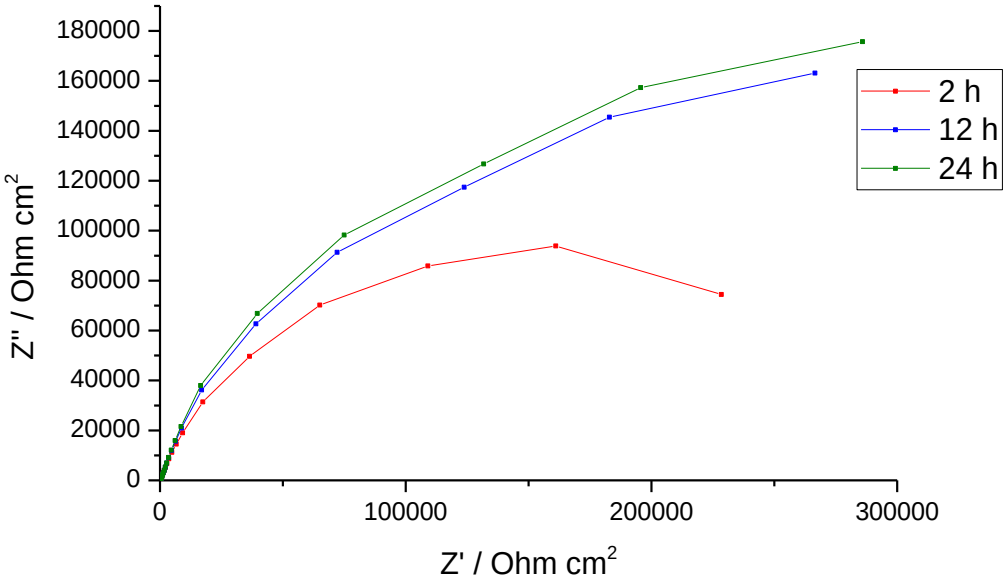

Figure 5.3.12 - Selected Nyquist plots obtained for the aluminium surface in an uninhibited 0.6M sodium chloride solution for the three electrode system

The aluminium surface shows large resistance within the impedance spectra, consistent with the presence of aluminium oxide on the surface, which becomes more protective at later timeframes. Whilst the uninhibited system was followed for the full 72 hour observation period, only results obtained for the initial 2 hour exposure will be used in the inhibitor efficiency calculations, as per previous chapters.

Strontium Aluminium Polyphosphate

Figure 5.3.13, Figure 5.3.14 and Figure 5.3.15 show selected Nyquist plots obtained on the steel, zinc and aluminium surfaces respectively for the strontium aluminium polyphosphate inhibited system.

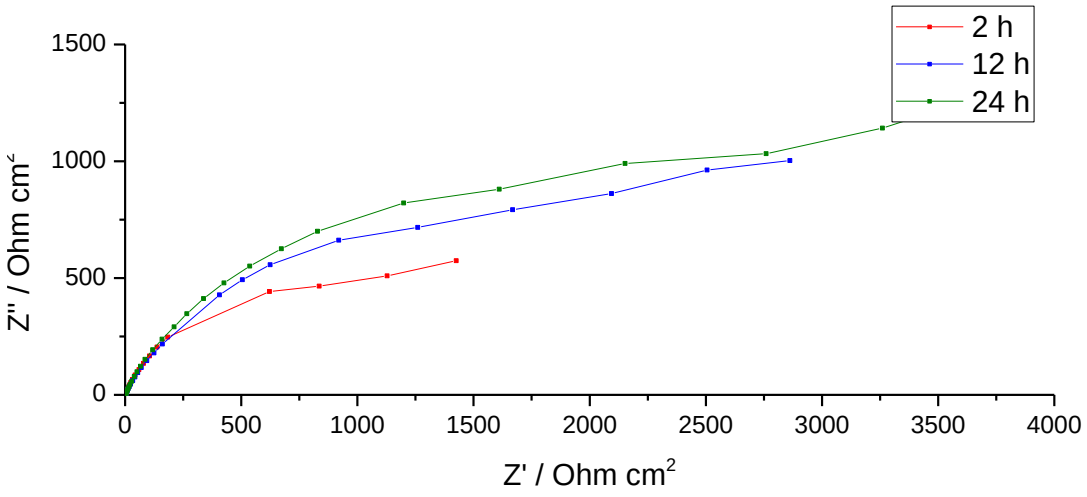

Figure 5.3.13 - Selected Nyquist plots obtained for the steel surface in a saturated strontium aluminium polyphosphate inhibited 0.6M sodium chloride solution for the three electrode system.

After adding SAPP inhibitor to the environment, the resistance shown is seen to increase compared to the uninhibited environment. However, it is also worth noting that there is also a depression of the capacitive semi-circle.

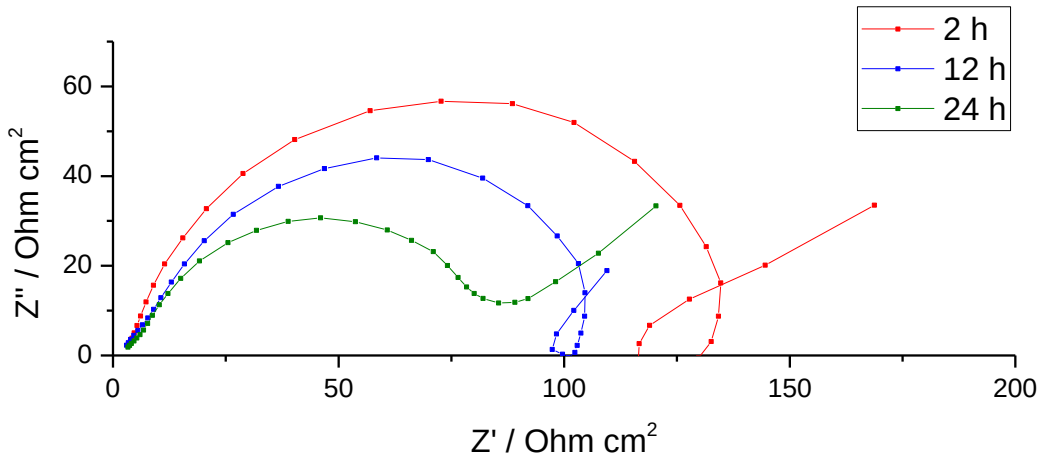

Figure 5.3.14 - Selected Nyquist plots obtained for the zinc surface in a saturated strontium aluminium polyphosphate inhibited 0.6M sodium chloride solution for the three electrode system.

The zinc electrode, when the SAPP pigment is introduced, also shows relatively low resistance, which reduces over longer exposure times. Inductive loops are also seen to be present on the low frequencies at earlier exposure times. This is expected to be due to small changes in corrosion potential.

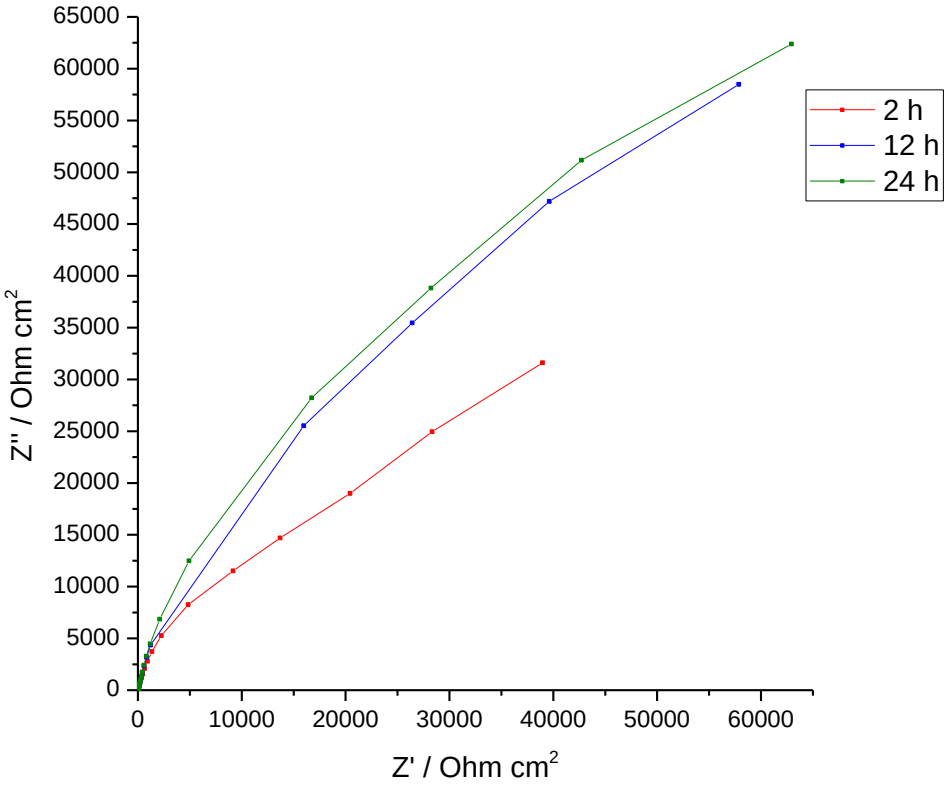

Figure 5.3.15 - Selected Nyquist plots obtained for the aluminium surface in a saturated strontium aluminium polyphosphate inhibited 0.6M sodium chloride solution for the three electrode system.

The aluminium surface shows large resistance within the impedance spectra, consistent with the presence of aluminium oxide on the surface, which becomes more protective at later timeframes. The inhibitor efficiency of strontium aluminium polyphosphate on the aluminium surface is calculated to be approximately 66%.

Calcium Aluminium Polyphosphate

Figure 5.3.16, Figure 5.3.17 and Figure 5.3.18 show selected Nyquist plots obtained on the steel, zinc and aluminium surfaces respectively for the calcium aluminium polyphosphate inhibited system.

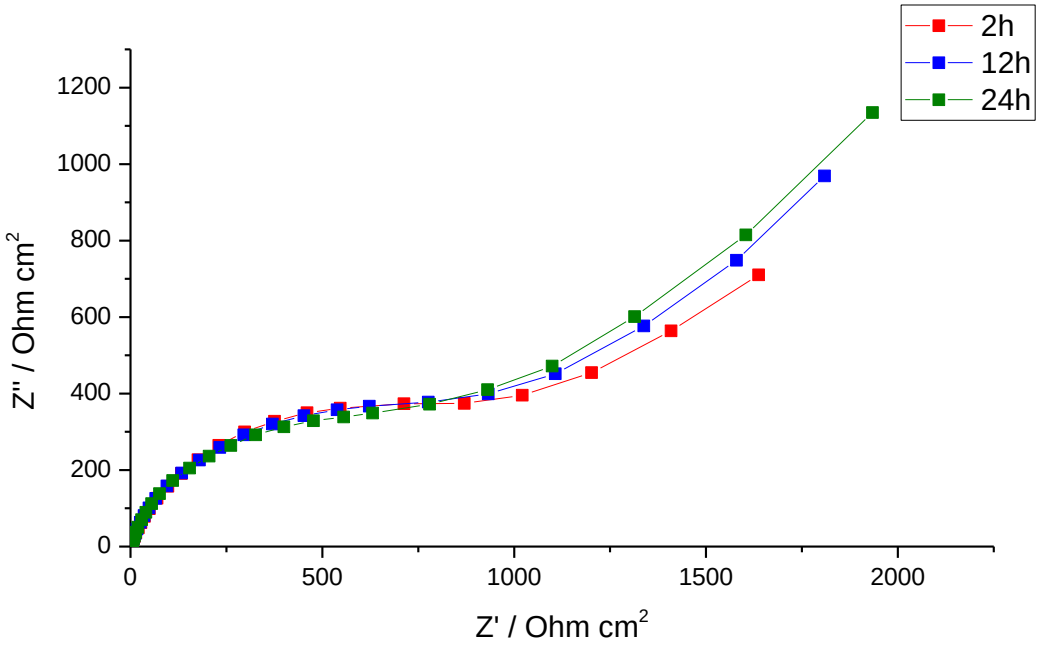

Figure 5.3.16 - Selected Nyquist plots obtained for the steel surface in a saturated calcium aluminium polyphosphate inhibited 0.6M sodium chloride solution for the three electrode system.

The steel surface when calcium aluminium polyphosphate is added shows an increase in resistance in the initial stage compared to the uninhibited environment. However, it can also be seen that the behaviour observed on the steel surface remained consistent throughout the first 24 hours of exposure.

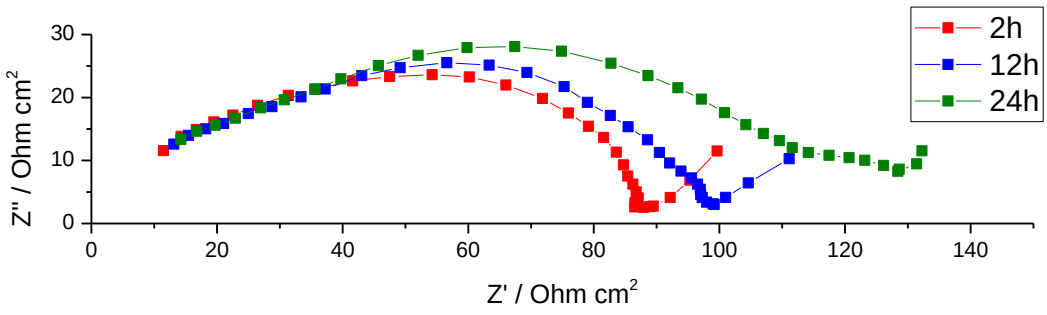

Figure 5.3.17 - Selected Nyquist plots obtained for the zinc surface in a saturated calcium aluminium polyphosphate inhibited 0.6M sodium chloride solution for the three electrode system.

With calcium aluminium polyphosphate added to the environment, the impedance spectra obtained exhibit heavily depressed semi-circles. The calculated resistances are larger than that exhibited by the uninhibited samples, and the resistance is shown to increase over longer exposure times.

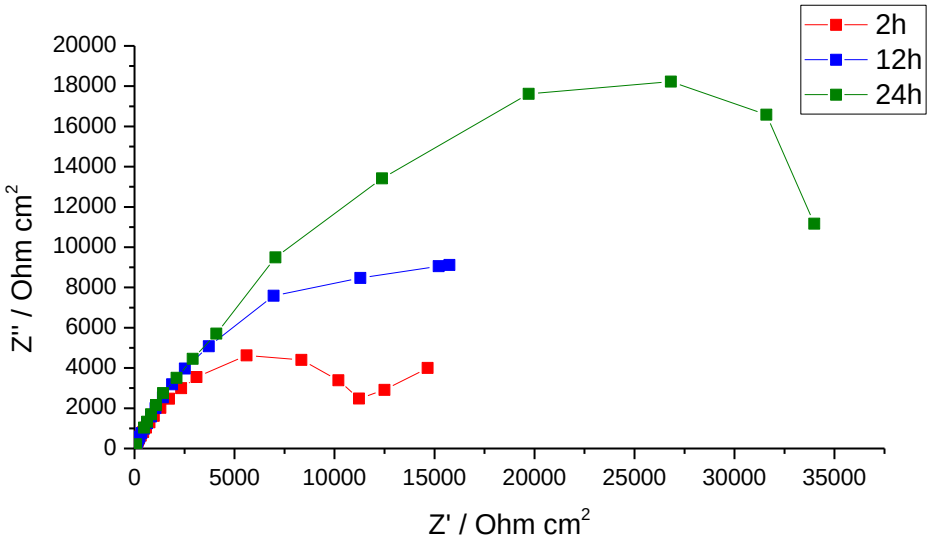

Figure 5.3.18 - Selected Nyquist plots obtained for the aluminium surface in a saturated calcium aluminium polyphosphate inhibited 0.6M sodium chloride solution for the three electrode system.

The aluminium impedance with calcium aluminium polyphosphate introduced into the environment exhibits a small reduction in the polarisation resistance at early exposure times. This resistance increases on the later exposure times.

Magnesium Aluminium Polyphosphate

Figure 5.3.19, Figure 5.3.20 and Figure 5.3.21 show selected Nyquist plots obtained on the steel, zinc and aluminium surfaces respectively for the strontium aluminium polyphosphate inhibited system.

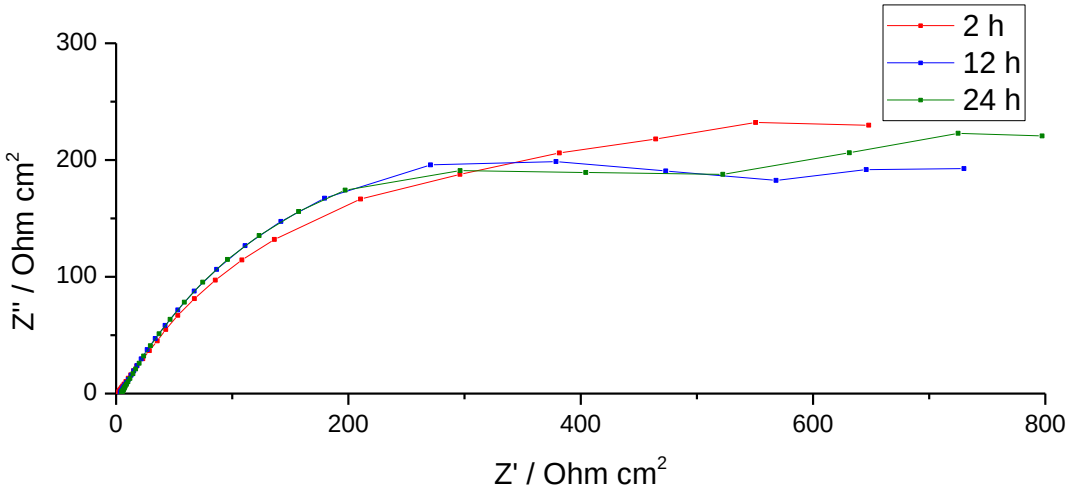

Figure 5.3.19 - Selected Nyquist plots obtained for the steel surface in a saturated magnesium aluminium polyphosphate inhibited 0.6M sodium chloride solution for the three electrode system.

The steel surface when magnesium aluminium polyphosphate is added shows an increase in resistance in the initial stage compared to the uninhibited environment. However, it can also be seen that the behaviour observed on the steel surface remained approximately consistent throughout the first 24 hours of exposure.

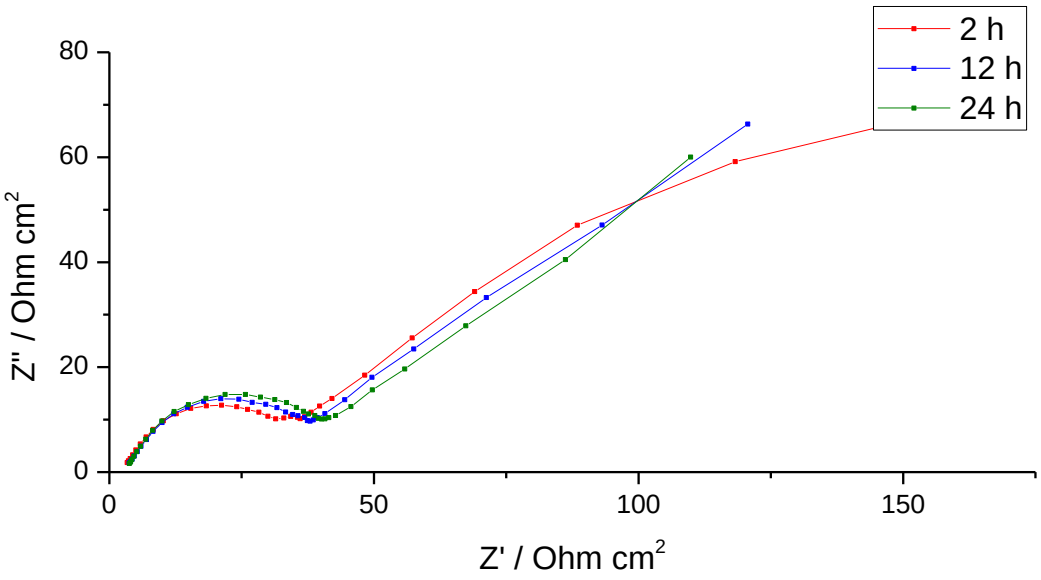

Figure 5.3.20 - Selected Nyquist plots obtained for the zinc surface in a saturated magnesium aluminium polyphosphate inhibited 0.6M sodium chloride solution for the three electrode system.

With magnesium aluminium polyphosphate added to the environment, the impedance spectra obtained exhibit heavily depressed semi-circles. The calculated resistances are lower than that exhibited by the uninhibited samples, suggesting a negative inhibitor efficiency, which remains approximately the same throughout the first 24 hours of exposure.

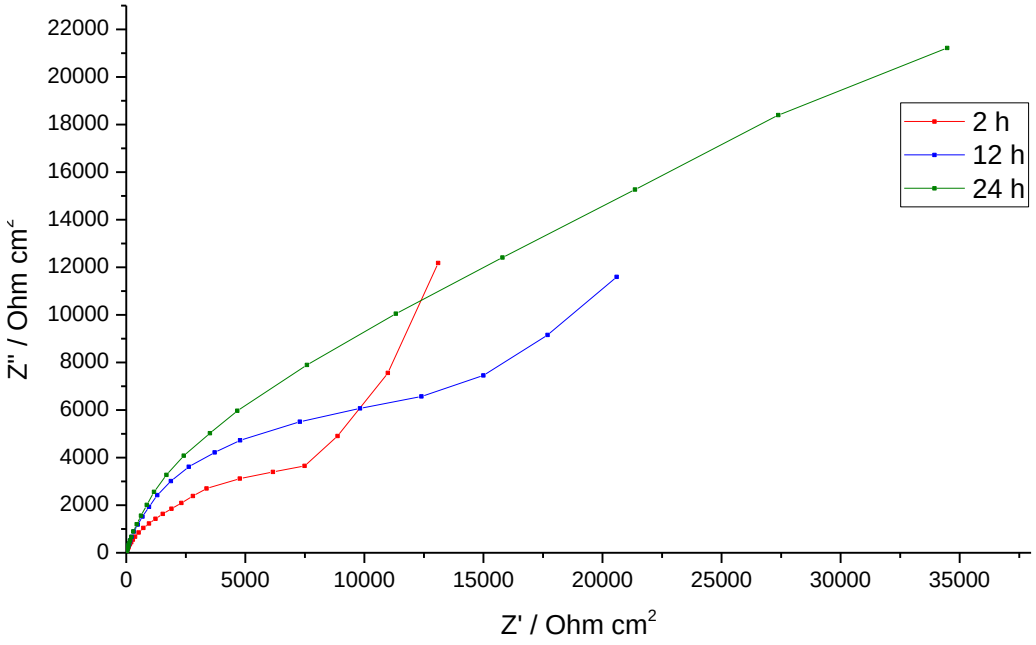

Figure 5.3.21 - Selected Nyquist plots obtained for the aluminium surface in a magnesium aluminium polyphosphate inhibited salt solution for the three electrode system.

The aluminium impedance with magnesium aluminium polyphosphate introduced into the environment exhibits a large reduction in the polarisation resistance at early exposure times. Looking at the potentiodynamic polarisation curve presented earlier, it can be seen that these are potentially impedance measurements done at an anodic potential as opposed to a cathodic one. It is also seen that the polarisation resistance of these samples increases with longer exposure times.

5.4 Discussion

Potentiodynamic Polarisation

General Observations

In this set of experiments, an additional experimental step, potentiodynamic polarisation, was added to take place following the 72 hour exposure period. For the initial analysis of the potentiodynamic polarisation results, the effects of the inhibitors on the individual metallic components are taken into consideration.

In the case of the steel surfaces, calcium aluminium polyphosphate exhibits the strongest cathodic inhibition, with a corrosion potential shift from -770 mV for the uninhibited solution to -900 mV. Cathodic inhibition is also clearly exhibited, to lesser extents, by strontium chromate, MAPP and the CES/ZMP mixture. Across the potential range, there are no notable changes in the measured currents, except for the calcium aluminium polyphosphate inhibitor pigment, which demonstrates a notable drop in measured current across the entire range of potentials. It is also worth noting that anodic areas with reduced rates of current increase are present for the CAPP, MAPP and strontium chromate inhibitors, suggesting areas approaching low levels of passivity.

For the zinc surface, strontium chromate shows an extended period of low corrosion current increase. It can be suggested that this represents efficacious anodic inhibition of the zinc surface, as opposed to an area of true passivity. Calcium aluminium polyphosphate also exhibits a reduction for the currents exhibited on the cathodic and anodic branches of the potentiodynamic polarisation curve by approximately one decade, similar in magnitude to that seen by strontium chromate, but with a corrosion potential that is not shifted to as negative values. For the remaining inhibitor systems, there are general negative shifts in the measured corrosion potential, but the magnitude of the cathodic and anodic branch currents are shown to be fairly similar to that of the uninhibited sample.

For the aluminium surface, a clear corrosion potential, through the presence of Tafel behaviour, is not evident in the case of the uninhibited system, as well as systems inhibited by ZMP and CES. These appear to exhibit similar behaviours with a sharp current increase evident at approximately -730 mV. This has been previously reported as the upper limit for the corrosion potential for pure aluminium[8]. This behaviour suggests that ZMP and CES have no effect on the corrosion behaviour of the aluminium component of this system.

In the case of the other inhibitors, the interpretation of their inhibitive behaviour requires further analysis of the curve behaviour. In the case of strontium chromate, this appears to exhibit an extended period of instable passivity in the anodic branch of the potentiodynamic polarisation curve. It is suggested that this has a physical manifestation through the pitting and subsequent repassivation of the surface.

However, in all but the calcium aluminium polyphosphate case, a full breakdown and increase in current is observed at potentials lower than -730 mV, as is seen in the cases of the uninhibited and poorly inhibited systems.

Calcium aluminium polyphosphate shows interesting behaviour on aluminium. The current branches seen on the potentiodynamic polarisation curve for the cathodic side can be considered to be at a relatively expected level, with suppression of the current down to levels seen for strontium aluminium polyphosphate, but slightly worse than that for strontium chromate. However, the anodic branch shows significantly modified behaviour to that of the other systems observed, with currents seen at a magnitude of approximately 1 decade lower than all other systems measured. As mentioned previously, calcium aluminium polyphosphate also exhibits a long, stable area of passivity, which only shows slight instabilities at potentials less negative than -680 mV.

The strontium aluminium polyphosphate inhibited aluminium surface shows similar profile to that seen by strontium chromate. Comparatively, the open circuit potential is seen to be shifted to less negative potentials by approximately 50 mV.

Magnesium aluminium polyphosphate is shown to provide the strongest cathodic potential shift within the inhibitors observed on the aluminium substrate. Strong inhibiting behaviour of the cathodic reaction on the aluminium surface, which would likely be the oxygen reduction reaction, could be influential on the production of the protective aluminium oxide. Therefore,

this observation may support the theory brought up in the discussion of the electrochemical impedance results that corrosion acceleration by magnesium aluminium polyphosphate is a result of the inhibitor interfering with the production of a coherent passivating layer. However, one consequence of the potential shift on the aluminium surface is that the mixed corrosion potential of the system in this case results in the aluminium electrode being polarised anodically. Within the inhibitor systems measured, this situation is unique and results in distinct behaviour for this pigment.

Analysing the general shapes of the potentiodynamic polarisation comparison for the overall responses, it can be seen that CAPP has the most significant shift to negative potentials, indicating strongest inhibition of the cathodic site. Indeed, all polyphosphates observed show a tendency towards cathodic inhibition. Strontium chromate has the greatest shift to more positive potentials, indicating strongest inhibition of the anodic sites. What can also be seen is that the observed current for the CAPP inhibitor are almost a level of magnitude lower than that of all other systems.

As per previous literature that was utilised in Chapter 2.1 for the inhibitors used for verification, ZMP displays cathodic inhibition whilst CES, and the inhibitor mixture containing both ZMP and CES exhibit mixed corrosion inhibition.

Using Tafel interpolation where appropriate, the corrosion potentials and corrosion currents were obtained for each individual electrode, alongside the overall system. Table 5.4-1 shows the values obtained.

Electrode	Steel		Zinc		Aluminium		Full System	
	Icorr / mA	*Ecorr* / mV	*Icorr* / mA	*Ecorr* / mV	*Icorr* / mA	*Ecorr* / mV	*Icorr* / mA	*Ecorr* / mV
UI	4.27E-03	-776	2.20E-02	-1064	*N/A*	*N/A*	1.66E-01	-1036
ZMP	2.79E-03	-718	1.22E-02	-1133	*N/A*	*N/A*	2.57E-01	-1083
CES	1.41E-03	-813	8.65E-03	-1080	*N/A*	*N/A*	8.36E-02	-1049
Mixture	4.20E-03	-845	2.26E-02	-1068	1.11E-03	-1003	1.65E-01	-1035
SAPP	9.95E-03	-752	1.26E-02	-1127	1.40E-04	-945	1.36E-01	-1062
CAPP	3.33E-03	-903	8.48E-04	-1171	1.03E-04	-868	2.35E-02	-1078
MAPP	1.82E-03	-790	2.06E-02	-1114	1.18E-04	-1120	1.93E-01	-1092
Chromate	1.28E-02	-883	8.76E-04	-1168	2.33E-04	-1006	5.88E-02	-972

Table 5.4-1 - A table showing the corrosion potential and corrosion currents calculated through Tafel interpolation of the potentiodynamic polarisation plots obtained. In the case of the uninhibited, zinc molyphosphate and calcium exchanged silica samples, no areas of Tafel behaviour were observed for the aluminium surface as it pits.

In some cases, Tafel interpolation was difficult or impossible as there were no activation state controlled processes occurring. For spectra obtained on some steel surfaces, the regions where Tafel behaviour might be expected contain noise. This means that any interpretations of these particular spectra are likely to be erroneous.

In the case of the spectra obtained on some of the aluminium surfaces, it is not possible to use Tafel interpolation to determine the corrosion current or potential as a clear shift between anodic and cathodic behaviour is not present within the spectra. It is possible that this is due to the corrosion potential of aluminium being outside the scan range of the experiment[9].

Whilst it would be possible to change the parameters of the experiment to extend the potential range, this would affect the results obtained on the zinc surface due to polarising the sample cathodic to the potential of zinc oxide, as the reduction potential of zinc oxide (approximately -1.2V) is close to that of the general corrosion potential of zinc (-0.78V)[9]. However, the most likely explanation is that the behaviour exhibited is consistent with pitting of the aluminium surface, which is expected at around -730 mV in this environment.

The applicability of the potentiodynamic polarisations is difficult to determine, whilst the Tafel interpolation of these curves may output some interesting information, ultimately the

corrosion potentials and currents of the individual parts of the system are not directly related to the coupled behaviour, as the corrosion potential is far from the individual open circuit potentials. Despite this, there are some interesting observations that are worth analysing.

Strontium chromate exhibits a significant reduction in the corrosion current for the zinc electrode, but unusually the highest corrosion current for the steel surface. As a well-known and highly effective corrosion inhibitor, this analysis can be considered incorrect. Indeed, no Tafel behaviour would be expected due to passive behaviour being exhibited. Despite this, Tafel analysis of the full system potentiodynamic polarisation plot shows one of the lowest corrosion currents and significant anodic inhibition compared to the uninhibited corrosion potential.

Indeed, throughout these tests, the steel inhibition across the board can considered to be fairly poor, with overall corrosion currents not varying much from that which was observed for the uninhibited system, yet some sizable shifts in corrosion potential. This would suggest that, in these cases, the inhibition of the anodic reactions is paired with a concurrent facilitation of the cathodic reaction (or vice versa).

In the case of magnesium aluminium polyphosphate, the corrosion current for the aluminium surface is seen to be low. Indeed, all polyphosphates (and strontium chromate) show corrosion currents an order of magnitude lower than that of the calcium exchanged silica/zinc molyphosphate mixture. This low corrosion current could be seen to be contradictory to the corrosion acceleration behaviour observed within the electrochemical impedance results. However, these polarisation results are taken after a greater period of time in which the corrosion acceleration effect could potentially have ended.

Additionally, it can be seen that MAPP has the most negative potential observed for the aluminium surface, suggesting inhibition of the cathodic reaction. This leads to the corrosion

potential of the system sitting anodic to the open circuit potential of the aluminium, which could explain the initial impedance behaviour. However, this is also the case for strontium chromate which does not exhibit this behaviour. Calcium aluminium polyphosphate shows the greatest positive shift in potentials for the aluminium surface, suggesting inhibition of anodic reactions on the surface.

Overall, the separated potentiodynamic polarisations can give some information in how the individual environments differ from the uninhibited systems. However, there are certainly some limitations.

Electrochemical Impedance

Justification of Equivalent Circuits

As was the case in the previous sections, the equation relating charge transfer resistance and inhibitor efficiency was used, following the calculation of the charge transfer resistance from equivalent circuit analysis of the obtained electrochemical impedance spectra. For the impedance spectra gained for the steel and zinc constituents of the multi-metal cell, the analysis was as described in the previous chapters, utilising the same equivalent circuits with the same justifications. In this set of experiments, the mixed corrosion potential of the systems was not significantly altered compared to that of the steel-zinc couple (i.e. the presence of aluminium did not cause large shifts in the potential of the system) and thus significant changes to the behaviour of these two components of the cell are not expected.

For impedance spectra obtained for the aluminium surface, the equivalent circuits shown in Figure 5.4.1 are representative of those that were used.

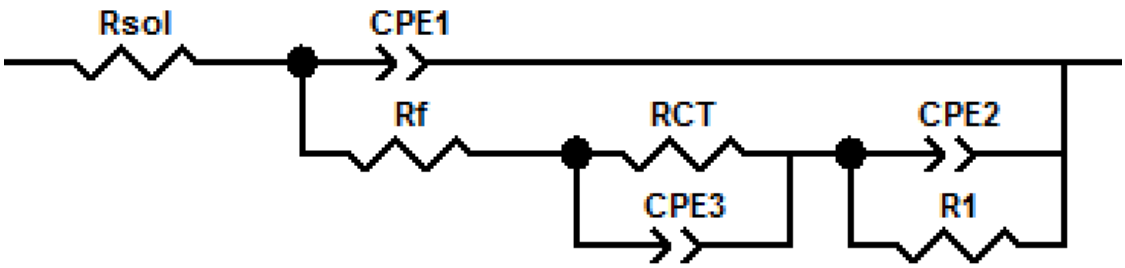

Figure 5.4.1 - Representative equivalent circuit used for the analysis of most electrochemical impedances obtained on the surface of aluminium.

For most aluminium samples, the presence of three time constants was detected, which utilised the equivalent circuit shown. The first is the parallel combination of the charge transfer resistance and double layer capacitance (a constant phase element has been used to take into account the imperfection in the capacitive behaviour). As is the case for the other samples, the charge transfer resistance of the corrosion process is what will be used to determine the overall inhibitor efficiency.

The second time constant that is present is attributed to the aluminium oxide layer at the surface. When using pure aluminium, like has been done in this section, the formation of aluminium oxide from contact with the air is almost unavoidable. Aluminium oxide at the surface is known to provide effective protection of the bulk sample, and it was seen in many of the observed samples that the calculated resistance was high[3]. Indeed, for some of the samples, the resistance was calculated to be beyond the limits of the programme. In these cases, the absence of the resistor from the equivalent circuit make little difference to the overall fitting, but are included for complete justification of the system.

The development of a third time constant in the lower frequency range is evident in many of samples. The stability of this third time constant can be considered to improve when looking at the samples with longer exposure times. It is suspected that this third time constant is either due to damage within the oxide layer[4] or the deposition of a secondary protective layer due to the presence of corrosion inhibitor within the solution[5].

Interpretation of Equivalent Circuit Analysis

To understand the behaviour better, the inhibitor efficiencies of the polyphosphate inhibitors, and strontium chromate, were calculated using the equation given in Chapter 2.1. Table 5.4-2 shows the calculated inhibitor efficiencies for each of the inhibitor species.

		Inhibitor Efficiency / %			
Metal	**Exposure Time**	**SrCrO4**	**SAPP**	**CAPP**	**MAPP**
Steel	*2h*	69	65	44	36
	12h	63	78	44	58
	24h	97	81	43	66
Zinc	*2h*	78	56	34	-60
	12h	85	46	40	-46
	24h	86	31	50	-41
Aluminium	*2h*	63	14	-159	-288
	12h	86	66	3	-116
	24h	85	66	31	-30

Table 5.4-2 - Calculated inhibitor efficiencies for strontium chromate and the observed polyphosphate inhibitors for the three electrode segmented electrochemical impedance experiments

These calculated inhibitor efficiencies give more detail of the overall picture, and can put some of the previous observations into context. Firstly, the inhibition observed for strontium chromate is seen to be effective across all three metallic surfaces, and over the observation period, in most cases, it can be seen to be the inhibitor with the highest efficiency. This observation highlights the flexibility and effectiveness that has led to the wide use of hexavalent chromium compounds, and the subsequent struggle to replace them.

Secondly, the suggested reduction in charge transfer resistance for the MAPP samples manifests itself as negative efficiencies in the calculation table. The physical meaning behind negative inhibitor efficiencies is suggested to be corrosion acceleration. This is seen on the aluminium surface, and to a lesser extent the zinc surface, for the MAPP inhibited samples.

The benefits to corrosion acceleration from a corrosion prevention standpoint can be considered to be non-obvious. However, in this case, initiating the corrosion of aluminium

could potentially be mechanistically important for the effective inhibition of the overall system.

As the three electrode set-up is designed to be a model of the galvanising alloy Galvalume, the behaviour of this alloy must be taken into consideration. One of the major advantages of using Galvalume as a metallic coating has been reported as improvements in results from salt spray tests[6]. It is suspected that this is due self-passivation that is a direct result of the high aluminium content present at the material surface[7]. This can be considered to be a useful outcome in the case of small coating defects in which only the alloy coating is exposed.

However, this behaviour can be potentially problematic in scenarios where the underlying steel is exposed to the environment, such as at the cut edge. In this scenario, sufficient self-passivation of the galvanic layer would lead to the steel becoming vulnerable to corrosive attack. In the case of a Galvalume system inhibited by MAPP, the corrosion acceleration effect could, in theory, allow the metallic coating to act as a sacrificial anode and thus protect the underlying steel substrate.

Within the polyphosphate inhibitors, strontium aluminium polyphosphate is shown to be the most consistent, with the best inhibition across all metallic surfaces. However, SAPP appears to get less efficient over the observation period on the zinc surface.

Applicability of Technique

This set of experiments attempted to expand the applicability of the electrochemical impedance experiments utilising two distinct electrodes in an attempt to study more complex systems.

As discussed in Chapter 2, there are some limitations to the information that can be obtained from the electrochemical impedance plots that are obtained from segmented electrode experiments. In moving from measuring at the open circuit potential of a particular metal to

the mixed corrosion potential of the overall system, it was determined that the obtained results were generally dominated by a single time constant, which is suspected to refer specifically to either the anodic or cathodic reaction. This means that the extent of inhibition for the individual reactions is what can be ascertained from the results, whereas most mechanistic information will be difficult to establish from the impedance results alone.

In applying this technique to a three electrode system, more points can be raised. The addition of further electrodes that have distinct electrochemical behaviours, in addition to the two electrodes utilised in the original experimental setup, may produce a non-binary distinction between anode and cathode. Whilst this does not appear to have created many issues with the results presented in this work, the application of this methodology to other systems may result in some data that is difficult to interpret.

Additionally, in using a pure aluminium electrode, problems can arise from the strongly passivating properties of naturally occurring aluminium oxide. This results in the measurement of strongly capacitive behaviour with large charge transfer resistances that can only be calculated through extrapolation and are therefore likely to have a large degree of inaccuracy. However, it appears that the overall behaviour of the plot can be interpreted through simple comparisons with relative confidence.

Overall Picture

A greater understanding of the inhibitor pigments, and the effects that they have on the three electrode system, can be obtained through combining the results of the potentiodynamic polarisation with the electrochemical impedance plots.

Strontium chromate exhibits the same flexibility and effectiveness that has resulted in wide use and ultimately the issues in replacing it. Consistently high calculated inhibitor efficiencies within the impedance results are also corroborated with significant inhibition that is noted in the potentiodynamic polarisation results.

With regards to the polyphosphate inhibitor pigments, anecdotal evidence from natural testing and in-service behaviour as suggested by the industrial sponsors indicates that the magnesium aluminium polyphosphate inhibitor pigment is the most effective for reducing corrosion behaviour when used in paints applied to a Galvalume coated steel substrate. It is also suggested in the literature, as previously stated, that the use of Galvalume for various applications is a result of improved corrosion testing results when compared to zinc coated steel, such as in salt spray.

One suggestion for this behaviour is that the high aluminium content of the alloy results in self passivation through the formation of an adherent aluminium oxide layer at the surface. This would be effective at lowering corrosion rates in standard testing but would also result in poor performance in situations where the steel is exposed, such as in scribes, or at the cut edge in real world scenarios, due to not providing sufficient sacrificial protection to the underlying steel substrate.

In the case of magnesium aluminium polyphosphate, it has been shown in previous chapters of this work that it is a reasonably effective inhibitor with a quick onset of action for the simple case of two electrode system utilising steel and zinc electrodes. In the case of Galvalume, it is suggested that it also provides an additional effect in the ability to disrupt the aluminium oxide layer and thus accelerate aluminium corrosion. In doing so, this allows the galvalume to act as a sacrificial anode in such scenarios where it is necessary to do so. In this way, the corrosion of the steel substrate is reduced sufficiently to allow the inhibitor to work.

5.5 Conclusions

In this chapter, the segmented electrode electrochemical methodology was expanded to employ further electrodes by introducing aluminium to the original zinc and steel electrode set-up. Following the analysis of the results obtained from these experiments, the following conclusions can be drawn:

- The application of the segmented electrode technique to three electrodes appears to be successful, with analysable data obtained across all three electrodes.
- In the case of aluminium, the presence of the naturally occurring passive oxide layer on the surface results in large charge transfer resistances in a non-inhibited medium.
- Strontium chromate is seen to be an effective inhibitor, with inhibitor efficiencies greater than 80% across all three surfaces compared to the polyphosphate inhibitors, which are often seen with inhibitor efficiencies lower than 60%.
- Magnesium aluminium polyphosphate shows unusual corrosion acceleration behaviour (negative inhibitor efficiencies) on the aluminium surface
    - This may be indicative of a mechanism which would allow cut edge protection, suggesting an interruption of aluminium oxide production allowing the aluminium parts of the microstructure to provide sacrificial protection
    - Magnesium aluminium polyphosphate is the only inhibitor where the aluminium corrosion potential/passivation potential is situated at a more negative potential than that of the system mixed potential, and this means that the aluminium component can therefore provide sacrificial protection to the steel
- Aluminium surface is generally seen to be cathodic, with the oxygen reduction reaction taking place at a rate generally between one and three orders of magnitude lower than that of the steel surface
- Most system potentials are situated within 100 mV of the corrosion potential of zinc.

- The addition of a potentiodynamic polarisation step following the completion of the final electrochemical impedance adds an extra dimension to the analysis that can be done of the overall system.
    - However, traditional Tafel interpolation may be insufficient or inappropriate for the analysis of the multiple metal set-up, as the corrosion potential of the system may be several hundred millivolts away from the Tafel region observed on the individual metal.
- The range selection for potentiodynamic polarisation may be incompatible for systems containing both zinc and aluminium. In some of the systems presented, it is possible that the aluminium Tafel region may be present at a more negative potential than the -1200 mV limit which was selected.
    - However, selecting a limit more negative than this is likely to shift the Tafel behaviour on the zinc sample from zinc to zinc oxide.

5.6 Chapter References

[1] Selverian JH, Marder AR, Notis MR. J Electron Microsc Tech 1987;226:223.

[2] Bush GW, Jones DA, Nair NR, Biber HE, Townsend HE, Borzillo AR, Friet JJ, Graedel TE, Allegra L, Dutton RJ, Kriner SA, Berke NS, Meyer L, Selige A, Midorikawa H, Minato A, Kubo M, Katayama K, Sato K, Yasunaga H, Yoshihara T, Fujita Y, Kyono K, Patent US, Higuchi S, Tano K, Kamada M, Okamoto S, Zoccola JC, Meitzner CF, Horton JB, Pelerin J, Bramaud B, Nouville JF, Coutsouradis D, Herrshaft DC, Serais JP, Radtke SF, Lee HH, Gomersall DW, Leckie HP, Sievet WC, Legault RA, Ichiyama K, Kobayashi J, Sugimoto S, Lynch RF, Lin KL, Ho JK, Kubaschewski O. Corrosion 1991;47:17.

[3] Juttner K, Lorenz W. Corros Sci 1989;29:279.

[4] Oh HJ, Jang KW, Chi CS. Bull Korean Chem Soc 1999;20:1340.

[5] Pan J, Thierry D, Leygraf C. Electrochim Acta 1996;41:1143.

[6] Edavan RP, Kopinski R. Corros Sci 2009;51:2429.

[7] Zhang X, Vu T-N, Volovitch P, Leygraf C, Ogle K, Wallinder IO. Appl Surf Sci 2012;258:4351.

[8] Burleigh TD, Rennick RC, Bovard FS. Corrosion 1993;49:683.

[9] Aylward G, Findlay T. SI Chemical Data, 6th editio. Milton, Queensland: Wiley; 2008.

6 Conclusions

The issue of replacing the carcinogenic hexavalent chromium compounds from being used in corrosion inhibition applications is one that is both difficult and real. Particularly in the coil coating industry, where the inherent defect of an exposed cut edge means that efficient and effective corrosion inhibition is required for almost all applications, it is a problem which requires a solution. These works have looked at a potential alternative, or addition, to long and costly real world exposure tests. Alongside this, they have also attempted to gain some understanding into how, or why, some of the proposed alternatives work in certain conditions. The conclusions that have been made from the contained works are:

- A methodology was developed for looking at the behaviour of corrosion inhibitors on multi-metal systems. This was tested on a simplified zinc and steel system using pigments in which the corrosion behaviour is relatively well known. Analysis of the obtained results showed good matching between the expected behaviour and that which was shown by the electrochemical impedance, suggesting that the methodology is valid.
- The methodology was applied to lesser understood and industrially relevant modified aluminium polyphosphate inhibitor pigments on the simple zinc and steel substrate configuration. Distinct behaviours were shown for each of the aluminium polyphosphates, particularly strontium aluminium polyphosphate which exhibited time-dependant behaviour, suggesting differing mechanisms of action.
- The zinc and steel configuration was modified to look at local effects after seeing time dependent behaviour in samples exposed with the strontium aluminium polyphosphate inhibitor. Following the change in the sample configuration, the time dependent behaviour was absent. This indicated that some mechanistic information could be predicted by manipulating the substrates and using the simultaneous electrochemical impedance methodology.

- Optical microscopy, scanning electron microscopy and energy-dispersive X-ray spectroscopy were used on steel samples exposed to polyphosphate inhibitors with and without the presence zinc chloride. The structure, adhesion and elemental composition of the corrosion products and surface deposits was seen to change when zinc chloride was added to the solution.
- X-ray photoelectron spectroscopy showed several composition changes with the presence of zinc chloride in solution. In particular, the presence of zinc chloride in solution was shown to result in greater concentrations of phosphorus on the surface for strontium aluminium polyphosphate at all measured exposure times, and to accelerate the deposit of phosphorus on the surface with calcium aluminium polyphosphate. It is therefore considered that the presence of zinc has an effect on the mechanism of deposition/inhibition for these polyphosphates. The effect of zinc on magnesium aluminium polyphosphate was shown to be minimal.
- The minimum concentration level of added zinc chloride to the solution for effective changes to the rate of phosphate deposition was determined to be between the approximate concentrations 1 and 2 mM within the bulk solution. At 1 mM and below, it was seen that the effect on phosphorus was inconsistent. An increased concentration of zinc chloride, 4 mM, was seen to improve the phosphorus deposition levels beyond that of 2 mM. A maximum level of effectiveness was not determined within the scope of this thesis.
- Limited initial results showed the potential for improving the efficacy of modified aluminium polyphosphate corrosion inhibition through the addition of alternative cationic sources. The addition of calcium in particular showed positive effects of phosphate levels similar to that of zinc in the other studies.
- The expanded simultaneous electrochemical impedance methodology was shown to be useful for a three working electrode set-up. Interesting mechanistic information

regarding the magnesium aluminium polyphosphate inhibitor was suggested through apparent corrosion acceleration behaviour. However, the highly resistive nature of naturally occurring aluminium oxide does mean that it can be somewhat difficult to gain accurate equivalent circuit analysis from the aluminium surface in the particular metallic configuration used within these tests.

- Simultaneous potentiodynamic polarisations were attempted with the three electrode cell set-ups. Whilst some potentially useful analysis could be made, the overall applicability of traditional Tafel interpolation is perhaps tenuous at best. However, graphical overlays do appear to give some comparative idea of how each individual part of the cell is interacting with the corrosion inhibitors.

7 Suggestions for Future Work

Whilst the work carried out and discussed within this report can be considered complete and has resulted in the conclusions presented, there are definite logical extensions to the work that can be suggested for future study. This section will provide some potential avenues for the continuation of the work shown in this thesis.

- Whilst the simultaneous electrochemical impedance methodology has been verified and can simply be compared with traditional electrochemical impedance spectroscopy, it has not been thoroughly compared with other advanced techniques. It is suggested that results obtained from the developed methodology are compared to what can be obtained from localised techniques, such as scanning vibrating electrode technique, localised electrochemical impedance spectroscopy and scanning kelvin probe.
- Some experimentation went into the expansion of the developed methodology into more complex metallic systems with three working electrodes. The addition of aluminium proved to be somewhat problematic. Therefore, it is suggested that further verification work is required on the systems with greater numbers of working electrodes. For example, adding more benign metals into the system such as copper or tin and observing how the system changes.
- In addition to the previous point, zinc magnesium aluminium ternary alloys are of interest due to becoming more commonly used within the coil coating industry. Therefore, testing additional analogue models for some of the more complex alloy coatings. This could also include introducing some non-pure metallic elements (alloys) into the models.
- Some mechanistic information was predicted through the change of experimental parameters (distance between electrodes) within this work. This means there is the

potential for more information to be gathered through similar parameter changes. One potential parameter to observe is to perform the impedance measurements at potentials offset from the measured mixed potential to understand how that might affect the inhibitor effects.

- In the work as presented, the x-ray photoelectron spectra are relatively crudely analysed with respect to the overall thickness/deposition. One proposal for the extension of this work is to introduce angle-resolved XPS measurements, as well as sputtering experiments, could be methods applied to gain a fuller understanding of both the overall thickness of the deposited material, as well as any through-thickness changes. XPS mapping could also be used to determine overall quality of coverage.
- All surface characterisation presented in these works concentrated on the steel surface which, whilst important, does not present a full view of the inhibitor action over the cut edge. A series of experiments analysing the surface of zinc would be important for the simple galvanised steel case.
- Further surface characterisation techniques could be utilised to gain a fuller understanding of the surface deposition by the inhibitor molecules. Atomic force microscopy could be used to determine the structure of the deposits, and comparing this with the structure produced in the presence of additional cationic species may give a better idea of why greater phosphorus deposition was seen for strontium aluminium polyphosphate when zinc is present.
- Further to the previous point, it would be of interest to see whether any structural changes occur on surface or in solution. In an attempt to determine this, a series of experiments involving recrystallization of inhibitor species from solutions containing cationic species could be done. Following this, various characterisation methods, such as differential scanning calorimetry, infrared spectroscopy or powder x-ray diffraction, could be used to determine whether any in-solution changes occur.

- There is the potential for more work to be done on the competing cationic species series of experiments. Firstly, further characterisation of the systems already studied could be useful. Specifically, observing the electrochemistry of systems containing additional cations and comparing the results with the XPS results.
- Introduction of cationic species experiments have thus far only used simple chloride additions to the bulk solution. Whilst this is useful for the experimental side, this will not have much use in real systems. Therefore, it is also proposed that pigment systems that can potentially provide the synergistic effects that the cationic species provide are looked at.